Distribution Agreement

In presenting this thesis or dissertation as a partial fulfillment of the requirements for an advanced degree from Emory University, I hereby grant to Emory University and its agents the non-exclusive license to archive, make accessible, and display my thesis or dissertation in whole or in part in all forms of media, now or hereafter known, including display on the world wide web. I understand that I may select some access restrictions as part of the online submission of this thesis or dissertation. I retain all ownership rights to the copyright of the thesis or dissertation. I also retain the right to use in future works (such as articles or books) all or part of this thesis or dissertation.

Signature:

_____   _____
Riley Edward Antares Perszyk   Date

A study of N-methyl-D-aspartate receptor allosteric modulators with diverse mechanisms

of action

By

Riley Edward Antares Perszyk
Doctor of Philosophy

Graduate Division of Biological and Biomedical Science
Molecular and Systems Pharmacology

_____
Stephen F. Traynelis, Ph.D.
Advisor

_____
Shannon Gourley, Ph.D.
Committee Member

_____
Criss Hartzell, Ph.D.
Committee Member

_____
John Hepler, Ph.D.
Committee Member

Accepted:

_____
Lisa A. Tedesco, Ph.D.
Dean of the James T. Laney School of Graduate Studies

_____
Date

A study of N-methyl-D-aspartate receptor allosteric modulators with diverse mechanisms

of action

By

Riley Edward Antares Perszyk
B.S., Georgia Institute of Technology, 2009

Advisor: Stephen F. Traynelis, Ph.D.

Abstract

A study of N-methyl-D-aspartate receptor allosteric modulators with diverse mechanisms

of action

By Riley Edward Antares Perszyk

N-methyl-D-aspartate receptors (NMDARs) are obligatory heterotetrameric ionotropic cell-surface receptors. Throughout the brain, NMDARs are expressed in synaptic and extrasynaptic spaces. Glutamate release at excitatory synapses leads to NMDAR activation, subsequent depolarization, and calcium influx. There are many endogenous molecular modulatory factors that influence NMDAR activity, including the co-agonist glycine, magnesium ions, zinc ions, neurosteroids, and extracellular protons. Additionally, NMDAR activity is controlled by the membrane potential due to extracellular block by magnesium ions. NMDARs play a role in initiating several forms of plasticity, integrating synaptic signals, and brain development. Modulation of NMDARs has been proposed as beneficial intervention in numerous neurological disorders. Previous attempts to target NMDARs have not been fruitful due to on-target side effects. A more detailed understanding of various NMDAR subtypes or subpopulations and how these factions contribute to the overall NMDAR function is required. This knowledge along with the development of novel pharmacological agents, with selective capabilities, will enhance future endeavors of producing safe and tolerated NMDAR-targeting drugs.

In this dissertation, three new compound series are evaluated for their actions on NMDARs and their utility in neural tissues. One series contains analogs with opposing

actions and particular properties that should allow these compounds to selectively act based on the pattern of synaptic stimulation. The subunit selectivity of a series of positive allosteric modulators allows for selective targeting of a subpopulation of neurons and enhanced excitability of those cells. A non-selective NMDAR positive allosteric modulator series may have cell-type preferring actions in neuronal tissue derived from to differences in potentiation across the NMDAR subunits. Study of these compound series has aided in a greater understanding of NMDAR allosteric modulation and how their use might alter physiological NMDAR-dependent processes. A discussion of various theoretical models of NMDAR modulation includes their potential use and limitations. The potential utility of these novel modulators will also be discussed. This work has utility in furthering our understanding of NMDARs and in the development of new pharmacological compounds that possess diverse modes of action.

A study of N-methyl-D-aspartate receptor allosteric modulators with diverse mechanisms

of action

By

Riley Edward Antares Perszyk
B.S., Georgia Institute of Technology, 2009

Advisor: Stephen F. Traynelis, Ph.D.

A dissertation submitted to the Faculty of the
James T. Laney School of Graduate Studies of Emory University
in partial fulfillment of the requirements for the degree of
Doctor of Philosophy
in Graduate Division of Biological and Biomedical Science
Molecular and Systems Pharmacology
2018

Acknowledgments

The completion of this dissertation would not have happen without many people, groups and organizations. I would like to acknowledge Emory University for being a wonderful collaborative place to study. The Traynelis lab has been a challenging and intriguing place to work and develop as a scientist; all of the lab members that have come through the lab have been wonderful to work with and around. I would like to thank Carrie and the Jenkins lab for teaching me how to patch-clamp and giving me the first taste of the type of research that constitutes the bulk of this dissertation.

I was able to cope with the stresses of graduate school and dissertating thanks to many people. I cannot express in words the gratitude I have for the Atlanta cycling community in helping me get through one of the darkest periods in my life and the continued delight it brings me. I'm thankful for the opportunity to lead Emory Spokes council that allowed me to engage and work towards bettering the local cycling community. The SARSenites for keeping it interesting on the 5th floor of Rollins. Playing Frisbee, board games, and soccer with many people helped keep me balanced throughout the years. I am indebted to the spaceteam team for their help in escaping many blackholes. I'd also like to thank everyone who has, either knowingly or unknowingly, helped motivate me to get outside to hike, bike or camp more. I fully appreciate and value highly the relationships that have persisted though the most trying of times.

And lastly, I would not have made it to this point if it weren't for the unconditional support of my parents, Sara and Tony; my brother, Tysen; my nieces, Arcadia, Hazel, and Zinnia; and extended family, Kathryn, the Serebin's and the Perszyk's.

Table of Contents

List of Figures

List of Tables

List of Abbreviations

Acetonitrile (ACN);

agonist binding domain (ABD);

α-amino-3-hydroxy-5-methyl-4-isoxazolepropionic acid (AMPA);

(2)-amino-5-phosphonovaleric acid (APV);

amino terminal domain (ATD);

artificial cerebral spinal fluid (aCSF);

(3-Bromophenyl)[3,4-dihydro-6,7-dimethoxy-1-[(4-methoxyphenoxy)methyl]-2(1H)-isoquinolinyl]methanone (BIQ);

(3-Chlorophenyl)[3,4-dihydro-6,7-dimethoxy-1-[(4-methoxyphenoxy)methyl]-2(1H)-isoquinolinyl]methanone (CIQ);

central nervous system (CNS);

7-chlorokynurenic acid (7-CKA);

coding deoxyribonucleic acid (cDNA);

coding ribonucleic acid (cRNA);

confidence interval (CI);

3,3' diaminobenzidine (DAB);

effective concentration (EC);

enantiomeric excess (EE);

excitatory postsynaptic current (EPSC);

(3-Flourophenyl)[3,4-dihydro-6,7-dimethoxy-1-[(4-methoxyphenoxy)methyl]-2(1H)-isoquinolinyl]methanone (FIQ);

γ-Aminobutyric acid (GABA);

γ-Aminobutyric acid type A Receptor (GABA$_A$R);

human embryonic kidney cells 293 (HEK293);

inhibitory concentration (IC);

inhibitory postsynaptic current (IPSC);

(3-Iodophenyl)[3,4-dihydro-6,7-dimethoxy-1-[(4-methoxyphenoxy)methyl]-2(1H)-

isoquinolinyl]methanone (IIQ);

kinetically derived affinity constant (K$_d$);

Methanethiosulfonate ethylammonium (MTSEA);

miniature excitatory postsynaptic currents (mEPSC);

N-methyl-D-aspartate receptors (NMDAR);

negative allosteric modulators (NAMs);

polymerase chain reaction (PCR);

positive allosteric modulators (PAMs);

reverse transcription PCR (RT-PCR);

structure activity relationship (SAR);

spontaneous inhibitory postsynaptic current (sIPSC);

transmembrane domain (TMD);

two-electrode voltage-clamp (TEVC);

complementary deoxyribonucleic acid (cDNA);

Chapter 1: Introduction

The primordial nervous system is an evolutionary development that has allowed multicellular organisms to coordinate their response to internal and external stimuli (Mackie 1990). The central nervous system (CNS) is an adaptation that allows for more interconnection between the peripherally acting neurons and specialization, where specific brain regions receive and send specific information (Sherrington 1910). Having more interconnections creates a greater ability for the association of diverse stimuli, higher ordered computation, and more complex responses. These associative properties were developed alongside with adaptive properties that allowed animals to alter their neuronal processes in response to their environment and experiences (Ryan and Grant 2009). These traits allowed the kingdom *Animalia* to be a widely successful branch of life on earth.

For hundreds of years, philosophers and scientists have wondered about how the brain functions, how memories are formed, and behaviors learned. With the advent of cellular identification methods, studies focused on the structures and interconnections of neurons (Golgi 1873, Ramon y Cajal 1894). Theories of learning and memory involved remodeling of dendrites and axons (Tanzi 1893, Ramon y Cajal 1894). Later, Hebb postulated that neurons should have the capability to detect coincidences in neural signaling and make adaptive alterations (Hebb 1949). Technical advances allowed for low-noise current-clamp recordings leading to the foundational principles of neurotransmission (Goldman 1943, Hodgkin and Huxley 1952, del Castillo and Katz 1954, Katz and Miledi 1972). Advancement in the pharmacological sciences allowed for the identification of cell-surface receptor families (Arunlakshana and Schild 1959). The discovery that high frequency stimulation paradigms could reliably induce a form of

neuronal plasticity was a major step forward towards identifying Hebb's postulated coincidence detector (Bliss and Lømo 1973). The invention of the patch-clamp method allowed scientists to perform highly precise electrical recordings from small patches of cellular membranes, which minimized signal noise and activity from individual channels could be resolved (Neher and Sakmann 1976). Newly developed pharmacological tools identified NMDARs as being critical for certain forms of neuronal plasticity, including Hebbian plasticity (Evans 1979, Evans 1982, Collingridge 1983). NMDAR antagonists were additionally shown to block certain types of memory formation (Morris 1986, Danysz 1988, Bolhuis and Reid 1992), but not the retrieval of formed memories, mimicking the actions of NMDAR antagonist impact on long term potentiation (Morris 1989, Staubli 1989, Shapiro and Caramanos 1990).

Technological advancements in genetic and biochemical methods led to a greater appreciation of the biological and pathological roles of NMDARs. Cloned NMDAR subunits could be used in heterologous cell systems to characterize the biophysical properties of specific NMDAR subtypes (Moriyoshi 1991, Ikeda 1992, Kutsuwada 1992, Meguro 1992, Monyer 1992, Sugihara 1992, Hollmann 1993, Ishii 1993, Monyer 1994, Vicini 1998). Additionally, advancements in genetic methodology allowed for identification of developmental and spatial expression patterns of NMDAR subunits (Akazawa 1994, Laurie and Seeburg 1994, Monyer 1994, Standaert 1994). NMDARs were identified as playing a role in several neurological disorders, including stroke and traumatic brain injury (Lipton and Rosenberg 1994). A vast amount of medicinal chemistry efforts led to highly efficacious and potent compounds targeting NMDARs, and many clinical trials were run (Chenard 1995, Fischer 1997, Yenari 1998, Palmer

2001). Most of these clinical trials failed for various reasons, including some that failed due to inadequate trial design, heterogeneity in endpoint selection, and some that failed due to on-target side effect profiles that could not be disentangled from the compounds therapeutic actions (Ikonomidou and Turski 2002, Chen and Lipton 2006).

Reflections upon the failures of NMDAR-targeting clinical trials suggest therapeutic benefit may still be achieved by modulating NMDARs, but a new generation of compounds with novel mechanism of actions is required (Hallett and Standaert 2004, Kalia 2008, Coyle 2012, Collingridge 2013, Paoletti 2013). Many neurological disorders where NMDARs have been implicated, including Alzheimer's disease, Parkinson's disease, stroke, and schizophrenia remain poorly managed (Mangialasche 2010, Cohen 2015, Gonzalez 2015, Kalia 2015, Chamorro 2016, Gooch 2017). NMDAR-targeting compounds with diverse activity are desired to test potential therapeutic benefits in these diseases. As stated above, this new generation of drugs will need to possess more selective targeting of NMDAR subtypes to reduce on-target side effects; this may be achieved by subunit-selectivity, activity-dependence or other mechanisms of action that limits a drug's unintentional wide-spread impact. In order for clinical success, a clear understanding of NMDAR function, expression, biophysical properties and potential for modulation is needed.

In this dissertation, development of three distinct allosteric modulator series with distinct mechanism of action will be presented. Prior to these studies, a summary of NMDAR's pathological implications, physiological roles and the properties that control receptor function will be discussed. Existing NMDAR ligands will also be summarized to provide context to what is known about the orthosteric and allosteric NMDAR

pharmacological agents. Following the presentation of these novel modulator series, models capable of representing the actions of many of these allosteric modulators will be presented. The diverse mechanistic properties of these compounds will be discussed as they may be useful in basic science research of NMDARs functional roles and as important features of potential therapeutic interventions.

Pathological roles of NMDA receptors

NMDARs are causal or contributing factors in many neurological diseases, such as intellectual disability, epilepsy, schizophrenia, traumatic brain injury, stroke and Parkinson's disease (Hallett and Standaert 2004, Kalia 2008, Coyle 2012, Collingridge 2013, Paoletti 2013). A large economic and societal burden arises from caring for individuals suffering from these diseases (Borlongan 2013, Gooch 2017). For many neurological diseases, the current standard of care begs for innovative therapies, as the current treatment options are not well tolerated, do not address all symptoms, and may not be curative (Mangialasche 2010, Gonzalez 2015, Kalia 2015, Chamorro 2016, Macrez 2016). The following is a brief overview of some of the potential ways NMDAR function or dysfunction may lead to or contribute to disease.

Due to the enhanced efficiency in genome sequencing, an increasing number of *de novo* mutations in NMDAR subunits are being identified in patients with epilepsy, schizophrenia, and intellectual disability diagnoses, as mutations segregate with the disease and significantly alter receptor function (Awadalla 2010, Endele 2010, Hamdan 2011, Fromer 2014, Swanger 2016, Chen 2017, Ogden 2017). These mutations either have a direct causal relationship with the disease or alter neuronal activity leading to

pathological state in neuronal networks (Swanger 2016). A primary theory of the pathogenesis of schizophrenia is due to hypofunction of NMDARs in cortical interneurons (Lau and Zukin 2007, Coyle 2012). NMDAR involvement in schizophrenia arises from genetic association studies and the observation that NMDAR channel blockers induce behaviors that are indistinguishable from disease symptoms (Krystal 1994, Cohen 2015). Compounds capable of rescuing this NMDAR hypofunction are desired for clinical investigation (Cohen 2015).

NMDARs contribute to acute and chronic neurodegeneration conditions (Lipton and Rosenberg 1994, Surmeier 2010, Collingridge 2013). After a traumatic brain injury or stroke, the tissue around the damaged tissue is metabolically compromised leading to a breakdown of ionic gradients and aberrant glutamate release (Choi and Rothman 1990, Kostandy 2012). The synergy of these conditions results in NMDAR activation, subsequent influx of Ca^{2+}, cellular stress and excitotoxicity (Kostandy 2012). Numerous studies have illustrated that blocking NMDARs, following a traumatic brain injury or stroke, provides robust neuroprotection (Palmer 2001, Wang and Shuaib 2005, Lipton 2007). Potential therapies must reduce aberrant NMDAR activity while sparing normal activity, to be ultimately successful (Ikonomidou and Turski 2002, Lai 2014). In chronic neurodegenerative diseases, such as Parkinson's disease, degeneration occurs slowly over time with neurons dying over many years (Lipton 2006, Surmeier and Schumacker 2013). Studies suggest a multitude of factors that impact cellular homeostasis leading to increased stress on at-risk neurons. NMDARs contribute to homeostatic stress and inhibiting them modifies the progression of certain neurodegenerative disease animal models (Lipton 2006, Kari 2009). Inhibiting NMDARs may also rectify imbalances in

network activity, due to NMDA expression in key basal ganglia nuclei that have increased activity in the disease (Hallett and Standaert 2004, Kari 2009).

NMDARs are potential therapeutic targets for the above mentioned diseases, as well as others. In various cases, either increasing or decreasing NMDAR activity is predicted to be beneficial. Interventions must address NMDAR's role in pathology but also take into account their biological roles (discussed in the next section). Currently only a few drugs targeting NMDARs are approved for clinical use, despite many dozens of clinical trials and a plethora of preclinical data (Palmer 2001, Wang and Shuaib 2005, Lipton 2006, Lipton 2007, Iacobucci 2017). Clinic trials have failed due to a variety of factors (Ikonomidou and Turski 2002, Muir 2006), thus new strategies are needed that produce beneficial actions while subverting on-target side-effects (Chen and Lipton 2006, Kalia 2008).

Neurological roles of NMDA receptors

NMDARs are found at most excitatory synapses in the central nervous system (Traynelis 2010). In the brain, the primary excitatory synaptic neurotransmitter is glutamate, which has a high affinity for the NMDAR. Synaptic glutamate concentrations reach a high level (>1 mM) but are tightly controlled by glutamate transporters (Rusakov and Kullmann 1998). Additionally, there are extra- and pre-synaptic NMDARs that are exposed to prolonged but lower concentrations of glutamate, either from synaptic spill-over or astrocytic release (Rusakov and Kullmann 1998, Collingridge 2004, Haydon and Carmignoto 2006). Glycine and D-serine are the physiological co-agonists of NMDARs (Johnson and Ascher 1987, Kleckner and Dingledine 1988, Mothet 2000). In the brain,

glycine and D-serine transporters control the level of the co-agonists, which can tune the activity level of NMDARs (Bergeron 1998, Foster 2016). Most NMDAR studies have considered glycine as the main co-agonist; differences are minor and so only glycine will be referred to in this document, for simplicity. Additionally, extracellular Mg^{2+} ions block NMDARs at hyperpolarized membrane potentials. Consequentially, when glutamate and glycine are bound, a neuron must be partially depolarized in order for full receptor activity (Evans 1977, Ault 1980, Mayer 1984, Nowak 1984, Monyer 1994, Vicini 1998).

Predating the identification of NMDARs, it was postulated that there must be a process of coincidence detection by neurons in the brain that leads to changes that enhance the detection of the coincidental signal (Hebb 1949). Hebbian plasticity, as this type of neuronal plasticity was then called, would allow an organism to better detect and respond to important stimuli in the future (Buchanan 2013). Early studies of the concept of neuroplasticity showed that repeated stimulation of axon fibers (sub-second time scale) led to an enhancement of the postsynaptic response, which was maintained for a long time (hour time scale) (Bliss and Lømo 1973). Years later, this phenomenon was shown to be blocked with (2R)-amino-5-phosphonovaleric acid (APV), a competitive antagonist of the glutamate binding site of NMDARs (Collingridge 1983). NMDARs were suggested as the molecular coincidence detector outlined by Hebb as they are blocked by Mg^{2+} at resting states (Cotman and Monaghan 1988). Additionally, NMDARs are highly permeable to Ca^{2+} ions allowing them to initiate intracellular signaling cascades and changes in the postsynaptic neuron (MacDermott 1986, Mayer and Westbrook 1987, Ascher and Nowak 1988, Ghosh and Greenberg 1995, Lisman 2012). These properties of

NMDARs are consistent with the properties that Hebb postulated should exist (Bliss and Collingridge 1993). Currently, NMDARs are considered to be one of the primary initiating factors in LTP and other forms of neuronal plasticity (Malenka and Nicoll 1999, Morris 2013). Many forms of plasticity are known, including some forms of LTP that are NMDAR-independent (Sweatt 2016). Neuronal plasticity, including a predominant role of NMDARs, has been implicated in several forms of learning and memory induction in animals (Martin 2000, Morris 2013).

In more recent years, new roles have been proposed for NMDARs due to the diversity in functional properties and subcellular cell-surface expression patterns conferred by various GluN2 subunits. Differences in the deactivation time course, following rapid glutamate removal, of NMDAR subtypes suggest that the NMDAR subtypes confer different windows of synaptic integration and summation (Magee 2000). The resting membrane potential of a neuron is controlled by a number of voltage-gated, leak and other channels, which normally restricts NMDAR activation to the stimulus conditions discussed in the previous paragraph. In some cell types, the membrane potential may be reduced or oscillates in a range where the Mg^{2+} block of NMDARs is partially relieved, such as in tonically active cell types (Hage and Khaliq 2015). In addition, Mg^{2+} affinity differs among NMDAR subtypes. In these situations, NMDARs may have a different role in neuronal excitability.

For any NMDAR-targeted drug candidate, consideration needs to be given to the candidate drug's actions on physiological NMDAR function during normal activity. Effective and tolerated drugs must limit their impact of the normal neurological roles of NMDARs and other physiological processes. Selectivity for NMDARs involved in

pathological processes may be achieved in various ways, which will be discussed in greater detail later, but is highly dependent on the NMDAR composition.

Molecular Composition and Function of NMDA Receptors

NMDARs are obligatory heterotetramers and typically consist of GluN1 and GluN2 subunits (Traynelis 2010, Paoletti 2013). In one tetramer, there are two GluN1 and two GluN2 subunits, assembled in an alternating pattern (Laube 1998, Schorge and Colquhoun 2003, Ulbrich and Isacoff 2008, Karakas and Furukawa 2014, Lee 2014). One gene (*Grin1*) can be differently spliced into eight distinct GluN1 transcripts (Moriyoshi 1991, Sugihara 1992, Hollmann 1993). Four *Grin2* genes exist and give rise to the four GluN2 subunits, GluN2A-D (Ikeda 1992, Kutsuwada 1992, Meguro 1992, Monyer 1992, Ishii 1993). Both GluN1 splice variants and GluN2 subunits have developmental and spatial expression patterns that create different subunit combinations in various brain regions (Akazawa 1994, Laurie and Seeburg 1994, Monyer 1994, Standaert 1994, Landwehrmeyer 1995). In the brain, NMDARs exist as diheteromeric (two distinct subunits in the tetramer) and triheteromeric (three distinct subunits) receptors (Sheng 1994, Chazot and Stephenson 1997, Luo 1997, Brickley 2003, Jones and Gibb 2005, Brothwell 2008, Tovar 2013, Hansen 2014). NMDAR properties are controlled by the subunits incorporated into each receptor (Monyer 1994, Vicini 1998, Vance 2012). The most common type of triheteromeric receptors are those with two distinct GluN2 subunits, although triheteromeric receptors with different splice variants of GluN1 or four distinct subunits could exist. Additionally, single nucleotide polymorphisms have been identified in human populations, which may increase the heterogeneity of heteromeric

receptor compositions (Swanger 2016). The GluN3 subunits bind glycine, can co-assemble with GluN1 to form a glycine receptor, and show sequence similarity with NMDAR subunits, but it is unclear what role they have in biology (Ciabarra 1995, Sucher 1995, Low and Wee 2010, Paoletti 2013).

NMDAR subunits have different amino acid sequence identities but have similar overall tertiary structure. This general structure of an NMDAR will be discussed next, followed by the differences in receptor function that different subunits confer.

Architecture of NMDA Receptors

Each subunit of an NMDAR consists of four modular semi-autonomous domains. Each has a modulatory amino-terminal domain (ATD), an agonist binding domain (ABD), a transmembrane domain (TMD), and an intracellular carboxyl-terminal domain (CTD) (Karakas and Furukawa 2014, Lee 2014). Interestingly, each semi-autonomous domain is homologous to other proteins, ancestral or otherwise. Specifically, the ATD is homologous to a bacterial periplasmic binding protein, the ABD is homologous to the glutamine-binding protein that can be found in *E. coli*, and the pore forming region of the TMD is homologous to K^+ channels (O'Hara 1993, Armstrong 1998, Panchenko 2001). These domains each have specific roles in the overall function of NMDARs.

The ATD is the most distal extracellular domain that binds some endogenous and exogenous modulators (Williams 1996, Perin-Dureau 2002, Karakas 2009, Mony 2011, Tajima 2016). The ATD exerts control over the desensitization and activity level of the receptor (Gielen 2009, Yuan 2009). The ABD is a clamshell-like domain consisting of two non-contiguous segments of the polypeptide. Agonist binds facilitating clamshell

closure that subsequently causes additional conformational changes, leading to the opening of the ion channel gate (Furukawa 2005, Vance 2012, Hansen 2013, Cooper 2015). The ABD of GluN1 binds glycine (Johnson and Ascher 1987, Kleckner and Dingledine 1988, Furukawa 2005). The ABD of GluN2 binds glutamate (Laube 1997, Furukawa 2005). The TMD consists of three membrane crossing α-helices and one reentrant loop (Wo and Oswald 1995, Wood 1995, Karakas and Furukawa 2014, Lee 2014). Parts of the M2 reentrant loop interact, constricting the channel pore and creating the selectivity filter of the NMDAR channel (Kuner and Schoepfer 1996, Wollmuth 1996, Wollmuth 1998). A sequence of amino acids in the M3 helix is one of the most conserved segments in the iGluR family and operates as the channel gate. After agonist binding, the M3 helices undergo a dilatation, two of them kink, and ions to flow through the unrestricted channel (Villarroel 1995, Zarei and Dani 1995, Wollmuth and Sobolevsky 2004, Twomey and Sobolevsky 2017). The CTD is the most variable domain and is thought to contain signaling sequences for intracellular binding partners (Carroll and Zukin 2002, Chen and Roche 2007, Choi 2013).

Recent structures of the AMPAR have greatly enhanced our understanding of the conformational changes that occur in the function of iGluRs (Yelshanskaya 2014, Twomey and Sobolevsky 2017, Twomey 2017, Twomey 2017, Yelshanskaya 2017). To date, there are multiple AMPAR crystal structures and a series of cryo-EM structures that illustrate several of the primary states that iGluRs can adopt, including apo (lacking agonist), agonist-bound shut, open channel and desensitized states. These structures have provided a general schematic for all iGluR motions, but discrepancies between the AMPAR and NMDAR structures are known to exist, for instance the ATDs and ABDs

are more closely associated in NMDARs and NMDAR are obligatory heterotetramers whereas several AMPARs are homotetramers (Karakas and Furukawa 2014, Lee 2014, Twomey and Sobolevsky 2017). This structural data has complemented and confirmed many postulates of receptor function made since the identification of the receptor family, such as the subunit arrangement and key gating elements (Karakas and Furukawa 2014, Lee 2014, Twomey and Sobolevsky 2017).

NMDA Receptor Function

Since the cloning of the genes encoding the glutamate receptor family, the NMDAR subtypes have been studied in order to understand how they function, what differences in activity they have, and why they exist (Traynelis 2010, Paoletti 2013, Swanger 2016). The general flow of receptor activation is believed to include agonist binding, domain closure, conformational changes in the ABD-TMD linkers, and rearrangement of the transmembrane helices (Twomey and Sobolevsky 2017). Single channel recordings demonstrate the dynamic nature of channel activity. In the presence of saturating glutamate and glycine, rapid channel opening and closing occurs (Nowak 1984, Cull-Candy and Usowicz 1987, Jahr and Stevens 1987). Upon agonist removal, random receptor transitions lead it back to a state where agonist can dissociate (Lester 1990). NMDARs can, also, enter a long-lived desensitized state where the open state is not achieved while agonist remains bound (desensitization is discussed in greater detail below).

The subunits in the tetrameric assembly control all properties of NMDARs (briefly summarized in Table 1.1). An important feature of synaptic receptors is their

Table 1.1. Summary of diheteromeric NMDAR receptor properties.

Receptor	Glu [a] EC_{50}	Gly [b] EC_{50}	Glu [c] Deactivation	Ca^{2+} [d] Perm.	Mg^{2+} [e] Block	Conductance (pS) [f]	Po [g]
GluN1/ GluN2A	3.3	1.1	55-120	+++	++	51, 38	0.50
GluN1/ GluN2B	2.9	0.72	280-400	+++	++	51, 39	0.12
GluN1/ GluN2C	1.7	0.34	260-380	++	+	36, 19	0.01
GluN1/ GluN2D	0.51	0.13	1700-4800	++	+	35, 17	0.01

[a] (Erreger 2007), [b] (Chen 2008), [c] (Monyer 1994, Vicini 1998), [d] (Burnashev 1995, Schneggenburger 1996, Wollmuth 1996, Siegler Retchless 2012), [e] (Kuner and Schoepfer 1996, Kotermanski and Johnson 2009), [f] (Stern 1992, Stern 1994, Wyllie 1996), [g] (Erreger 2005, Dravid 2008, Yuan 2009)

deactivation rate, since high levels of neurotransmitter is released, leading to rapid activation. Neurotransmitter is quickly removed due to transporter or enzymatic activity, thus the impact of the synaptic event is based on the amplitude of the response as well as the time frame of receptor deactivation (Lester 1990). The deactivation rates of the various diheteromeric receptors vary from the relatively quick GluN1/GluN2A, to the intermediate GluN1/GluN2B and GluN1/GluN2C, and to the slow GluN1/GluN2D (Monyer 1994, Vicini 1998). Receptor deactivation is related to the agonist potency. Since deactivation involves the unbinding of the agonist and the potency of a ligand is determined by its dissociation rate, thus glutamate and glycine potencies also vary greatly based on subtype. At GluN1/GluN2D the glutamate and glycine EC_{50}s are sub-micromolar whereas at GluN1/GluN2A the EC_{50}s are in the micromolar range (Erreger 2007, Chen 2008). Synaptically-released glutamate is thought to reach the millimolar range in the synaptic cleft, saturating any synaptic NMDAR. Alternatively, extrasynaptic glutamate concentrations are thought to be much less (Rusakov and Kullmann 1998), and may result in greater activity at NMDAR subtypes with higher glutamate potency (e.g. GluN1/GluN2D).

The dual properties of high Ca^{2+} permeability (MacDermott 1986, Mayer and Westbrook 1987, Ascher and Nowak 1988) and voltage dependent Mg^{2+} blockade (Evans 1977, Ault 1980, Mayer 1984, Nowak 1984) of NMDARs distinguishes them from other ionotropic glutamate receptors (Traynelis 2010). Specifically, GluN1/GluN2A and GluN1/GluN2B are more permeable to Ca^{2+} than GluN1/GluN2C and GluN1/GluN2D (Burnashev 1995, Schneggenburger 1996, Wollmuth 1996). Additionally, Mg^{2+} block is stronger in GluN1/GluN2A and GluN1/GluN2B as compared to GluN1/GluN2C and

GluN1/GluN2D (Kuner and Schoepfer 1996, Kotermanski and Johnson 2009). Conductance levels of NMDARs are also divided along these lines. Each diheteromeric NMDARs has one or two conductance levels, based on the absence or presence of extracellular Ca^{2+} (Wyllie 1996). The channel conductance levels for GluN1/GluN2A and GluN1/GluN2B receptors are larger than GluN1/GluN2C and GluN1/GluN2D (Stern 1992, Stern 1994, Wyllie 1996). The open probability of the diheteromeric receptors vary greatly; GluN1/GluN2C and GluN1/GluN2D have the lowest open probability, GluN1/GluN2B has an intermediate open probability, and GluN1/GluN2A has the highest open probability (Wyllie 1998, Erreger 2005, Dravid 2008). Interestingly, many of these permeation properties of NMDARs are controlled by a divergent residue (S632 in GluN2A, S633 in GluN2B, S643 in GluN2C, and L657 in GluN2D) in the M3 GluN2 subunit (Siegler Retchless 2012).

NMDARs can also desensitize in the continued presence of glutamate and glycine in a manner that is independent of several other forms of desensitization that are dependent on different ligands (discussed later). This desensitization is sensitive to intracellular dialysis, being more prominent in excised outside-out membrane patches (Sather 1990, Sather 1992). A wide range of mutations in various domains, including the conserved M3 gating motif, the pre-M1 linker region, and the ion channel pore, the ABD, and the TMD-ABD interface perturb this form of desensitization (Chen 2004, Hu and Zheng 2005, Alsaloum 2016). Interestingly, this generalized form of desensitization affects GluN1/GluN2A and GluN1/GluN2B whereas it spares GluN1/GluN2C and GluN1/GluN2D (Erreger 2005, Dravid 2008, Vance 2013). Recent studies of AMPAR hold pertinent structural information regarding the conformational changes during

NMDAR desensitization (Twomey and Sobolevsky 2017, Twomey 2017) but needs to be interpreted with caution as differences in the structures of these related iGluRs have been noted (Karakas and Furukawa 2014, Lee 2014). These differences in desensitization may be derived from specific NMDAR subtypes structural conformations, but it is difficult to make any specific predictions given the lack of structural information of multiple NMDAR subtypes.

Glycine-dependent NMDAR desensitization is present only in sub-saturating glycine concentrations, and occurs as a result of a negative allosteric interaction between the glutamate and glycine binding sites, such that the binding of glutamate decreases the glycine affinity, and vice versa (Mayer 1989, Benveniste 1990, Lester 1993). Thus, when glutamate binds GluN2 in the presence of subsaturating of glycine, the current will relax to a new equilibrium as glycine unbinds from the receptor following the allosteric reduction in glycine affinity. This form of desensitization is dictated by glycine unbinding, which is temporally similar to the synaptic NMDAR time course, raising the possibility that glycine-dependent desensitization could impact synaptic signaling when glycine is subsaturating.

NMDARs also undergo Ca^{2+}-dependent desensitization or inactivation, which requires an increase in intracellular Ca^{2+} over several seconds (Clark 1990, Legendre 1993, Vyklicky 1993, Rosenmund 1995). The magnitude of this form of desensitization varies at different NMDAR subtypes. GluN2A-containing NMDARs exhibits the greatest extent of desensitization, GluN2B- containing NMDARs exhibits a lesser extent, and GluN2C-containing NMDARs exhibits a very low level of Ca^{2+}-dependent desensitization (Medina 1995, Krupp 1996). Increases in the intracellular Ca^{2+} in the

vicinity of the NMDAR triggers uncoupling of the receptor from filamentous actin (Rosenmund and Westbrook 1993). In addition, calmodulin binding to the GluN1 CTD may play a role in this form of desensitization (Ehlers 1996, Ehlers 1998, Zhang 1998, Krupp 1999).

These differences in molecular composition and functional properties allow for selective modulator action. Divergent sequence identity may result in selectivity, if there are differences in tertiary structure (see ifenprodil and PYD-106 below) or if similar pockets exist and clashes between side chain residues and ligands occur (see TCN, MPX and GNE GluN2A-selective PAMs). Additionally, given that receptors experience complex interactions in the microenvironment, a compound may derive selectivity from the synthesis of these complex interactions or the activity of a receptor, i.e. selectivity of low affinity channel blockers derived from an interaction with Mg^{2+} (discussed below). More detailed evaluations of the regulation of NMDARs by endogenous and exogenous factors and the kinetic nature of NMDAR function are discussed in the following sections.

Intercellular Consequences of NMDA Receptor Activity

NMDAR activation leads to the influx of Na^+ and Ca^{2+}. The Na^+ ions serve to depolarize the postsynaptic cell and which has a prolonged impact, due to NMDAR's relatively long deactivation time course. The Ca^{2+} ions cause depolarization but also are important intercellular factors due to their capacity to activate calcium dependent signaling cascades. These mechanisms are heavily dependent on cell type expression of many factors, such as calcium binding proteins, calcium transporters that sequester

calcium, kinases and factors that calcium activates (see Figure 1.1) (Thomas and Huganir 2004, Marambaud 2009, Dityatev 2010, Kotaleski and Blackwell 2010, Murakoshi 2011, Saneyoshi and Hayashi 2012, Koleske 2013). These calcium signaling cascades can lead to several endpoints, including AMPAR phosphorylation, AMPAR insertion into the membrane, synaptic AMPAR removal, gene transcription, protein synthesis, influence actin dynamics and influence structural plasticity. Most notably, Ca^{2+} signaling leads to neuronal plasticity (Malenka and Nicoll 1999). NMDAR activity can lead to the insertion of new AMPARs into the synapse via activation of the calmodulin/CAMKII pathway, which is thought to occur during long term potentiation (Buard 2010, Kotaleski and Blackwell 2010). Additionally, it can lead to gene transcription and protein synthesis via PKC and ERK pathway which can cause longer term alteration in neuronal activity (Thomas and Huganir 2004). Ca^{2+} signaling also influences structural plasticity of spines via the Rho/Rock pathway (Dityatev 2010, Koleske 2013).

The network of Ca^{2+} signaling is complex and intricate. For instance, during transient Ca^{2+} signaling the Rho and CDC42 actin remodeling pathways are activated whereas in sustained Ca^{2+} signaling leads to primarily Rho pathway activation due to CDC42 diffusion (Murakoshi 2011, Saneyoshi and Hayashi 2012). This highlights the importance of the orientation and placement of these effector proteins in these signaling pathways. NMDARs are typically found in the post-synaptic density and have many protein binding recognition sites which may facilitate the activation of particular signaling cascades (Traynelis 2010). These signaling networks also can contain feedback mechanism and interweaving of pathways, for instance calmodulin binds to the CTD GluN1 and inhibit receptor activation whereas calmodulin activation due to NMDAR
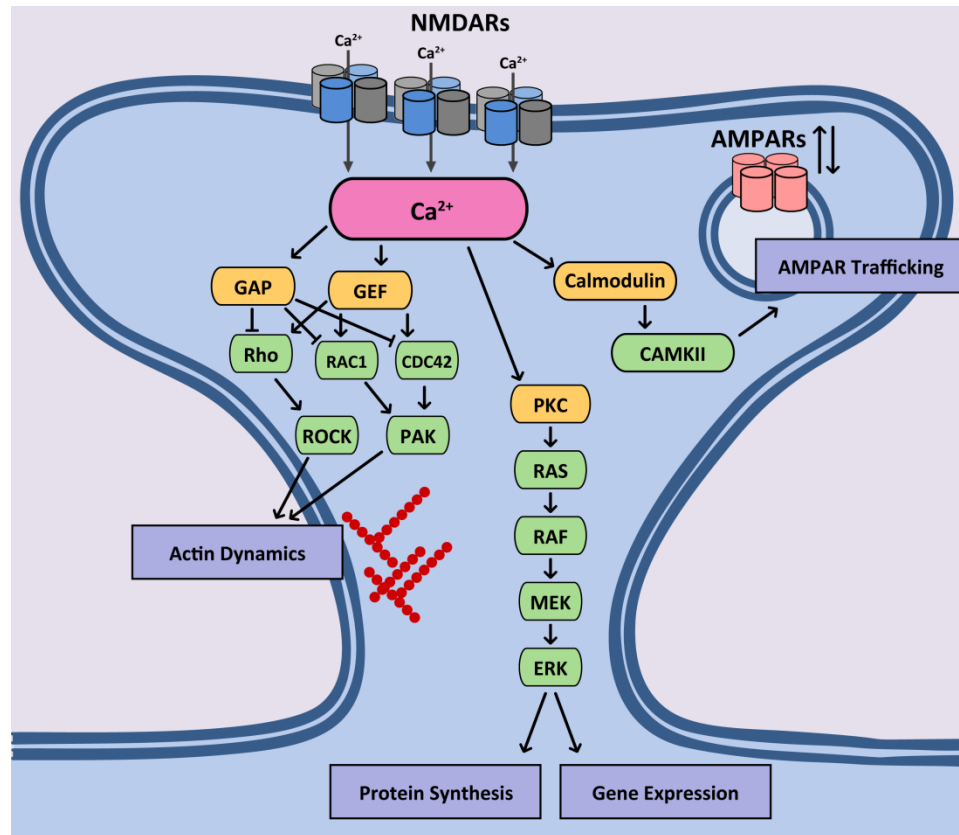
Figure 1.1. An overview of Ca^{2+} signaling pathways.

A cartoon illustrating the signaling pathway map of some of the interactions that occur upon NMDAR activation and the influx of calcium is shown. Ca2+ influx can activate many effector proteins, such as calmodulin, PKC, GEFs, and GAPs, leading to several functional consequences, such as influencing AMPAR trafficking, gene expression, protein synthesis, and actin dynamics.

activity in important in activating CAMKII and causing long term potentiation (Ehlers 1996, Rycroft and Gibb 2004). More thorough reviews of these important protein interactions of NMDARs and post-translational modifications exist (Kohr and Seeburg 1996, Carroll and Zukin 2002, Maki 2012, Lussier 2015).

Mechanisms of NMDA receptor allosteric modulation

As discussed, NMDARs are complex macromolecular membrane-bound structures. Many properties of NMDARs function can be altered by extracellular ions, endogenous compounds, and exogenous compounds. This suggests that potentially there are diverse avenues to exploit for therapeutic intervention. Historically, NMDAR identification relied on selective pharmacology that differentiated them from other iGluRs. The use of selective agonists (Watkins 1962, Curtis and Watkins 1963, Evans 1978, Evans 1979), antagonists (Biscoe 1977, Davies and Watkins 1979, McLennan and Lodge 1979, Evans 1982), and channel blockers (Anis 1983, Wong 1986) identified the sub-family of iGluRs, which was eventually named after the selective agonist N-methyl-D-aspartate. Since then, newer generations of compounds have been developed with diverse chemical structures and activity. Currently, a number of compounds have selective action by exploiting differences in GluN2 subunits. Additionally, several modulator series have been discovered with other properties that contribute to their mechanism of action. Some of these properties include use-dependence, agonist-dependence, agonist-potency enhancement, and the ability to partition into the lipid bilayer. In the following section, the actions of various NMDAR ligands based on their site of action will be discussed (see Figure 1.2).
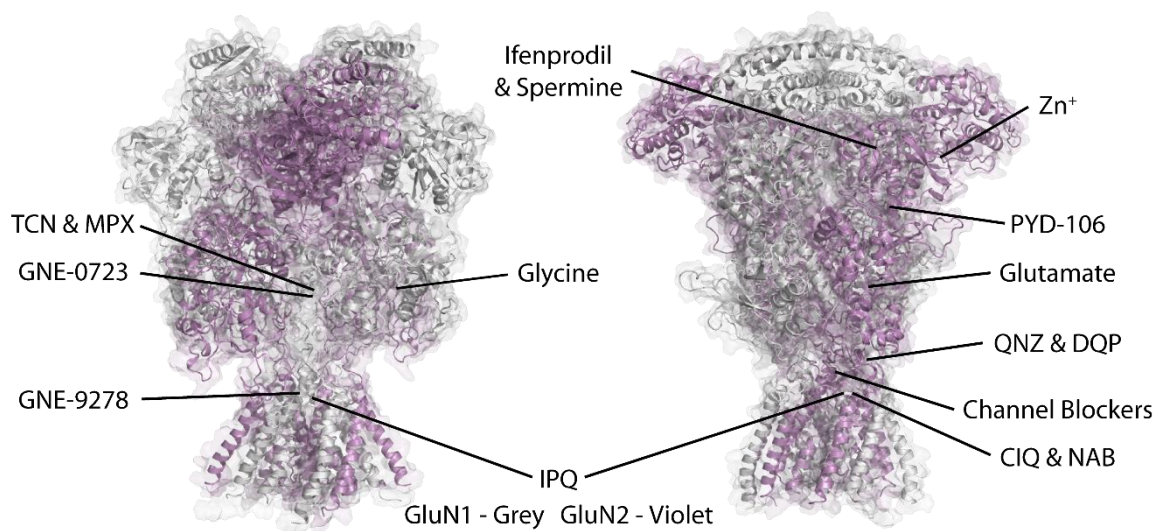
Figure 1.2. A map of known NMDAR ligands.

Images of a homology model of an NMDAR based on recent iGluR structures (Karakas and Furukawa 2014, Lee 2014, Yelshanskaya 2016). Highlighted are the approximate, binding sites of the many compounds discussed in this chapter. The *left* image has ligands that primarily bind to the GluN1 subunit and the *right* image has ligands that primarily bind to the GluN2 subunit.

Regulation of NMDA receptor function by allosteric ligands of the ATD
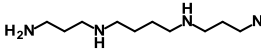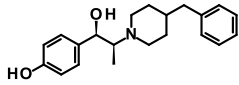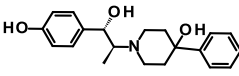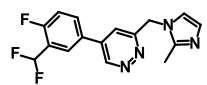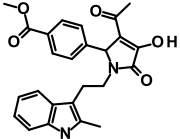
Protons

Extracellular protons completely inhibit NMDAR function with an IC_{50} of 50 nM and suggest a single isotherm, which corresponds to a pH of about 7.3 (Table 1.2) (Giffard 1990, Traynelis and Cull-Candy 1990, Vyklicky 1990, Traynelis and Cull-Candy 1991). This IC_{50} inhibition by protons aligns with the physiological pH of cerebrospinal fluid, also about 7.3, leading to tonic inhibition in normal conditions. This means that NMDARs are poised to respond to changes in extracellular pH that can occur under physiological conditions, for instance due to vesicular release or due to proton or bicarbonate transporters or channels (Chesler 2003).

Proton inhibition is voltage-independent and without effect on glutamate potency; however low pH produces small shifts in the glycine potency (Traynelis and Cull-Candy 1990, Traynelis and Cull-Candy 1991). The precise structural determinants underlying proton inhibition are unknown, although data suggests the agonist binding domain heterodimer interface is pH-sensitive. In addition, mutations to the linkers, pore forming elements, and the reentrant loop can all influence pH sensitivity (Low 2003, Gielen 2008). Interestingly, GluN1/GluN2A, GluN1/GluN2B, and GluN1/GluN2D have proton IC_{50}'s that match pH values ranging from 7.0 to 7.4, whereas GluN1/GluN2C appears insensitive (IC_{50} is 6.0) (Traynelis 1995, Low 2003). Altogether, this suggests that NMDAR gating is tightly coupled to proton inhibition of the receptor.

The actions of several ATD modulators appear to involve a change in the pKa of the proton sensor that leads to enhancement or reduction of tonic proton inhibition at physiological pH. For instance, Zn^{2+} and ifenprodil, two ATD inhibitory ligands enhance

Table 1.2. Summary of allosteric modulators with ATD associated binding sites.

Compound		Activity at GluN1/GluN2X (in μM)			
		2A	2B	2C	2D
Zn^{2+}		IC_{50}[a] 0.02	2.5	23	14
H^+		IC_{50}[b] 0.080	0.060	0.825	0.065
Spermine		EC_{50}[c] NE	127	NE	NE
Ifenprodil		IC_{50}[d] 39.5	0.114	29.1	75.9
CP-101,606		IC_{50}[e] NE	0.039	NE	NE
Ro 25-6981		IC_{50}[f] 52	0.009	-	-
EVT-101		IC_{50}[g] -	0.012	-	-
PYD-106		EC_{50}[h] NE	NE	16	NE

[a] (Traynelis 1998), [b] (Traynelis 1995, Low 2003), [c] (Mony 2011), [d](Hess 1996), [e](Mott 1998), [f](Fischer 1997), [g](Stroebel 2016), [h](Khatri 2014). All determinations were made using two-electrode voltage-clamp experiments with *Xenopus* oocytes.

- denotes not determined and NE denotes no effect at the highest concentrations evaluated.

proton sensitivity (Pahk and Williams 1997, Mott 1998, Traynelis 1998, Choi and Lipton 1999, Erreger and Traynelis 2008, Bhatt 2013). In contrast, the binding of extracellular polyamines reduce the receptors sensitivity to protons, which results in potentiation at physiological pH levels (Traynelis 1995, Kashiwagi 1996, Kashiwagi 1997).

Extracellular Zn^{2+}

Extracellular Zn^{2+} shows high affinity at the GluN2A ATD, with an IC_{50} value in the nanomolar range (Table 1.2) (Williams 1996, Chen 1997, Paoletti 1997, Traynelis 1998). Alternatively, the IC_{50} of Zn^{2+} inhibition at GluN1/GluN2B receptors is in the low micromolar range. Crystallographic and functional data suggests the Zn^{2+} binding site is located within the cleft formed by the two lobes of the ATD (Karakas 2009). Binding of Zn^{2+} stabilizes a conformation of the GluN2 ATD, which presumably is accompanied by structural changes at the GluN1/GluN2 ABD subunit interface that favor channel closure (Gielen 2008). Reports have suggested that Zn^{2+} binding enhances proton sensitivity of the receptor (Traynelis 1998, Choi and Lipton 1999, Low 2000). Interestingly, triheteromeric GluN1/GluN2A/GluN2B receptors retain a high affinity Zn^{2+} binding site, although there is reduced inhibition at maximally effective concentrations of Zn^{2+} (Hatton and Paoletti 2005, Hansen 2014, Stroebel 2014). Zn^{2+} can also block the channel in a voltage-dependent manner, but this action occurs at concentrations above 10 μM (Williams 1996).

The activity of Zn^{2+} also induces a rapid component of desensitization during agonist application (Chen 1997). This effect is similar to glycine-dependent desensitization, but is a result of positive intrasubunit allosteric interactions with

glutamate binding (Zheng 2001, Erreger and Traynelis 2005). If the concentration of Zn^{2+} is subsaturating, glutamate-binding enhances Zn^{2+} affinity and establishes a new Zn^{2+} ion equilibrium. Thus, the time-course for Zn^{2+}-dependent desensitization follows the time course for Zn^{2+} binding.

Ifenprodil and other GluN2B selective negative allosteric modulators (NAMs)

Ifenprodil and other mechanistically similar analogs have been widely used tool compounds since the discovery that they are GluN2B-selective (Williams 1993). Ifenprodil inhibits GluN1/GluN2B receptors with potency in the nM range and 200-400 fold selectivity over GluN1/GluN2A (Table 1.2). The inhibition of GluN1/GluN2A by high concentrations (>10 μM) of ifenprodil reflects low-affinity non-selective channel block, suggesting selectivity of this allosteric site is much higher (Williams 1993). The binding site for ifenprodil resides in the interface between the GluN1 and GluN2B ATD heterodimer (Masuko 1999, Karakas 2011). Recent evaluation of the GluN2A ATD heterodimer shows that contact residues are largely conserved for ifenprodil binding, however differences in the ATD conformation restricts ligand access (Romero-Hernandez 2016).

Allosteric modulation by ifenprodil induces an enhancement in agonist potency, making inhibition dependent on agonist concentration (Kew 1996). At saturating agonist concentrations, ifenprodil inhibition is incomplete with a residual response of 10-20% (Williams 1993, Kew 1996, Mott 1998, Masuko 1999). The glycine concentration is inversely correlated with the magnitude of inhibition (Williams 1993). In addition, the effects of ifenprodil are different depending on glutamate concentrations. Ifenprodil

modulation increases glutamate affinity, which reduces inhibition at sub-saturating agonist concentrations and at very low levels of glutamate, potentiation can be observed (Kew 1996). Interestingly, the interaction between ifenprodil and glutamate binding sites is an opposite allosteric action as compared to Zn^{2+} (Paoletti 1997, Zheng 2001). As mentioned before, there is an interaction between ifenprodil (and other similar modulators) and extracellular pH (Pahk and Williams 1997, Mott 1998). In a physiological context, this interaction may be an important determinant of ifenprodil modulation.

GluN2B-selective NAMs have been extensively studied by both in industry and academia, resulting in many diverse scaffolds and numerous analogs (Santangelo 2012, Hashimoto 2013, Lai 2014, Shipton and Paulsen 2014, Strong 2014). Compound have been developed with improved potency, improved selectivity (e.g. Ro 25-6981 and CP-101,606, Table 1.2) (Chenard 1995, Fischer 1997), and novel features, such as context dependent sensitivity to extracellular pH (Yuan 2015). Crystallographic data show that similarly acting GluN2B-selective NAMs ifenprodil-like ligands and EVT-101 (Table 1.2) have partially overlapping binding site (Stroebel 2016).

Endogenous Polyamines

Polyamines, such as spermine and spermidine, are GluN2B-selective potentiators of NMDAR function (Table 1.2). They interact with clusters of negatively charged residues in the lower R2 lobes of GluN1 and GluN2B ATDs (Mony 2011). Although the precise location of this binding site on the ATD remains to be identified, it has been shown using FRET that spermine binding opens the GluN2B ATD clamshell (Sirrieh

2015). Aminoglycosides analogs can also potentiate GluN2B-containg receptors by a similar mechanism of action (Masuko 1999). Furthermore, a model has been proposed where the positively charged spermine shields the negatively charged residues in the ATDs, thereby eliminating electrostatic repulsion between the two lower R2 lobes (Mony 2011). Consistent with this model, other cations can also potentiate GluN2B-containing NMDARs in manner similar to spermine; for example, extracellular Mg^{2+}, in addition to its pore-blocking capabilities, can enhance GluN1/GluN2B responses at millimolar concentrations (Paoletti 1995).

The PYD series of GluN2C-selective positive allosteric modulators (PAMs)

A series of pyrollidinones (PYD compounds) are the only currently reported purely GluN2C-selective PAMs (Khatri 2014, Zimmerman 2014). This series has stereo-selective actions (Zimmerman 2014), and displays a high degree of selectivity that discriminates between GluN2C- and GluN2D-containing NMDARs. PYD analogs are capable of potentiating saturated GluN1/GluN2C receptor responses over 200% of control, with potencies in the low μM range (Table 1.2) (Khatri 2014, Zimmerman 2014). Interestingly, PYD-106 is selective for the diheteromeric GluN1/GluN2C receptors and does not potentiate triheteromeric GluN1/GluN2A/2C or GluN1/GluN2B/2C receptors (Khatri 2014, Kaiser 2017). PYD-106 has a weak effect on glutamate potency, and modestly prolongs the glutamate deactivation time-course (Khatri 2014). The structural determinants of action of PYD-106 reside at the interface of the GluN2C ATD and the upper lobe of the GluN2C ABD (Khatri 2014). Structural modelling of the GluN1/GluN2C receptor, based on recent GluN1/GluN2B crystal structures (Karakas and
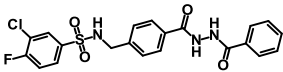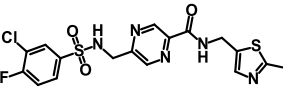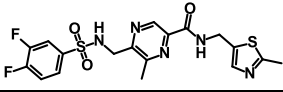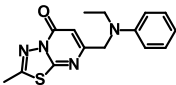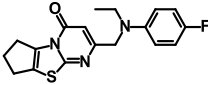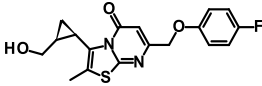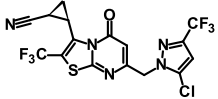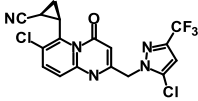
Furukawa 2014), suggests that residues contributing to PYD-106 actions form a large pocket that rationalizes for the structure activity relationship of the series (Khatri 2014, Kaiser 2017). Additionally, this pocket could be transferred to other GluN2 subunits strengthening the idea that this pocket represents a *bone fide* novel modulatory site of GluN1/GluN2C NMDARs. It remains an open question if a similar site exists on other NMDARs (Kaiser 2017).

Regulation of NMDA receptor function by allosteric ligands of the agonist binding domain

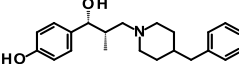The TCN and MPX series of GluN2A-selective NAMs

The first series of GluN2A-selective NAMs described in the literature (Bettini 2010) highlighted analogs TCN-201 and TCN-213. These compounds are potent (i.e. K_D for TCN-201 was 27-70 nM, see Table 1.3) and highly selective for GluN2A over other GluN2 subunits (Edman 2012, Hansen 2012, Yi 2016). Surprisingly, TCN-201 inhibition of GluN2A is diminished in high concentrations of glycine but not glutamate; a paradoxical result given the subunit that defines TCN selectivity (GluN2A) binds glutamate (Bettini 2010, Edman 2012, Hansen 2012). The apparent interaction between TCN-201 and glycine can be described by an allosteric model of inhibition rather than direct competition (Edman 2012, Hansen 2012). Crystallographic data shows that TCN-201 binds at the GluN1 and GluN2A ABD heterodimer interface and has interactions with residues that are 16 Å from the GluN1 glycine binding site (Hansen 2012, Hackos 2016, Yi 2016). These structures show that NAM binding stabilizes the open conformation of the GluN1 ABD, facilitating glycine unbinding (Yi 2016). Key residues

Table 1.3. Summary of allosteric modulators with ABD associated binding sites.

Compound			Activity at GluN1/GluN2X (in μM)			
			2A	2B	2C	2D
TCN-201		K_B^a	0.045	NE	NE	NE
		K_B^b	0.070	NE	NE	NE
		K_B^c	0.027	NE	NE	NE
MPX-004		IC_{50}^d	0.079	NE	-	NE
		IC_{50}^e	0.198	NE	NE	NE
MPX-007		IC_{50}^d	0.027	NE	-	NE
		IC_{50}^e	0.143	ND	NE	NE
GNE-3419		EC_{50}^f	2.03	NR	NR	NR
GNE-8324		EC_{50}^f	2.43	NR	NR	NR
GNE-6901		EC_{50}^f	0.33	NR	NR	NR
GNE-0723		EC_{50}^g	0.021	ND	7.4	6.2
GNE-5729		EC_{50}^h	0.037	ND	4.7	9.5

[a]determined using Schild analysis (Hansen 2012), [b]determined using Schild analysis (Edman 2012), [c]determined using Schild analysis using TEVC (Yi 2016), [d]determined using Ca^{2+} imaging (Volkmann 2016), [e]determined using TEVC (Volkmann 2016), [f]determined using Ca^{2+} imaging (Hackos 2016), [g]determined using Ca^{2+} imaging (Volgraf 2016), [h]determined using Ca^{2+} imaging (Villemure 2017)

- denotes not determined, NE denotes no effect at the highest concentrations evaluated, and ND indicates that the compound displayed some activity, but the affinity or potency could not be determined. NR denotes some activity, but that the numerical affinity value was not reported.

form a molecular switch that distinguishes a low- and high-affinity NAM binding states, establish selectivity, and result in allosteric inhibition (Yi 2016). MPX-004 and MPX-007 are two GluN2A-selective NAMs with improved potency (79 and 27 nM, respectively, Table 1.3), improved solubility (Volkmann 2016), and improved saturating inhibition over TCN-201 (Volkmann 2016, Yi 2016). Additionally, the MPX-004 and MPX-007 are less dependent on glycine, than TCN analogs, which enhance their pharmacological utility.

The GNE series of ABD interface positive allosteric modulators

In 2016, the first GluN2A-selective positive allosteric modulator series (PAMs) possessing more than 10-fold selectivity for GluN2A over other GluN2 subunits was published (Table 1.3) (Hackos 2016). Following this initial report, a considerable effort went into developing this series, and several studies have probed the structure-activity relationship of this series, typified by GNE-0723, GNE-5729 and GNE-6901 (Hackos 2016, Volgraf 2016, Villemure 2017). Data suggest this series binds to the GluN1 and GluN2A ABD heterodimer interface and partially overlaps with the binding sites of TCN and MPX, potentially this site that can be tuned between allosteric inhibition and potentiation. The GluN2A-seletive PAMs interact with the same residue (Val783) in GluN2A that controls selectivity of GluN2A NAMs, exemplified by TCN-201 (Hackos 2016, Yi 2016). Introduction of this residue into GluN2B confers sensitivity to both GluN2A-selective PAMs and NAMs (Hansen 2012, Hackos 2016). GluN1/GluN2A ABD heterodimer in complex with the GluN2A-selective modulators reveal distinct binding modes for both positive and negative allosteric modulators. Interestingly, some analogs

have PAM activity at AMPARs (i.e. GNE-3419), with a similar potency as compared to NMDARs (Hackos 2016).

The potentiation produced by these GluN2A-selective PAMs is inversely correlated with the concentration of agonist used to stimulate responses. Less potentiation is observed when saturating concentrations of agonist are used. The presented data for these series does not clearly delineate this relationship, which precludes a mechanistic interpretation. For example, GNE-0723 potentiation can range from 2-fold to 5-fold based on agonist concentration but it is unclear if the EC_{50} of GNE-0723 also changes in different conditions (Hackos 2016, Volgraf 2016). A complex relationship appears to exist between GluN2A-selective modulator structure, efficacy, and the degree of prolongation of glutamate deactivation rate (Volgraf 2016). A set of experiments using analogs, with different abilities to potentiation and enhance agonist potency, have different actions on NMDAR responses in hippocampal brain slice recordings (Hackos 2016).

The UBP series of mixed mode compounds

Development of early competitive antagonist led to the discovery that some analogs had modest selectivity for GluN1/GluN2C and GluN1/GluN2D receptors, including PPDA and UBP141 (Buller and Monaghan 1997, Feng 2004, Feng 2005, Morley 2005). Of these analogs, UBP141 achieved the greatest selectivity being seven-fold more potent at GluN1/GluN2D over GluN1/GluN2B, but has intermediate potencies at GluN1/GluN2A and GluN1/GluN2C decreasing its actual selectivity (Table 1.4). This degree of selectivity does not allow for clear dissection of the contribution of GluN2D-

Table 1.4. Brief summary of GluN1 and GluN2 antagonists.

Compound			2A	2B	2C	2D
			Activity at GluN1/GluN2X (in µM)
APV		K_i^a GluN2	0.28	0.46	1.6	3.7
(R)-CPP		K_i^a GluN2	0.041	0.27	0.63	1.99
(R)-α-AA		K_i^a GluN2	6.5	25	44	110
selfotel		K_i^a GluN2	0.15	0.58	0.58	1.1
7-CKA		K_B^b GluN1	0.6	0.2	-	-
5,7-DCKA		K_i^c GluN1	0.03	0.05	0.17	0.09
NVP-AAM077		K_B^d GluN2	0.015	0.078	-	-
ST3		K_B^e GluN2	0.052	0.782	0.107	0.400
PBPD		K_i^f GluN2	15.8	5.0	9.0	4.3
PPDA		K_i^g GluN2	0.55	0.31	0.096	0.125
UBP141		K_i^h GluN2	14.2	19.3	4.2	2.8

[a](Feng 2005), [b]K_B was calculated from inhibition of glycine activated responses in mouse L(tk-) cells using the Cheng-Prusoff method (Priestley 1995), [c](Hess 1998), [d]determined using Schild analysis (Frizelle 2006), [e]determined using Schild analysis (Lind 2017), [f]determined using the Cheng-Prusoff method (Buller and Monaghan 1997), [g]determined

using the Cheng-Prusoff method (Feng 2004), [h]determined using the Cheng-Prusoff method (Morley 2005). - denotes not determined.
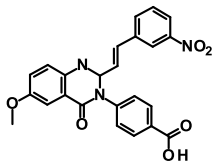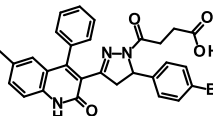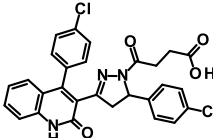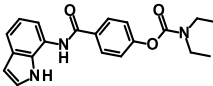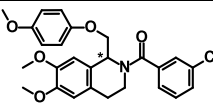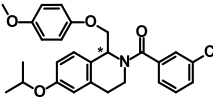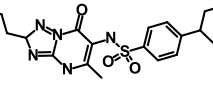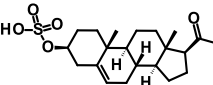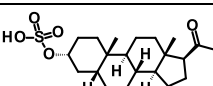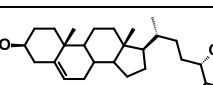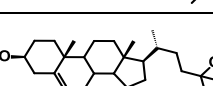
containing receptors in a mixed population of receptors. However more recently, compounds with some chemical similarities appear to be allosteric modulators, which suggest renewed scrutiny of the mechanism of action may be required (Costa 2010). Further development of the chemical space around the UBP-141 scaffold led to the discovery of a series of mixed-action modulators such as UBP-710, UBP-512 and UBP-551 (Costa 2010). UBP-710 displays complex effects at high concentration (100 μM or greater), which include potentiation of GluN1/GluN2A and GluN1/GluN2B, but inhibition of GluN1/GluN2C and GluN1/GluN2D (Costa 2010). UBP-551 may be selective for GluN2D-containing NMDARs, showing a biphasic concentration-effect relationship, with maximal potentiation of GluN1/GluN2D observed at 30 μM, which inhibits other NMDARs (Costa 2010). Data suggest these mixed-action compounds are allosteric modulators but their precise site of action is unknown; chimeric receptor studies suggest the action of these modulators is influenced by the GluN2 ABD S2 segment (Costa 2010). The utility of these complex mixed-action UBP compounds is limited by poor physiochemical properties, low potency, and modest subunit selectivity.

Regulation of NMDA receptor function by allosteric ligands of the TMD

Glutamate-dependent GluN2C- and GluN2D-selective negative allosteric modulators

The first potent and highly selective series with GluN2C- and GluN2D-selectivity was described in 2010 containing a quinazolin-4-one (QNZ) core (Table 1.5) (Mosley 2010). QNZ-46 is a negative allosteric modulator of NMDARs showing ~50-fold selectivity for GluN2C- or GluN2D-containing NMDARs with potency in the low micromolar range (Mosley 2010, Hansen and Traynelis 2011). QNZ-46 has minimal

Table 1.5. Summary of allosteric modulators with TMD associated binding sites.

Compound			Activity at GluN1/GluN2X (in μM)			
			2A	2B	2C	2D
QNZ-46		IC_{50}^{a}	229	ND	6	3
		IC_{50}^{b}	182	193	7.1	3.9
DQP-1105		IC_{50}^{c}	ND	113	7.0	2.7
DQP-26		IC_{50}^{d}	21	22	0.77	0.44
NAB-14		IC_{50}^{e}	5200	3000	3.7	2.2
CIQ, (+)-CIQ*		EC_{50}^{f}	NE	NE	2.7	2.8
		EC_{50}^{g}	NE	NE	$9.0^{\ddagger}$	$8.0^{\ddagger}$
IPQ-2, (+)-IPQ-2*, (-)-IPQ-2*		EC_{50}^{h}	$7.4^{\dagger}$	5.2	2.0	3.0
		EC_{50}^{i}	NE	NE	0.71	1.0
		EC_{50}^{i}	-	3.0	3.1	3.8
GNE-9278		EC_{50}^{j}	3.2	15.7	6.6	6.7
PS		EC_{50}^{k}	34	63	83	78
		IC_{50}^{k}	1301	553	114	62
PA-S		IC_{50}^{l}	62 (-)	38 (-)	12 (-)	14 (-)
24-(S)		EC_{50}^{m}	>30 +	>30 +	>30 +	>30 +
SGE-201		EC_{50}^{m}	>30 +	>30 +	>10 +	>30 +

[a](Mosley 2010), [b](Hansen and Traynelis 2011), [c](Acker 2011), [d] (Acker 2013), [e](Swanger 2017), [f](Mullasseril 2010), [g](Santangelo Freel 2013, Santangelo Freel 2014), [h](Strong 2017), [i]unpublished data, [j](Wang 2017), [k]determined using patch-clamp

electrophysiology recordings from HEK293 cells (Horak 2006), [l](Malayev 2002), [m]activity profile displayed in (Paul 2013) and rough potency taken from oocyte TEVC data presented in a conference poster. All determinations were made using two-electrode voltage-clamp experiments with *Xenopus* oocytes.

[*] The chiral carbon of (+)-CIQ and the enantiomers of IPQ-2 are denoted by the asterisk in the chemical structure.

[‡] The apparent lower potency for (+)-CIQ compared to the racemic mixture is likely due to better estimation of maximum potentiation, since the active enantiomer has increased abundance in solution at concentrations close to the solubility limit (i.e the pure enantiomers can be evaluated at higher concentrations compared racemic CIQ).

- denotes not determined, NE denotes no effect at the highest concentrations evaluated, and ND indicates that the compound displayed some activity, but the affinity or potency could not be determined.

[†] The EC_{50} was determined at a sub-saturating agonist concentration (0.3 glutamate, 0.07 glycine)

actions on AMPA and kainate receptors, even though it shares a scaffold with a series of AMPA-selective NAMs, including CP-465,022. Interestingly, the inhibition by QNZ-46 is dependent on glutamate, but not glycine; glutamate binding results in an increase in QNZ-46 potency (Hansen and Traynelis 2011). A reciprocal effect of cooperativity between QNZ-46 glutamate potency occurs, which can be observed as a prolongation of the glutamate deactivation time course by QNZ-46. Consistent with the idea, it appears as if QNZ-46 must first dissociate before glutamate can unbind (Hansen and Traynelis 2011). Chimeric and mutagenesis studies suggest that the structural determinants of QNZ-46 action reside in the membrane-proximal surface of the GluN2D ABD (Hansen and Traynelis 2011). A recent GluA2 AMPA receptor crystal structure shows CP-465,022 bound to the upper portion of the TMD. Given the similarity in structure of these two molecules, it is possible that the agonist-dependent high affinity binding site of QNZ-46 involves both of these regions (Hansen and Traynelis 2011, Yelshanskaya 2016).

Another series of negative allosteric modulators with strong selectivity for GluN2C/GluN2D-containing NMDARs was published around the same time. A series of compounds with a dihydroquinolone-pyrazoline (DQP) core has similar properties to QNZ-46 (Acker 2011). DQP-1105, a representative member of this class, is approximately 50-fold selectivity for GluN2C/D-containing NMDARs with single digit IC_{50} values (Table 1.5) (Acker 2011). Like QNZ-46, inhibition by DQP-1105 appears to be dependent on glutamate binding (Acker 2011), suggesting a shared mechanism of action. Additionally, DQP-1105 and QNZ-46 appear to have overlapping binding sites (Acker 2011). The elucidation of the DQP structure-activity relationship identified enantiomers of new analogues with nanomolar IC_{50} values, making this series more

potent and selective than QNZ-46 (Acker 2013). Different compounds of this series display various degrees of glutamate-dependency (unpublished observations). If so, an SAR may be assembled around this property if sufficient compounds could be assayed.

A new, highly selective class of negative allosteric modulators has recently been described (Swanger 2017). This series is built around an N-aryl benzamide core. NAB-14 is a prototypical member of this class, with an IC_{50} value of 3.7 and 2.2 μM at GluN1/GluN2C and GluN1/GluN2D receptors (Table 1.5). This series shows 200-fold selectivity for GluN2C/GluN2D over other GluN2 subunits, has minimal off-target actions, and is active at native synaptic NMDARs. NAB-14's structural determinants are distinct from QNZ-46 or DQP-1105, and appear to overlap with those of the positive allosteric modulator CIQ (see below). NAB-14 binding, like QNZ-46 and DQP-1105, has glutamate-dependency, but to a lesser degree, and lacks glycine-dependency.

The CIQ series of GluN2C- and GluN2D-selective positive allosteric modulators

CIQ is a selective GluN2C/GluN2D-selective positive allosteric modulator of NMDARs (Table 1.5) (Mullasseril 2010). The CIQ series has been extensively explored; a detailed structure-activity relationship has been developed showing stereo-selective actions with robust selectivity for GluN2C/D-containing receptors and micromolar to submicromolar EC_{50} values (Santangelo Freel 2013, Santangelo Freel 2014). CIQ and related analogues can potentiate the responses of triheteromeric receptors with only one copy of either GluN2C or GluN2D, but with a reduced maximal extent of potentiation (Mullasseril 2010). Only the (+)-enantiomer of CIQ is active, making it a better tool compound than racemic CIQ due to enhanced pharmacological properties with fewer off-

target actions (Perszyk 2016). Interestingly, whereas CIQ does not alter the GluN1/GluN2D deactivation time course, it prolongs the deactivation of GluN1/GluN2C after glutamate removal (Mullasseril 2010). The structural determinants of CIQ potentiation of GluN1/GluN2D reside within the M1 transmembrane helix and a short pre-M1 helix in the GluN2D subunit (Mullasseril 2010, Ogden and Traynelis 2013). However, it is unknown whether these regions directly contribute to the CIQ binding site. Racemic CIQ and the active enantiomer (+)-CIQ have been used as tool compounds in multiple studies exploring the role of GluN2D in synaptic transmission (Yamamoto 2013, Hildebrand 2014, Ogden 2014, Suryavanshi 2014, Zhang 2014, Swanger 2015, Perszyk 2016).

The IPQ series of non-selective positive allosteric modulators

Development of the CIQ scaffold led to the discovery of a series of modification that converts the GluN1/GluN2C- and GluN1/GluN2D-selective into non-selective positive allosteric modulators (Table 1.5) (Strong 2017). Several IPQ-2 analogs have enantiomers with differential actions on NMDARs. One enantiomer typically has CIQ-like actions whereas the other can modulate all NMDARs. The non-selective modulators can potentiate GluN1/GluN2B, GluN1/GluN2C, and GluN1/GluN2D receptors activated by saturating concentrations of agonist but can also potentiate GluN1/GluN2A at sub-saturating agonist concentrations. Both enantiomers are capable of inducing an allosteric enhancement of agonist potency to varying degree based on their subunit selectivity. Interestingly, the enantiomers of IPQ-2 have different determinants of action. The

structural determinants of the CIQ-like enantiomer track to the GluN2 subunit and the non-selective enantiomer track to the GluN1 subunit.

GNE-9278, a non-selective positive allosteric modulators

A report was published in 2017, highlighting a novel non-selective and highly efficacious PAM, GNE-9278 (Wang 2017). Although the scaffold of GNE-9278 is similar to the GluN2A-selective GNE PAM the activity and mechanism of action differ. GNE-9278 robustly potentiates all NMDARs and can enhance agonist potency; however the enhancement of agonist potency has not been shown for all GluN2 subunits. GNE-9278 is selective for NMDARs over AMPARs, but displays little selectivity for GluN2 subunits (Table 1.5). Interestingly, this compound appears to have divergent structural determinants of action as compared to the GluN2A-selective PAMs. Mutagenesis studies indicate modulation dependence on the TMD, including several residues on the M1 and M3 helices of GluN1. Interestingly, GNE-9278 actions are dependent on glutamate binding.

Neurosteroids

Several neurosteroid analogs have been shown to modulate NMDAR activity. The actions of these lipophilic molecules are complex. For instance, pregnenolone sulfate (PS) has dual actions on NMDAR responses, having both inhibitory and potentiating activity over a wide range of potencies (Table 1.5) (Horak 2006). The potentiating actions of PS are most predominant when applied before receptor activation, whereas inhibitory actions arise when applied continuously (Horak 2006). The dual actions of PS

lead to divergent actions depending on the GluN2 subunit; when applied during steady state NMDAR responses, GluN1/GluN2A and GluN1/GluN2B are potentiated and GluN1/GluN2C and GluN1/GluN2D are inhibited.

Other neurosteroid analogs are pan-inhibitors, e.g. pregnanolone sulfate (PA-S), and others, and pan-potentiators, e.g. 24(S)-hydroxycholesterol (24(S)-HC), SGE-201 and other SGE-analogs (Malayev 2002, Borovska 2012, Paul 2013, Vyklicky 2015). Some of these neurosteroid (PA-S and others) analogs have been shown to have agonist dependency (Petrovic 2005, Borovska 2012, Vyklicky 2015). This concept is complicated since some neurosteroids have been shown to have different actions on NMDARs given divergent actions based on the timing of modulator application (i.e. PS actions above). Additionally, evidence suggests these steroid derivatives may partition into the membrane in route to their active site, which alters the concentration-response relationship of their actions (Borovska 2012, Vyklicky 2015). A recent study reported that cholesterol modulates NMDAR function and its removal causes inhibited receptor activity (Korinek 2015), which suggest that the membrane environment influences NMDA receptor activity and may be an important determinate of neurosteroid analog action. A clear binding site has not been resolved, so it is possible that neurosteroid derivatives interact directly on the receptor or through influencing the lipid membrane environment around the receptor. A subset of neurosteroid inhibitors also have voltage dependent actions, suggesting that they may inhibit NMDARs through blocking the channel (Vyklicky 2015). These findings further complicate the interpretation of neurosteroid derivative data and require additional study to clearly delineate a clear mechanism of action of these compounds.

Competitive antagonists of NMDA receptor

Competitive antagonists have historically been useful in identifying NMDARs (Biscoe 1977, Davies and Watkins 1979, McLennan and Lodge 1979, Evans 1982). Additionally, they have utility in biological tissues when there is need to isolate other iGluR responses or to confirm NMDAR-dependent activity. Most NMDAR competitive antagonists have widely ranging affinities (nM to μM, Table 1.4) but have a limited capacity for subunit selectivity due to the fact that the agonist binding sites are highly conserved. The maximum selectivity identified for any competitive antagonist is roughly five- to ten-fold (Feng 2005, Frizelle 2006). With this degree of subunit selectivity, no concentration of antagonist can reliably differentiate NMDAR subtypes.

Some confusion concerning one competitive antagonist, NVP-AAM007, arose from the initial report that derived simple IC_{50} values using a fixed agonist concentration. The data were interpreted to suggest that NVP-AAM007 had >100-fold selectivity for Glu1/GluN2A over GluN1/GluN2B (Auberson 2002). A more rigorous study was performed using Schild analysis, which showed NVP-AAM007 only possesses five-fold selectivity (Frizelle 2006). Despite this lack of selectivity, many labs have still use NVP-AAM007 (also known as PEAQX) as a way to argue for subunit specific roles, some even from the first few weeks of 2018 (Aroniadou-Anderjaska 2018, Eyo 2018). This highlights the importance of thorough characterization and a clear understanding of the mechanism of action of pharmacological reagents being used in any study.
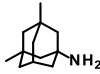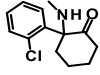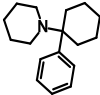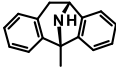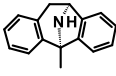
Until recently pharmacological limitations given the homology surrounding the agonist binding site have limited the subunit selectivity of competitive antagonists.

However, recently, a series of competitive antagonists with more robust selectivity over certain NMDAR subunits have been reported (Lind 2017). The lead compound, ST3, is 15 fold more selective for GluN1/GluN2A over GluN2B. A cavity near the agonist binding pocket was occupied by this series to achieve high affinity and selectivity. This level of selectivity was capable of discriminating between GluN2A- and GluN2B-containing NMDARs in rapid solution exchange experiments using heterologous expression system. Caution should still be had when attempting to these new competitive antagonists to identify NMDAR subtype in native tissue as ST3 has intermediate affinity for the GluN2C and GluN2D diheteromeric receptors (Lind 2017). However, lower affinity antagonists can be utilized in determining biologically relevant agonist concentrations in certain scenarios (Diamond 2001, Harris and Pettit 2008).

Channel blockers of NMDA receptors

Several series of NMDAR channel blockers have been discovered (Table 1.6) (Anis 1983, Wong 1986). This class includes the only NMDAR-targeted drugs approved for clinical use (Strong 2014). Typically, channel blockers, or un-competitive antagonists, are thought to enter the channel pore from the extracellular side in an activity dependent manner. It is thought that there are different classes of channel blockers, including "trapping" and "foot-in-door" blockers (Sobolevsky 1999, Sobolevsky and Yelshansky 2000, Bolshakov 2003, Johnson and Kotermanski 2006). A "trapping" blocker is one that is retained in the pore upon channel gate closure and agonist unbinding, remaining there until subsequent agonist exposure and channel reopening. A "foot-in-door" blocker is one that prevents gate closure and must dissociate before the receptor can deactivate, since

Table 1.6. Summary of open channel blockers of NMDA receptors.

Compound			Activity at GluN1/GluN2X (in μM)			
			2A	2B	2C	2D
Memantine, +1mM Mg^{2+}		$IC_{50}{}^{a}$	0.80, 13	0.57, 10	0.52, 1.6	0.54, 1.8
Ketamine, +1mM Mg^{2+}		$IC_{50}{}^{a}$	0.33, 5.4	0.31, 5.08	0.51, 1.2	0.83, 2.9
PCP		$IC_{50}{}^{b}$	0.82	0.16	0.16	0.22
Mg^{2+}		$IC_{50}{}^{c}$	2.4	2.1	14.2	10.2
(+)-MK-801		$IC_{50}{}^{b}$	0.015	0.009	0.024	0.038
(-)-MK-801		$IC_{50}{}^{b}$	0.35	0.32	0.038	0.17

[a]determined using patch-clamped HEK293 cells (Kotermanski and Johnson 2009), [b]determined using TEVC (Dravid 2007), [c]determined using TEVC holding the oocytes at -100 mV (Kuner and Schoepfer 1996)

the channel gate must close before the ABDs can reopen and allow for agonist unbinding. MK-801 is a trapping blocker (Huettner and Bean 1988) and has been used to study extrasynaptic receptors by initially driving activity dependent blockade of synaptic NMDARs in order to study the extrasynaptic (Hardingham 2002, Tovar and Westbrook 2002, Harris and Pettit 2007, Bordji 2010, Liu 2013). Recently study of several channel blockers suggests that these compounds (including memantine, ketamine and MK-801) may partition into the membrane before accessing the NMDAR pore (Glasgow 2016, Wilcox 2017). These findings have not yet been published, but if fully validated this property would necessitate a reevaluation of experiments utilizing these channel blockers to block synaptic stimulated receptors.

Some of these compounds have clinical utility, including the low affinity channel blocker memantine (Alzheimer's disease) and ketamine (dissociative anesthetic) (Johnson and Kotermanski 2006, Iacobucci 2017). These compounds may be tolerated due to mimicry of Mg^{2+}. In neurodegenerative diseases cellular metabolism can be compromised leading to a failure to maintain the resting membrane potential and aberrant NMDAR signaling due to the loss of Mg^{2+} block (Surmeier and Schumacker 2013, Zhang 2016). Memantine is capable of blocking this aberrant activity and potentially restoring normal NMDAR function. The channel pore is highly conserved leading to low subunit selectivity. However, it is known that key residues in the permeation pathway alter the affinity of Mg^{2+}, creating a modest difference in affinity at GluN1/GluN2A and GluN1/GluN2B versus GluN1/GluN2C and GluN1/GluN2D (Siegler Retchless 2012). Interestingly, this difference in Mg^{2+} affinity results in a modest enhancement of subunit selectivity in physiological conditions of memantine and ketamine. Several channel

blockers show an approximate 10-fold selectivity for GluN1/GluN2C and GluN1/GluN2D over GluN1/GluN2A and GluN1/GluN2B (Kotermanski and Johnson 2009) due to this difference in Mg^{2+} affinity. Essentially, memantine and ketamine compete with Mg^{2+} for access to their binding sites. Mg^{2+} has lower potency at GluN1/GluN2C and GluN1/GluN2D, or dissociates more rapidly (Clarke and Johnson 2006), which allows memantine and ketamine to gain access to their binding sites more readily at these receptors than GluN1/GluN2A and GluN1/GluN2B and result in different IC_{50}s. This modest subunit selectivity may contribute to their clinical tolerability.

Regulation of NMDA receptor function by the carboxyl-terminal domain

Comparatively less is known about the precise role of the CTD than other domains, summarized in (Kohr and Seeburg 1996, Carroll and Zukin 2002, Maki 2012). It is known that there are many differences in the CTDs between the GluN1 and the 4 GluN2 subunits in terms of their amino acid sequence identities, intercellular binding partners and post-translational modulatory sites; including calmodulin, CaMKII, phosphorylation sites, PDZ binding domains, etc (Kornau 1995, Niethammer 1996, Gardoni 1998, Strack and Colbran 1998, Leonard 1999, Leonard 2002, Ataman 2007). These play a large and important role in controlling expression, cellular localization and internalization which are crucial components in achieving proper NMDAR signaling. Being that the CTD is an intracellular domain, chances for pharmacological manipulation with exogenous compounds is more restricted. Little is known about how the CTD specifically modulates NMDARs function, but some studies have shown that the CTD influences channel properties (Rossi 2002, Maki 2012, Punnakkal 2012).

Summary of modulation mechanisms

Currently, a large number of non-agonist NMDAR ligands are known. They have diverse actions on receptor function, including competitive antagonists, channel-blockers, positive allosteric modulators and negative allosteric modulators. Within these general classes of ligand, there are mechanistic differences that alter their actions on receptor function and may underlie their difference in clinical utility. For instance, the differences of the mechanism of action of the channel blockers explain why memantine is tolerated clinically, whereas MK-801 produces psychosis and ketamine produces anesthesia (Javitt and Zukin 1991, Johnson and Kotermanski 2006). The more recent wave of subunit selective allosteric modulators has yet to be tested clinically and may contain successful drugs. The differences in the mechanism of action of all ligands need to be dutifully characterized in order to understand their therapeutic potential.

Models of NMDA receptor behavior

Throughout the years, biological phenomena have been modeled to provide greater insight into the workings of these processes, in order to simplify and define parameters that control the inputs and outputs process. One can observe the voltage of a cell, the responsiveness of a contracting muscle or current passed through ion channels all by stimulating fibers of axons that enervate these other cells but a model of these processes is required to explain how the stimulation input leads to the observed biological output. Using robustly characterizing measureable parameters of a biological process (voltage, contraction, scintillation, current, etc.), models allow one to define previously unmeasurable properties (affinity, efficacy, conduction, permeability, etc.). In terms of

receptors, models have been used to represent how various stimuli (ligands, voltage, temperature, etc.) affect the activity of a receptor (current flow, intercellular signaling, transporter activity, etc.). Usually this is done by constructing a relationship between different hypothetical receptor states that are controlled by instinct rates, condition dependent rates, or ligand-dependent rates (controlled by ligand-receptor affinity). If utilized correctly, models have predictive capabilities to determine responses not yet tested experimentally and when data does not conform to currently held models, the discrepancy may be suggestive that an alternative model may be more accurate.

One example of a receptor model, that has been widely useful, describes the behavior of receptor antagonists. Inhibition produced by an antagonist was found to conform to a model based on the interaction of a receptor and an antagonist (Gaddum 1937, Arunlakshana and Schild 1959). Based on the law of mass action, the model proposed an antagonist's interaction with a receptor blocks an agonist from associating. This model was powerful since the parameters defining the interaction of the receptor and antagonist (affinity, K_b) was independent of the agonist used to stimulate a response. Additionally, this affinity was a universal property, which meant antagonists could be used to identify receptors in various cell types. Also, this model can be used to calculate the inhibition status of a receptor given different concentrations of agonists and antagonists, allowing for confidence when probing receptor activity in biological experimentation.

Study of agonists actions on receptors lead to the appreciation that affinity alone was not sufficient to characterize the activity of a receptor (Del Castillo and Katz 1957). Their observations lead them to propose a model with two steps, the first step

representing binding (defined by affinity) and the second step representing activation (now defined as efficacy). This was necessary as partial agonist actions cannot be represented solely on their binding affinity. This model allowed for more representative characterization of the concentration response of full agonists, partial agonists, and even antagonists, as they could be represented as having an efficacy of zero.

Another type of ligand-protein interaction was first identified in the study of enzymes. The end-products of an enzymatic pathways were found to bind to the earlier enzymes in the pathway, in a way that does not interact with the active site but inhibited enzymatic activity; this interaction was referred to as allosteric (meaning allo- "other", -steric "body/solid", e.i. not the enzymatic binding site) inhibition (Monod and Jacob 1961, Monod 1963). These sites were thought to be evolutionarily preserved allowing for a convenient form of feed-back control of the enzymatic pathway; where the end-product of a pathway could shut down the process of its production, once it reached a desired level. This concept was expanded to explain the behaviors of any symmetrical oligomeric proteins; oligomer conformational changes occur naturally, influencing the other oligomers due to cooperativity, and ligands stabilize certain conformational states of the oligomers (Monod 1965). This model, later known as the MWC (Monod, Wyman and Changeux) model, was also suggested to occur in cell surface receptors, including pentameric ligand gated ion channels (Karlin 1967, Thron 1973). The two-state model, which is essentially the same as the MWC model, was adapted for GPCRs (Lüllmann 1969, Clark and Mitchelson 1976, Leff 1995). The two-state model has a strict requirement that the functional effect is coupled to changes in apparent affinity of the ligands. Later, the ternary complex model was developed, created to accommodate

agonist and G-protein binding to the same receptor (De Lean 1980, Stockton 1983, Ehlert 1988). Importantly in these models, these effects are reciprocal, the enhancement or diminishment of agonist potency also impacts modulator potency. A further expansion of this concept, resulted in combining these allosteric principles into the allosteric two-state model capable of recapitulating many behaviors of the two-state or the ternary complex models (Hall 2000). This model can account for perplexing cases, compared to the ternary complex model, for instance where allosteric inhibition of receptor activity is coupled with increases in agonist potency (Hall 2000).

In terms of NMDARs, multiple models have been created that accurately represent the activation of different NMDAR subtypes. Models can be adapted that can predict the activities of the orthosteric and allosteric ligands discussed above. These models will facilitate a clear understanding of the abilities and limitations of the use of these ligands in biological contexts and drive forward the development of useful therapeutic compounds. An overview of published models, which approximate NMDAR agonist activation, is presented below.

Macroscopic models of NMDA receptors

After the cloning of the NMDAR subunits, specific receptor models were used to rationalize receptor responses of different NMDAR subtypes. The first proposed model was based on the most basic operations of NMDARs (Lester and Jahr 1992). This model contains two binding steps, an agonist-bound shut state, a desensitized state, and an open state (see Scheme 1.1).

$$R \underset{b_-}{\overset{2b_+}{\rightleftharpoons}} RA \underset{2b_-}{\overset{b_+}{\rightleftharpoons}} RA_2 \underset{k_-}{\overset{k_+}{\rightleftharpoons}} O_1$$

with D_1 connected to RA_2 by rates d_+ and d_-.

Scheme 1.1:
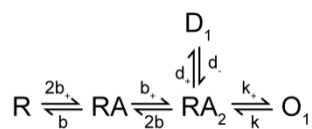
This model can be used to quantify the transition rates between different receptor states. This is achieved by reducing the vast number of possible conformations of the receptors into a small set of explicitly defined states, based on known steps in receptor activation. Thus, R represents the unbound receptor, A is an agonist molecule, RA represents a receptor with one agonist bound, RA_2 represents a fully agonist-bound shut state, D is a desensitized state, and O is an open state. The binding rates are represented by $b_{+/-}$, the desensitization rates are represented by $d_{+/-}$, and the gating rates are represented by $k_{+/-}$. Scheme 1.1 was used to model macroscopic currents, not microscopic currents. With this model, all the transition rates can be measured with various experimental paradigms. This model provided a means to compare the macroscopic response time-course for various agonists and partial agonists. Also, it was consistent with the idea that the deactivation time-course of synaptic activity is controlled by the biophysics of the receptor (Lester 1990).

Microscopic models of NMDA receptors

The Lester and Jahr model, however, cannot reproduce the properties identified in patch clamp recordings of single channels. In Figure 1.3, a single channel record of a GluN1/GluN2A receptor is displayed; the deficiencies in the Lester and Jahr model should become apparent through careful observations of these records. The open
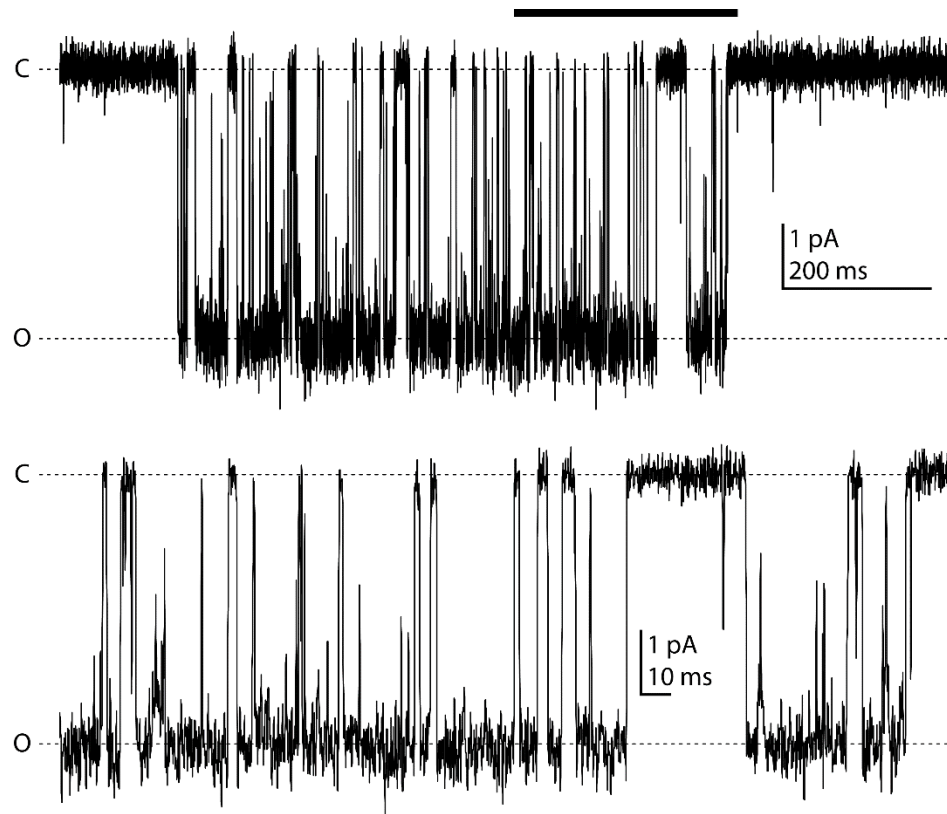
Figure 1.3. The nature of ionotropic receptor activation.

Representative GluN1/GluN2A single channel recording that illustrates the stochastic

nature of receptor activation. In the continued presence of saturating glutamate and

glycine, the receptor rapidly transition from a shut (C) and open (O) state. The receptor

open and shut dwell times are determined by biophysical and biochemical properties of

receptor gating and agonist binding.

probability, or Po, is a property of each receptor type and can be calculated from the gating transition rates. The gating equilibrium of the Lester and Jahr model can approximate a mean Po. However, single channel recordings consist of complex sequence of open and shut states that have different durations, which cannot be accounted for by the simplicity of the Lester and Jahr model. For instance, in the single channel record (Figure 1.3) the receptor shuts for drastically different amounts of time. The histogram of shut states can be fit by multiple exponential functions with very brief time-constants (< 1 ms), intermediate time-constants (1-10 ms), and long time-constants (10's-100's ms). This suggests that the shut state is cannot be a simply represented by a single equilibrium reaction.

With multiple observations of different NMDAR channel recordings (Nowak 1984, Cull-Candy and Usowicz 1987, Jahr and Stevens 1987, Gibb and Colquhoun 1992), there was a need for more accurate models that could quantify the parameters of their activity and provide a way to compare different subtypes. Since open and shut dwell times histograms of NMDAR can be fit with multiple exponential functions, models with multiple connected open and shut states were proposed (Banke and Traynelis 2003, Popescu and Auerbach 2003, Popescu 2004, Auerbach and Zhou 2005, Erreger 2005, Erreger 2005, Schorge 2005, Dravid 2008, Vance 2013). The diversity in open and shut dwell times arise from a stochastic random-walk process where receptor transitions between various states. Models with different connectivity and transition rates produce different patterns of open and shut times. The idealized records of single channel can be fit with a hidden Markov least likelihood algorithm to derive transition rates that best predict the sequence of open and shut times (Colquhoun and Sigworth 1995).

In designing models, one approach focused on different linear combinations of states (Popescu and Auerbach 2003, Popescu 2004, Auerbach and Zhou 2005), similar to successful models of nicotinic acetylcholine receptor function. One model that has been more widely used and contains three agonist-bound shut and two open states (Popescu 2004).

Scheme 1.2:
$$R \underset{b_-}{\overset{2b_+}{\rightleftharpoons}} RA \underset{2b_-}{\overset{b_+}{\rightleftharpoons}} RA_2 \underset{k_{1-}}{\overset{k_{1+}}{\rightleftharpoons}} R^+A_2 \underset{k_{2-}}{\overset{k_{2+}}{\rightleftharpoons}} R^*A_2 \underset{k_{3-}}{\overset{k_{3+}}{\rightleftharpoons}} O_1 \underset{k_{4-}}{\overset{k_{4+}}{\rightleftharpoons}} O_2$$
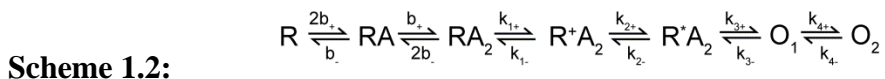
This model has improved ability to fit single channel data from GluN1/GluN2A and GluN1/GluN2B receptors, using a shut dwell-time cut-off, or t_{crit}, to exclude supposed desensitization states. Many models remove supposed desensitization states from single channel idealizations to fit microscopic records, but this may alter fitted rates and abilities of these models. Scheme 1.2 has short-comings when simulating macroscopic currents, especially for low open probability receptors (Dravid 2008, Vance 2013). The fitted rates for GluN1/GluN2C and GluN1/GluN2D do not allow for rapid rise time of macroscopic currents of these receptors given their low open probability.

A different type of model was proposed using structural information of NMDARs. A cyclic gating model was proposed where, after the binding of agonist, two possible gating transitions could occur in any order (Banke and Traynelis 2003). This model attempted to reflect the potential independence of the gating transitions of the GluN1 and GluN2 subunits in a receptor.

Scheme 1.3a:

$$D_1 \quad \overset{d_{1+}}{\underset{d_{1-}}{\Updownarrow}} \quad \overset{k_{f+}}{\underset{k_{f-}}{\nearrow\!\!\!\nearrow}} \quad R^+A_2 \quad \overset{k_{s+}}{\underset{k_{s-}}{\searrow\!\!\!\searrow}}$$

$$R \overset{2b_+}{\underset{b_-}{\rightleftharpoons}} RA \overset{b_+}{\underset{2b_-}{\rightleftharpoons}} RA_2 \qquad O_1 \overset{k_{1+}}{\underset{k_{1-}}{\rightleftharpoons}} O_2$$

$$D_2 \quad \overset{d_{2-}}{\underset{d_{2+}}{\Updownarrow}} \quad \overset{k_{s+}}{\underset{k_{s-}}{\searrow\!\!\!\searrow}} \quad R^+A_2 \quad \overset{k_{f+}}{\underset{k_{f-}}{\nearrow\!\!\!\nearrow}}$$
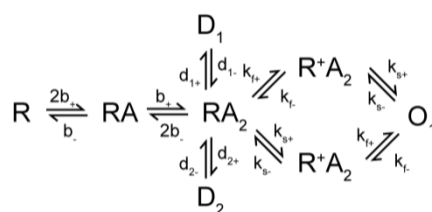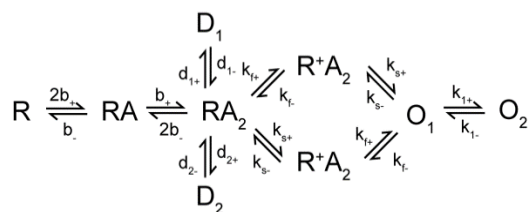
Scheme 1.3b:

In these models, the two random order transitions were referred to as a "fast" and a "slow" step. This cyclic model and the previous linear (scheme 1.2) have relatively similar capabilities to fit open and shut time histograms. Several extensions from this cyclic model have also been made including one used in fitting GluN1/GluN2C responses (Dravid 2008).

$$D_1$$

$$R \overset{2b_+}{\underset{b_-}{\rightleftharpoons}} RA \overset{b_+}{\underset{2b_-}{\rightleftharpoons}} RA_2 \quad R^+A_2 \quad R^*A_2 \overset{k_{1+}}{\underset{k_{1-}}{\rightleftharpoons}} O_1 \overset{k_{2+}}{\underset{k_{2-}}{\rightleftharpoons}} O_2$$

$$D_2$$
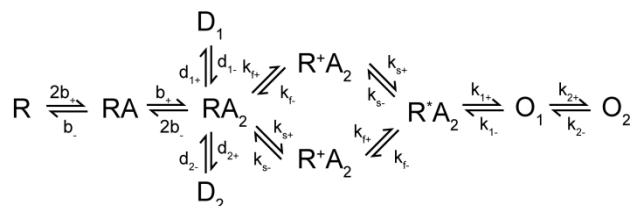
Scheme 1.4:

This model had improved capabilities to fit the low open probability of GluN1/GluN2C while accurately reflecting macroscopic responses. A study (Dravid 2008) compared the linear model (Scheme 1.2) and cyclic model (Scheme 1.4), fitting the same dataset. Interestingly, the fitted rates were highly similar although the rise time of a simulated rapid agonist application produced by the cyclic model was more accurate. An additional cyclic model was proposed to account for open and shut dwell time correlations observed in channel records (Schorge 2005).

$$D_1$$

$$RA_2 \quad R^xA_2 \quad R^*A_2 \overset{k_{3+}}{\underset{k_{3-}}{\rightleftharpoons}} O_1$$

$$R^+A_2$$

$$O_2$$
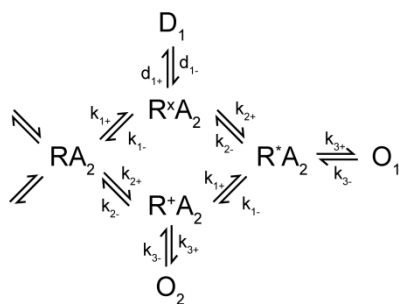
Scheme 1.5:

This model included glutamate and glycine binding steps (not shown, connects in a grid like fashion on the left of the model, the final binding transition steps are included) and was fit simultaneously to patches exposed to various concentrations of agonists. The open and shut time histograms were similar at different agonist concentration allowing the authors to conclude that the receptor operates in an all-or-none fashion, requiring all subunits to be bound to agonists before the channel can gate (Schorge 2005). This differentiates NMDARs from AMPARs, for which data suggests that each subunit contributes to receptor responses (Rosenmund 1998).

Another model was used in describing the function of GluN1/GluN2D receptors (Vance 2012). This model contains two parallel arms that confer a lower and higher Po.

Scheme 1.6:

$$R_a \underset{b_-}{\overset{2b_+}{\rightleftharpoons}} RA_a \underset{2b_-}{\overset{b_+}{\rightleftharpoons}} RA_{2a} \underset{k_{1-}}{\overset{k_{1+}}{\rightleftharpoons}} R^+A_{2a} \underset{k_{2-}}{\overset{k_{2+}}{\rightleftharpoons}} R^*A_{2a} \underset{k_{3-}}{\overset{k_{3+}}{\rightleftharpoons}} O_{1a} \underset{k_{4-}}{\overset{k_{4+}}{\rightleftharpoons}} O_{2a}$$

$$\;k_{5+}\updownarrow k_{5-} \quad k_{5+}\updownarrow k_{5-} \quad k_{5+}\updownarrow k_{5-} \quad k_{5+}\updownarrow k_{5-} \quad k_{5+}\updownarrow k_{5-}$$

$$R_b \underset{b_-}{\overset{2b_+}{\rightleftharpoons}} RA_b \underset{2b_-}{\overset{b_+}{\rightleftharpoons}} RA_{2b} \underset{k_{6-}}{\overset{k_{6+}}{\rightleftharpoons}} R^+A_{2b} \underset{k_{7-}}{\overset{k_{7+}}{\rightleftharpoons}} R^*A_{2b} \underset{k_{8-}}{\overset{k_{8+}}{\rightleftharpoons}} O_{1b} \underset{k_{9-}}{\overset{k_{9+}}{\rightleftharpoons}} O_{2b}$$
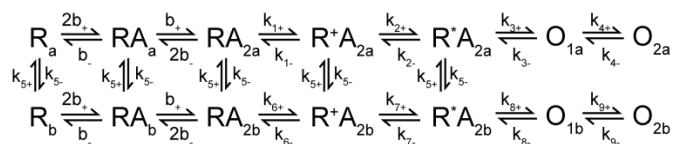
This partially recalls earlier theory about modal gating, which was proposed to account for observations of GluN1/GluN2A receptors (Popescu and Auerbach 2003) but this two arm model was necessary to achieve rapid activation of GluN1/GluN2D receptors (Vance 2012). Modal gating was later shown to be influenced by Zn^{2+} and H^+ (Schorge 2005). GluN1/GluN2D only rarely displays modal gating (Vance 2013). This model was capable of fitting the sequence of single channel open and shut times as well as macroscopic GluN1/GluN2D records. A splice variant of the GluN1, containing the amino acids encoded by exon5 significantly altered several gating constants using scheme 1.6. Simulations of models, containing or lacking exon5, spent different amounts of time in

the high-Po and low-Po arms of the model, suggesting that the ATD plays a role in modal gating of GluN1/GluN2D (Vance 2012, Vance 2013).

Uses of NMDA receptor models

In addition to the above mentioned characterization of different NMDAR subtypes, models of NMDARs have been utilized in numerous ways to understand specific properties of the receptor or perturbations to receptor function. Some of these studies have illustrated the differences of agonists and partial agonists, the function of receptor domains, the actions of allosteric modulators, and the effects point mutations (Erreger 2005, Cais 2008, Kussius and Popescu 2009, Yuan 2009, Mullasseril 2010, Acker 2011, Yuan 2014, Korinek 2015, Amin 2017, Ogden 2017). Some studies do not fit hidden Markov models explicitly but utilize the concept of these models to interpret channel records and draw conclusions about the effects of various manipulations.

The following are some specific examples of NMDAR models that have assisted in interpretation experimental data. Homoquinolinate activation was compared glutamate activation using scheme 1.3b (Erreger 2005). To control for variation of different patches due to recording conditions, the Po was scaled using the relative efficacy of homoquinolinate (62% of glutamate). Many rates of the model varied but the only significant change was in the slow transition forward rate, which decreased by 21%. This suggests the primary difference in efficacy caused by homoquinolinate is potentially due to this specific step in receptor activation (Erreger 2005). Another study used a linear model to determine the effects of several partial agonists, primarily SYM2081 (a 72% glutamate partial agonist) and alanine (a 79% glycine partial agonist), found that partial

agonists of either type had longer shut time and shorter open time components than full agonists (Kussius and Popescu 2009). Most of the fitted linear models gating transition rates were different for both SYM2081 and alanine datasets compared to glutamate and glycine, however the partial agonist model rates were similar. The authors interpreted the result based on this model as further confirmation of NMDAR's all-or-none gating requirement, that glutamate and glycine work in concert with one another to activate the receptor (Kussius and Popescu 2009). Although, the construction of this model may not have allowed for independent contribution of the GluN1 and GluN2 subunits to gating, and may have led to a false conclusion based on the model's construction. The role of the ATD in receptor function was probed using ATD deletion constructs of the GluN2 and GluN2D subunits and single channel recordings (Yuan 2009). Divergent effects were observed in these chimeric deletion constructs, the open probability of GluN1/GluN2A decreased with ATD deletion, whereas the deletion of GluN2D ATD increased open probability. However, the models that best fit the dataset possessed different combinations of states that prohibited direct comparison of transition rates (Yuan 2009). The actions of CIQ on GluN1/GluN2D channel recordings were examined (Mullasseril 2010). Single channel recording were not obtained, preventing precise characterization, however CIQ did not cause a change in channel open time suggesting that its main modulatory actions occur at earlier gating steps (Mullasseril 2010). In a different study, cholesterol-depletion of the lipid membrane was shown to dramatically inhibit NMDARs but channel open times were unaffected (Korinek 2015). On the other hand, a point mutation in the pre-M1 helix of GluN2A, P552R, was capable of increasing the open times of single channel recordings (Ogden 2017). Interestingly, the mutation was

required in both GluN2A subunits of the diheteromeric receptor in order to see a significant effect, whereas other effects occurred when only one GluN2A subunit contained the mutation (Ogden 2017).

The above examples show that if used properly receptor models can allow for highly specific quantification of the actions of perturbations to receptor function and allow for deeper interpretation of experimental data. However, these NMDAR models must be utilized carefully as they are highly dependent on the connectivity of the model, the assumptions, the simplifications, and the data used to fit the models (ionic concentrations, recording limitations) (Colquhoun 1998, Schorge 2005). The selection of an ill-chosen model may result in an incorrect conclusion or a conclusion drawn where one should not be made. However, accurate models of novel NMDAR modulator action would be highly useful as they may have predictive potential in suggesting how modulators would alter NMDARs in neuronal tissue. Currently, there is a lack of models that represent allosteric modulators of NMDARs, likely due to the effort required to collect sufficient data to fit these model.

Conclusion

The study of NMDARs has developed over the past 30 years and has shown their importance in the CNS. NMDARs have many important biological roles, including in neuronal processing and in the induction of certain forms of neuronal plasticity. NMDARs contribute to the diversity in synapse signaling complexity that allows for higher ordered behaviors. In addition, NMDARs are implicated in many neurological diseases. Many of these diseases are in need of novel therapies. Targeting NMDARs is complicated given their numerous roles and wide expression. Throughout the years, there

have been many pharmacological agents identified that act on NMDARs. Through careful evaluation of the properties and actions of compounds, gaining more knowledge concerning the function and role of NMDARs will pave the way future clinical utility.

Chapter 2: Materials and Methods

Molecular biology

All procedures using animals were reviewed and approved by the Institutional Animal Care and Use Committee of Emory University and NICHD. cDNAs for rat wild type NMDAR subunits GluN1-1a (GenBank U11418, U08261; hereafter GluN1), GluN2A (D13211), GluN2B (U11419), GluN2C (M91563), GluN2D (L31611), modified as described (Monyer 1994), GluA1 (X17184), and GluK2 (Z11548) were provided by Drs. S. Heinemann (Salk Institute), S. Nakanishi (Kyoto University), and P. Seeburg (University of Heidelberg). Plasmids containing the genes for the $GABA_A$ (α1β2γ2s), $GABA_C$ (ρ1), glycine (α1), serotonin ($5-HT_{3A}$), nicotinic acetylcholine receptor (nAChR, α1β1δγ, α2β4, α4β3, α7) and purinergic (P2X2 rat, P2X2 human) receptors were provided by Drs. Heinemann (Salk), Weiss (Univ. of Texas, San Antonio), Papke (Univ. of Florida), and Hume (Univ. of Michigan). For expression in *X. laevis* oocytes, cDNA constructs were linearized by restriction endonuclease digestion, purified using the QIAquick PCR Purification Kit (Qiagen, North Rhine-Westphalia, Germany), and used as templates to transcribe cRNAs using the mMessage mMachine kit (ThermoFisher Scientific, Massachusetts, USA) following the manufacturer's protocol.

Two-electrode voltage-clamp recordings from *Xenopus laevis*

Xenopus laevis stage VI oocytes (Ecocyte Biosciences, Texas, USA) were isolated as previously described (Hansen 2013), and injected with 50 nl of water containing 5-10 ng of cRNA encoding the GluN1 and GluN2 NMDAR subunits (3:7 ratio). Oocytes were stored at 15°C in media containing (in mM) 88 NaCl, 2.4 $NaHCO_3$, 1 KCl, 0.33 $Ca(NO_3)_2$, 0.41 $CaCl_2$, 0.82 $MgSO_4$, 5 Tris-HCl (pH was adjusted to 7.4 with

NaOH), 1 U/mL penicillin, 0.1 mg/mL gentamicin sulfate, and 1 μg/mL streptomycin. Two to seven days after injection, two-electrode voltage-clamp recordings were performed at room temperature. All extracellular solutions contained (in mM) 90 NaCl, 1 KCl, 10 HEPES, 0.5 $BaCl_2$, 0.01 EDTA (pH 7.4 with NaOH). Gravity-applied solutions (4-5 ml/min) were exchanged by an 8 port Modular Valve Positioner (Hamilton Company, Nevada, USA) and controlled by custom software. Voltage and current electrodes were filled with 0.3 M and 3.0 M KCl, respectively. Oocyte currents were recorded at a holding potential of -40 mV, maintained by a two-electrode voltage-clamp amplifier (OC-725B or C, Warner Instruments, Connecticut, USA). For some recordings, 1 mM 2-(hydroxypropyl)-β-cyclodextrin was added to wash solutions to ensure modulators did not adhere to the tubing, valves, or recording chamber.

(+)-CIQ and related analogue stocks were prepared as a 20 mM solution in DMSO, and working solutions were prepared during rapid stirring immediately before the experiment. For concentration-response curve recordings, 1-5 mM 2-(hydroxypropyl)-β-cyclodextrin was used to increase the solubility of modulators and subsequently added to all agonist solutions to control for any direct effects. Unless indicated otherwise, current responses were elicited by application of 100 μM glutamate plus 30 μM glycine.

Whole cell patch-clamp recordings of heterologous cells

HEK293 cells (CRL-1573, ATCC, Manassas, VA) were maintained and transfected using a $CaPO_4$ protocol to express the diheteromeric NMDARs as previously described (Hansen 2013). cDNA ratios for transfection were 1:1:1 (GluN2D) or 1:1:5

(GluN2A) for GluN1:GluN2:GFP. Cells were maintained in 5% CO_2 at 37^oC for 12-36 hours post-transfection. Prior to and during recording, cells were bathed in a solution containing (in mM) 150 NaCl, 10 HEPES, 3 KCl, 0.5 $CaCl_2$, 0.01 EDTA (pH 7.4). Cells were patched with borosilicate glass micropipettes (3-4 MΩ) that were filled with internal recording solution that contained (in mM) 95 CsGluconate, 5 CsCl, 40 HEPES, 8 NaCl, 5 $MgCl_2$, 10 BAPTA, 0.6 EGTA, 2 Na_2ATP, and 0.3 NaGTP (pH 7.35). The whole cell recording conformation was achieved, and the cell lifted into the flow of solution from a two barreled theta glass or a triple barrel square glass perfusion system to perform rapid solution exchange experiments. The theta/triple barreled glass was translated using a piezoelectric manipulator to exchange the solution around the cell. Calibration of the perfusion manifold was performed each day to ensure the 10-90% rise time of the solution exchange (switching between 0/100% and 50/50% H_2O/external solution) around an open tip was less than 1.5 ms for a theta tube and 4 ms for a transition into an outside lane and 2 ms for a transition between lanes for a triple barreled manifold. For some recordings, 1 mM 2-(hydroxypropyl)-β-cyclodextrin was added to wash solutions to ensure modulators did not adhere to the tubing, valves, or recording chamber.

Electrophysiological recordings of rodent hippocampus

Horizontal hippocampal brain slices (300 μm) were made from C57Bl/6 mice (post-natal day 7-14 or P7-14, unless otherwise stated) using a vibratome (TPI, Missouri, USA). During preparation, the slices were bathed in ice-cold (0-2°C) artificial cerebral spinal fluid (slicing-aCSF containing in mM, 75 NaCl, 2.5 KCl, 1.25 NaH_2PO_4, 25 $NaHCO_3$, 5 $MgCl_2$ or $MgSO_4$, 0.5 $CaCl_2$, 20 glucose, 70 sucrose, and bubbled with 95%

O_2/5% CO_2). After preparation, slices were allowed to recover for 1 hour at 37°C before use in experimentation.

Whole-cell voltage-clamp recordings of stimulated excitatory postsynaptic currents (EPSCs) from C57Bl/6 mice (post-natal day 7-14) were made using an aCSF containing in mM, 130 NaCl, 2.5 KCl, 1.25 NaH_2PO_4, 25 $NaHCO_3$, 0.1 $MgCl_2$ or $MgSO_4$, 2.5 $CaCl_2$, and 20 glucose, supplemented with 0.01 mM bicuculline methobromide or gabazine, 0.01 mM DNQX, and 0.005 nimodipine. Stimulated EPSC experiments were performed at room temperature. Whole-cell voltage-clamp recordings of miniature EPSCs (mEPSCs) were made using the same aCSF as above supplemented with 0.01 mM bicuculline methobromide or gabazine, 0.005 mM nimodipine and 0.5 μM tetrodotoxin (TTX). Patch recording electrodes filled with an internal solution containing in mM, 110 Cs-gluconate, 30 CsCl, 5 HEPES, 4 NaCl, 0.5 $CaCl_2$, 2 $MgCl_2$, 5 BAPTA, 2 Na-ATP, 0.3 Na-GTP, supplemented with 1 mM QX-314 and 0.1% biocytin (pH 7.35, 285-295 mOsm). The bath temperature was maintained at 29-32°C using an in-line solution heater and a bath chamber heating element (Warner Instrument Corporation, Hamden, CT, USA). Thin walled borosilicate glass (1.5 mm outer and 1.12 mm inner diameter, WPI Inc., FL, USA) was used to fabricate recording electrodes (3-5 MΩ), which were positioned using a micromanipulator (Luigs and Neumann, North Rhine-Westphalia, Germany) for whole-cell patch-clamp recording; currents were recorded using an Axopatch 1D and filtered at 1 kHz and digitized at 2 kHz by a Digidata 1440A for analysis off line (Molecular Devices, California, USA). To minimize uncontrolled voltage-gated receptor activation when changing the membrane holding potential during an experiment, the holding potential was slowly altered at a rate less than 4 mV/s.

For experiments testing the effects of (+)-CIQ on mEPSC properties, slices were first equilibrated with aCSF supplemented with the $GABA_A$ receptor antagonist gabazine (10 μM) and containing reduced Mg^{2+} (0.1 mM). Following equilibration, mEPSCs were recorded 3-6 minutes to determine the baseline properties. We subsequently recorded with either a vehicle solution of the same composition or a solution that contained 10 μM (+)-CIQ. (+)-CIQ solutions were made from 20 mM DMSO stock and mixed immediately before the switch in perfusion; an equivalent amount of DMSO was added to the vehicle recording solution (Figure 5A). We subsequently switched to aCSF supplemented with the competitive NMDAR-selective competitive antagonist APV (200 μM) to confirm that the slow component we recorded was mediated by NMDARs, followed by a switch to aCSF supplemented with both APV and DNQX (10 μM) to confirm that the mEPSCs we analyzed arose from AMPA receptors; no mEPSCs could be detected in the presence of DNQX. The tubing and chamber were washed with ethanol followed by extensive aCSF rinsing between recordings from each cell to remove any residual (+)-CIQ from tubing and slice-chamber.

For field recordings, horizontal brain slices (500 μm) from Sprague Dawley rats (P14-21) were prepared. To maintain the brain slices during experimentation a high flow rate (3-5 mL/min) was used to perfuse both sides of the brain slice. The bath temperature was clamped at 32°C using a custom built apparatus with an isolated 500 ml liquid heat reservoir immediately beneath the recording chamber. Thin walled borosilicate glass electrodes (similar to above) were filled with external solution and used to record the field potentials of the slice. The monopolar stimulating electrode (RD1, FHC, Bowdoin, ME, USA) and the recording electrode were maneuvered with mechanical

micromanipulators to find a robust response that requires a small amount of stimulation (30-100 µA) and had a well-defined fiber volley. Low frequency excitatory postsynaptic potentials (EPSPs) were stimulated every 30 seconds and a theta burst was stimulated by 3 sets (200ms interval) of 4 stimulations of 100 Hz.

For whole-cell voltage-clamp recordings of spontaneous inhibitory postsynaptic currents (sIPSCs), using brain slices from C57Bl/6 mice (post-natal day 7-14). An aCSF containing in mM, 130 NaCl, 2.5 KCl, 1.25 NaH_2PO_4, 25 $NaHCO_3$, 1.0 $MgCl_2$, 2.0 $CaCl_2$, and 20 glucose using patch recording electrodes filled with the same internal solution used for recording mEPSC supplemented with 1 mM QX-314 and 0.1% biocytin (pH 7.35, 285-295 mOsm). $GABA_AR$-mediated currents were isolated by performing recordings at the reversal potential for EPSCs, which in these recording solutions was +10 mV.

Intracellular recording solutions for some electrophysiology experiments contained biocytin (0.1-0.2%), which allowed for anatomical reconstruction after the experiment conclusion. Biocytin-filled cells were stained with Alexa dye-conjugated avidin (Molecular Probes/Invitrogen, California, USA). Slices were fixed in 4% paraformaldehyde (PFA) in PBS for 12-60 hours at 4°C, and then rinsed twice with PBS and maintained in PBS until further processing. Slices were re-sectioned, mounted on slides, and imaged as previously reported (Matta 2013). Neurons were classified by their cell body localization as well as dendritic and axonal arborization.

Miniature and spontaneous post synaptic current detection and analysis

Minianalysis (Synaptosoft, Georgia, USA) was used to detect mEPSCs using amplitude and integral threshold cut-offs. Recordings were filtered using a 250 Hz low pass Butterworth filter only for detection purposes. For the detection of composite AMPAR/NMDAR-mediated currents while holding the membrane voltage at -60 mV, an amplitude threshold from 8-12 pA and an area of 40 fC were used to identify mEPSCs, which were aligned on the time of the peak of the response. Amplitude threshold was selected based on the variance (>3 times the standard deviation of a stretch of recording with no mEPSCs) of the control recording in each experiment. An amplitude threshold of 8 pA and an area of 80 fC were used to detect NMDAR-mediated spontaneous synaptic currents at a holding voltage at +40 mV. The same detection parameters were used throughout analysis of each data set from every experiment. Each detected current was evaluated for synaptic-like shape (rapid 10-90 rise < 2 ms, an exponential decay) and rejected if there was a second mEPSC or any non-synaptic recording artifact present during the mEPSC. Following detection of mEPSCs, the original recorded mEPSC (digitized at 2 kHz) was aligned on the rising phase of the response and the time course averaged. The experimenter was blinded to the identity of the recording group while sorting mEPSCs. mEPSCs selected for inclusion were further analyzed using custom written Matlab scripts to determine mEPSC peak amplitude, decay time constants, the amplitude of the NMDAR-component of the mEPSC. The deactivation time course for the rapid (AMPAR) and slower (NMDAR) components of the mEPSC were evaluated by non-linear least-squares fitting of a dual exponential equation to the synaptic waveform as follows:

$$I = Amplitude_{\text{FAST}} \, e^{\left(\frac{time}{-\tau_{\text{FAST}}}\right)} + Amplitude_{\text{SLOW}} \, e^{\left(\frac{time}{-\tau_{\text{SLOW}}}\right)} \qquad (2.1)$$

where *I* is the current response, *Amplitude*$_{\text{FAST}}$ is the amplitude of the fast component, *time* is the time of the response in reference to the peak response amplitude, τ_{FAST} is the deactivation time constant of the fast component, *Amplitude*$_{\text{SLOW}}$ is the amplitude of the slow component, and τ_{SLOW} is the deactivation time constant of the slow component. In mEPSC recordings, τ_{FAST} was assumed to reflect the AMPAR-component, and determined by fitting the response in the presence of the competitive NMDAR antagonists APV. To estimate the amplitude of the NMDAR-mediated component of EPSC, the mean current between 40-50 ms after the peak of the AMPAR response was measured. The AMPAR/NMDAR ratio was calculated by dividing *Amplitude*$_{\text{FAST}}$ by *Amplitude*$_{\text{SLOW}}$.

The NMDAR-mediated evoked EPSC peak amplitude was measured within a 2 ms window around the peak of the waveform obtained from the average of 30-40 individual EPSCs. Rise time was determined as the time for the current to rise from 20 to 80% of the peak amplitude. The EPSC time course was analyzed by fitting a single exponential component to the averaged waveform between 90% and 20% of the peak amplitude. For these experiments, EPSC decay kinetics were measured using the second EPSC waveform evoked by the paired stimuli and the paired-pulse ratio was calculated as P2/P1, where P1 represents the amplitude of the first evoked current and P2 the amplitude of the second synaptic current measured from the averaged EPSC waveform.

Spontaneous IPSCs (sIPSCs) were detected using Minianalysis as described above, with an amplitude threshold of 6-8 pA and an area of 30 fC at a holding potential of +10 mV. sIPSC recordings were analyzed for their relative frequency throughout the

experiment. A rolling average (60 second window) of the sIPSC frequency was normalized to a 60 second period in pre-treatment control phase of experiment for each cell and the resulting plots averaged between cells to produce the composite response for all recordings in an experimental group. The comparable 60 second periods in the baseline and at the end of the application of (+)-CIQ phases was used to determine the change in sIPSC frequency and amplitude. To determine the integral of the spontaneous activity, the mean current in a stretch of the recording free of sIPSCs was subtracted from the full record. The current response in a 50 second window was integrated during the baseline, at the end of the (+)-CIQ phases, and in the presence of gabazine. The gabazine current was subtracted from baseline and (+)-CIQ and the ratio presented.

Hippocampal field tissue preparation and western blotting for GluN2D

Wild type C57Bl/6 P9, P17, P30, P58 and P74 mice (both male and female, 3 in each age group) were used for western blot analysis of GluN2D expression. Experiments included analysis of three *GRIN2D*-/- mice at P9. Animals were euthanized by isoflurane overdose, the brains rapidly were removed, and 500 µm slices were cut in ice-cold PBS on a vibratome (TPI, Missouri, USA). The whole hippocampus was dissected out for some slices and tissue punches of the CA1 region, the CA3 region, and the dentate gyrus/hilar region collected using a 0.75 mm Stoelting tissue punch from other slices. The tissue was frozen on dry ice, and subsequently homogenized in lysis buffer containing (in mM) 150 NaCl, 50 Tris, 50 NaF, 5 EDTA, 5 EGTA, 1% Triton, 1% SDS, and protease inhibitors (cat. number 88266, Pierce, Thermo Scientific) at pH 7.4. A Bradford assay was used to quantify and normalize total protein concentrations, and the

samples were then mixed with 4x Laemmli buffer (containing 40% glycerol, 240 mM Tris/HCl pH 6.8, 8% SDS, 0.04% bromophenol blue, 175 mM DDT). After samples were heated to 95°C for 5 min, they were separated by electrophoresis using a 4-20% SDS-PAGE gel, and transferred to a PVDF membrane (cat. number 162-0177, Bio-Rad). The mouse anti-GluN2D (Millipore, MAB5578, 1:5000), mouse anti-tubulin (Sigma-Aldrich, 1:50,000), and horseradish peroxidase-conjugated goat anti-mouse (Jackson Immunoresearch, 1:10,000) antibodies were used. Between probing for different primary antibodies, Restore Stripping Buffer (Pierce) was applied for 10 min to strip off previous probe. Band intensities were imaged (Bio-Rad Gel Doc XR+ Imager, cat. number 1708195) from films exposed to chemiluminescence signals, and band intensity was analyzed using ImageJ.

Modelling receptor function

Matlab (Mathworks, Natick, MA) scripts were written based on previously described approaches to modelling channel function (Colquhoun and Hawkes 1977, Colquhoun and Hawkes 1995). Briefly, a Q matrix was constructed for a model that accounts for macroscopic responses (Lester and Jahr 1992). The glutamate association and dissociation rates were from (Erreger 2005), and unidirectional rate constants for gating and modulator binding were chosen to allow the model to be used for modulator competition. The differential equations derived by the Q matrix were solved using an ordinary differential equation solver (ode23s, Matlab) and occupancy of each state was determined at equilibrium given the concentrations of the theoretical ligands.

Statistical analysis

Concentration-response curves for both positive and negative modulators were fitted by the Hill equation:

$$\frac{I}{I_{[M]=0}} = 1 + Extent \left(\frac{[M]^h}{[M]^h + EC_{50}{}^h} \right) \tag{2.2}$$

where *I* is the measured response of receptor activation, *Extent* is the maximal predicted modulation of the glutamate/glycine response, *[M]* is the concentration of the modulator being used, *h* is the Hill slope, and EC_{50} is the half-maximal effective concentration of the modulator. Modulator concentration response data was plotted as a percentage of unmodulated response and displayed fitted curves were obtained by fitting all data simultaneously.

Glutamate and glycine concentration-response curves were fit by the Hill equation as follows:

$$\frac{I}{I_{Max}} = \left(\frac{[A]^h}{[A]^h + EC_{50}{}^h} \right) \tag{2.3}$$

where *I* is the measured response of receptor activation, *[A]* is the concentration of the agonist, *h* is the Hill slope, and EC_{50} is the half-maximally effective concentration of the agonist. Agonist concentration-response data, unless otherwise stated, were plotted as a percentage of maximal response and displayed fitted curves were obtained by fitting all data simultaneously with the appropriate Hill equation.

The time course for the onset of negative modulation was fitted using a single exponential function:

$$I = Ae^{-time/\tau} + c \tag{2.4}$$

where A is the amplitude of the exponential, τ is the time constant for the exponential and c is a constant. Additionally, some of the complex modulator time-courses were fitted with the sum of a single exponential equation and a linear component

$$I = Ae^{-time/\tau} + mt + c \tag{2.5}$$

where m is the slope.

Measurements are given as mean $\pm$ SEM unless otherwise indicated. Number of replicate experiments used chosen to ensure a power level of at least 0.80 when $\alpha = 0.05$ and when detecting appropriate effect sizes. EC_{50} and IC_{50} values and confidence intervals reported were calculated by averaging the $\log(EC_{50})$ or $\log(IC_{50})$ value, determining confidence intervals for mean $\log(EC_{50})$ or $\log(IC_{50})$, and converting back to units of molarity. Statistical significance evaluations (α set to 0.05) were performed using a one-way ANOVA with Dunnett's multiple comparison test, a paired t–test, or other appropriate tests as described.

Data are shown as mean $\pm$ SEM unless otherwise indicated. Number of replicate experiments used ensured a power level of at least 0.80 when detecting a 40% change. Data were evaluated for statistical significance using a one-way ANOVA with Dunnett's multiple comparison test with α set to 0.05 or a paired t–test, as appropriate. For statistical testing of EC_{50} values, a one-way ANOVA with Dunnett's multiple comparison test was calculated using the logarithm of the EC_{50} values with α set to 0.05.

Chapter 3: An NMDAR positive and negative allosteric modulator series share a binding site and are interconverted by methyl groups.[1]

Abstract

N-methyl-D-aspartate receptors (NMDARs) are an important receptor in the brain and have been implicated in multiple neurological disorders. Many non-selective NMDAR-targeting drugs are poorly tolerated, leading to efforts to target NMDAR subtypes to improve the therapeutic index. We describe here a series of negative allosteric NMDAR modulators with submaximal inhibition at saturating concentrations. Modest changes to the chemical structure interconvert negative and positive modulation. All modulators share the ability to enhance agonist potency and are use-dependent, requiring the binding of both agonists before modulators act with high potency. Data suggest that these modulators, including both enantiomers, bind to the same site on the receptor and share structural determinants of action. Due to the modulator properties, submaximal negative modulators in this series may spare NMDARs at the synapse, while augmenting the response of NMDARs in extrasynaptic spaces. These modulators could serve as useful tools to probe the role of extrasynaptic NMDARs.

Introduction

N-methyl-ᴅ-aspartate receptors (NMDARs) are a subtype of ionotropic glutamate receptors that are broadly expressed in the brain and are important for normal development, neuronal plasticity and memory formation (Traynelis 2010, Paoletti 2013). NMDARs contribute a slow, Ca^{2+} permeable component to fast excitatory neurotransmission that is voltage dependent by virtue of its sensitivity to pore block by extracellular Mg^{2+} (Traynelis 2010). The typical NMDAR is comprised of 2 GluN1 and 2 GluN2 subunits, creating the potential for diversity given that there are 8 splice variants of GluN1 and 4 independent genes encoding GluN2 subunits (A-D) (Traynelis 2010). The regulation and functional properties of the NMDAR are controlled by the subunits incorporated into the receptor (Monyer 1994, Vicini 1998, Vance 2012). NMDARs are expressed at most excitatory synapses, and are also found in peri- and extrasynaptic locations (Sans 2000, Steigerwald 2000, Groc 2006, Traynelis 2010). Although NMDARs have been studied extensively, there are still important questions about the different roles that NMDARs may play given differences in subunit composition and synaptic localization (Hardingham and Bading 2010, Gladding and Raymond 2011, Paoletti 2013). Pharmacological approaches can be useful for probing these questions, but tool compounds to differentiate these NMDAR subtypes have been limited (Ogden and Traynelis 2011, Monaghan 2012, Santangelo 2012, Strong 2014, Zhu and Paoletti 2015). Whereas NMDAR receptors have been implicated in many neurological diseases, there remains a dearth of clinically-approved drugs that target NMDARs (Kalia 2008, Traynelis 2010, Paoletti 2013, Strong 2014).

Multiple endogenous and exogenous modulatory sites in the NMDAR recently have been described. In addition, nearly complete NMDAR structures obtained using crystallographic approaches are now available (Karakas and Furukawa 2014, Lee 2014), and these data, together with recent cryo-EM structures in the receptor super family (Twomey and Sobolevsky 2017, Twomey 2017, Twomey 2017), illustrate the overall topography of the NMDAR and suggest a mechanism for some allosteric modulators, such as GluN2B-selective ifenprodil (Tajima 2016, Zhu 2016). However, a complete understanding of how other modulatory sites operate and can be exploited has been elusive. Advances in the understanding of specific roles of particular NMDAR subunits have led to renewed interest in targeted therapeutic intervention, and recent work has yielded a growing tool box of novel ligands that act on NMDARs with diverse sites and mechanisms (Ogden and Traynelis 2011, Monaghan 2012, Hackos and Hanson 2017). To date, there are positive and negative modulators that bind to the amino-terminal domain (ATD), agonist binding domain (ABD), or transmembrane domain (TMD). Each new class of compounds discovered enriches our understanding of the function of NMDAR and how these receptors can be modulated. The information gained from these modulators has the potential to provide insight into both NMDAR function and therapeutic strategies to treat complex neurological diseases.

This study describes a series of compounds that includes both positive allosteric modulators (PAMs) as well as negative allosteric modulators (NAMs) of NMDAR function (Katzman 2015). A set of aliphatic substitutions off an ester linkage to the scaffold interconverts these compounds between positive and negative allosteric modulators. Remarkably, the difference between the positive and negative modulation to

the same chemical scaffold was influenced by the addition or removal of individual methyl groups. These modulators appear to bind to a shared site to bring about opposing actions, and share mechanistic features, such as agonist dependence and enhancement of agonist potency. The spectrum of properties in this series of modulators could serve as useful tool compounds for probing the role of NMDARs in circuits in both healthy brain and in neuropathological situations.

Results

Identification of a new class of positive allosteric modulators of NMDAR function

We have previously described the structure-activity relationship (SAR) of a series of negative allosteric pan-NMDAR modulators that contained a amidothiophene core, the most potent possessing a tetrahydrobenzothiophene, with different alkyl and aryl substitutions connected via an ester linkage at the 3-position (Katzman 2015). These compounds inhibited the response to saturating concentration of co-agonists at NMDARs expressed in *Xenopus laevis* oocyte experiments, typified by **EU1794-2** (compound **4** in Katzman 2015). We describe here a new set of closely related analogues that can either potentiate or inhibit responses depending on subtle changes in structure and agonist concentration. As shown in Figure 3.1 and Table 3.1, **EU1794-4** contained an ethyl ester similar to **EU1794-2** and lacked a methyl substituent on the tetrahydrobenzothiophene core (data from P. Le, J. Zhang, and R. Perszyk). **EU1794-4** potently inhibited GluN1/GluN2D with a substantial residual current remaining at saturating concentrations (Figure 3.1B,C, Table 3.1). Interestingly, ester substitutions that had a larger calculated functional group volume than the ethyl ester in **EU1794-4** potentiated NMDAR responses to saturating concentrations of glutamate and glycine. For example, the isopropyl ester (**EU1794-5**) potentiated GluN1/GluN2D responses to nearly 200% of control (Figure 3.1A-C). Restoration of the methyl to the tetrahydrobenzothiophene core restored negative allosteric modulation (**EU1794-19**, Figure 3.1B,C). Thus, the direction of modulation (positive or negative) could be determined by the size of the alkyl ester and substitution to the tetrahydrobenzothiophene core. Moreover, the size of the ester-linked substituent controlled the extent and potency of positive modulation. The *t*-butyl
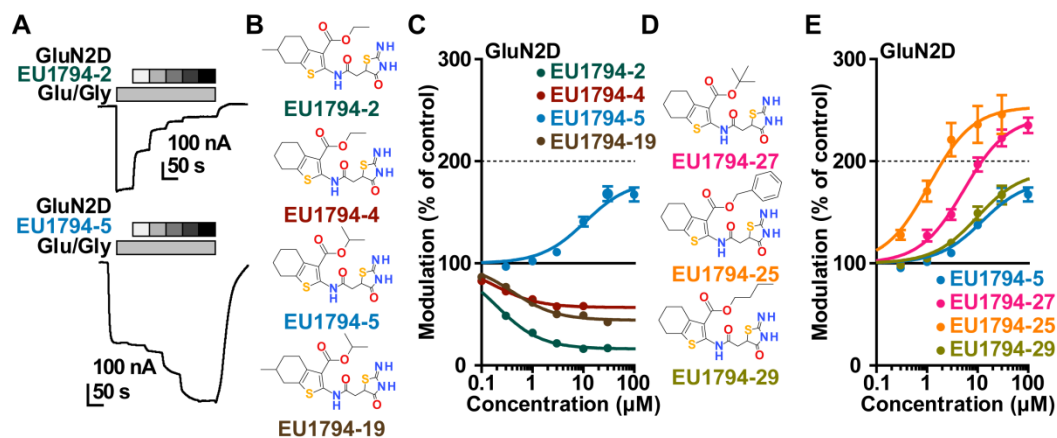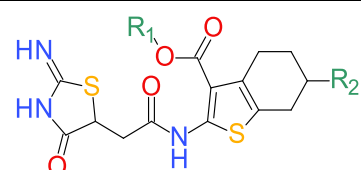
Figure 3.1. The **EU1794** series of NMDAR NAMs can be converted to PAMs with subtle structural modifications.

A) Representative concentration-response experiments for a negative (**EU1794-2**, above) and positive (**EU1794-5**, below) allosteric modulator using two-electrode voltage-clamp recordings of GluN1/GluN2D NMDARs activated by saturating concentrations of agonist. 100/30 µM glutamate/glycine application is represented by the grey bar and increasing concentrations of modulator are shown by grey scale boxes (0.3, 1, 3, 10, 30 µM for **EU1794-2** and 1, 3, 10, 30, 100 µM for **EU1794-5**). B) Chemical structures of the NAMs **EU1794-2**, **EU1794-4, EU1794-19** and PAM **EU1794-5** are given. C) The concentration-response curves for the compounds shown in (B) acting on GluN1/GluN2D NMDARs activated by maximally effective concentrations of co-agonists and fitted by the Hill equation. D) Chemical structures of the PAMs **EU1794-25, EU1794-27** and **EU1794-29** are given. E) Concentration-response curves for **EU1794** PAMs on the responses of GluN1/GluN2D NMDARs to maximally effective concentrations of co-agonists. See Table 3.1 for fitted EC_{50} values at all diheteromeric NMDARs. Data represent 4-18 oocytes recorded in at least 2 independent experiments. Data are from P. Le, J. Zhang, and R. Perszyk, and analyzed by R. Perszyk.

Table 3.1. The effect of alkyl ester and tetrahydrobenzothiophene ring substitutions on the potency and efficacy of **EU1794** analogues.

Compound	R_1	R1 volume (Å^3)	R_2	GluN2A	GluN2B	GluN2C	GluN2D
				EC_{50} (μM) [conf. int.][a] Maximal Degree of Modulation (% of control)[b]
EU1794-4	Et	45.15	H	2.2 [1.8, 2.8] 32 ± 3%	2.6 [1.4, 4.8] 67 ± 4%	0.42 [0.28, 0.61] 52 ± 2%	0.36 [0.29, 0.45] 51 ± 3%
EU1794-2	Et	45.15	Me	0.60 [0.44, 0.82] 6 ± 2%	1.2 [0.8, 1.9] 10 ± 3%	0.26 [0.21, 0.31] 14 ± 1%	0.20 [0.17, 0.25] 14 ± 1%
EU1794-5	iPr	62.16	H	18 [9.0, 36] 36 ± 5%	2.5 [1.4, 4.4] 71 ± 4%	4.0 [3.5, 4.6] 140 ± 3%	9.3 [8.1, 11] 169 ± 7%
EU1794-19	iPr	62.16	Me	1.1 [0.5, 2.3] 19 ± 6%	1.1 [0.9, 1.3] 43 ± 2%	0.74 [0.57, 0.96] 32 ± 3%	0.43 [0.32, 0.59] 46 ± 2%
EU1794-27	tBu	79.23	H	7.4 [5.3, 10] 52 ± 7%	1.4 [1.2, 1.7] 130 ± 3%	2.8 [2.5, 3.2] 230 ± 10%	2.4 [1.8, 3.3] 250 ± 8%
EU1794-25	Bn	98.87	H	-	1.0 [0.9, 1.2] 220 ± 13%	0.77 [0.56, 1.0] 180 ± 12%	1.0 [0.95, 1.1] 250 ± 19%
EU1794-29	n-Bu	79.12	H	3.7 [1.7, 8.0] 59 ± 5%	1.4 [1.1, 1.8] 140 ± 3%	3.8 [2.6, 5.7] 130 ± 7%	5.7 [5.1, 6.4] 166 ± 8%

[a]EC_{50} values for potentiation of responses to saturating glutamate and glycine (100 μM, 30 μM) were obtained by least-squares fitting of data from individual experiments by the Hill equation. EC_{50} values are given as the mean with the 95% confidence interval determined from $\log(EC_{50})$. [b]The maximal degree of modulation is given as mean ± SEM. For all compounds, data are from 4-18 oocytes recorded in at least 2 independent experiments. Data were not fit (shown as -) if the response recorded at 30 μM of test

compound did not differ by more than 15% from control. Data are from P. Le, J. Zhang, and R. Perszyk, and analyzed by R. Perszyk.

ester **EU1794-27** potentiated GluN1/GluN2D NMDARs with greater efficacy and higher potency, increasing responses to maximally effective glutamate and glycine to 250% of control with an EC_{50} value of 2.4 μM (Figure 3.1D,E). The benzyl ester (**EU1794-25**) also strongly potentiated responses with a potency similar to **EU1794-27** (Figure 3.1D,E). However, **EU1794-29**, which had a longer substitution, *n*-butyl, reduced both the maximal potentiation and potency, suggesting an optimal substituent size and shape (Figure 3.1D,E).

Allosteric modulation of agonist potency by NAMs and PAMs

The tetrahydrobenzothiophene-containing NAMs reported here inhibit all diheteromeric NMDARs without substantial subunit selectivity, similar to those that we previously described (Katzman 2015). By contrast, the novel PAMs described here show distinct GluN2 dependence (Table 3.1). All PAMs are active at GluN1/GluN2C and GluN1/GluN2D, but do not enhance the response of GluN1/GluN2A to maximally effective concentrations of agonist, in some cases resulted in inhibition of these responses. Most PAMs also were capable of potentiating GluN1/GluN2B (Table 3.1, Figure 3.2A). As seen with other series of NMDAR PAMs (Malayev 2002, Horak 2004, Horak 2006, Wang 2017) (Hackos and Hanson 2017), allosteric modulation can be dependent on agonist concentrations. Thus, we assessed the ability of **EU1794-27** to modulate NMDAR responses activated by sub-saturating co-agonist concentrations (Figure 3.2B, Table 3.2, data from P. Le and R. Perszyk). In these conditions, **EU1794-27** positively modulated all NMDAR subtypes and enhanced previously potentiated
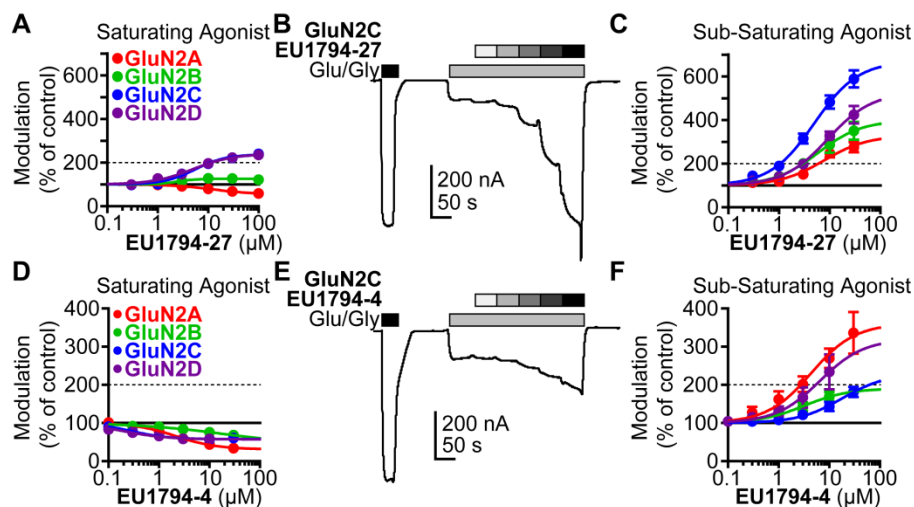
Figure 3.2. Modulation of both **EU1794** PAMs and NAMs is dependent on agonist concentration.

A) The concentration-response relationship for **EU1794-27** at diheteromeric NMDARs activated by 100/30 µM glutamate/glycine (data for GluN1/GluN2D shown in Figure 3.1E is included here for clarity). GluN1/GluN2C and GluN1/GluN2D (which are superimposed) are potentiated to a greater extent than GluN1/GluN2B; there appears to be slight inhibition of GluN1/GluN2A. B) A representative concentration-response recording of **EU1794-27** at GluN1/GluN2B activated by sub-saturating concentrations of agonist. The initial response was activated using saturating 100/30 µM glutamate/glycine (black box) followed by 1/0.3 µM glutamate/glycine (grey box, roughly resulting in an activity state that was 20% of the maximal response) administered in the absence and presence of increasing concentrations of **EU1794-27** (0.3, 1, 3, 10, 30 µM). C) Concentration-response relationship for **EU1794-27** at diheteromeric NMDARs activated by sub-saturating concentration of agonist (glutamate/glycine concentrations used for GluN1/GluN2A were 2/0.6 µM, GluN1/GluN2B and GluN1/GluN2C were 1/0.3 µM, and GluN1/GluN2D were 0.6/0.2 µM). Note potentiation of all subunits. D-F) Similar

experiments as in A-C, but using the NAM **EU1794-4** at saturating (D) or sub-saturating (E,F) concentrations of agonist (glutamate/glycine concentrations used for GluN1/GluN2A, GluN1/GluN2B and GluN1/GluN2C were 1/0.3 μM, and GluN1/GluN2D were 0.3/0.09 μM); data for GluN1/GluN2D presented in Figure 3.1C are included here for comparison. Note the inhibition by the NAM at saturating agonist concentration (D) compared to potentiation in submaximal concentrations of agonist in (E,F). Data represent 4-13 oocytes recorded in 2 independent experiments. Data are from P. Le and R. Perszyk, and analyzed by R. Perszyk.

Table 3.2. Effect of **EU1794-4** and **EU1794-27** at sub-saturated NMDAR responses.

	EC_{50} (µM) [conf. int.][a]			
	Maximal Degree of Modulation (% of control)[b]			
	GluN2A	**GluN2B**	**GluN2C**	**GluN2D**
EU1794-4	3.9	4.3	15	14
	[0.78, 20]	[1.3, 14]	[6.5, 35]	[6.5, 29]
	$500 \pm 32\%$	$210 \pm 6.8\%$	$220 \pm 20\%$	$540 \pm 190\%$
EU1794-27	8.1	6.3	5.0	8.3
	[5.7, 12]	[5.0, 8.0]	[3.7, 6.6]	[5.3, 13]
	$340 \pm 32\%$	$400 \pm 50\%$	$680 \pm 50\%$	$580 \pm 86\%$

[a]EC_{50} values of modulator action on responses to sub-saturating glutamate/glycine concentrations were obtained by least-squares fitting of data from individual experiments by the Hill equation. For **EU1794-4** modulation of GluN1/GluN2A, GluN1/GluN2B and GluN1/GluN2C, glutamate/glycine concentrations were 1/0.3 µM; for GluN1/GluN2D glutamate/glycine were 0.3/0.09 µM. For **EU1794-27** potentiation, glutamate/glycine concentrations were 2/0.6 µM (GluN1/GluN2A), 1/0.3 µM (GluN1/GluN2B, GluN1/GluN2C), and 0.6/0.2 µM (GluN1/GluN2D). EC_{50} for potentiation values are given as the mean with the 95% confidence interval determined from $\log(EC_{50})$. [b]The extent of modulation is given as a percent of the control response in the absence of test compound. The maximal degree of modulation is given as mean $\pm$ SEM. For all compounds, data are from 4-13 oocytes recorded in 2 independent experiments. Data are from P. Le and R. Perszyk, and analyzed by R. Perszyk.

subtypes to a greater extent than in saturating agonist (compare Figure 3.2A and 3.2C). We hypothesized that this agonist-dependence was due to **EU1794-27** altering the agonist potency. Therefore, we determined the glutamate and glycine EC_{50} values in the absence and presence of **EU1794-27** (Figure 3.3A,B, Table 3.3). **EU1794-27** produced modest but significant decreases (higher potency) in the EC_{50} values for both glutamate and glycine at all NMDARs (Table 3.3, Figure 3.4). Given this effect by the PAMs in this series, we subsequently considered whether the NAMs in the series shared this mechanism. We selected **EU1794-4** for use in evaluating actions on agonist potency since it retains a large steady-state current even for receptors that have bound **EU1794-4** (saturated inhibition is between 40-70% of control, Figure 3.2D). We co-applied **EU1794-4** during responses stimulated by sub-saturating concentrations of agonist (glutamate and glycine concentrations that resulted approximately in a EC_{20} response), which resulted in positive modulation (Figure 3.2E,F, Table 3.2). Furthermore, the negative modulator **EU1794-4** enhanced the glutamate and glycine potencies (Figure 3.3C,D, Table 3.4, Figure 3.4). Interestingly, positive modulation elicited by 10 µM **EU1794-4** is dependent on the sub-saturating agonist concentrations used (Table 3.5). **EU1794-4** inhibited GluN1/GluN2C responses to saturating concentrations of agonist to 54% of control, and positively modulated equivalent EC_{30} responses (equal effective concentrations of glutamate and glycine concentrations that when applied resulted in a 30% of a maximal response) to 140% of control, and positively modulated average equivalent EC_3 responses by 660% (Table 3.5). We did not observe augmentation of sub-saturating agonist responses by **EU1794-2**, most likely due to its greater extent of
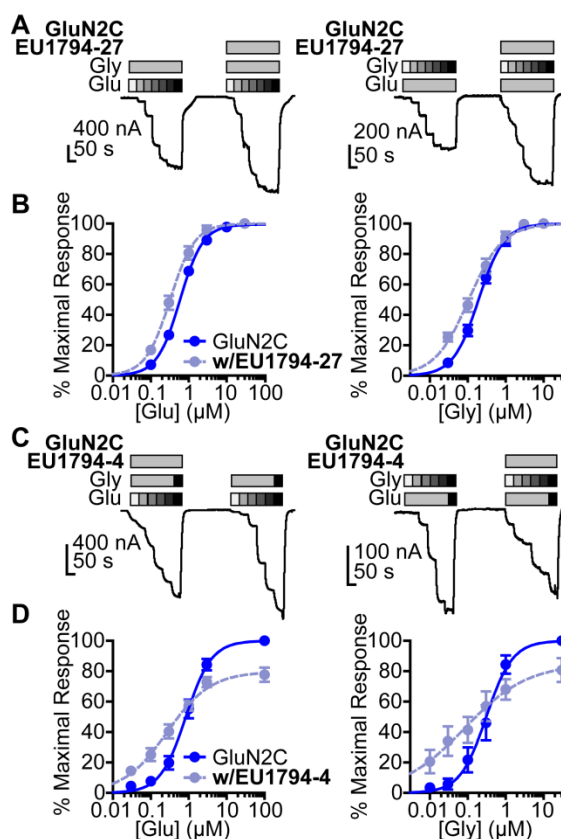
Figure 3.3. EU1794 PAMs and NAMs enhance glutamate and glycine potency.

A) Representative glutamate (left) and glycine (right) concentration-response curves of oocytes expressing GluN1/GluN2C with and without **EU1794-27** (10 μM, grey box). The glutamate concentration-response curve (0.1, 0.3, 1, 3, 10, 30 μM) was generated with 30 μM glycine and the glycine concentration-response curve (0.03, 0.1, 0.3, 1, 3, 10 μM) was recorded in 100 μM glutamate. B) Mean concentration-response data for glutamate (left) and glycine (right) at GluN1/GluN2C (see Figure 3.4 for other subunits). Each curve was normalized to the maximal response in the absence of **EU1794-27** to illustrate the actions of **EU1794-27** on agonist EC_{50}. C,D) A similar set of experiments as in (A,B), but with **EU1794-4** are shown (10 μM, grey box). Note the variation of the order of **EU1794-4** application in experimental traces, which was selected randomly. The glutamate concentration-response curve (glutamate concentration are 0.03, 0.1, 0.3, 1, 3,

and 100 μM and glycine concentrations are 10 and 30 μM) and the glycine concentration-response curve (glycine concentrations are 0.01, 0.03, 0.1, 0.3, 1, 30 μM, and glutamate concentration are 30 and 100 μM). Each curve was normalized to the maximal response from each oocyte in the absence of **EU1794-4**. Data are from 4-12 paired oocytes recordings from at least 2 independent experiments.

Table 3.3. EU1794-27 effects on glutamate and glycine EC$_{50}$ values.

	EC_{50} (µM) [conf. int.]^a					
	Control Glutamate	**EU1794-27 Glutamate**	**Fold Difference**	**Control Glycine**	**EU1794-27 Glycine**	**Fold Difference**
GluN2A	2.9 [2.2, 4.0]	1.1 [0.88, 2.1]	2.3*	0.57 [0.34, 0.96]	0.38 [0.23, 0.64]	1.6
GluN2B	1.2 [1.1, 1.3]	0.65 [0.49, 0.85]	2.0*	0.28 [0.22, 0.36]	0.14 [0.08, 0.24]	2.9*
GluN2C	0.67 [0.61, 0.73]	0.22 [0.16, 0.31]	3.3*	0.23 [0.13, 0.40]	0.10 [0.07, 0.15]	2.4
GluN2D	0.21 [0.17, 0.27]	0.054 [0.028, 0.11]	5.3*	0.086 [0.077, 0.095]	0.020 [0.013, 0.029]	4.9*

^{a} Glutamate EC$_{50}$ values (in the presence of 30 µM glycine) and glycine EC$_{50}$ values (in the presence of 100 µM glutamate) were obtained by least-squares fitting of data from independent oocyte recordings by the Hill equation. EC$_{50}$ values are given as the mean with the 95% confidence interval determined from log(EC$_{50}$). Data in the absence and presence of **EU1794-27** were obtained from the same oocyte. Data are from 5-12 paired oocytes recordings from at least 2 independent experiments. *indicates paired measurements with non-overlapping confidence intervals.
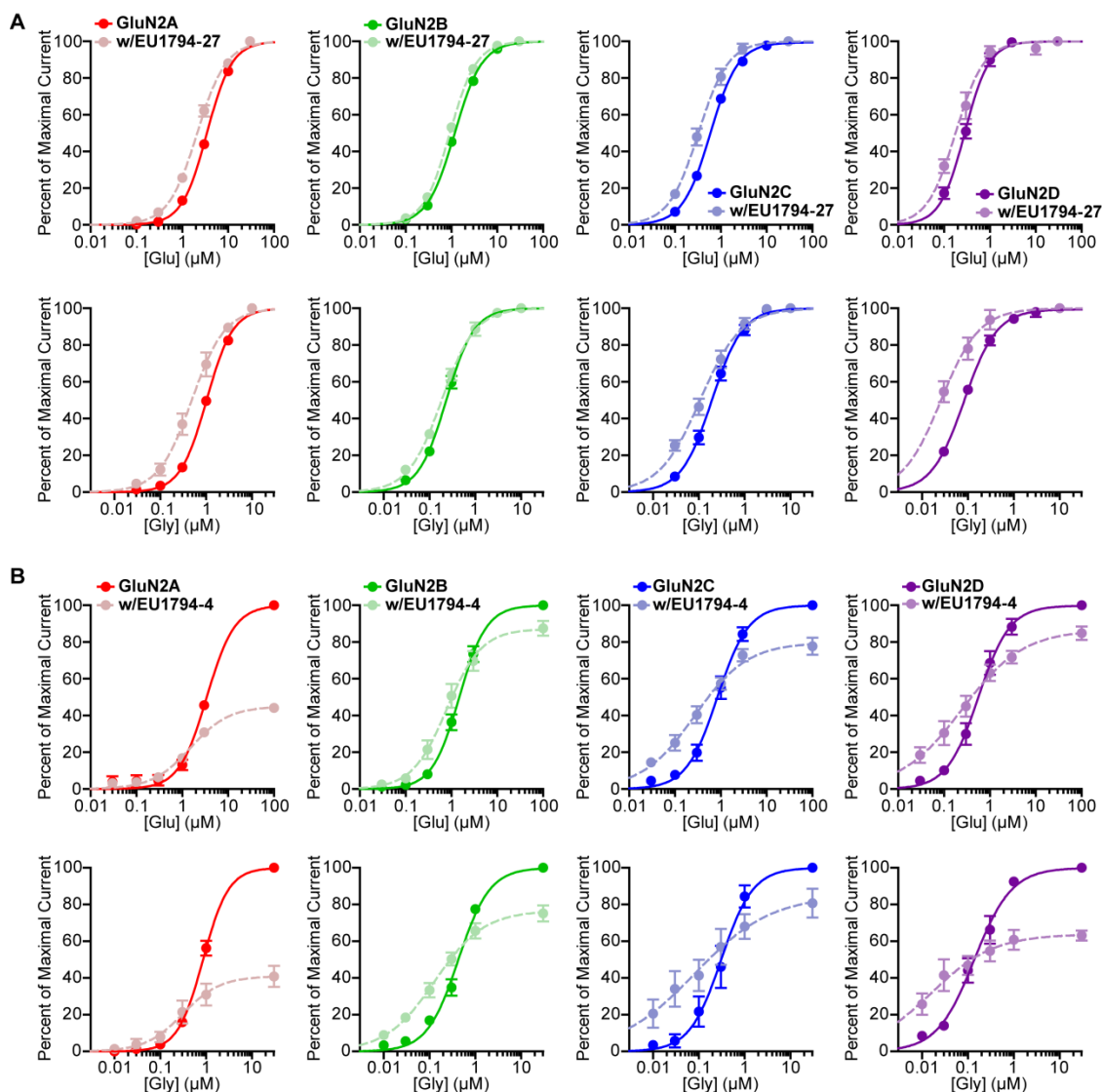
Figure 3.4. The effects of **EU1794-27** and **EU1794-4** on agonist potency of all diheteromeric NMDARs.

A) Mean concentration response data for glutamate (*top*) and glycine (*bottom*) at each diheteromeric NMDAR with and without 10 μM of the PAM **EU1794-27**. Each curve was normalized to the maximal response (either in the absence or presence of **EU1794-27**) to better illustrate the shift in agonist EC_{50}. B) A similar set of plots as in (A) but with 10 μM of the NAM **EU1794-4**. Each set of curves was normalized to the maximal

response from each cell in the absence of **EU1794-4**. Data are from 4-12 paired oocytes

recordings from at least 2 independent experiments.

Table 3.4. EU1794-4 effects on glutamate and glycine EC$_{50}$ values.

	EC$_{50}$ (μM) [conf. int.]^{a}					
	Control Glutamate	**EU1794-4 Glutamate**	**Fold Difference**	**Control Glycine**	**EU1794-4 Glycine**	**Fold Difference**
GluN2A	3.6 [3.3, 4.0]	1.5 [1.2, 2.1]	2.4*	0.89 [0.72, 1.1]	0.35 [0.17, 0.70]	2.8*
GluN2B	1.5 [1.2, 2.0]	0.8 [0.48, 1.3]	2.0*	0.46 [0.37, 0.56]	0.14 [0.12, 0.17]	3.3*
GluN2C	0.84 [0.57, 1.2]	0.29 [0.15, 0.55]	3.2*	0.31 [0.15, 0.62]	0.08 [0.024, 0.25]	4.6*
GluN2D	0.63 [0.41, 0.95]	0.17 [0.065, 0.43]	3.9*	0.15 [0.089, 0.24]	0.016 [0.007, 0.038]	8.9*

^{a} Glutamate EC$_{50}$ values (in the presence of 10 μM glycine) and glycine EC$_{50}$ values (in the presence of 30 μM glutamate) were obtained by least-squares fitting of data by the Hill equation. EC$_{50}$ values are given as the mean with the 95% confidence interval determined from log(EC$_{50}$). Data in the absence and presence of **EU1794-4** were obtained from the same oocyte. Data are from 4-8 paired oocytes recordings from 2 independent experiments. *indicates paired measurements with non-overlapping confidence intervals.

Table 3.5. Comparison of **EU1794-27**, **EU1794-4**, and **EU1794-2** effects at GluN1/GluN2C NMDAR responses to sub-saturating agonist.

GluN2C	Glu/Gly (μM)	Relative Agonist Response[a] (% of maximal response)	Modulation by 10 μM[b] (% of control)
EU1794-27	100/30	-	$190 \pm 10\%$
	1/0.3	20 ± 1.6	$480 \pm 31\%*$
EU1794-4	100/30	-	$54 \pm 1.6\%$
	1/0.3	27.7 ± 3.3	$140 \pm 12\%*$
	0.3/0.09	2.8 ± 0.7	$660 \pm 110\%*$
EU1794-2	100/30	-	$16 \pm 1.0\%$
	0.6/0.2	21.5 ± 6.8	$43 \pm 2.1\%*$

The data presented are mean ± SEM. [a]Reported average responses to sub-saturating agonist were normalized to a 100/30 μM glutamate/glycine response. [b]The degree modulation is reported as a percent of the control response to sub-saturating agonist. Some of these data points correspond to those used to calculated EC_{50} values for each modulator in Table 3.1, Table 3.2 or Table 3.6. Data are mean ± SEM. [*]$p < 0.05$ as compared to 100/30 μM glutamate/glycine response, determined by an unpaired t-test, n=4-10 cells. Some saturating agonist response data are from P. Le.

inhibition (Figure 3.5, Table 3.6). However, the degree of inhibition produced by EU1794-2 was reduced on sub-saturating responses at GluN1/GluN2C from 16% to 45% of control (Table 3.5).

PAM and NAM display both glutamate and glycine dependence

We studied NMDARs expressed in HEK293 cells to investigate the time course of modulator action. Concentration-dependent association of **EU1794-2**, **EU1794-4** and **EU1794-27** and concentration-independent disassociation were evaluated by co-applying modulator with glutamate and/or glycine (Figure 3.6A,B). We analyzed the concentration-dependence of the exponential time course describing the onset of action during co-application with saturating concentrations of glutamate plus glycine to determine modulator association and dissociation rates. From these we calculated the kinetically-determined affinity constant (K_d), which we found to be similar to the EC_{50} values determined from concentration-response experiments. **EU1794-2** K_d was 1.1 μM at GluN1/GluN2D (Figure 3.6A,B). Complex actions of **EU1794-4** and **EU1794-27** were observed, with two temporally-distinct phases of modulation evident for the association of these modulators (Figure 3.6A). Both compounds produced a rapid inhibition followed by a slowly developing potentiating phase for **EU1794-27**. The rapid association rate determined during the rapid inhibition produced by **EU1794-4** was approximately 3 times faster than **EU1794-2**; similarly, the dissociation rate was also faster for **EU1794-4** than **EU1794-2**. Quantitative analysis of the slower phases was challenging due to its lower signal-to-noise ratio. Likewise, the rapid inhibitory phase was also difficult to measure for **EU1794-27** because its rapid time course was convolved with the potentiation time
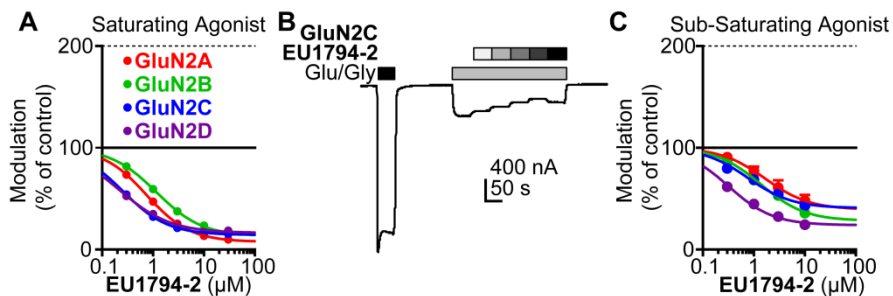
Figure 3.5. EU1794-2 actions possess modest agonist concentration-dependence.

A) Concentration-response relationship for **EU1794-2** at each diheteromeric NMDAR activated by saturating concentration of agonist (100/30 μM glutamate/glycine; data for GluN1/GluN2D is reproduced from Figure 3.1C). B) A representative recording of the response to **EU1794-2** at GluN1/GluN2C NMDARs activated by sub-saturating concentrations of agonist. The initial response was activated using saturating concentrations (100/30 μM glutamate/glycine, black box) of agonist followed by sub-saturating concentrations of agonist (0.6/0.2 μM glutamate/glycine, grey box) co-applied with increasing concentrations of **EU1794-2** (0, 0.3, 1, 3, 10, 30 μM). C) Concentration-response relationship for **EU1794-2** at each diheteromeric NMDAR activated by sub-saturating concentration of agonist (as noted in B). Saturating data are from 4-18 oocytes from at least 2 independent experiments and sub-saturating data are from 6 oocytes. Data are from P. Le and R. Perszyk, and analyzed by R. Perszyk.

Table 3.6. Comparison of **EU1794-2** effects on NMDAR responses to saturating and sub-saturating concentrations of agonist

| EU1794-2 | EC_{50} (μM) [conf. int.][a] | | | |
| | Maximal Degree of Modulation (% of control)[b] | | | |
	GluN2A	GluN2B	GluN2C	GluN2D
Saturating agonist	0.60 [0.44, 0.82][†] 6 ± 2%	1.2 [0.8, 1.9] [†] 10 ± 3%	0.21 [0.18, 0.25][†] 15 ± 1%	0.20 [0.17, 0.25][†] 14 ± 1%
Sub-Saturating agonist	1.8 [1.1, 3.0] 37 ± 7%	1.4 [1.1, 1.7] 28 ± 1%	0.72 [0.52, 1.0] 41 ± 3%	0.32 [0.26, 0.40] 24 ± 3%

[a] EC_{50} values were obtained by least-squares fitting of data from individual experiments by the Hill equation. EC_{50} values are given as the mean with the 95% confidence interval determined from $\log(EC_{50})$. Sub-saturating agonist concentrations were 0.6 μM glutamate and 0.2 μM glycine. [b]The extent of modulation is given as a percent of the control response in the absence of test compound. The maximal degree of modulation is mean ± SEM. Sub-saturating agonist data are from 6 oocytes. [†] Data from Table 3.1 is included here for clarity. Data are from P. Le and R. Perszyk, and analyzed by R. Perszyk.
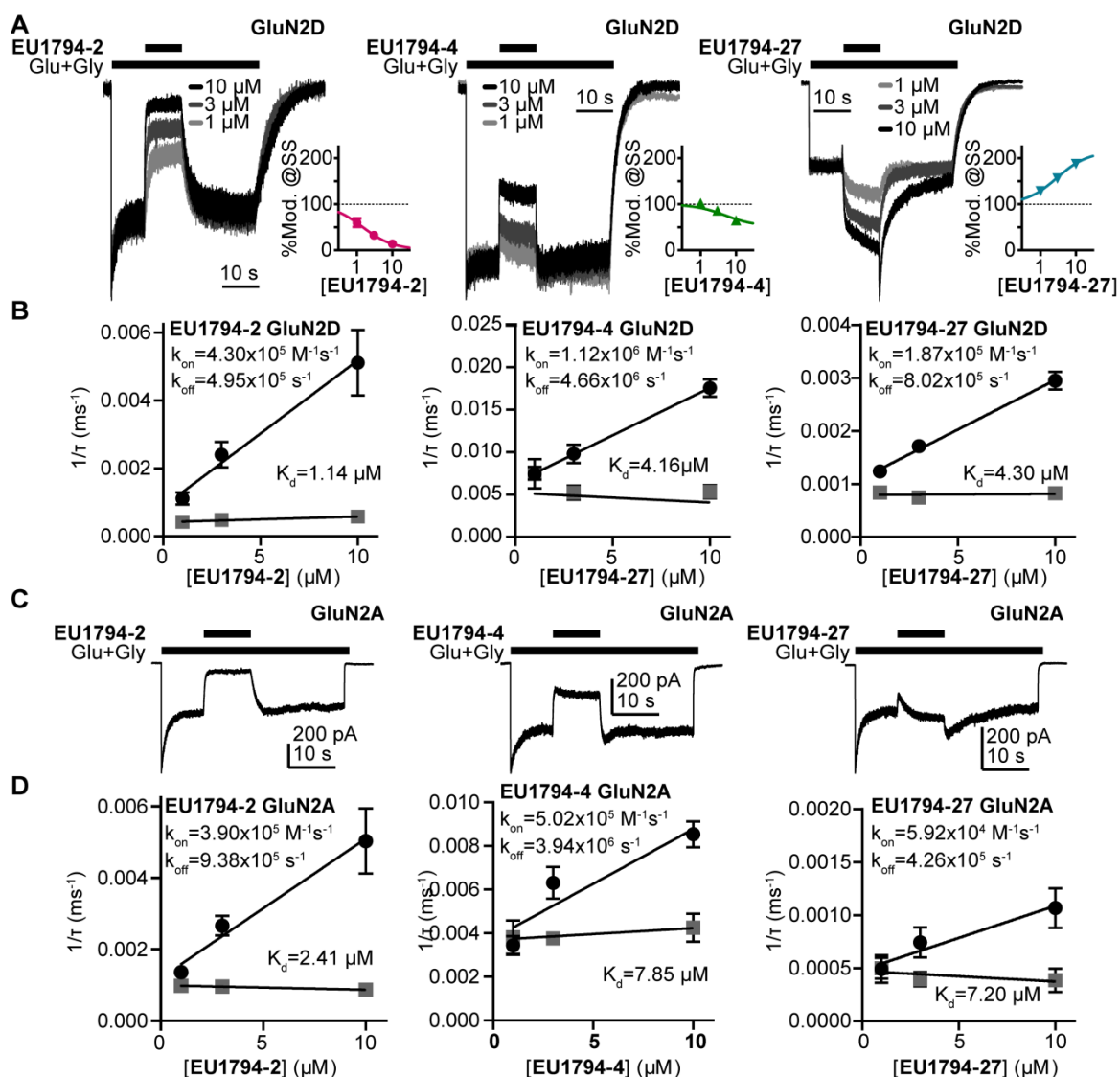
Figure 3.6. The **EU1794** series has agonist dependence that alters the response time-course.

A) Representative whole-cell current recordings of GluN1/GluN2D NMDARs exemplifying the modulation time course of **EU1794-2**, **EU1794-4** and **EU1794-27** (1, 3, 10 µM). Responses were evoked by 100/30 µM glutamate/glycine and were normalized for display. Insets show the steady state modulation extent from the HEK cell experiments fit by the Hill equation (Hill slope fixed to 1). B) Analysis of the time course for the onset of PAM and NAM action as a function of concentrations for **EU1794-2**

(*left*), **EU1794-4** (*left*) and **EU1794-27** (*right*) used to determine the association rate k_{ON} (black circles) and dissociation rate k_{OFF} (grey squares), from which we can calculate K_d for each modulator. Data are from at least 3 cells for each concentration of modulator. For **EU1794-27** the association and dissociation rate linear component was also found to be concentration dependent (m_{on} = -0.98 pA/(ms*μM), m_{off} = 0.62 pA/(ms*μM)). C,D) Similar set of panels as A,B but examining **EU1794-2**, **EU1794-4** and **EU1794-27** modulation of GluN1/GluN2A. In example recordings, all modulator concentrations are 10 μM. Data are from at least 3 cells for each concentration of modulator. For **EU1794-27** time-course was fitted with the sum of an exponential and linear function, and both the time constant and slope were concentration dependent (m_{on} = -0.33 pA/(s*μM), m_{off} = 0.16 pA/(s*μM)).

course. Additionally, the depotentiation time course is preceded by a transient enhancement of the current response, followed by a relaxation to the pre-modulation level. The time course for potentiation and depotentiation were best fit with an exponential function summed with an additional linear component after the rapid phase subsided. K_d determined from the association and dissociation rates of **EU1794-4** was 4.2 µM and **EU1794-27** was 4.3 (Figure 3.6B). All modulatory effects were independent of voltage (Figure 3.7A). The steady state modulator responses from HEK293 cells approximately match the concentration-response relationship determined from TEVC recordings from *X. laevis* oocytes (Figure 3.6A, *inset graphs*). The time-course of modulator binding of **EU1794-2**, **EU1794-4** and **EU1794-27** was also determined for GluN1/GluN2A (Figure 3.6C,D). Higher K_d values (lower potency) were determined for each molecule at GluN1/GluN2A as compared to GluN1/GluN2D that parallel EC_{50} values determined using *X. laevis* oocytes. Similar to oocyte data, robust inhibition was produced by **EU1794-2**, modest inhibition was produced by **EU1794-4,** and transient inhibition and recovery was observed by the application of **EU1794-27**. Interestingly, the extent of steady-state modulation for this series appeared to be dependent on the level of desensitization of the receptors at the time of modulator application. When classifying the cells as either having high or low levels of desensitization (using 35% steady-state/peak response as a cut-off), the extent of modulation by 10 µM was significantly different for **EU1794-27** (p=0.02, unpaired t-test, N=4,2). The low desensitized group (40% average desensitization) was modulated by 107%, whereas the high desensitized group (10% average desensitization) was modulated to 247% of control by 10 µM **EU1794-27**.
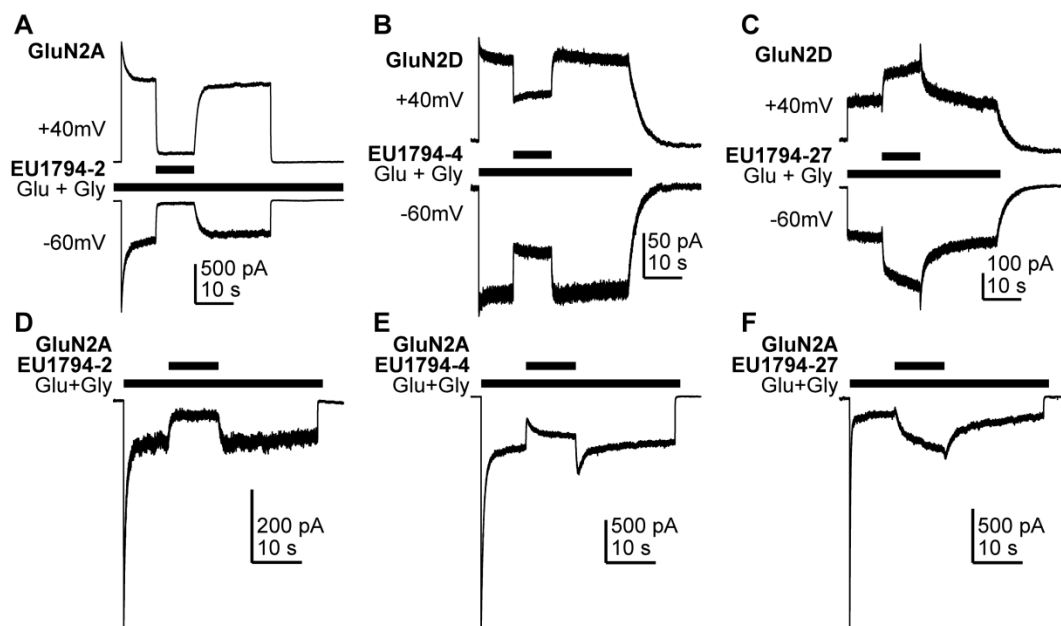
Figure 3.7. The actions of **EU1794** modulators are voltage-independent and are influenced by the desensitization level.

A-C) A representative current response of **EU1794-2** (A, the ratio of the % modulation by **EU1794-2** at +40 mV and -60 mV was 1.1 ± 0.27, n = 3), **EU1794-4** (B, the ratio of modulation at +40 mV and -60 mV was 0.88 ± 0.06, n = 6) and **EU1794-27** (C, the ratio of modulation at +40 mV and -60 mV was 0.99 ± 0.15, n = 3) modulation with the Vm held at +40 mV and -60 mV; all responses shown were using 10 μM of test compound. D-F) Representative whole-cell current recordings exemplifying the modulation time course of 10 μM **EU1794-2** (D), **EU1794-4** (E), and **EU1794-27** (F) on GluN1/GluN2A NMDAR responses with a high degree of desensitization. Responses were evoked by 100/30 μM glutamate/glycine and were normalized for display. **EU1794-2** modulated low desensitized steady state responses by 12.9% (drug/control) and high desensitized steady state responses by 32.0% (n = 3, 1). **EU1794-4** modulated low desensitized steady state responses by 46.9% and high desensitized steady state responses by 79.2% % (n = 2, 1). **EU1794-27** modulated low desensitized steady state responses by 107 ± 16% and

high desensitized steady state responses by 247 ± 31% (n = 2, 4; p = 0.028 unpaired t-test).

Given that other NMDAR modulators have displayed agonist-dependence (Petrovic 2005, Acker 2011, Hansen and Traynelis 2011, Borovska 2012, Vyklicky 2015, Wang 2017), we performed rapid solution exchange experiments to examine if these modulators had different affinities at agonist-bound and apo receptors (Figure 3.8A,B). The instantaneous current response to a rapid step into glutamate/glycine (from glycine alone) gives an estimate of whether a modulator was pre-bound to receptors with only glycine (but not glutamate) bound. The immediate NMDAR activation after a rapid switch to a solution containing glutamate and glycine should occur faster than modulator binding. We found that the peak current was similar when cells were preincubated in glycine with or without 3 μM **EU1794-2**, suggesting that **EU1794-2** does not bind appreciably to the receptor in the absence of glutamate (Figure 3.8A,C). After the rapid step into glutamate where glycine and modulator were pre-exposed, we observed a relaxation to a new response level that was similar in amplitude to that observed with steady state co-application of glutamate plus glycine and modulator (Figure 3.8A,C). Interestingly, we also observed a similar effect for the converse experiment, in which we pre-applied glutamate with or without **EU1794-2**, followed by a rapid step into glutamate plus glycine and **EU1794-2** (Figure 3.8B,C). We interpret these data to suggest that **EU1794-2** associates with the receptor with high affinity (μM) after glutamate and glycine binding.

We repeated these use-dependent experiments with **EU1794-27**, which yielded a similar result, although a slightly different experimental design was required for consistent responses. The pre-application of glycine with **EU1794-27** produced a similar level of immediate activation following glutamate application (Figure 3.8D,E). This was then followed by the complex actions observed when **EU1794-27** was applied to steady-
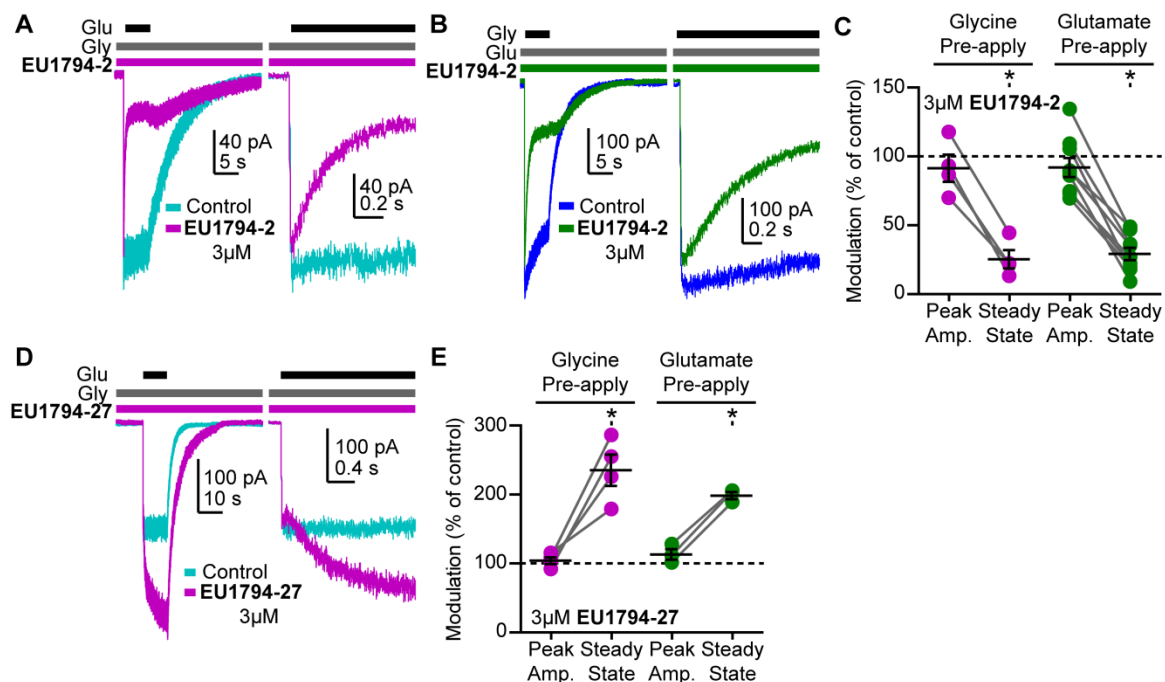
Figure 3.8. The **EU1794** series has agonist dependence that alters the response time-course.

A) Representative whole-cell recordings of GluN1/GluN2D NMDARs exemplifying the **EU1794-2** dependence on glutamate binding. The cell was exposed continuously to 30 μM glycine with/without 3 μM **EU1794-2**, and then was rapidly stepped into a solution additionally containing 100 μM glutamate. The *right panel* shows an expanded view of the rise of the receptor activation and the rapid time course of **EU1794-2** action. B) Representative whole-cell current recordings of GluN1/GluN2D NMDARs exemplifying the **EU1794-2** dependence on glycine binding. The cell was exposed continuously to 100 μM glutamate with/without 3 μM **EU1794-2**, and then was rapidly stepped into a solution additionally containing 30 μM glycine. The *right panel* shows an expanded view of the rise of the receptor activation and the rapid kinetics of **EU1794-2** action. C) Quantification of the modulation of the immediate peak response and steady state data (shown as a percentage **EU1794-2**/control for each phase) from use-dependence

experiments for **EU1794-2** (3 µM, from A,B and 3.9B). * signifies $p < 0.05$ as determined by a Bonferroni's multiple comparison test where only **EU1794-2** vs control was compared for both peak and steady state conditions after a significant repeat measures ANOVA ($F_{(3,3)} = 7.66$ for pre-applied glycine and $F_{(3,7)} = 12.4$ for pre-applied glutamate). D) Representative whole-cell current recordings of GluN1/GluN2D NMDARs exemplifying the **EU1794-27** dependence on glutamate binding. The cell was exposed continuously to 30 µM glycine with/without 3 µM **EU1794-27,** and the solution was rapidly changed to one additionally containing 100 µM glutamate. The *right panel* is an expanded view of the activation kinetics of the responses and the onset of modulation. E) Quantification of the modulation of the immediate peak and steady state response (shown as a percentage **EU1794-27**/control for each phase) from use-dependence experiments for **EU1794-27** (3 µM, from D and 3.9A). Similar to C, * signifies $p < 0.05$ from the *post hoc* Bonferroni's multiple comparison test ($F_{(3,3)} = 17.8$ for pre-applied glycine and $F_{(3,2)} = 13.5$ for pre-applied glutamate).

state responses of NMDARs (Figure 3.8D, *right panel*). Using the same protocol to pre-apply glutamate became problematic for some cells due the degree to which **EU1794-27** enhances agonist potency, a feature exemplified by the prolongation of deactivation. This action of **EU1794-27** was able to render nanomolar contaminate levels of glycine (when present) more active, which necessitated a different experimental design (Figure 3.9A). When **EU1794-2** was used in this experimental paradigm, inhibition of the contaminate level of activity was observed upon modulator application (Figure 3.9B). Nevertheless, we still observed a similar result with pre-application of glycine and **EU1794-27**, with the instantaneous response reaching the control level, followed by a slow relaxation to a new potentiated level that reflected the time course for association of **EU1794-27** after binding of both glutamate and glycine (Figure 3.8E). This result illustrates a requirement for glycine to be bound to the receptor for high-affinity binding of **EU1794-27**. To circumvent any ambiguity associated with glycine contamination, we utilized another experimental design described by Vyklicky et al. 2015. Glutamate was pre-applied with 7-CKA (100 μM) to antagonize the glycine site, blocking any occupancy by contaminant glycine. The receptor was activated by switching to a solution that lacked 7-CKA and contained glycine plus glutamate (with or without modulator, Figure 3.9C). To test the ability of **EU1794-27** to bind to the receptor with the GluN1 ABD bound to antagonist, **EU1794-27** (3 μM) was added to the solution containing 7-CKA. Upon the switch from the 7-CKA/**EU1794-27** solution containing glutamate to a solution just containing glutamate and glycine, no detectable change in the response rise time or peak amplitude was observed. If **EU1794-27** bound during the 7-CKA phase prior to agonist binding, we would have expected an increased instantaneous peak current upon switching to
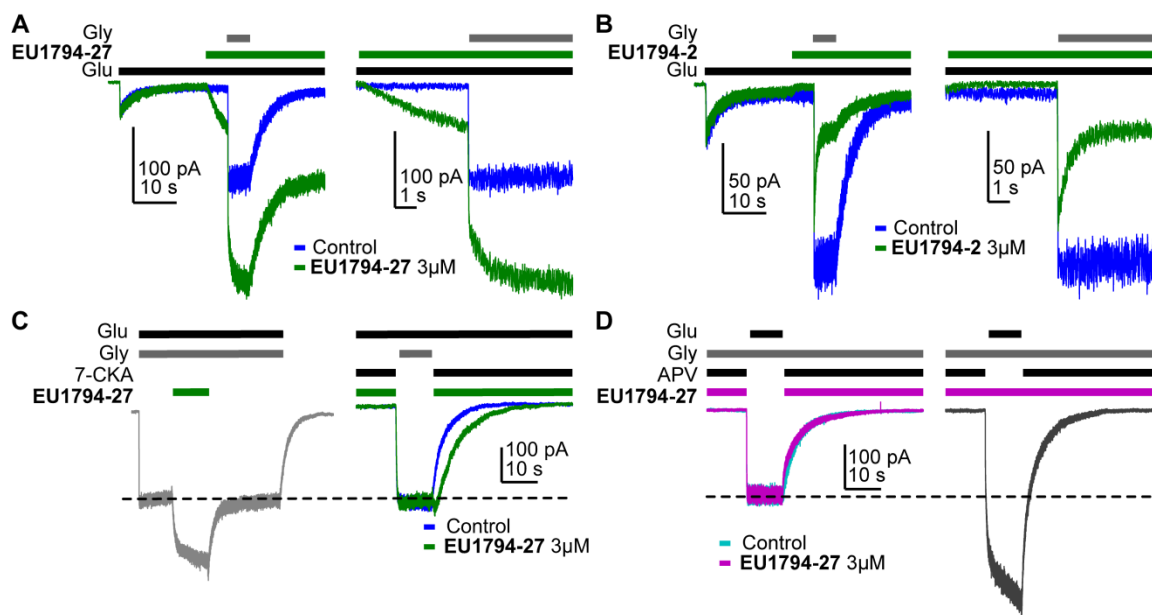
Figure 3.9. EU1794 modulators are dependent on co-agonist binding.

A) Representative whole-cell current recordings of GluN1/GluN2D NMDARs exemplifying the **EU1794-27** modulation in the presence of contaminant levels of glycine. The *left panel* shows the response to glutamate in the absence of 3 μM **EU1794-27** but with a low, unknown level of glycine. Note the initial response to just glutamate, which fades with time to a small constitutive current. When 3 μM **EU1794-27** is applied in the presence of only glutamate, there is a slowly rising response as **EU1794-27** binds and increases glycine potency, allowing the receptor to re-equilibrate with the contaminant level of glycine. The cell was then rapidly stepped to a solution containing 30 μM glycine (in addition to the previous ligands). The *right panel* shows an expanded view (grey box in the *left panel*) of the rise of the receptor activation and the rapid kinetics of **EU1794-27** action once the receptor is fully activated. Note the difference in modulation kinetics prior to full activation and during full activation. B) Representative whole-cell current recordings of GluN1/GluN2D NMDARs exemplifying **EU1794-2** modulation that is similar to the trace shown in Figure 3.8B. C) Representative whole-

cell current recordings of GluN1/GluN2D NMDARs exemplifying the **EU1794-27** modulation dependence on the closed GluN1 ABD. The left current response shows the steady state response to 3 μM **EU1794-27.** The right current response is shown for the same cell to 100 μM glutamate plus 100 μM 7-CKA either with or without 3 μM **EU1794-27** followed by a rapid change to a solution lacking 7-CKA and **EU1794-27** with 30 μM glycine. Similar results were observed in 3 cells. D) Representative whole-cell current recordings of GluN1/GluN2D NMDARs exemplifying the **EU1794-27** modulation dependence on the closed GluN2 ABD. The *left trace* shows the exposure of GluN1/GluN2D to 100 μM glutamate, 100 μM APV, and either with or without 3 μM **EU1794-27** followed by a rapid change to a solution lacking APV and **EU1794-27** but containing 30 μM glycine. The *right trace* generated from the same cell shows the response if both solutions contained **EU1794-27**. Similar results were observed in 2 cells.

glutamate plus glycine given that the dissociation of **EU1794-27** is slower than 7-CKA (compare the steady state jump and the 7-CKA jump in Figure 3.9C). Additionally, comparable experiments were performed with 100 μM APV with similar results, as APV stabilizes the GluN2 agonist binding domain (ABD) open-cleft conformation, and thereby prevents the pre-binding of **EU1794-27** (Figure 3.9D). When **EU1794-27** (3 μM) was included in all solutions, potentiation was observed but APV unbinding was a required prior to modulation (Figure 3.9D). Together these data suggest that the **EU1794** series is capable of high affinity binding only when glutamate and glycine are bound to the receptor.

Evaluation of interactions with known modulatory sites

To identify the molecular determinants of action for the **EU1794** series, we evaluated the ability of GluN2 ATD deletion, GluN1 ATD splice variants, and co-application of known modulators to alter the effects of the **EU1794** modulators. The ATD harbors the binding site for the GluN2B-selective negative allosteric modulator ifenprodil. Deletion of the ATD from GluN2A, GluN2B, or GluN2C had no effect on the actions of the PAM **EU1794-27**; deletion of the ATD from GluN2D reduced but did not eliminate potentiation (Figure 3.10A). Similarly, inclusion of 21 residues in the ATD encoded by alternatively spliced GluN1 exon5 only slightly altered the extent of potentiation of **EU1794-27**, but was without effect on EC_{50} for potentiation of GluN2B- and GluN2D-containing NMDARs activated by saturating agonist (Figure 3.10B). We previously described a similar result for the negative allosteric modulator **EU1794-2**
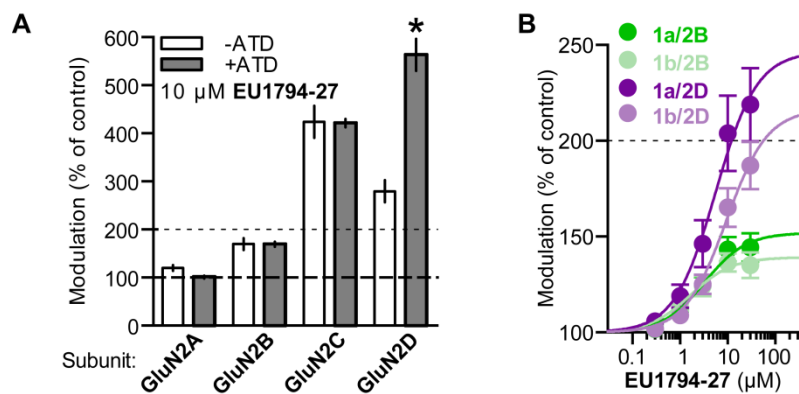
Figure 3.10. EU1794 series effects are not altered by ATD perturbations.

A) 10 µM **EU1794-27** potentiates GluN2-ΔATD NMDARs (n = 4-12). B) Concentration-response curves for **EU1794-27** potentiation of GluN2B and GluN2D with GluN1-1a and GluN1-1b (with and without exon5, respectively, n = 6-10). * signifies $p < 0.05$ as determined by an unpaired t-test.

(Katzman 2015). These data are consistent with minimal involvement of the GluN1 or GluN2 ATD in the actions of **EU1794** modulators.

We next screened for interaction with known modulators to focus our search for the molecular determinants of **EU1794** series modulation (Mullasseril 2010, Acker 2011, Hansen and Traynelis 2011, Hansen 2012, Khatri 2014, Ogden 2014, Hackos 2016, Tajima 2016, Yi 2016) (Figure 3.11A). In these experiments, a known positive or negative modulator was co-applied with either **EU1794-2** or **EU1794-27**, with each pair always containing one PAM and one NAM. If there is no interaction between paired modulators, their combined activity should be predicted by multiplying the extent of their independent actions. Co-application of the modulator pairs ifenprodil/**EU1794-27**, **EU1794-2**/CIQ and **EU1794-2**/PYD-106 produced levels of modulation that largely could be predicted from their independent actions (Figure 3.11B, *top row*). Modest differences from predictions were observed with modulators that bind to the ABD interface, TCN-201/**EU1794-27**, **EU1794-2**/GNE-6901 and **EU1794-2**/GNE-0723 (Figure 3.11B, *bottom left*). Co-application of the GluN2C/GluN2D-selective negative allosteric modulators QNZ46 and DQP-1105 paired with **EU1794-27** resulted in the greatest divergences from predictions, raising the possibility that these modulators have partially overlapping binding sites (Figure 3.11B, *bottom right*) or similar downstream mechanisms.

We also examined the ability of **EU1794-2** and **EU1794-27** to modulate NMDARs harboring mutations within the structural determinants for other known allosteric modulators. Mutations in GluN1 (I519A, R755A) and GluN2A (L780A, G786A) that block TCN-201 inhibition were evaluated for effects on **EU1794** series of
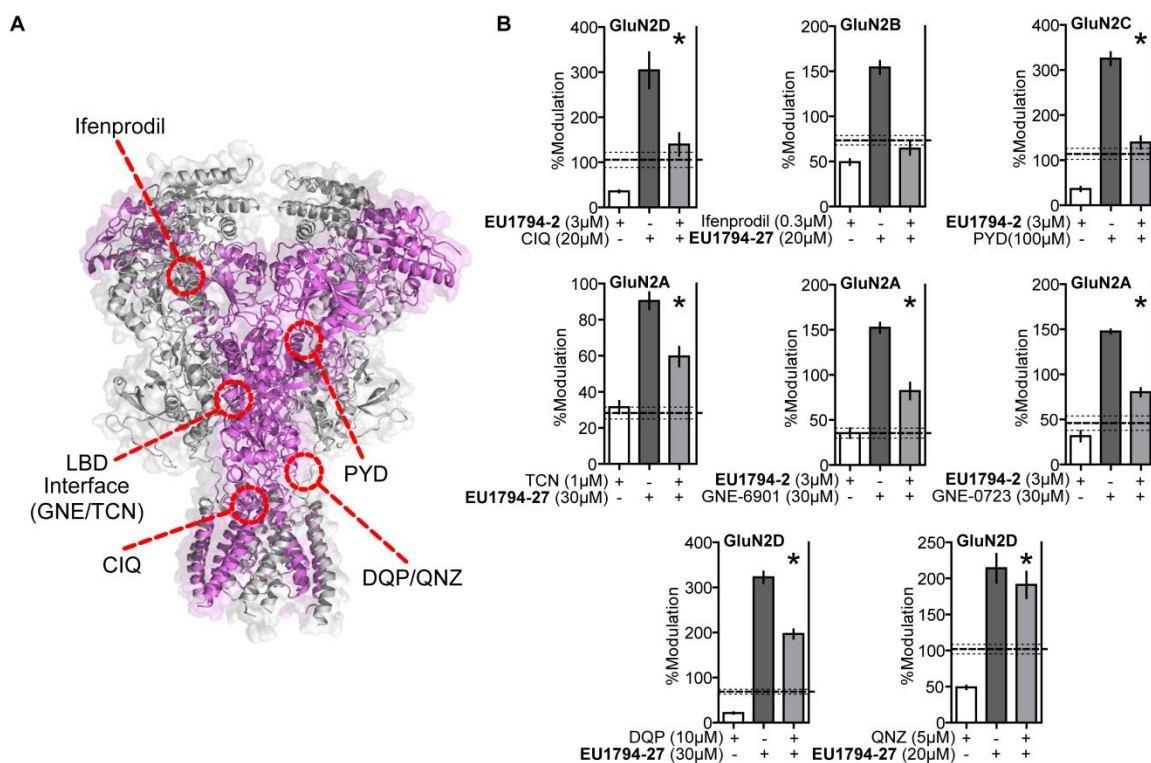
Figure 3.11. Compound competition screen of the **EU1794** series with NMDAR modulators highlights potential interactions with the ABD and the TMD.

A) Overlaid surface and ribbon representations of the GluN1/GluN2D model highlighting proposed ligand binding sites for ifenprodil (Karakas 2011), PYD-106 (Khatri et al 2014), CIQ (Ogden and Traynelis 2013), GNE-6901 (Hackos and Hanson 2017), TCN-201 (Yi 2016), DQP-1105 (Acker 2011), and QNZ-46 (Hansen and Traynelis 2011). B) Single concentration competition experiments are summarized for ifenprodil (0.3 μM, on GluN1/GluN2B, n=10), CIQ (20 μM, GluN1/GluN2D, n=15), PYD-106 (100 μM, GluN1/GluN2C, n=14), TCN-201 (1 μM, 1 μM glycine, GluN1/GluN2A, n=11), GNE-6901 (30 μM, GluN1/GluN2A, n=6), GNE-0723 (30 μM,GluN1/GluN2A, n=6), DQP-1105 (10 μM, GluN1/GluN2D, n=10), and QNZ-46 (5 μM, GluN1/GluN2D, n=8) co-administered with maximally effective glutamate and glycine plus either **EU1794-2** (3 μM) or **EU1794-27** (20 μM). The individual average effects of the pairs of modulators

along with the co-applied effect are plotted, and the predicted mean net effect of the modulators is displayed as a dashed line (surrounded SEM, dotted lines). * signifies p < 0.05 as determined by a paired t-test comparing co-applied modulators and predicted net effect of modulator actions. All pairs were tested during two independent experiments sessions.

modulators (Vance 2012). NMDARs that contained GluN1/GluN2A(L780A), GluN1/GluN2A(G786A), GluN1(R755A)/GluN2D, GluN1(I519A)/GluN2D were equally sensitive as wild type receptors to inhibition by EU1794-2 or potentiation by EU1794-27 (Figure 3.12A). GluN1/GluN2A(E530A), GluN1/GluN2A(V783W), GluN1(Y535W)/GluN2A, GluN1(Y535V)/GluN2D and GluN1(Y535W)/GluN2D, which reduce the actions of GNE-6901 and GNE-0723 (Hackos and Hanson 2017), produced no significant effects on inhibition by **EU1794-2** or potentiation by **EU1794-27** (Figure 3.12B). Inhibition by **EU1794-2** of GluN1/GluN2C(K470G) and GluN1/GluN2C(S472T), which block PYD-106 potentiation of GluN1/GluN2C (Ogden 2014), was similar to wild type NMDARs (Figure 3.12C). Interestingly, inhibition by **EU1794-2** and potentiation by **EU1794-27** was not significantly changed by GluN1/GluN2D(Q701Y) and GluN1/GluN2D(L705F), mutations that appear to confer subunit selectivity for GluN2C/D over GluN2A/B for QNZ-46 and DQP-1105 (Figure 3.12D) (Acker 2011, Hansen and Traynelis 2011).

Mutagenesis suggests shared structural determinants of action for PAMs and NAMs

The result obtained with the QNZ-46/DQP-1105 interaction test suggested that the two residues we evaluated for QNZ-46 and DQP-1105 insufficiently probed the structural determinants of action for these compounds. We therefore examined a GluA2 AMPA receptor structure bound to CP-465,022, which shares a core scaffold with QNZ modulators (Yelshanskaya 2016). Residues identified as being important for CP-465,022 binding in Yelshanskaya et al. (2016) were aligned to the GluN1 and GluN2D subunits to map this site onto the NMDAR subunits, in addition to critical residues for GNE-9278 in
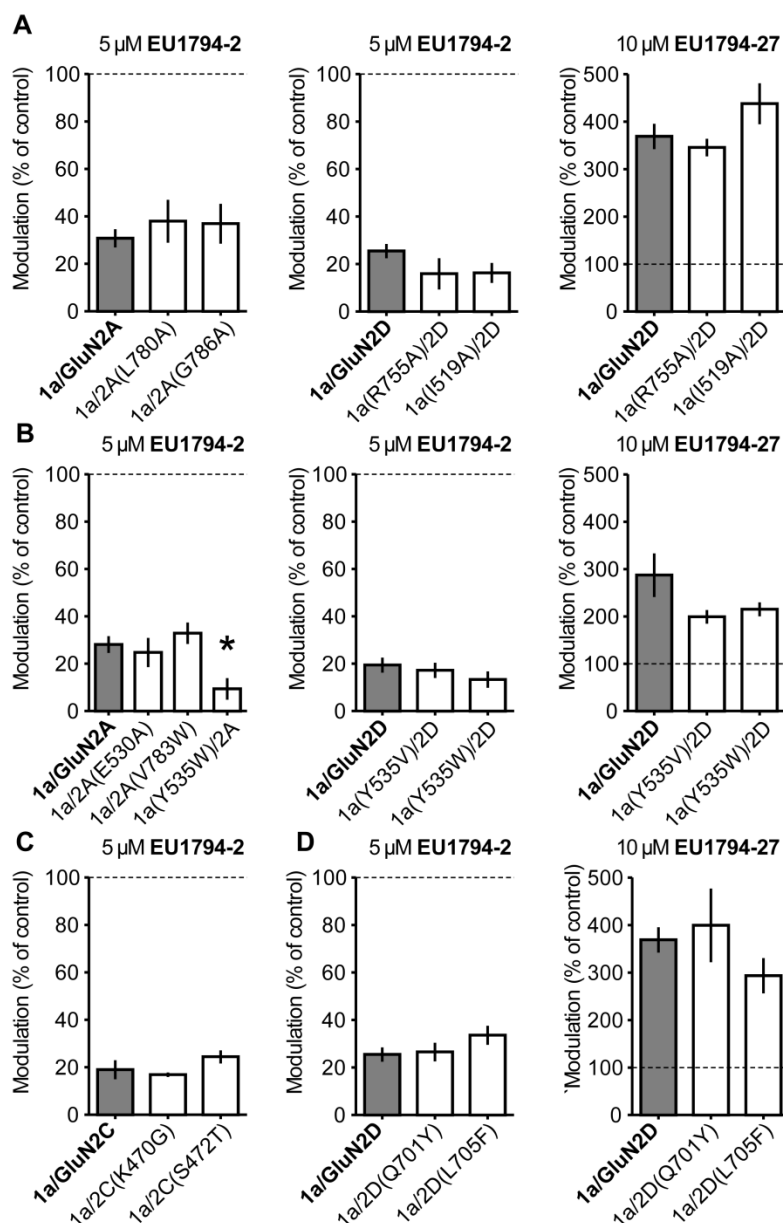
Figure 3.12. Residues in known modulator binding sites do not perturb actions of the **EU1794** series.

A) Inhibition by 5 μM **EU1794-2** (*left* and *middle*) and potentiation by 10 μM **EU1794-27** (*right*) on NMDARs possessing mutations known to alter the activity of TCN-201 as compared to wild type GluN1/GluN2A (*left*) and GluN1/GluN2D (*middle* and *right*) (Vance 2012, Yi 2016). B) Inhibition by 5 μM **EU1794-2** (*left* and *middle*) and

potentiation by 10 μM **EU1794-27** (*right*) on NMDARs possessing mutations that alter the activity of GNE-6901 and GNE-0723 as compared to wild type GluN1/GluN2A (*left*) and GluN1/GluN2D (*middle* and *right*) (Hackos and Hanson 2017). C) Inhibition by 5 μM **EU1794-2** on NMDARs possessing mutations that alter the activity of PYD-106 as compared to wild type GluN1/GluN2C (Ogden 2014). D) Inhibition by 5 μM **EU1794-2** (*left*) and potentiation by 10 μM **EU1794-27** (*right*) on NMDARs possessing mutations that alter the activity of DQP-1105 and QNZ-46 as compared to wild type GluN1/GluN2D (Acker 2011, Hansen and Traynelis 2011). Wild type GluN1/GluN2D data is the same as in (A). Data represent recordings from 3-9 oocytes.

this same region (Figure 3.13A) (Wang 2017). This broader range of residues were located on the pre-M1, M3, and pre-M4 regions of both GluN1 and GluN2D, which have previously been suggested to cooperate to control gating (Chen 2017, Ogden 2017). These residues were suggested by Yelshanskaya et al. (2016) to constitute a binding site in homomeric GluA2 AMPARs. However, mapping the homologous residues onto NMDAR structures yields two pockets given the multimeric subunit architecture, one of which consists of the residues of GluN1 and the other of residues of GluN2. Certain residues of M3, depending on their position on the helix, could point towards either pocket, rendering the two pockets to be lined by a mixture of GluN1 and GluN2 residues. 15 GluN1 and 15 GluN2D residues in these two regions that probed these pockets were identified and mutated to allow a test of the contribution of each residue to EU1794-2 inhibition and EU1794-27 potentiation. Inhibition by EU1794-2 was significantly altered by substitutions at 6 residues in GluN1 and 2 GluN2D residues (Figure 3.13B), which were found on pre-M1 and M3 regions of both GluN1 and GluN2D. Potentiation by EU1794-27 was more labile, being altered in mutations at 9 GluN1 residues and 6 GluN2D residues (Figure 3.13B). Residues that perturbed the actions of EU1794-27 were spread across all regions tested except for the GluN2D pre-M1. Modulation was observed to be altered in 3 different ways by the mutations studied here: activity could be reduced, increased, or inverted.

The distributions of residues that altered modulation by **EU1794-2** and **EU1794-27** shows clear overlap (Figure 3.13C). Inhibition by **EU1794-2** was altered primarily by mutations in GluN1, whereas potentiation by **EU1794-27** was perturbed by residues both in GluN1 and in the M3 helix of GluN2D. Interestingly, the mutations that invert activity
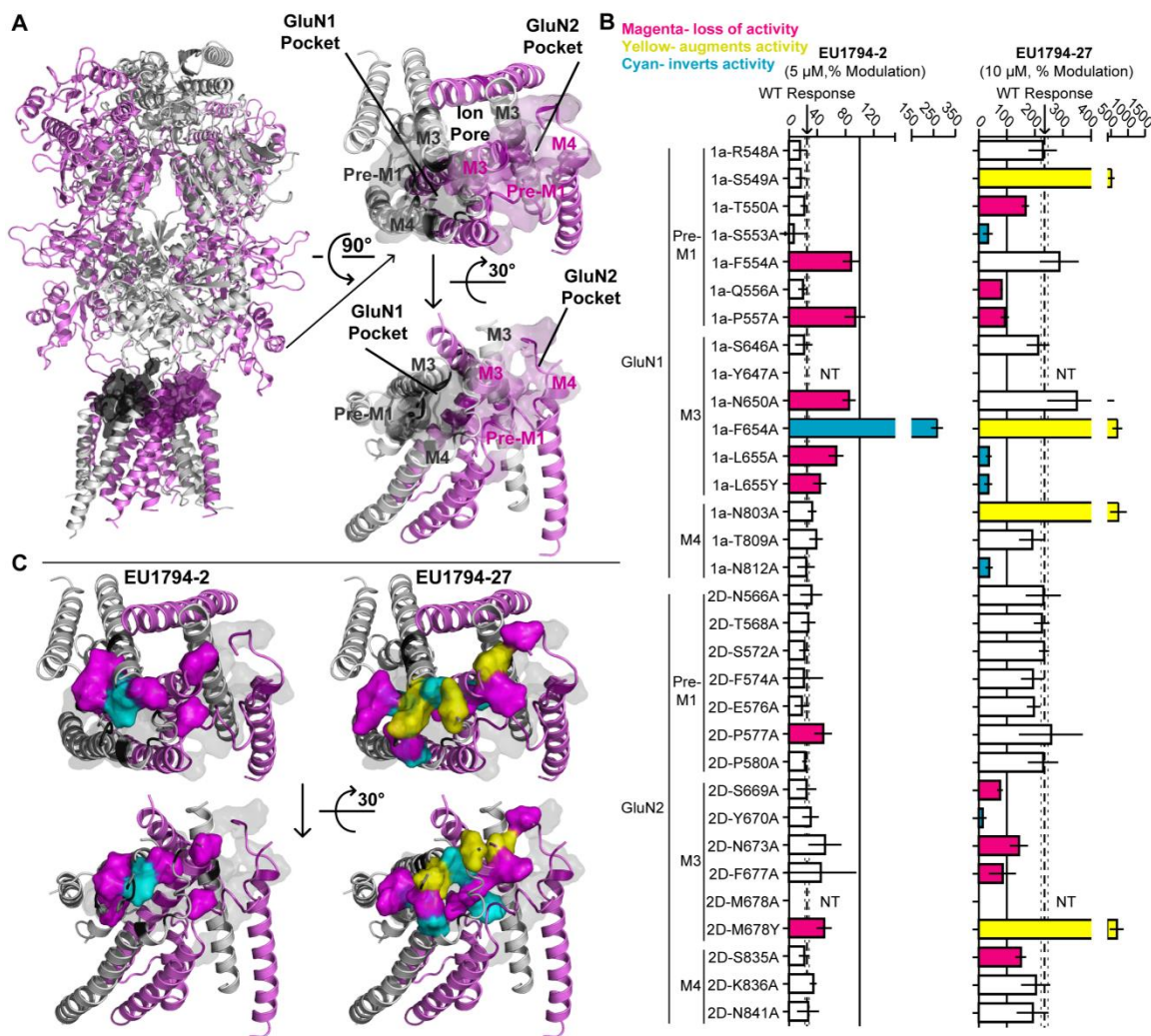
Figure 3.13. Distinct and overlapping pattern of residues contribute to the actions of **EU1794** modulators with opposing actions.

A) Ribbon representation (*left*) of a GluN1/GluN2D model based on published crystal structures of GluN1/GluN2B and GluA2 (Karakas and Furukawa 2014, Lee 2014, Yelshanskaya 2016). The GluN1 subunits are grey and the GluN2D are purple; surface shell indicate residues of interest in GluN1 and GluN2D, including residues that are homologous to those identified in recent studies investigating transmembrane domain interacting modulators of NMDAR and AMPAR (Yelshanskaya 2016, Wang 2017). These GluN1 and GluN2D residues were changed to alanine (or tyrosine in two cases, as

previously reported) and tested for effects on the NMDAR sensitivity to **EU1794-2** and **EU1794-27**. Top down (*right top*) and side (*right bottom*) view of the model TMD and linker segments, to highlight one set of pockets the foreground GluN1 and GluN2 TMD are displayed in full along with the background GluN1 and GluN2 M3 helices. The residues comprise two pockets, one primarily associated with GluN1 and the other GluN2. B) The modulation response (mean ± 99% CI) of **EU1794-2** (5 μM, *left*) and **EU1794-27** (10 μM, *right*) are shown as a % of the mutant receptor response to 100 μM glutamate and 30 μM glycine in the absences of the test compound. The wild type mean response is shown by the dashed line, surrounding dotted lines, which indicate the 99% confidence interval. Residues with non-overlapping confidence intervals with the wild type are colored with red indicating apparent loss of activity, cyan indicating augmented activity, and purple indicating robust inverted modulation. Data for the mutations shown represent 4-18 oocytes from at least 2 independent experiments and the wild type response shown represent 83 oocytes for **EU1794-2** and 76 oocytes for **EU1794-27,** recorded each experimental day to ensure consistency. We were not able to test all mutant receptors due to low expression for some (NT, not tested). C) The residues (shown by the space-filling shell) identified in (B) that altered the effects of **EU1794-2** (*left*) and/or **EU1794-27** (*right*) were mapped onto the model with colors as described in (B). Views are the same as (A), with the all residues probed shown as grey transparent shell representation. Data are from H. Kusumoto and R. Perszyk, and analyzed by R. Perszyk.

of **EU1794-2** and **EU1794-27** were distinct, but in some cases were in close proximity. For example, **EU1794-2** was inverted by GluN1-F654A, whereas mutation of the adjacent residue GluN1-L655A/Y inverted the modulatory action of **EU1794-27** (Figure 3.13B,C). **EU1794-27** potentiation was also converted to inhibition by 4 mutations at residues residing on the 3 areas of GluN1 that were investigated (pre-M1, M1, M3) and also on the M3 GluN2D helix, which were in close proximity to each other (Figure 3.13C). **EU1794-27** actions on GluN1-L655A/Y and GluN2D-M678Y, which are homologous residues immediately downstream of the SYTANLAAF motif, resulted in opposite effects (GluN1-L655A/Y converts **EU1794-27** to an inhibitor and GluN2D-M678Y increases the potentiation of **EU1794-27**). We interpret these results to suggest that the activity of both PAMs and NAMs of the **EU1794** series is dependent on multiple residues in the GluN1 subunit, some of which are overlapping. Furthermore, potentiation by **EU1794-27** is dependent on a wider range of GluN1 and GluN2 residues. One possible way to account for this would be if both modulators bound near the GluN1 pre-M1 helix, with potentiator actions dependent on the nearby GluN2 M3 residues associated with the GluN1 pocket (Fig 3.13A,C).

PAMs and NAMs exert their opposing effects via a shared binding site on NMDARs

Given the similarity in chemical structure between positive and negative modulators in this series, we hypothesized that they might have overlapping binding sites. In order to conduct a detailed functional analysis of competition between allosteric modulators, we first used modeling to examine a receptor's functional response to co-application of positive and negative modulators acting at the same or different sites. We

evaluated two models of modulator binding built into a scheme first proposed by (Lester and Jahr 1992) to evaluate the equilibrium response of modulator action. *Model 1* describes receptors with a single binding site that can accommodate either PAM or NAM, but not both. *Model 2* describes a receptor to which both modulators can bind at the same time in different sites (Figure 3.14A, Figure 3.15). We evaluated hypothetical responses from these models (see *Methods*, Figure 3.15A-C). Responses to maximally effective concentrations of agonist were simulated at various concentrations of the positive and negative modulators. When the modulators compete for the same binding site, they act similarly to stated theory about competitive antagonists (Arunlakshana and Schild 1959, Christopoulos and Kenakin 2002), with the PAM causing a rightward shifting NAM IC_{50} and generating a linear relationship in dose ratio analysis (Figure 3.14B, Figure 3.15D,E, *Model 1*). By contrast, there is no apparent EC_{50} shift when the two modulators are capable of binding simultaneously (Figure 3.14C, Figure 3.15D,E, *Model 2*). Additional simulations showed the reciprocal effect of NAM on PAM EC_{50} (Figure 3.15F,G). We subsequently performed competition experiments to test the hypothesis that this series of PAMs and NAMs compete for a mutually exclusive modulatory pocket (Figure 3.14D). We observed that fixed concentrations of the PAM **EU1794-27** caused parallel shifts in the concentration-response curve of the NAM **EU1794-2** (Figure 3.14E, Table 3.7). A similar phenomenon was shown for the reverse, as fixed concentrations of **EU1794-2** caused parallel shifts in the **EU1794-27** concentration-response curves (Table 3.7). These results closely match *Model 1*, where PAMs and NAMs bind in a mutually exclusive fashion. This suggests that the opposing modulators in the **EU1794** series share
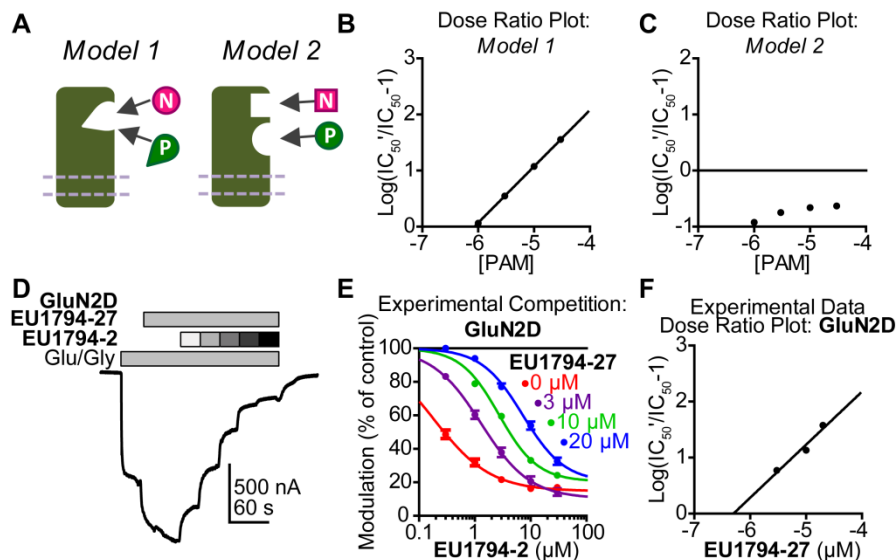
Figure 3.14. EU1794 PAMs and NAMs act in a competitive manner that matches receptor models with mutually exclusive modulator binding.

A) Cartoon models of potential modulator binding schemes. *Model 1* possesses mutually exclusive modulator binding whereas *Model 2* can bind either or both modulators. Ligands are denoted by [N] (NAM) and [P] (PAM). B,C) Dose-ratio plots of the simulated concentration response curves of the NAM in various concentration of the PAM for *Model 1* (B) and *Model 2* (C). IC_{50}' is the observed NAM IC_{50} in the presence of a fixed concentration PAM. D) A representative TEVC recording (fixed 3 μM **EU1794-27** and 0.3, 1, 3, 10, 30 μM **EU1794-2**) of GluN1/GluN2D NMDARs (top). E) The mean steady state responses in (D) were fitted by the Hill equation. Concentration-response data in the absence of **EU1794-27** are included for comparison from Figure 1C. F). Dose-ratio analysis of experimental data determining the shift in the IC_{50} of the NAM as a function of PAM concentration. Data are from at least 6 oocytes evaluated from 2 independent experiments.
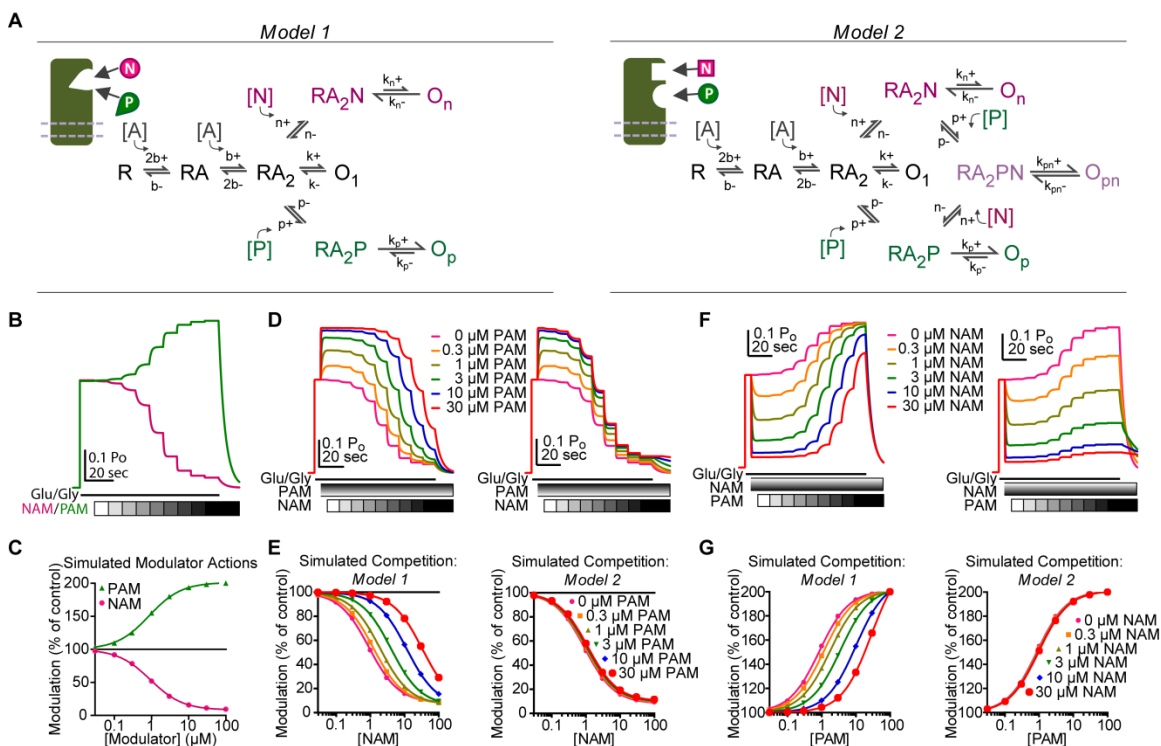
Figure 3.15. EU1794 PAMs and NAMs act in a competitive manner that suggests mutually exclusive modulator binding.

A) Cartoon and Markov models of potential modulator binding schemes. *Model 1* possesses mutually exclusive modulator binding whereas *Model 2* can bind either or both modulators. Ligand dependent transitions are denoted by [A] (agonist), [N] (NAM), [P] (PAM). B) Simulated concentration-response curves of hypothetical modulator actions on an agonist-saturated response of *Model 1* and *2* (NAM EC_{50} 0.89 μM, PAM EC_{50} 0.85 μM). C) Simulation of co-administered hypothetical modulators for *Model 1* (left) and *Model 2* (right) to an agonist-saturated response. Responses to NAM concentrations (0.03, 0.1, 0.3, 1, 3, 10, 30, 100 μM) were simulated in the presence of fixed concentrations of PAM (0, 0.3, 1, 3, 10, 30 μM). D) Simulated concentration-response data fit by the Hill equation for *Model 1* (left) and *Model 2* (right). F) Simulated responses for co-application of multiple modulators using *Model 1* and *Model 2* (*left and*

right, respectively). The current response to saturating agonist concentration was simulated in the presence of eight PAM concentration responses (0.03, 0.1, 0.3, 1, 3, 10, 30, 100 µM) and fixed concentrations of NAM (0, 0.3, 1, 3, 10, 30 µM). G) The steady-state responses from each condition was plotted as a function of concentration and fit by the Hill equation. Rates used are (concentration dependent rates in µM s^{-1}) $b^+ = 10.4$ $[A]*s^{-1}$, $b^- = 73\ s^{-1}$, $k^+ = 501.6\ s^{-1}$, $k^- = 790\ s^{-1}$, $n^+ = 0.786\ [N]*s^{-1}$, $n^- = 0.393\ s^{-1}$, $p^+ = 0.786\ [P]*s^{-1}$, $p^- = 0.786\ s^{-1}$, $k_n^+ = 25.08\ s^{-1}$, $k_n^- = 790\ s^{-1}$, $k_p^+ = 1003.2\ s^{-1}$, $k_p^- = 790\ s^{-1}$, $k_{pn}^+ = 50.16\ s^{-1}$, $k_{pn}^- = 790\ s^{-1}$. Data are from at least 6 oocytes evaluated from 2 independent experiments.

Table 3.7. The response to co-application of **EU1794-2** and **EU1794-27** suggest a common binding site.

	EU1794-2 IC_{50} (µM) [conf. int.]^a				EU1794-27 EC_{50} (µM) [conf. int.]^a		
	+ EU1794-27				+ EU1794-2		
	0 µM	3 µM	10 µM	20 µM	0 µM	1 µM	3 µM
GluN2A	0.60† [0.44, 0.82]	2.5* [1.9, 3.1]	3.6* [2.4, 4.8]	8.0* [1.3, 15]	-$^\#$	-$^\#$	-$^\#$
GluN2B	1.2† [0.8, 1.9]	NR	3.5* [2.1, 4.9]	12 [~, 26]	1.4† [1.2, 1.7]	6.0* [4.6, 7.4]	8.4 [~, 18]
GluN2C	0.21† [0.18, 0.25]	1.2* [0.91, 1.4]	2.4* [1.8, 3.0]	6.0* [4.1, 7.8]	2.8† [2.5, 3.2]	7.3* [5.9, 8.8]	7.3 [2.1, 11.74]
GluN2D	0.20† [0.17, 0.25]	1.4* [1.2, 1.6]	2.7* [2.3, 3.2]	7.3* [4.6, 9.9]	2.4† [1.8, 3.3]	7.5* [5.6, 9.3]	7.8 [1.1, 14]

A 5 point concentration response curve was obtained for modulator effects on responses to maximally effective concentrations of glutamate and glycine (100/30 µM) for **EU1794-2** co-administered with increasing concentrations of **EU1794-27**, and for **EU1794-27** in increasing concentrations of **EU1794-2**. $^a IC_{50}$ and EC_{50} values were obtained by least-squares fitting of data by the Hill equation. IC_{50} and EC_{50} values are given as the mean with the 95% confidence interval determined from $\log(IC_{50})$ or $\log(EC_{50})$. Data are from at least 6 oocytes evaluated from 2 independent experiments for the **EU1794-2** IC_{50} determinations and from at least 3 oocytes evaluated from 1 experiment for the **EU1794-27** EC_{50} determinations. NR, Given the low potency for modulators at GluN2B, the **EU1794-2** concentration-response curve with 3 µM **EU1794-27** determination was not recorded. *indicates non-overlapping 95% confidence interval with the **EU1794-2** IC_{50} without **EU1794-27** or **EU1794-27** EC_{50} without **EU1794-2**. $^\#$**EU1794-27** does not potentiate GluN2A responses to maximally effective concentrations of glutamate and glycine. †Data from Table 3.1 is included here for clarity. ~ indicates that the confidence interval hit a theoretical limit ($EC_{50} < 0$).

overlapping binding sites instead of the coincidence that the subtle chemical differences confer unique binding sites. The enantiomers of **EU1794-27** were separated to determine whether the racemic activity reflected the actions of only one enantiomer. **(-)-EU1794-27** potentiated NMDAR responses similarly to the racemic mixture (Figure 3.16A, Table 3.8). By contrast, **(+)-EU1794-27** exhibited only weak potentiation of GluN1/GluN2C and GluN1/GluN2D, which may be due to the purity achieved via chiral separation (Table 3.8). We previously reported (Katzman 2015) that purified enantiomers were likely to racemize in aqueous solutions, which should proceed by a first-order reaction dependent on multiple factors such as ionic strength, pH, buffer, etc. (Smith 1978). Thus, to quantitatively determine if racemization would impact our experiments using the enantiomers, we performed a functional assessment of this property in our standard experimental solution. We observed racemization of the enantiomers of **EU1794-27** with a half-life of 197 minutes (Figure 3.16A, Table 3.8). Both enantiomers of **EU1794-4** inhibited NMDAR responses, but with different potencies (Figure 3.16C, Table 3.9). A similar rate of racemization was observed for the enantiomers of **EU1794-4** (196 min, Figure 3.16D), consistent with the idea that the structural determinants of positive and negative modulation by **EU1794-27** and **EU1794-4** are distal to the chiral center. All enantiomer studies, other than the racemization time-course, were performed rapidly to minimize any racemization, being completed in less than 80 minutes after making the aqueous solution of modulator. Similar to results in oocytes, when the enantiomers of **EU1794-27** were applied to steady-state GluN1/GluN2D responses in HEK cells, (-)-**EU1794-27** potentiated responses whereas (+)-**EU1794-27** had a slight inhibitory effect
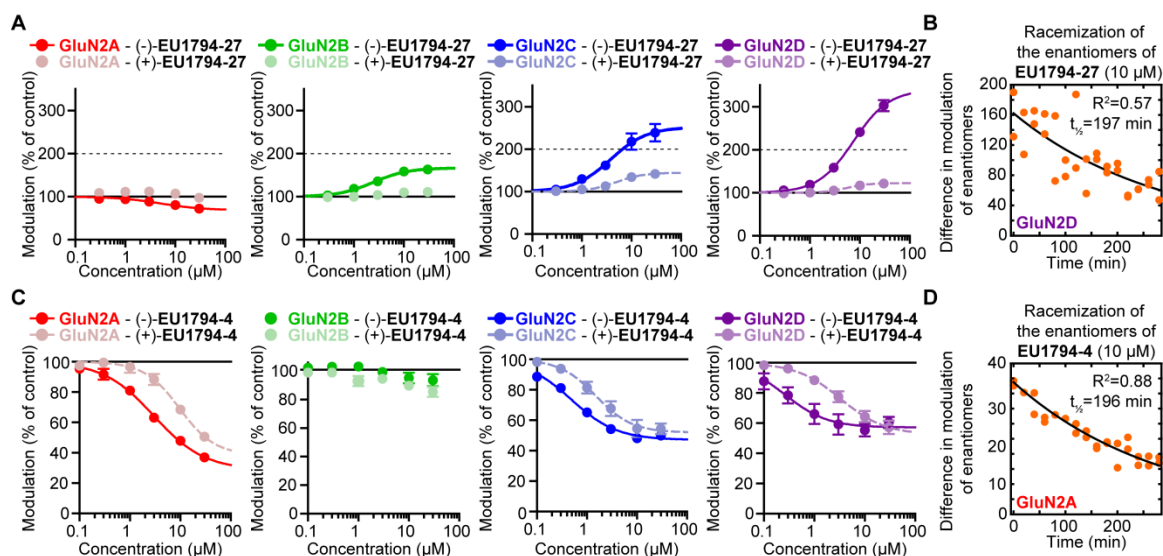
Figure 3.16. Activity of the enantiomers of **EU1794-27** and **EU1794-4**.

A) The concentration-response relationships illustrate the selective action of the enantiomer (-)-**EU1794-27**. Responses were activated with 100/30 μM glutamate/glycine and modulated with 0.3, 1, 3, 10, and 30 μM of each enantiomer. B) The time course is shown for **EU1794-27** enantiomer racemization in working solutions. Individual paired differences in the % modulation of the enantiomers are plotted versus time. As previously reported (Katzman 2015), this series appears prone to racemization in aqueous solution, which may account for differences in activity due to the time the enantiomers spend in the working solution. The difference in the extent of modulation of the enantiomers of **EU1794-27** was reduced slowly over time, producing modest racemization over the time frame of enantiomer experiments. C) The concentration-response relationships illustrate the selective action of one enantiomer of **EU1794-4**. Responses were activated with 100/30 μM glutamate/glycine and modulated with 0.1, 0.3, 1, 3, 10, and 30 μM of each enantiomer. Data are from 4-7 oocytes from at least 2 independent experiments. D) The time course of **EU1794-4** enantiomer racemization in working solutions is shown; all data are from one racemization experiment (1-2 recordings at each time point). The

difference in the extent of modulation of the enantiomers of **EU1794-4** was reduced slowly over time.

Table 3.8. Enantiomeric preference of **EU1794-27**.

Compound	EC_{50} (µM) [conf. int.]^a Maximal Modulation Extent (% of control)			
	EU1794-27	(-)-EU1794-27	(+)-EU1794-27	
GluN2A	7.4 $[5.3, 10]^{\dagger}$ $52 \pm 7\%$	5.6 [2.7, 12] $67 \pm 5\%$	-	*
GluN2B	1.4 $[1.2, 1.7]^{\dagger}$ $130 \pm 3\%$	2.8 [2.0, 3.8] $170 \pm 10\%$	-	*
GluN2C	2.8 $[2.5, 3.2]^{\dagger}$ $230 \pm 10\%$	5.1 [4.1, 6.4] $260 \pm 24\%$	7.1 [3.6, 14] $160 \pm 6.2\%$	*
GluN2D	2.4 $[1.8, 3.3]^{\dagger}$ $250 \pm 8\%$	8.2 [6.7, 9.9] $340 \pm 21\%$	7.4 [3.7, 15] $130 \pm 4.7\%$	*

^{a}EC$_{50}$ values were obtained by least-squares fitting of data from individual experiments by the Hill equation. EC$_{50}$ values are given as the mean with the 95% confidence interval determined from log(EC$_{50}$); the maximal degree of modulation is given as mean $\pm$ SEM. Data are from 4-7 oocytes from at least 2 independent experiments. Data were not fitted (shown as -) if the response recorded at 30 µM of test compound did not differ by more than 15% from control. †Data from Table 3.1 is included here for clarity. *indicates significant unpaired t-test between the percent modulation between 30 µM **(-)-EU1794-27** and **(+)-EU1794-27**.

Table 3.9. Enantiomeric preference of **EU1794-4**.

Compound	IC$_{50}$ (µM) [conf. int.]^{a}		
	Maximal Modulation Extent (% of control)		
Compound	**EU1794-4**	**(-)-EU1794-4**	**(+)-EU1794-4**
GluN2A	2.2 [1.8, 2.8]† 32 ± 3%	4.9 [2.1, 12] 17 ± 10%	12 [7.4, 20] 41 ± 6%
GluN2B	2.6 [1.4, 4.8]† 67 ± 4%	-	-
GluN2C	0.42 [0.28, 0.61]† 52 ± 2%	0.48 [0.27, 0.86] 47 ± 1%	1.7 [0.99, 3.0] 50 ± 4%	*
GluN2D	0.36 [0.29, 0.45]† 51 ± 3%	0.46 [0.10, 1.1] 54 ± 3%	3.5 [1.6, 7.5] 47 ± 6%	*

^{a}EC$_{50}$ values were obtained by least-squares fitting of data from individual experiments by the Hill equation. EC$_{50}$ values are given as the mean with the 95% confidence interval determined from log(IC$_{50}$); the maximal degree of modulation is given as mean ± SEM. Data are from 4-5 oocytes from 2 independent experiments. Data were not fitted (shown as -) if the response recorded at 30 µM of test compound did not differ by more than 15% from control. †Data from Table 3.1 is included here for clarity. *indicates non-overlapping IC$_{50}$ confidence intervals of **(-)-EU1794-4** and **(+)-EU1794-4**.
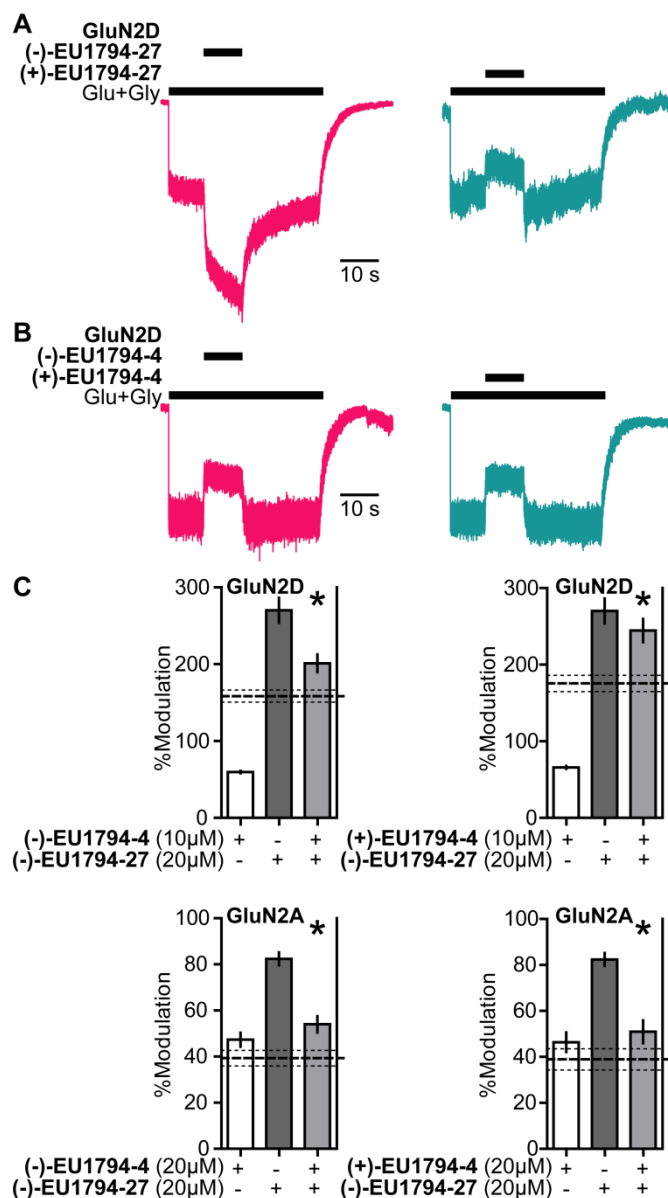
Figure 3.17. The actions of **EU1794-4** and **EU1794-27** enantiomers

A) Representative modulation of GluN1/GluN2D responses by the enantiomers of **EU1794-27** (both 10 μM, 100/30 μM glutamate/glycine). Similar results were observed in at least 3 cells to fresh modulator solution made less than one hour before experiment conclusion. B) Representative modulation of GluN1/GluN2D responses by the enantiomers of **EU1794-4** (both 10 μM, 100/30 μM glutamate/glycine). Similar results were observed in at least 3 cells to fresh modulator solution made less than one hour

before experiment conclusion. C) Single concentration competition experiments illustrating an interaction between both enantiomers of **EU1794-4** (+ and -) and the positive modulating enantiomer of **EU1794-27** (-) at GluN1/GluN2D. The individual average effects of the pairs of modulators along with the co-applied effect are plotted, and the predicted mean net effect of the modulators is displayed as a dashed line (SEM is represented by the dotted lines, n=10 from two independent experiments). * signifies $p < 0.05$ as determined by a paired t-test comparing co-applied modulators and predicted net effect of modulator actions.

(Figure 3.17A). In additional, 10 µM of both enantiomers of **EU1794-4** had similar inhibitory actions on GluN1/GluN2D responses to maximally effective concentrations of glutamate and glycine (Figure 3.17B).

To assess whether both enantiomers bound to similar or distinct sites on the NMDAR, we performed single concentration competition experiments. Co-application of each enantiomer of **EU1794-4** with the **(-)-EU1794-27** resulted in a degree of modulation that was significantly different than that predicted for independent sites of action at both GluN1/GluN2A and GluN1/GluN2D (Figure 3.17C). Interestingly, the competition by **EU1794-4** was not dependent on the direction of modulation by **(-)-EU1794-27**, which had a potentiating action at GluN1/GluN2D (Figure 3.17C, *top panels*) and an inhibitory effect at GluN1/GluN2A (Figure 3.17C, *bottom panels*). Although there remain potential caveats, the evidence suggests that the co-application of **(-)-EU1794-27** with either enantiomer of **EU1794-4** displays mutual exclusivity in modulator binding.

Discussion

This study highlights how subtle chemical variations in a series of NMDAR allosteric modulators can result in fundamentally different actions on NMDAR responses to maximally effective concentrations of agonists. This series of small molecule allosteric modulators show a spectrum of effects ranging from strong negative modulation to robust positive modulation. In addition, there are features that are shared across this series, including agonist-dependence and the ability to enhance agonist potency. Thorough analysis of the actions of this series illustrates a potential way forward in designing new analogues to achieve a wide range of activities. Additionally, the novel features found in this class of modulators suggest potential new strategies for targeting distinct populations of NMDARs, such as extrasynaptic receptors that typically are not activated by high concentrations of glutamate or distinct patterns of stimulation.

The site and mechanism of action for the EU1794 series

In the evaluation of the kinetic properties of modulator action, we observed complex actions of **EU1794-4** and **EU1794-27**, which could arise from multiple binding sites, enantiomers of these compounds, or could reflect distinct modulator-dependent mechanistic actions from occupancy of a single binding site. The modulation by **EU1794-4** and **EU1794-27** is voltage independent, eliminating potential channel block within the ion channel pore by potential cationic species as a confounding site that contributes to the observed effects. Given that there is high homology between GluN1 and GluN2, especially in the ABD and the TMD, a reasonable hypothesis is that multiple binding sites exist for **EU1794** series modulators in homologous regions on GluN1 and

GluN2 subunits. However, the mutagenesis data argues against this idea, given that the residues at which mutations perturbed the actions of **EU1794-2** and **EU1794-27** overlapped and clustered around the pre-M1, M3, and M4 of the GluN1 subunit. Whereas there were a few residues of the GluN2 M3 helix that influenced **EU1794-27** modulation, the structural NMDAR models suggest that these residues face the M3 helix, and thus could interact with the pocket adjacent to the GluN1 pre-M1 helix. Additionally, it's likely the M3 helixes of both GluN1 and GluN2, which are in close contact, act in concert with one another to control rapid pore opening or closing. If these residues identified by mutagenesis controlled conformational changes downstream of the **EU1794** binding site(s), it would limit potential binding site candidates to the interface between the GluN1 and the GluN2 ABDs, which would then have only 2 identical binding sites in diheteromeric NMDARs. Therefore there would be less potential for non-identical binding sites that contribute to the mixed actions that are observed for **EU1794-27** and **EU1794-4**. For these reasons, the idea that the positive and negative allosteric actions reflect modulator specific mechanisms from occupancy of a single site seems the most plausible interpretation.

Evaluation of the effects of enantiomers provides further insight into the binding site of the **EU1794** series. **EU1794-27** exhibits strong stereoselectivity, with the (-) enantiomer showing a typical potentiation time course and the (+) enantiomer producing inhibition. The enantiomers of **EU1794-4** are both capable of producing inhibition but with the (-) enantiomer being more potent (3-10 fold) than the (+) enantiomer. Additionally, both enantiomers of **EU1794-4** appear to compete with **EU1794-27** for access to the binding site, suggesting that enantiomers may interact differently with the

same binding site. An alternative explanation for lack of additivity of the effects of the two compounds could be that there are shared residues downstream of the PAM and NAM binding sites that mediate their effects, additional studies are required to evaluate this hypothesis. However, the idea that the enantiomers of the **EU1794** series act at the same site suggests their complex actions on NMDARs expressed in HEK is a mixture of receptors bound to one or the other enantiomer for of racemic **EU1794-27** and **EU1794-4**. The available enantiomeric data further supports the idea that positive and negative modulators within the **EU1794** series share a single or overlapping binding site.

EU1794 series links positive and negative allosteric modulators that act at the TMD.

An increasing number of NMDAR and AMPAR modulators have been identified with structural determinants of action that reside in transmembrane linker regions and extracellular portions of the transmembrane domain (Mullasseril 2010, Acker 2011, Hansen and Traynelis 2011, Ogden and Traynelis 2013, Yelshanskaya 2016, Swanger 2017, Wang 2017). Other cell surface receptor families have bi-directional modulator pockets, including multiple GPCRs as well as the benzodiazepine binding site in GABA-A receptors (Barnard 1998, Rudolph and Knoflach 2011, Wootten 2013). Among all ionotropic glutamate receptor modulators interacting with this region of the receptor, there are positive (CIQ, GNE-9278) and negative (DQP-1105, QNZ-46, CP-465,022, GYKI 52466) modulators with diverse scaffolds. However, the **EU1794** compounds represent the first bidirectional NMDAR modulator series with structural determinants of activity within this region, low micromolar potency and with a clear rules to control modulation. The similarity in structure of positive and negative modulators illustrates

how subtle differences in the ligand can interconvert functional actions between inhibition and potentiation of NMDARs. The ability to potentiate NMDAR seems to be unique to **(-)-EU1794-27,** which may have a specific interaction with the receptor achieved only by its stereoselective active pose in the binding pocket. Work with this series may lead to an understanding of the mechanistic link between the PAMs and NAMs that interact in this portion of the receptor.

Differential actions on synaptic and extrasynaptic receptors by submaximal EU1794 analogues

The **EU1794** series has a property of use-dependence, requiring both glutamate and glycine to be bound before the putative binding site adopts a high potency orientation for members of the series. The property of use-dependence is best understood for open channel blockers (e.g. memantine, MK-801, ketamine, etc.) that inhibit the receptor through interactions within the ion permeation path, and thus rely on pore opening (Traynelis 2010). Given that the **EU1794** series are allosteric modulators are not voltage-dependent, the mechanism of their use-dependence is unclear. Previously, the NAMs QNZ-46, DQP-1105, and NAB-14 have been reported to show varying degrees of glutamate- but not glycine-dependence (Acker 2011, Hansen and Traynelis 2011, Swanger 2017). Moreover, neurosteroid derivatives with NAM activity have also been shown to have glutamate- and glycine-dependence (Vyklicky 2015), and the PAM GNE-9278 was reported to be glutamate-dependent (Wang 2017). Thus, the **EU1794** series is the first series of positive and negative modulators that has been shown to possess the property of being both glutamate and glycine use-dependence. Our working hypothesis is

that the **EU1794** series of modulators requires conformational changes in both GluN1 and GluN2 subunits that reflect pre-gating or gating transitions, after which its affinity for its binding site is increased. However, we cannot rule out at this time the possibility that the pore must open to increase modulator binding. Resolving the specific mechanism of the **EU1794** may lead to a more complete understanding of the activation transitions NMDAR.

We believe that **EU1794-4** highlights a novel sub-class of NMDAR modulators that have the capability to selectively act at extrasynaptic NMDARs based on the combinations of its properties. Extrasynaptic NMDAR are hypothesized to respond to glutamate spillover or glial release of glutamate (Rusakov and Kullmann 1998, Haydon and Carmignoto 2006, Sahlender 2014). The potential ability to preferentially act at these non-synaptic sites arises from three mechanistic features of the allosteric mechanism: (1) the submaximal inhibitory effects at saturating concentrations of modulator and agonist, (2) the agonist-dependent and slow association rate, which might limit activity at synaptic receptors, and (3) the ability to enhance NMDAR responses to low agonist concentrations. A similar property has been described for the GluN2B-selective agent ifenprodil (Kew 1996), although the extent to which **EU1794-4** can enhance the response to low concentrations of agonist is amplified by the large degree of residual current at saturating levels of **EU1794-4** (30-60%) compared to ifenprodil (~10%). There are numerous studies that suggest the importance of extrasynaptic NMDARs in normal biology but study of them requires complex experimental paradigms (Harris and Pettit 2008, Paoletti 2013, Papouin and Oliet 2014). Alternatively, the use-dependence of **EU1794-4** may alter this capability in instances of repeated stimulation. In either case,

EU1794-4 is a unique compound that may act as a tool that could be used to probe the contribution of distinct types of NMDARs or their activity in circuit function. Further work is required to fully understand the utility of this modulator as a probe for extrasynaptic NMDARs.

Chapter 4: GluN2D-containing NMDA receptors mediate synaptic transmission in

hippocampal interneurons and regulate interneuron activity[1]

Abstract

NMDA receptors (NMDARs) are ionotropic glutamatergic receptors that have been implicated in learning, development, and neuropathological conditions. They are typically composed of GluN1 and GluN2A-D subunits. Whereas a great deal is known about the role of GluN2A- and GluN2B-containing NMDARs, much less is known about GluN2D-containing NMDARs. Here we explore the subunit composition of synaptic NMDARs on hippocampal interneurons. GluN2D mRNA was detected by single-cell PCR and *in situ* hybridization in diverse interneuron subtypes in the CA1 region of the hippocampus. The GluN2D subunit was detectable by immunoblotting and immunohistochemistry in all subfields of the hippocampus in young and adult mice. In whole-cell patch-clamp recordings from acute hippocampal slices, (+)-CIQ, the active enantiomer of the positive allosteric modulator CIQ, significantly enhanced the amplitude of the NMDAR-component of miniature excitatory postsynaptic currents (mEPSCs) in CA1 interneurons but not pyramidal cells. (+)-CIQ had no effect in slices from *GRIN2D-/-* mice, suggesting that GluN2D-containing NMDARs participate in excitatory synaptic transmission onto hippocampal interneurons. The time course of the NMDAR-component of the mEPSC was unaffected by (+)-CIQ potentiation and was not accelerated in slices from *GRIN2D-/-* mice compared to wild type receptors, suggesting that GluN2D doesn't detectably slow the NMDAR EPSC time course at this age. (+)-CIQ increased the activity of CA1 interneurons as detected by the rate and net charge transfer of spontaneous inhibitory postsynaptic currents (sIPSCs) recorded from CA1 pyramidal cells. These data provide evidence that interneurons contain synaptic NMDARs

possessing a GluN2D subunit, which can influence interneuron function and signal processing.

Introduction

NMDA receptors (NMDARs) are tetrameric assemblies comprises GluN1 subunits and GluN2 subunits. Whereas GluN3 subunits can be incorporated into NMDARs, our understanding of their role remains incomplete. Four independent genes (*GRIN2A*, *GRIN2B*, *GRIN2C*, and *GRIN2D*) encode GluN2A-D subunits, which have distinct spatial and developmental expression patterns (Traynelis 2010). Among the GluN2 subunits, little is known about the role of GluN2D in brain function, even though anatomical studies have suggested that it is expressed in many cell types, such as hippocampal interneurons (Akazawa 1994, Monyer 1994, von Engelhardt 2015). Receptor pharmacology has been studied extensively in heterologous expression systems showing incorporation of different GluN2 subunits into NMDARs confers strikingly different functional properties to the receptors, with GluN1/GluN2D receptors showing an unusually slow deactivation and low open probability (Monyer 1994, Vicini 1998, Vance 2012, Vance 2013, Wyllie 2013). Given that the deactivation time course, following removal of glutamate, controls the time course of the NMDAR-mediated component of the excitatory postsynaptic current (EPSC) (Lester 1990), the presence of GluN2D-containing receptors might alter the signal processing by changing the time course of the composite excitatory synaptic current. GluN1/GluN2D receptors also show reduced Ca^{2+} permeability and reduced Mg^{2+} sensitivity (Clarke and Johnson 2006, Retchless 2012), suggesting that inclusion of this subunit into synaptic receptors may alter synaptic signaling in multiple ways.

NMDARs have been implicated in a number of neurological processes and disorders. Accordingly, this receptor class has been the focus of intense study as a

potential target for the treatment of a wide range of neurological problems including Alzheimer's disease, depression, epilepsy, Parkinson's disease, schizophrenia, and traumatic brain injury (Choi 1992, Palmer 2001, Coyle 2003, Hallett and Standaert 2004, Preskorn 2008, Coyle 2012, Preskorn 2015, Yuan 2015). Expression of different GluN2 subunits in different cells and nuclei (Akazawa 1994, Monyer 1994, Standaert 1994, Rudolf 1996) may provide an opportunity to selectively target specific circuits using subunit-selective modulators. This approach should allow for enhanced efficacy and greater safety for new therapeutic strategies by restricting actions of drugs to the brain regions and synapses involved in the pathology. While GluN2A and GluN2B receptors are expressed in principal cells, a number of studies suggest GluN2D is expressed in cortical and hippocampal interneurons (Monyer 1994, Landwehrmeyer 1995, Rudolf 1996, Thompson 2002), which should confer unique circuit properties in these regions. Here we evaluate the role of GluN2D in hippocampal interneuron function using genetic, anatomical, pharmacological, and functional experiments.

We previously described a series of GluN2C/GluN2D-selective positive allosteric modulators (PAMs) exemplified by the prototypical chiral compound CIQ (Mullasseril 2010, Santangelo Freel 2013, Santangelo Freel 2014). This pharmacological tool was recently used to evaluate subunit composition of NMDAR-mediated EPSCs onto spinal and subthalamic neurons (Hildebrand 2014, Swanger 2015). Here, we describe in detail the properties and selectivity of the active enantiomer (+)-CIQ and several closely related analogues. We subsequently use (+)-CIQ to assess the subunit composition of the synaptic NMDARs in CA1 hippocampal interneurons. Our anatomical and functional data suggest that GluN2D is expressed in hippocampal interneurons, participates in

synaptic transmission, and in *ex vivo* preparations (+)-CIQ can increase the activity of these inhibitory interneurons.

Results

Enantiomeric preference of a series of GluN2C/D-selective NMDAR positive allosteric modulators

To explore the subunit composition of the NMDARs underlying EPSCs in CA1 interneurons, we utilized a series of GluN2C/GluN2D-selective allosteric modulators (Mullasseril 2010, Santangelo Freel 2013). Racemic CIQ was described as the first GluN2C and GluN2D subunit-selective positive allosteric modulator for NMDARs (Mullasseril 2010), with virtually all activity residing in the (+) enantiomer (Santangelo Freel 2013). Although the stereochemistry of the two enantiomers has not been absolutely resolved, a model of the stereoselective reduction during the chiral synthesis of the enantiomers predicts that the (+)-enantiomer is the (R)-enantiomer (Santangelo Freel 2014). In the absence of a crystal structure of either enantiomer, however, we will refer to the active enantiomer as (+)-CIQ (Figure 4.1B).

We first evaluated the properties of purified (+)-CIQ as well as closely related halogen-substituted analogues of CIQ (Table 4.1). In agreement with previous work using (±)-CIQ, neither (+)-CIQ nor (-)-CIQ affected responses of GluN1/GluN2A or GluN1/GluN2B diheteromeric NMDARs expressed in *Xenopus laevis* oocytes when activated by 100 μM glutamate and 30 μM glycine (Figure 4.1C and D, Table 4.1). (+)-CIQ enhanced the response of GluN1/GluN2C and GluN1/GluN2D NMDARs activated by maximally effective co-agonist concentrations, whereas (-)-CIQ had minimal effects at these NMDARs (Figure 4.1E, and F, Table 4.1). To further examine the enantiomeric specificity of this class of modulator, other enantiopure halogenated isoquinolines (FIQ,
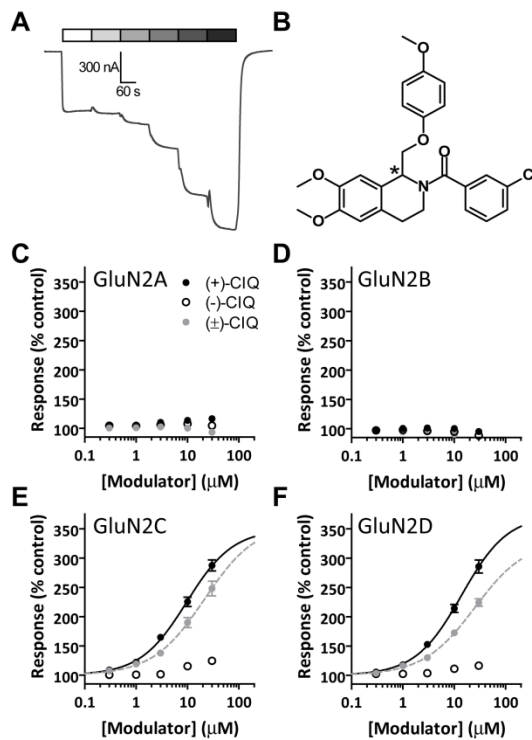
Figure 4.1. (+)-CIQ but not **(–)-CIQ** potentiates NMDA receptor-mediated currents in *X. laevis* oocytes.

(**A**) Representative response of a GluN1/GluN2D NMDAR (activated by 100 μM glutamate and 30 μM glycine) in the absence and presence of increasing concentrations of (+)-CIQ (0, 0.3, 1, 3, 10, 30 μM). (**B**) The chemical structure of CIQ is shown with the chiral carbon indicated by the asterisk (Santangelo Freel 2013, Santangelo Freel 2014). (**C-F**) Concentration-response relationships show the effects of the purified enantiomers of (+)-CIQ, (-)-CIQ and racemic CIQ on the diheteromeric NMDARs, recorded under two electrode voltage clamp from *X. laevis* oocytes. Data are from P. Le and J. Zhang.

Table 4.1: Stereoselective potentiation of GluN2C- and GluN2D-containing NMDARs

Compound	I (30 μM) / I (control) (%)				EC_{50} (μM) [conf. int.]^{a} (% max. modulation)	
	GluN2A	GluN2B	GluN2C	GluN2D	GluN2C	GluN2D
(+)-FIQ	100 ± 2.9	102 ± 2.1	192 ± 6.4	177 ± 3.5	N.A.	N.A.
(-)-FIQ	97 ± 0.9	96 ± 0.9	102 ± 3.5	106 ± 4.9	N.E.	N.E.
(+)-CIQ	118 ± 1.9	98 ± 1.3	250 ± 15	285 ± 11	7.8 [6.8, 9.0] (286 ± 23)	10.5 [9.5, 11.7] (322 ± 18)
(-)-CIQ	105 ± 2.7	88 ± 2.7	125 ± 4.7	117 ± 5.6	N.E.	N.E.
(+)-BIQ	87 ± 0.5	99 ± 0.8	318 ± 28	326 ± 16	3.8 [3.2, 4.5] (352 ± 47)	5.5 [5.1, 6.0] (354 ± 21)
(-)-BIQ	89 ± 5.7	84 ± 0.6	100 ± 5.0	96 ± 3.2	N.E.	N.E.
(+)-IIQ	98 ± 1.4	97 ± 0.7	197 ± 14	273 ± 15	2.1 [1.9, 2.2] (204 ± 16)	3.5 [3.1, 4.0] (289 ± 16)
(-)-IIQ	88 ± 3.6	85 ± 1.3	98 ± 5.4	85 ± 3.8	N.E.	N.E.

Values for current ratio and EC_{50} are mean $\pm$ SEM from 8-22 oocytes obtained from at least 2 different frogs. ^{a}is the mean half-maximally effective concentration of modulators (see Methods). The value [95% confidence interval] was determined from fitting individual concentration-effect curves and averaging the fitted values on the *log* scale, and presented on linear scale. The Hill slopes ranged between 0.5-1.5. The fitted maximal response as a percent of control is given in parentheses. N.A. – Not analyzed; the concentration-effect curve could not be fitted by the Hill equation. N.E. – No effect; the ratio of current in 30 μM test compound to control current was less than 130%, our threshold for further analysis. Data are from P. Le and J. Zhang.

BIQ, IIQ) were assayed for their activity on recombinant GluN1/GluN2 diheteromeric NMDARs. In all cases, activity resided with the (+) enantiomers (Table 4.1).

A previous evaluation of potential off-target activity of racemic CIQ suggested it was highly selective (Santangelo Freel 2013), with a few notable exceptions, such as low µM actions on 5-HT6 serotonin receptor, peripheral benzodiazepine receptor (PBR), and several nACh receptors. Off target analysis of 45 assayed receptors (see *Methods, Besnard 2012*) showed that 3 µM (+)-CIQ displaced bound ligand of the serotonin 5-HT1A receptor and PBR in the initial screening assay, prompting further evaluation of affinity. The K_i of (+)-CIQ was determined to be greater than 10 µM (which was the upper boundary for this assay) for the 5-HT1A receptor and 1.8 µM for the PBR receptor by the secondary assay. Additionally, 3 µM (-)-CIQ was found to displace bound ligand for serotonin 5-HT6, 5-HT7, and PBR receptors. Further evaluation determined that the K_i of (-)-CIQ was 1.0 µM for the 5-HT6 receptor, and greater than 10 µM for both the 5-HT7 receptor and the PBR. (+)-CIQ and (-)-CIQ were also screened at a higher concentration (20 µM) on a series of ionotropic receptors expressed in *Xenopus laevis* oocytes using two electrode voltage clamp (Perszyk 2016). Both (+)-CIQ or (-)-CIQ similarly inhibited nicotinic α1β1γδ acetylcholine receptors (42 ± 0.8% of control by (+)-CIQ *vs* 57 ± 17% by (-)-CIQ, unpaired t-test, p=0.54) and nicotinic α4β2 acetylcholine receptors (44 ± 5.1% by (+)-CIQ vs 34 ± 4.8% by (-)-CIQ, unpaired t-test, p=0.22), but did not significantly affect the other receptors tested. Due to reduced off-target activity, (+)-CIQ is a better tool compound than racemic CIQ for evaluation of GluN2C- and GluN2D-containing receptors.

GRIN2D mRNA and the GluN2D protein are expressed in hippocampal interneurons

Several studies suggest that cortical and hippocampal interneurons express *GRIN2D* mRNA (Monyer 1994, Rudolf 1996, Porter 1998, Cauli 2000), which encodes the GluN2D subunit. To provide more detailed information regarding interneuron subtype and NMDAR subunit expression patterns in the hippocampus, we performed single cell RT-PCR from various interneurons throughout the hippocampal formation. A total of 37 interneurons were recorded using whole-cell patch-clamp methods under current-clamp and classified by their spiking activity before harvesting their cytoplasmic contents for the analysis of mRNA (*see* Perszyk 2016 for details, data from collaborators). Patched cells were filled with biocytin, allowing for *post hoc* determination of soma and axon location (*see* Perszyk 2016). Single cell RT-PCR detected *GRIN2D* in multiple interneuron subpopulations of the hippocampus, including dendritic targeting bistratified and oriens-lacunosum molecular cells as well as fast spiking (parvalbumin) and regular spiking (cholecystokinin) perisomatic targeting basket cells. S*ee* Perszyk 2016 for the location and prevalence of NMDAR subunits for the 37 interneurons. Overall, amplified signals for *GRIN1*, *GRIN2A*, and *GRIN2B* were detected in most cells (33, 26, and 31 out of 37 interneurons, respectively). *GRIN2C* was only detected in 1 of the 37 interneurons. *GRIN2D* was detected in 29 of 37 cytoplasmic harvests from randomly recorded hippocampal interneurons.

To further investigate the cell-type specificity of *GRIN2D* subunit expression, we performed fluorescent *in situ* hybridization examining mRNA expression for *GRIN2D* and interneuron-specific molecular markers. Corroborating single-cell RT-PCR data, we found *GRIN2D* in cells positive for parvalbumin (PV), cannabinoid receptor type 1

(CB1R, a marker for cholecystokinin-expressing interneurons), and somatostatin (SOM, *see* Perszyk 2016).

As an independent assessment of GluN2D expression at the protein level, we performed immunohistochemistry on adult mouse brain sections from mice using a GluN2C/D polyclonal antibody (*see* Perszyk 2016, data from collaborators). Several reports suggest that expression of GluN2D decreases throughout development (Akazawa 1994, Monyer 1994). We thus used adult animals to test whether GluN2D protein persists at older ages. Diffuse neuropil staining was evident throughout the hippocampus, in addition to staining of cell bodies. Parallel experiments showed that staining was greatly diminished in these same regions in age-matched *GRIN2D*-/- mice (*see* Perszyk 2016), confirming the specificity of the immunoreactivity for the GluN2D subunit. These data suggest that the immunostaining observed in these neurons reflected primarily GluN2D rather than GluN2C, consistent with lack of detection of *GRIN2C* in RT-PCR analysis of interneuron mRNA.

To assess the protein expression of the GluN2D subunit across hippocampal regions and through early developmental periods, we collected whole hippocampal slices (Figure 4.2A, B, D) from acute mouse hippocampal slices (Figure 4.2C, E). The expression of GluN2D was not detected in P9 *GRIN2D*-/- hippocampal preparations (Figure 4.2C). To assess the expression of the GluN2D subunit in the different subfields of the adult hippocampus, micropunches of tissue were isolated from slices prepared from P74 mice (Figure 4.2B). The GluN2D subunit was detected in all regions, with lower levels in the CA1 as compared to the dentate gyrus (Figure 4.2B, D). Similarly to previous studies, GluN2D is expressed in the hippocampus of young and adult rodents
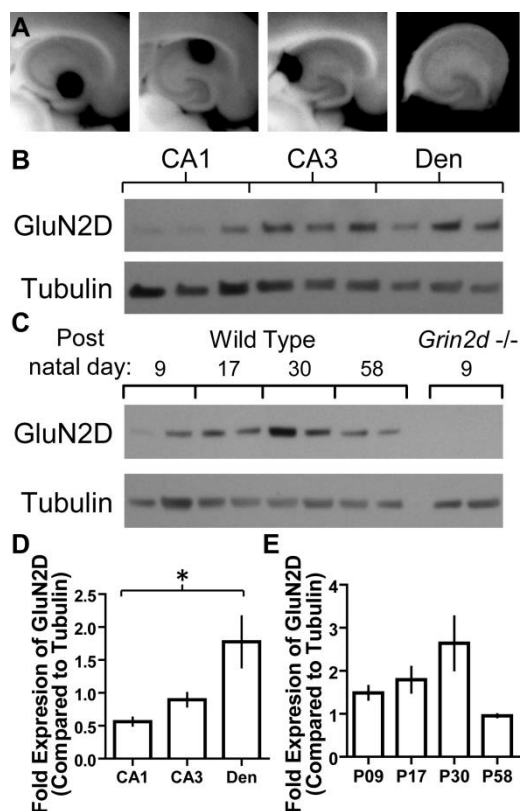
Figure 4.2. GluN2D protein expression across development and hippocampus subfield.

(**A**) Images of mouse brain slices illustrating typical tissue punches (diameter 0.75 mm) taken for protein analysis of (from left to right) the dentate gyrus, CA1, CA3, and a dissected whole hippocampus slice. (**B**) Representative western blot for GluN2D and tubulin from three different animals (p74) for the CA1, CA3 and dentate gyrus tissue punch samples. (**C**) Representative western blot of GluN2D and tubulin from whole hippocampus slices from wild type mice aged P9, P17, P30, P58 and *GRIN2D*-/- aged P9. (**D**) Densitometry measurements for the GluN2D levels normalized to tubulin, analyzed by one-way repeat measure ANOVA ($N=3$, $F(2,4) = 8.869$, $p = 0.034$, Tukey's multiple comparison test, comparisons that were $p < 0.05$ are denoted by *). Measurements from six replicate SDS-PAGE gels and western blots were used to produce the average for each animal's value. (**E**) Densitometry measurements for the GluN2D levels as a function

of age of wild type samples normalized to tubulin, analyzed by one-way ANOVA (N=3, $F(3,8) = 3.95$, $p = 0.054$). Measurements from three replicate SDS-PAGE gels and western blots were used to produce the average for each animal's protein value.

but decreases in adulthood (Akazawa 1994, Monyer 1994, von Engelhardt 2015).

The NMDAR-component of mEPSCs in hippocampal interneurons is potentiated by (+)-CIQ

To investigate the subunit composition of synaptic NMDARs in interneurons, we recorded from hippocampal interneurons in the CA1 stratum radiatum under voltage clamp (V_{hold} -60 mV) using the whole-cell patch-clamp method (Figure 4.3A). We chose animals aged P7-14 as these ages preceded a switch from GluN2B to GluN2A (Akazawa 1994, Monyer 1994, Edman 2012, McKay 2012); these ages were also similar to those used in a recent study of NMDAR expression in hippocampal neurons (von Engelhardt 2015). Slices were bathed in aCSF supplemented with 0.5 µM TTX, 10 µM gabazine or bicuculline, and extracellular Mg^{2+} reduced to 0.1 mM to record miniature EPSCs (mEPSCs). These inward currents had a rapid rise time and a dual exponential decay thought to reflect spontaneous release of a single vesicle of glutamate (Figure 4.3B). By detecting and aligning these mEPSCs, we could average them together to resolve a deactivation time course containing two components, a fast exponential component (typically about 5 ms decay tau) and a slow exponential component (typically over 100 ms decay tau). We consider these dual-component mEPSCs to reflect the activation of AMPARs and NMDARs (Figure 4.3C, D, Table 4.2). The NMDAR antagonist APV (200 µM) eliminated the slow component of the inward current, suggesting it is entirely generated by NMDARs (Figure 4.3E, F). Experiments were concluded by adding the AMPAR and kainate receptor antagonist DNQX (10 µM), which blocked all mEPSCs, confirming that they reflected glutamatergic synaptic currents. Using this recording
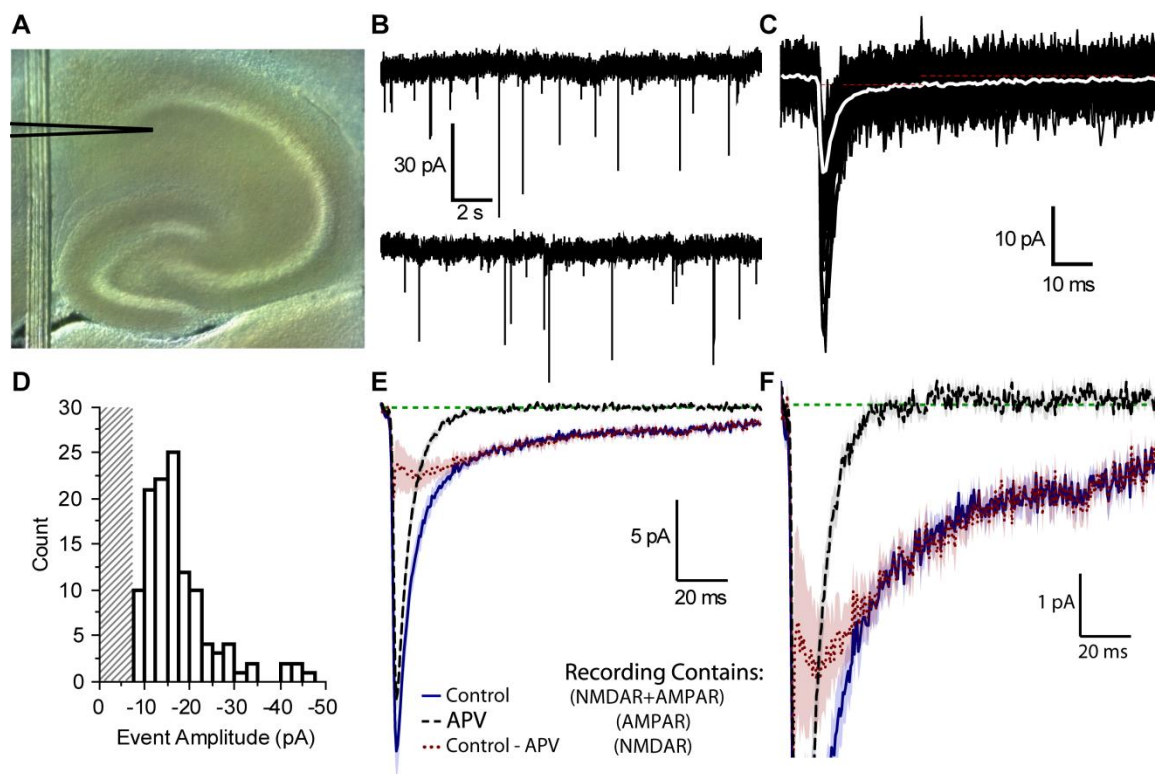
Figure 4.3. Characterization of mEPSCs in hippocampal CA1 interneurons from P7-14 mice.

(**A**) Visible light image of a mouse hippocampal slice showing a CA1 stratum radiatum interneuron in the whole-cell patch-clamp configuration; the outline of the recording electrode has been enhanced. (**B**) An illustrative recording (filtered at 0.25 kHz) of spontaneous glutamatergic activity from a CA1 interneuron in the presence of 0.5 μM TTX, 10 μM bicuculline, and 5 μM nimodipine. (**C**) Superimposed mEPSCs (black) and the mean response time course (white); the red dashed line illustrates pre-mEPSC baseline current level. (**D**) The mEPSC peak response amplitude histogram from the interneuron recording is shown in (**C**), the patterned area indicates amplitudes below the detection threshold. (**E**) Averaged composite mEPSC time course is shown for control conditions and in APV (200 μM); the difference current reveals the NMDAR-component of the mEPSC (average response is shown ± SEM indicated by the shaded area). (**F**) The

same recordings in (**E**) but at an expanded scale to better illustrate the NMDAR-component.

Table 4.2. Measured mEPSC characteristics of neurons from P7-14 mice

	AMPAR Time Constant (ms)	NMDAR Time Constant (ms)	AMPAR Amp. (pA)	NMDAR Amp. (pA)[a]	mEPSC Detection rate (s^{-1})	AMPAR/ NMDAR ratio[b]	N
Interneuron Wild Type	4.6 ± 0.5	138 ± 37	20 ± 1.6	2.1 ± 0.2	1.6 ± 0.4	9.7 ± 1.1	25
Interneuron *GRIN2D-/-*	3.9 ± 0.7	140 ± 48	24 ± 4.3	3.9 ± 1.3	1.0 ± 0.5	6.8 ± 0.7	4
Pyramidal Wild Type	6.5 ± 0.4	91 ± 8.6	21 ± 1.4	4.7 ± 0.6	0.92 ± 0.22	5.9 ± 0.9	17

[a]NMDAR amplitude is calculated from the amplitude of slower component of the dual exponential fit. [b]Recordings were performed in 0.1 mM Mg^{2+}. Values are mean $\pm$ SEM; N is the number of cells recorded from. Some data contributed by C.M. Low.

paradigm we assayed the actions of (+)-CIQ on mEPSCs from hippocampal CA1 interneurons (for observed mEPSC characteristics, Table 4.2; the protocol is given in Figure 4.4A).

(+)-CIQ (10 μM) had no significant effect on the amplitude of the AMPAR-component of the mEPSCs (99 ± 3%, Figure 4.5A and C, Table 4.3, repeat measure ANOVA, N=17, $F(2,32) = 5.651$, $p = 0.0079$, Dunnett's test, $p < 0.05$ for APV). By contrast, (+)-CIQ enhanced the amplitude of the NMDAR-mediated component of the mEPSC to 147 ± 10% of control (Figure 4.5B, D, Table 4.3, repeat measure ANOVA, N=17, $F(2,32) = 173.0$, $p < 0.0001$, Dunnett's test, $p < 0.05$). APV reduced the NMDAR amplitude to 18 ± 4% of control ($p < 0.001$, Dunnett's test). In vehicle experiments, the AMPAR-component amplitude of the mEPSCs did not significantly change nor did the NMDAR-component, the latter which was blocked by APV (NMDAR amplitude, 115 ± 22% vehicle/control, 14 ± 4% APV/control Figure 4.5E, Figure 4.4B-D, Table 4.3, repeat measure ANOVA, N=8, $F(2,14) = 22.31$, $p < 0.0001$, Dunnett's test, $p < 0.0001$ for APV). We also recorded mEPSCs from CA1 pyramidal neurons, which should lack the GluN2D subunit (Table 4.2). When (+)-CIQ was applied to pyramidal neurons, there were no detectable changes in the amplitude of the AMPAR-mediated fast component of the mEPSC (94 ± 15%) or the NMDAR-mediated slow components of the mEPSCs (109 ± 19%), the latter which was sensitive to APV (10 ± 2%, Figure 4.5A, B, F, Figure 4.4D, Table 4.3, repeat measure ANOVA, N=10, $F(2,18) = 76.94$, $p < 0.0001$, Dunnett's test p>0.05 for (+)-CIQ and $p < 0.0001$ for APV). (+)-CIQ also had no significant effect on the amplitude of the AMPAR or NMDAR component of the mEPSC in slices prepared from *GRIN2D*-/- mice (NMDAR amplitude, 90 ± 20% (+)-CIQ/control, 16 ± 3%
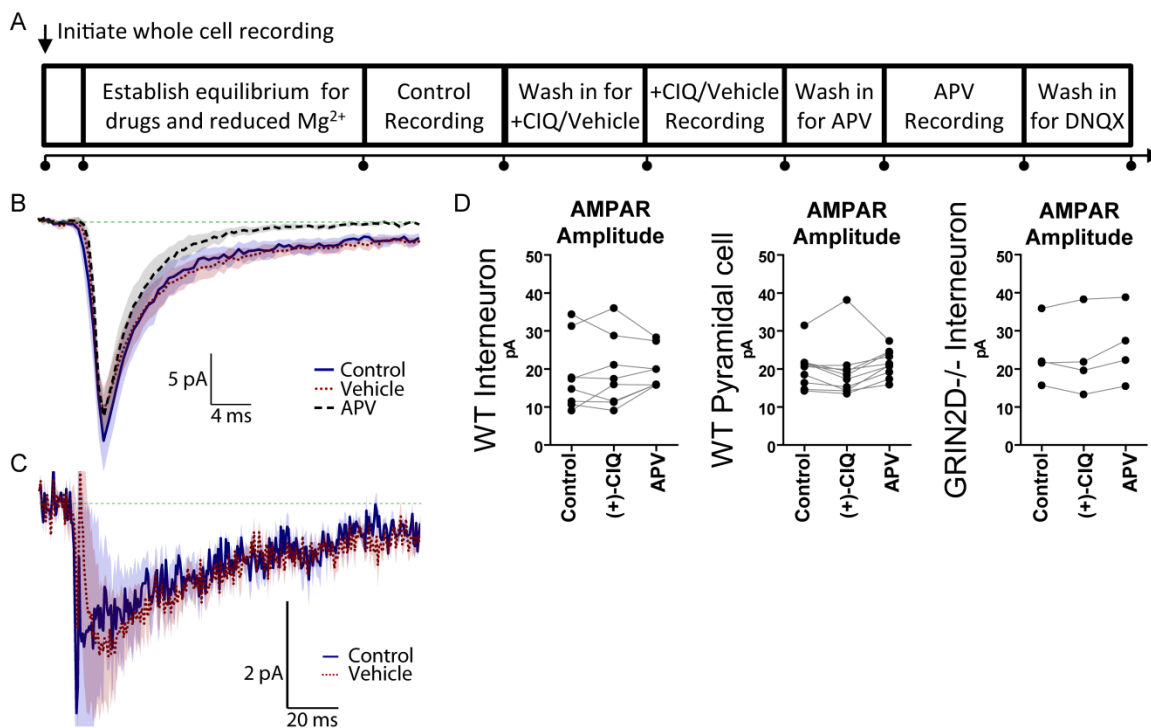
Figure 4.4. Vehicle-control mEPSCs experiment in P7-14 mice.

(**A**) The timeline illustrates the experimental protocol. (**B**) The average composite mEPSC response from (+)-CIQ WT pyramidal cell experiments. (**C**) Composite APV difference responses for (+)-CIQ WT pyramidal cell experiments. (**D**) The mean AMPAR amplitudes from WT interneuron vehicle, WT pyramidal cell (+)-CIQ and *GRIN2D*-/-interneurons (+)-CIQ recordings. Vehicle AMPAR WT interneuron response was 107 ± 21% of control (repeat measure ANOVA, *N*=8, $F(2,14) = 0.4923$, $p = 0.621$). (+)-CIQ AMPAR WT pyramidal response was 99 ± 2.9% of control (repeat measure ANOVA, *N*=10, $F(2,18) = 2.173$, $p = 0.1423$). (+)-CIQ AMPAR *GRIN2D*-/- response was 95 ± 21% of control (repeat measure ANOVA, *N*=4, $F(2,6) = 2.966$, $p = 0.1271$). 10 μM (+)-CIQ, 200 μM APV. Some data contributed by C.M. Low.
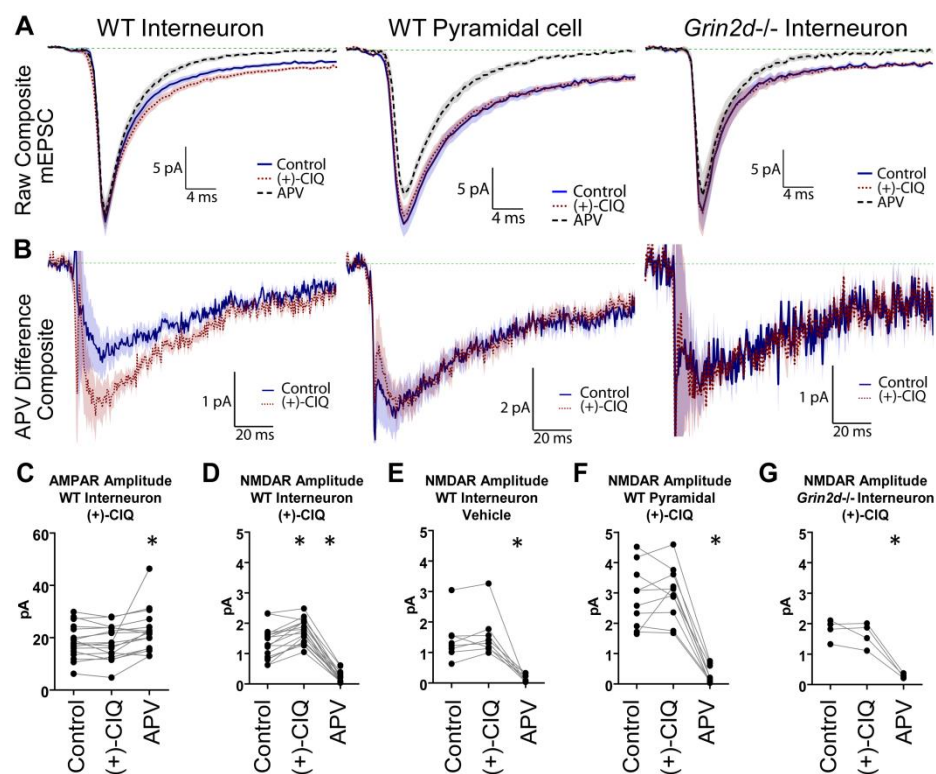
Figure 4.5. (+)-CIQ potentiates NMDAR currents in hippocampal CA1 stratum radiatum interneurons but not CA1 pyramidal neuron or in *GRIN2D*-/- interneurons from P7-14 mice.

(**A**) The average composite mEPSC response from each phase of the mEPSC experiment is shown. (**B**) Composite-APV difference current reveals the NMDAR-component of the mEPSC waveform. (**C**) The AMPAR amplitudes are shown for WT interneurons before and during (+)-CIQ application. (**D**) The measured mean NMDAR responses are shown for WT interneurons before and during (+)-CIQ application. (**E**) The measured mean NMDAR responses from WT interneurons before and during application of vehicle. (**F**) The measured mean NMDAR responses are shown from WT pyramidal cell (+)-CIQ recordings. (**G**) The measured mean NMDAR responses are shown from *GRIN2D*-/- interneurons before and during (+)-CIQ application. * indicates $p<0.05$ by Dunnett's test. 10 μM (+)-CIQ, 200 μM APV. Some data contributed by C.M. Low.

Table 4.3: Effects of (+)-CIQ on the AMPAR and NMDAR components of mEPSCs in P7-14 mice

		AMPAR Amplitude[a]			NMDAR Amplitude[b]			N
		Cont. (pA)	Comp. (pA)	Comp. /Cont.	Cont. (pA)	Comp. (pA)	Comp. /Cont.	
Interneuron								
Wild Type	Vehicle	18 ± 3.4	19 ± 3.3	1.07 ± 0.21	1.4 ± 0.25	1.6 ± 0.26	1.15 ± 0.22	8
Wild Type	(+)-CIQ	20 ± 1.8	20 ± 1.7	0.99 ± 0.03	1.2 ± 0.12	1.7 ± 0.11*	1.47 ± 0.10	17
GRIN2D-/-	(+)-CIQ	24 ± 4.3	23 ± 5.3	0.95 ± 0.21	1.8 ± 0.17	1.6 ± 0.20	0.90 ± 0.20	4
Pyramidal								
Wild Type	Vehicle	23 ± 2.6	19 ± 1.8	0.85 ± 0.16	2.5 ± 0.89	3.0 ± 1.0	1.33 ± 0.27	7
Wild Type	(+)-CIQ	20 ± 1.6	19 ± 2.4	0.94 ± 0.15	2.9 ± 0.32	3.0 ± 0.29	1.09 ± 0.19	10

[a]AMPAR amplitudes were measured by the amplitude of fast component of the fitted composite mEPSC (mean ± SEM). [b]NMDAR amplitudes were measured as the averaged response between 40-50 ms after the peak AMPAR response (mean ± SEM). *$p < 0.05$, Dunnett's test following a repeat measure ANOVA (Control vs Compound). Some data contributed by C.M. Low.

APV/control, Figure 4.5A, B and G, Figure 4.4D, Table 4.3, repeat measure ANOVA, N=4, $F(2,6) = 56.02$, $p < 0.0001$, Dunnett's test, $p > 0.05$ for (+)-CIQ and $p < 0.0001$ for APV). These data support that the potentiating effects of (+)-CIQ on interneuron mEPSCs reflect actions at the GluN2D subunit.

(+)-CIQ does not alter the NMDAR EPSC time course

We analyzed the time course of the NMDAR-component of the mean composite mEPSCs recorded in the presence of 1.5 mM extracellular Mg^{2+} at a holding current of +40 mV. These currents were larger and provide a more reliable analysis of the synaptic time course of the NMDAR-component of the mEPSC. These synaptic currents may arise from a mixed population of interneurons that have different AMPAR subtype expression. Some of these interneurons express GluA2-lacking AMPARs with inward rectifying current-voltage relationship in the presence of intracellular spermine (McBain and Dingledine 1993, Matta 2013). We measured the time course of the NMDAR component of the mEPSC in the presence of only $GABA_A$ antagonists for wild type and *GRIN2D*-/- stratum radiatum interneurons (Figure 4.6A). The average mEPSC response amplitude at +40 mV was 18 ± 1.2 pA in CA1 interneurons in slices from wild type mice, similar to mEPSCs in CA3 stratum radiatum interneurons (McBain and Dingledine 1993). By fitting the composite mEPSC time course to two exponential components, the amplitude of the NMDAR-component was 12 ± 1.2 pA and decayed with a tau of 200 ± 18 ms. The amplitude of the NMDAR-component under these recording conditions is likely higher than that determined at -60 mV due to the channel block produced by 0.1 mM Mg^{2+}, as well as the ability of Mg^{2+} at 1.5 mM (+40 mV) to potentiate GluN2B outward currents

mEPSC (+40mV)

— Wildtype
····· *Grin2d -/-*

20%
100 ms
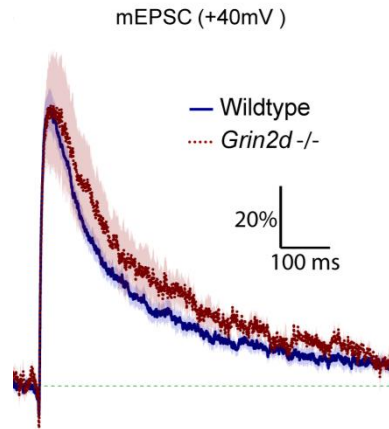
Figure 4.6. Synaptic response time course for GluN2D-containing receptors.

Normalized mEPSCs (V_{Hold} +40 mV) from wild type and *GRIN2D*-/- interneurons (P7-14) are superimposed (20% scale bar corresponds to 3.2 pA for wild type and 2.6 pA for *GRIN2D*-/-).

(Paoletti 1995). Additionally, we observed an increase in NMDAR-dependent noise in recordings at +40 mV, which altered the amplitude threshold for mEPSCs detection, potentially skewing our sample of mEPSCs to a subset with larger amplitudes. In CA1 interneurons held at +40 mV in slices from *GRIN2D-/-* mice, the mEPSC amplitude was 13 ± 1.9 pA (*GRIN2D-/-* compared to WT, unpaired t-test, p = 0.06, *N*=12,5). The amplitude of the NMDAR-mediated component of the *GRIN2D-/-* mEPSC was 9.7 ± 2.3 pA (*GRIN2D-/-* compared to WT, unpaired t-test, p = 0.33, *N*=12,5) with a tau of 300 ± 44 ms (*GRIN2D-/-* compared to WT, unpaired t-test, p = 0.02, *N*=12,5).

Additional experiments were performed with racemic CIQ to investigate the time course of the CIQ-responsive synaptic current (*see* Perszyk 2016). Pairs of evoked EPSCs were recorded from hippocampal interneurons at +40 mV from P14-21 slices (*see* Perszyk 2016). The evoked EPSC time course was determined in cells for which racemic CIQ produced a reversible increase of the NMDAR peak amplitude (at least 120% of control, 16 of 50 cells, *see* Perszyk 2016). Potentiation of the peak amplitude in these cells was on average 142 ± 6% of control (*see* Perszyk 2016). There was no detectable change by CIQ in the paired pulse ratio (summary data not shown, p = 0.34, one sample t-test, *see* Perszyk 2016). In this subset of CIQ-sensitive cells, the weighted time constant was not significantly different in CIQ compared to control (110 ± 5.7% of control, n=16, p = 0.08, paired t-test, *see* Perszyk 2016).

(+)-CIQ increases spontaneous interneuron activity in mouse hippocampal brain slices.

Hippocampal CA1 interneurons exhibit tonic firing activity that can be modulated by NMDAR activity (Lacaille 1987, Xue 2011). To determine whether (+)-CIQ could

influence interneuron activity through its actions on GluN2D-containing NMDARs, we recorded spontaneous inhibitory post synaptic currents (sIPSCs) from CA1 pyramidal cells from P7-14 mice. $GABA_A$ receptor-mediated sIPSCs (Figure 4.7A) were isolated by recording at the reversal potential of AMPARs and NMDARs (+10mV, see *Methods*). The baseline sIPSC frequency (3.51 ± 0.55 s^{-1}) was increased during application of (+)-CIQ by 1.48 ± 1.9 fold (Figure 4.7B, C, paired t-test, $p = 0.02$). In addition, (+)-CIQ significantly increase the total inhibitory charge transfer, measured as the integral of the sIPSC recordings, by 1.71 ± 0.3 fold of baseline (paired t-test t-test, $p = 0.04$, Figure 4.7C). There was no detectable difference in sIPSC peak amplitude (1.12 ± 0.12 fold of baseline, paired t-test t-test, $p = 0.32$).

In parallel experiments, 200 μM APV was applied to the slice, and did not detectably alter the mean sIPSC frequency (control 2.60 ± 0.54 s^{-1}, APV 2.18 ± 0.34 s^{-1}). Application of (+)-CIQ, in the presence of APV had no significant effect on sIPSC frequency (0.92 ± 0.13 fold of baseline, $p = 0.56$), amplitude (0.96 ± 0.08 fold of baseline, $p = 0.65$) or total inhibitory charge transfer (Figure 4.7B, C, 0.86 ± 0.15 fold of baseline, $p = 0.32$). These data suggest that the effects of (+)-CIQ that we measured were NMDAR-dependent.
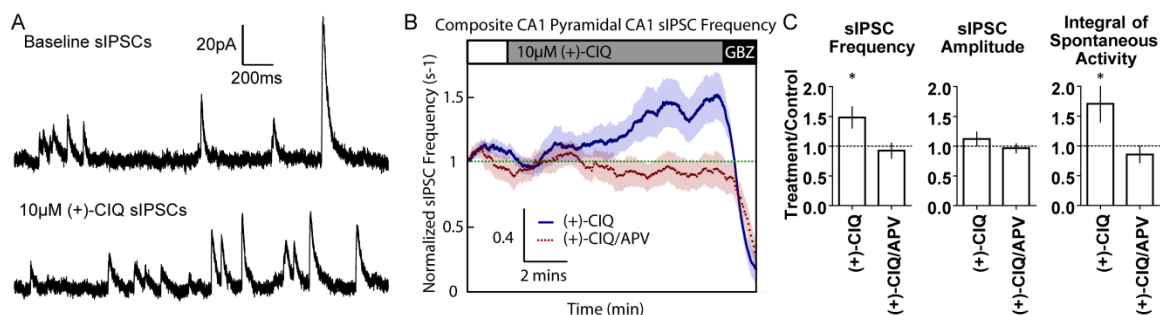
Figure 4.7. (+)-CIQ increases spontaneous interneuron activity in hippocampal brain slices from P7-14 mice.

(**A**) Representative sIPSC recordings from CA1 pyramidal cells before and during the application of (+)-CIQ. (**B**) Composite rolling average (30s window of sIPSC frequency from CA1 pyramidal cells in the presence of (+)-CIQ and (+)-CIQ/APV. A baseline sIPSC frequency was established (white box, aCSF/DMSO for (+)-CIQ recordings and aCSF/200 µM APV/DMSO for (+)-CIQ/APV recordings) followed by the addition of 10 µM (+)-CIQ (grey box). Experiments ended in 10 µM gabazine (black box) to ensure spontaneous sIPSCs reflected solely GABA$_A$ receptor-mediated transmission. The shaded area shows SEM across cells. (**C**) Average change (fold over baseline response) in sIPSC frequency, amplitude and integral of current response of spontaneous activity for (+)-CIQ and (+)-CIQ/APV recordings. *indicates $p < 0.05$ by unpaired t-test of fold change over baseline for test conditions.

Discussion

Three important conclusions can be drawn from this study. First, *GRIN2D* mRNA is present in a wide array of interneurons as assessed by single cell PCR and *in situ* hybridization experimentation. Second, GluN2D subunit immunoreactivity could be detected in the neuropil of all hippocampal subfields, and expression persisted in adult mice. Third, the GluN2C/GluN2D-selective positive allosteric modulator (+)-CIQ potentiates the NMDAR-component of synaptic events in WT hippocampal CA1 interneurons but not *GRIN2D*-/- interneurons. These data suggest that (+)-CIQ can increase the activity of hippocampal CA1 interneurons, which was confirmed in recordings of spontaneous IPSCs in hippocampal pyramidal cells. These data provide strong evidence that the GluN2D subunit contributes to the NMDARs that mediate excitatory synaptic transmission onto interneurons. In addition, we describe (+)-CIQ's improved pharmacological properties over its racemic mixture.

Expression of GluN2D in hippocampal interneurons has previously been inferred by various means (Monyer 1994, Thompson 2002, von Engelhardt 2015). Here, we provide direct functional pharmacological evidence supporting the expression of GluN2D at synapses in hippocampal interneurons. By contrast, GluN2D appears to be undetectable in the NMDARs that mediate excitatory synapses onto CA1 pyramidal cells at this developmental stage. Multiple lines of evidence in this study suggest that this population of synaptic NMDARs that are modulated by (+)-CIQ may be triheteromeric receptors that contain one GluN2D plus either a GluN2A or GluN2B subunit. The observed time course of the (+)-CIQ-sensitive currents (GluN2D-containing synaptic NMDAR responses) is distinct from that of recombinant diheteromeric GluN1/GluN2D

NMDARs *in vitro* (Vance 2012, Wyllie 2013, Swanger 2015). Diheteromeric GluN1/GluN2D NMDARs display an unusually long decay time constant following removal of glutamate (time constant ~1 s, at 32°C). If diheteromeric GluN1/GluN2D NMDARs were present at the synapse, we would expect a slower EPSC time course than observed, regardless of the GluN1 splice variant expressed (Vance 2012) given that the deactivation rate of the receptors expressed controls the time course of the EPSC (Lester 1990). However, the absence of a detectable increase in the deactivation time course of the NMDAR response by potentiating GluN2D-containing receptors suggests that the NMDAR pool does not contain a high portion of diheteromeric GluN1/GluN2D NMDARs. Recent data describing the time course of triheteromeric NMDARs suggest that the deactivation time course may be dominated by that of the faster deactivating subunit following rapid removal of glutamate (Hansen 2014). For example, the deactivation time course for triheteromeric GluN1/GluN2A/GluN2B NMDARs (57 ms, 23°C) was closer to that of the faster deactivating GluN1/GluN2A diheteromeric receptor (33 ms, 23°C) than the slower deactivating GluN1/GluN2B diheteromeric receptor (274 ms, 23°C, data from Hansen 2014). Thus, the EPSC time course that we detected here (200 ± 18 ms, 29-32°C) may reflect the more rapid deactivation of the GluN2 subunit that is co-assembled with GluN2D. In addition, racemic CIQ's actions on *in vitro* GluN1/GluN2A/GluN2D-containing NMDAR further suggest that (+)-CIQ acts on triheteromeric receptors in this study. The degree of potentiation by 10 μM (+)-CIQ (150%) observed here is similar to that described for CIQ actions on tri-heteromeric GluN1/GluN2A/GluN2D receptors, as opposed to diheteromeric receptors that contain 2 copies of GluN2D, which show >200% potentiation by CIQ (Mullasseril 2010). Together

these data suggest GluN2D-containing diheteromeric NMDARs are either not present at the synapse or constitute a small portion of the synaptic receptor pool of NMDARs.

There is also the possibility that only a subset of synapses express synaptic GluN2D-containing NMDARs, which would reduce the experimentally measured mean effect of (+)-CIQ from all synapses (as measured by mEPSC recordings). In addition, (+)-CIQ for unanticipated reasons might not reach all synapses in the recorded slices, preventing a fully potentiated state. The evoked EPSCs recorded at positive potentials revealed that approximately 1 in 3 cells are influenced by racemic CIQ. By contrast, data obtained for mEPSCs and single cell RT-PCR experiments, in which more than 75% of the cells show evidence of *GRIN2D* expression. This discrepancy in GluN2D detection may have a systematic cause. Single-cell RT-PCR samples the complete cellular contents of the neuron and detected mEPSCs should be sampled from the entire dendritic arbor of the neuron, whereas typical stimulating protocols activate release from only 5-10 synapses (approximated from the average stimulated response amplitudes and mEPSC amplitude at +40 mV in this study). The lower percentage of CIQ-sensitive synaptic cells may also reflect voltage-dependent plasticity of GluN2D, given the step to +40 mV might increase intracellular levels of Ca^{2+} that could momentarily overload the buffering capacity provided by the intracellular BAPTA and alter receptor expression or localization.

Our results agree with a recent study (von Engelhardt 2015), which uses genetic studies and pharmacological experiments that implies the expression of synaptic GluN2D by analyzing the effects of a GluN2B-selective inhibitor, ifenprodil, on hippocampal CA1 interneurons in WT and *GRIN2D*-/- mice. Our data from experiments showing the actions

of (+)-CIQ on mEPSCs deactivation taus suggest that the presence of a GluN2D-containing pool of synaptic NMDARs does not prolong the EPSC time course. This result differs from recent data showing that ifenprodil prolongs the EPSC time course (von Engelhardt 2015), which was interpreted to reflect the influence of GluN2D on synaptic currents in the absence of functional GluN2B. Additionally, our data with (+)-CIQ suggests that synaptic GluN2D-containing NMDARs in CA1 interneurons are potentially triheteromeric NMDARs. The discrepancy in the GluN2D-containing component of the NMDAR-EPSC synaptic time course between these two studies could be due to pharmacology of ifenprodil at these triheteromeric receptors. For instance, ifenprodil is known to increase glutamate affinity at GluN2B-containing NMDARs (Kew 1996, Kew and Kemp 1998), which slows the deactivation time course, an effect that might be pronounced in GluN2B/GluN2D triheteromeric NMDARs. A complete study of ifenprodil's actions at all possible triheteromeric receptors that can be made with GluN2A, GluN2B and GluN2D will need to be assessed to fully interpret these observations.

Interestingly, we detected a slower NMDAR synaptic time course in *GRIN2D*-/- neurons (300 ± 44 ms) than WT neurons (200 ± 18 ms), consistent with the result reported by von Engelhardt (2015) who showed at a lower recording temperature and different animal age a prolongation of the median time constant from 253 ms in WT mice to and 323 ms in *GRIN2D*-/- mice. This result is paradoxical since GluN2D has a longer deactivation time course, and the loss of GluN2D would therefore be expected to shorten the net NMDA deactivation time course, as is observed in the spinal cord and subthalamic nuclei (Hildebrand 2014, Swanger 2015). This may reflect an overall

difference in GluN2D expression or differences in GluN2D-containing NMDAR composition. Additionally, the *GRIN2D*-/- mice might have a disrupted GluN2A/GluN2B developmental switch that gives rise to this observed deactivation time course at this age (Liu 2004, Lu and Constantine-Paton 2004), or other compensatory mechanisms that alter the properties of synaptic receptors. More work needs to be done to further understand how specific NMDAR subunits such as GluN2D influence circuit-, network-, and systems-level dynamics

The finding that GluN2D is expressed in hippocampal interneurons has important implications for circuit function, exemplified by the ability of (+)-CIQ to increase the activity of CA1 interneurons. The presence of GluN2D could enable a different role of NMDARs in these cell types and in the hippocampal network. Co-assembly of GluN2D may change open probability and trafficking of synaptic receptors, and consequently alter where these receptors are expressed, what signals (i.e. synaptic, peri-synaptic, extra-synaptic) they receive, and how these signals are integrated. The interneurons of the hippocampus as well as neocortex control the excitability of local circuits, influencing other interneurons as well as principle cells, and thus sculpting the firing patterns of pyramidal/projection neurons. Furthermore, the GluN2D subunit may dictate distinct rules for the firing patterns that are capable of triggering NMDAR-dependent synaptic plasticity. If potentiation of GluN2D changes the synaptic NMDAR response to be more GluN2D-like (low open probability, low Ca^{2+} permeability, weak Mg^{2+} block) when the population of receptors are mixed, neuronal plasticity that depends on these properties, such as spike timing-dependent plasticity, may be altered by GluN2D potentiation (Hao and Oertner 2012, Verhoog 2013, Stefanescu and Shore 2015). A complete understanding

of the pharmacology of triheteromeric NMDARs containing GluN2D is required to understand how these receptors are behaving in the hippocampus. As shown by the increase in sIPSC frequency by (+)-CIQ, positive allosteric modulation of GluN2D-containing NMDARs could have important effects on circuit and network function. The ability of GluN2C/D-selective modulators to alter the network balance of hippocampus by selectively acting on interneurons (Bachtiar and Stagg 2014, Talaei 2016) might have significant actions on animal behavior, such as learning and memory (Kullmann and Lamsa 2007, Sweatt 2016). In addition, modulation of interneuron activity by GluN2C/D-selective allosteric modulators could have therapeutic implications (Collingridge 2013).

Chapter 5: 1622-14 is a highly efficacious NMDA-receptor positive allosteric modulator that acts on hippocampal pyramidal cells and interneurons

Abstract

N-methyl-D-aspartate receptors (NMDARs) have important roles in fast excitatory neurotransmission, are implicated in the induction of neuronal plasticity, and are associated with multiple neuropathologies. Neurological disorders often involve compromised neurotransmission that leads to pathological phenotypes, and multiple lines of evidence suggest manipulation of the NMDA receptor system could be beneficial. However, multiple candidate drugs acting on NMDARs have not been successful when tested clinically, and thus there continues to be a need for new modulators to test role of NMDA receptors in neurological disorders. Here, we describe a series of positive allosteric NMDAR modulators that have distinct actions on all NMDA receptors. The most active compound potentiates responses of GluN2B-, GluN2C- and GluN2D-containing NMDARs, of maximally effective concentrations of agonist, to approximately 300-900% of control, whereas it lacks the ability to potentiate GluN2A-containing receptors. The modulator is also capable of enhancing co-agonist potency with the strongest actions on GluN2A-containing NMDARs. At native receptors, this modulator robustly enhances the charge transfer of the NMDAR-component of excitatory postsynaptic currents in hippocampal neurons, and may preferentially augment interneuron NMDARs. This modulator has robust capabilities to potentiate theta-burst responses, which should influence the induction of plasticity. These modulators could serve as useful tools to probe the role of NMDARs throughout neuronal networks.

Introduction

N-methyl-D-aspartate receptors (NMDARs) are important excitatory ionotropic receptors in the brain (Paoletti 2013). They participate in fast excitatory neurotransmission and are a contributing factor in neuronal plasticity (Collingridge 2013). In the brain there are two major classes of neurons, which are pyramidal (projection) and interneurons (local). Together, multiple subtypes of these two neuron classes comprise neural networks and interplay between them controls signal processing and network output. The hippocampus is a brain region with a well-defined cytoarchitecture containing both classed of neurons (Klausberger and Somogyi 2008). The pyramidal cells are excitatory, receive inputs from and send their axons to other brain regions or other sub-regions of the hippocampus. Interneurons are inhibitory and provide feedforward and feedback control over the pyramidal cells (Freund and Buzsaki 1996). NMDARs are expressed in both types of neurons, although recent reports suggest that there are differences in the subunit expression profiles (von Engelhardt 2015, Perszyk 2016, Swanger 2017).

Neuronal plasticity is a process where neurons alter their connectivity or responsiveness due to specific patterns of afferent signaling (Collingridge 2004). One form of neuronal plasticity, known as long term potentiation, is a processes where high-frequency stimulation leads to persistent enhancement of low-frequency evoked responses of the same connections (Bliss and Lømo 1973). Later, NMDARs were demonstrated to be critical for long term potentiation induction, but are not involved in low-frequency evoked responses (Collingridge 1983). In hippocampal interneurons, the specifics of neuronal plasticity induction and consolidation are variable and not as clearly

delineated (Pelkey 2017). Additionally, how neuronal plasticity in interneurons contribute to memory and network function requires further study (Kullmann and Lamsa 2007). The precise role of NMDARs in hippocampal interneurons is also unknown, as hippocampal interneurons express NMDAR but expression of NMDAR-dependent and – independent forms of plasticity varies on cell type (Christie 2000, Hájos 2002, Oren 2009, Nicholson and Kullmann 2014, Pelkey 2017).

NMDAR small molecule pharmacology has been most extensively developed for orthosteric antagonists, partial agonists and channel-blockers that bind within the pore (Paoletti and Neyton 2007). For many years there was a striking lack of compounds with strong subunit-selectivity, with two exceptions, with ifenprodil (along with similarly acting compounds) and spermine being GluN2B-selective allosteric modulators (Ogden and Traynelis 2011). In recent years, many new allosteric modulator series have been discovered (Bettini 2010, Mullasseril 2010, Acker 2011, Hansen and Traynelis 2011, Katzman 2015, Volkmann 2016, Hackos and Hanson 2017, Strong 2017, Swanger 2017, Wang 2017). These series have various selectivity and capabilities. These series have been used to determine the expression of particular NMDAR subunits in different brain regions and to propose divergent roles for different populations of receptors (Edman 2012, McKay 2012, Hildebrand 2014, Swanger 2015, Perszyk 2016, Swanger 2017). NMDARs have been implicated in many neurological disorders (Paoletti 2013). Many of these diseases are associated with compromised signal processing and impaired circuit function, and aberrant NMDAR signaling may in some way contribute to circuit dysfunction (Hallett and Standaert 2004, Lisman 2008, Gilmour 2012, Dulla 2016). For example, in schizophrenia the lack of NMDAR signaling in cortical interneurons is

thought to lead to reduced inhibitory control (Lisman 2008). Moreover, distinct NMDARs are expressed in different cell types, and selective modulation of NMDARs that contain different subunits may be capable of altering network activity (Yang 2006, Zhang 2014, Swanger 2015, Perszyk 2016, Swanger 2017). In order to probe NMDAR's role in neuronal networks and the potential for therapeutic intervention, new ways to modulate NMDARs are needed.

Here we describe the structural determinants and mechanism of action of a novel NMDAR modulator series, **1622**, that can efficaciously potentiate NMDAR responses, activated by maximally effective agonist concentration, and also increases agonist potency. The best in class compound, **1622-14**, increases agonist potency leading to prolonged receptor response time-course due to slowed deactivation. In mouse brain slices, we see a robust augmentation by **1622-14** of NMDAR receptor response amplitude and a marked prolongation of the deactivation time course. We have found apparent preferential actions of **1622-14** on CA1 interneurons over pyramidal cells in the hippocampus, consistent with our finding of stronger effects of **1622-14** on GluN2D. In the hippocampus, modulation by **1622-14** is capable of enhancing burst signaling that is thought to lead to the induction of plasticity while lacking actions on low-frequency signaling.

Results

Identification of a new class of positive allosteric modulators of NMDAR function.

We identified a novel NMDA receptor potentiator containing a thienopyrimidine core, referred to as compound **1622** based on internal database numbering system. Two-electrode voltage-clamp recordings of NMDARs in *Xenopus leavis* oocytes show that **1622** possesses the capability to potentiate NMDAR responses to saturating concentrations of co-agonists from GluN1/GluN2B, GluN1/GluN2C, and GluN1/GluN2D receptors (Figure 5.1A, B, Table 5.1, data from P. Le, P. Lyuboslavsky, K. Vellano, J. Zhang). This compound is not particularly potent (EC_{50} value >10 μM), but possesses the ability to strongly augment receptor responses (240-430% of control, Figure 5.1C, Table 5.1). Analysis of the time course of **1622** modulation yields a K_d value of 21.9 μM for GluN1/GluN2B NMDARs, which closely matches concentration-response data (Figure 5.1D, E, Table 5.1, data from S. Swanger). **1622** has no direct actions on NMDARs in the absence of agonists (not shown, data from P. Le). As with other positive allosteric modulators (PAMs), modulation might result in subsequent actions on agonist potency. Agonist concentration-response experiments were performed in the absence and presence of 50 μM **1622**. We observe a modest but significant enhancement of glutamate potency in GluN1/GluN2B and GluN1/GluN2D (Figure 5.1F, Table 5.2, data from J. Zhang). Additionally, **1622** enhances glycine potency in GluN1/GluN2B NMDARs, but not in GluN1/GluN2D (Figure 5.1F, Table 5.2).

We sought to determine the binding site of this novel PAM. Preliminary data suggests that the determinants of **1622** series binding do not include the GluN2 amino-terminal domain (data not shown). A number of recent series of PAMs have determinants
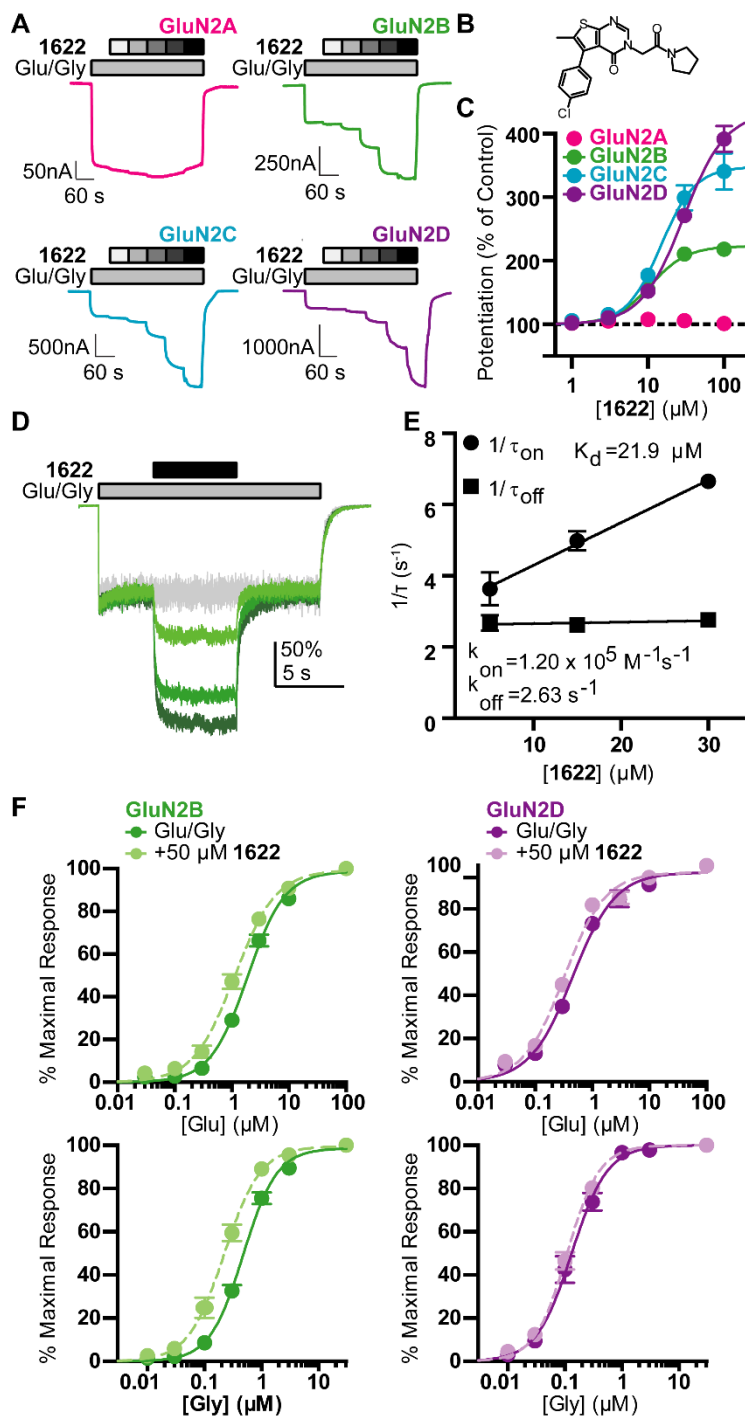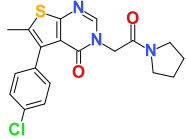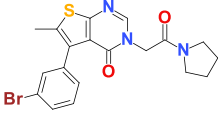
Figure 5.1. 1622 is small molecule positive allosteric modulator of NMDARs.

A) Representative two-electrode voltage-clamp oocyte recordings exemplifying the concentration-response of **1622** (gray scale boxes – 1, 3, 10, 30, 100 μM) on the diheteromeric NMDARs stimulated with saturating concentrations of agonist (gray bar,

100 µM glutamate and 30 µM glycine). B) Chemical structure of **1622**. C) Average concentration-response data of **1622**, fit by the Hill equation. D) Representative HEK293 cell patch-clamp recordings exemplifying the mass action of **1622** on GluN1/GluN2B receptors (0, 3, 15, 30 µM, lightest to darkest). E) Average time course of **1622** association and disassociation, fit with linear equations. F) Averaged agonist (glutamate *top*, glycine *bottom*) concentration-response data from GluN1/GluN2B (*left*) and GluN1/GluN2D (*right*) in the absence and presence of 50 µM **1622**, fit by the Hill equation. Data (except for panels **D** and **E**) were collected by P. Le, P. Lyuboslavsky, K. Vellano, J. Zhang. Data from panels **D** and **E** were collected and analyzed by S. Swanger.

Table 5.1. Actions of **1622** and **1622-14** on diheteromeric NMDARs activated by saturating and sub-saturating concentrations of agonist.

| ID | Structure | | EC_{50} (μM) [conf. int.][a] | | | |
| | | | **Maximal Degree of Modulation (% of control)[b]** | | | |
			GluN2A	GluN2B	GluN2C	GluN2D
1622		Saturating	-	15 [14, 17] 250 ± 12%	24 [22, 26] 410 ± 37%	37 [31, 44] 430 ± 20%
		Sub-saturating	NR	100 [78, 130] 770 ± 59%	NR	90 [29, 280] 4600 ± 16%
1622-14		Saturating	-	5.1 [4.4, 6.0] 310 ± 22%	11 [7.0, 16] 710 ± 59%	17 [14, 19] 930 ± 66%
		Sub-saturating	21 [18, 24] 990 ± 47%	14 [12, 16] 870 ± 31%	43 [37, 43] 4900 ± 350%	95 [81, 110] 8300 ± 800%

[a]EC_{50} values were obtained by least-squares fitting of data from independent recordings by the Hill equation. Hill slope value was fixed to 1. EC_{50} values are given as the mean with the 95% confidence interval determined from $\log(EC_{50})$. Data are from 5-12 oocytes recordings from at least 2 independent agonist-saturated experiments and 1 sub-saturating agonist experiment. For determination of **1622** modulation of sub-saturating responses of GluN1/GluN2B glutamate/glycine concentrations used were 1/0.3 μM and for GluN1/GluN2D were 0.3/0.1 μM. For determination of **1622-14** modulation of sub-saturating responses of GluN1/GluN2A glutamate/glycine concentrations were 1.5/0.8 μM, for GluN1/GluN2B were 1.5/0.45 μM, for GluN1/GluN2C were 0.85/0.2 μM, and for GluN1/GluN2D were 0.3/0.07 μM. [b]Underlined values represent the extent of modulation as a percent of the control response in the absence of modulator. The maximal degree of modulation is given as mean ± SEM. Data were not fit (shown as -) if the response recorded at 30 μM of test compound did not differ by more than 20% from

control. NR – indicates effect was not recorded. Data were collected by P. Le, P. Lyuboslavsky, K. Vellano, J. Zhang and sections were analyzed by R. Perszyk.

Table 5.2. 1622 actions on glutamate and glycine potency.

	EC$_{50}$ (µM) [conf. int.]^a					
	Glutamate	**+ 50 µM 1622**	**Fold Effect**	**Glycine**	**+ 50 µM 1622**	**Fold Effect**
GluN2B	1.88 [1.64, 2.15]	1.10 [0.85, 1.41]	1.71*	0.48 [0.40, 0.57]	0.22 [0.17, 0.29]	2.19*
GluN2D	0.46 [0.39, 0.55]	0.32 [0.28, 0.35]	1.45*	0.13 [0.10, 0.18]	0.11 [0.09, 0.13]	1.18

The glutamate concentration-response experiments were performed in the presence of 30 µM glycine and the glycine concentration-response experiments performed in the presence of 100 µM glutamate. ^{a}EC$_{50}$ values were obtained by least-squares fitting of data from independent recordings by the Hill equation. EC$_{50}$ values are given as the mean with the 95% confidence interval determined from log(EC$_{50}$). Data are from 8-13 oocytes recordings from at least 2 independent experiments. *indicates $p<0.05$ as determined by unpaired t-test. Data were collected by J. Zhang.

of action that include the transmembrane domain (Mullasseril 2010, unpublished data of the IPQ-2 series). Thus, we investigated the residues known to be important in the actions of these series. We probed the ability of 50 μM **1622** to modulate NMDARs containing a series of systematic mutations (all residues mutated to alanine, except for alanine that was mutated to cysteine, data are from P. Le, J. Zhang, and K. Ogden). Of the 27 GluN1 residues tested, 13 residues significantly alter modulation by 50 μM **1622**, the strongest effect arises from the mutations in pre-M1 and the portions of M1 positioned near the extracellular leaf of the plasma membrane. Additionally, of the 21 GluN2B residues tested, 14 residues significantly alter **1622** modulation. Further study of the potential determinants of action of **1622** led us to probe the effect of GluN1-exon5. Potentiation by **1622** is less efficacious on exon5-containing GluN1 splice variants expressed with GluN2B and GluN2D (Table 5.3, data from P. Le). It appears that the TMD of both subunits is critical for the full actions of **1622** and as well is influenced by other critical features of the receptor.

1622-14 is a more potent and efficacious analog of 1622.

We synthesized a series of analogs of **1622.** In *X. laevis* oocytes, **1622-14** (~90% pure) potentiates the agonist-saturated responses in GluN1/GluN2B, GluN1/GluN2C, and GluN1/GluN2D more potently and to a greater extent than **1622** (Table 5.1), but has no effect on GluN1/GluN2A response amplitude (Figure 5.2A, data from P. Le).

Given these properties, I subsequently evaluated the actions of **1622-14** on sub-saturating agonist responses. **1622-14** has pan-potentiating actions of all diheteromeric NMDARs, with greater maximal potentiation of GluN1/GluN2B, GluN1/GluN2C, and

Table 5.3. Actions of **1622** on NMDARs that contain exon5 in GluN1.

| Compound ID | EC_{50} (μM) [conf. int.][a] | | | |
| | **Maximal Degree of Modulation (% of control)**[b] | | | |
	GluN1a/2B	**GluN1b/2B**	**GluN1a/2D**	**GluN1b/2D**
1622	38 [35, 42] $\underline{260 \pm 10\%}$	-	53 [35, 81] $\underline{520 \pm 64\%}$	38 [31, 47] $\underline{300 \pm 20\%}$

[a]EC_{50} values for 1622 potentiation were obtained by least-squares fitting of data from independent recordings by the Hill equation. EC_{50} values are given as the mean with the 95% confidence interval determined from $\log(EC_{50})$. Data are from 9-10 oocytes recordings from 2 experimental recording set. [b]Underlined values represent the extent of modulation as a percent of the control response in the absence of test compound. The maximal degree of modulation is given as mean ± SEM. Data were not fit (shown as -) if the response recorded at 30 μM of test compound did not differ by more than 20% from control. Data were collected by P. Le.
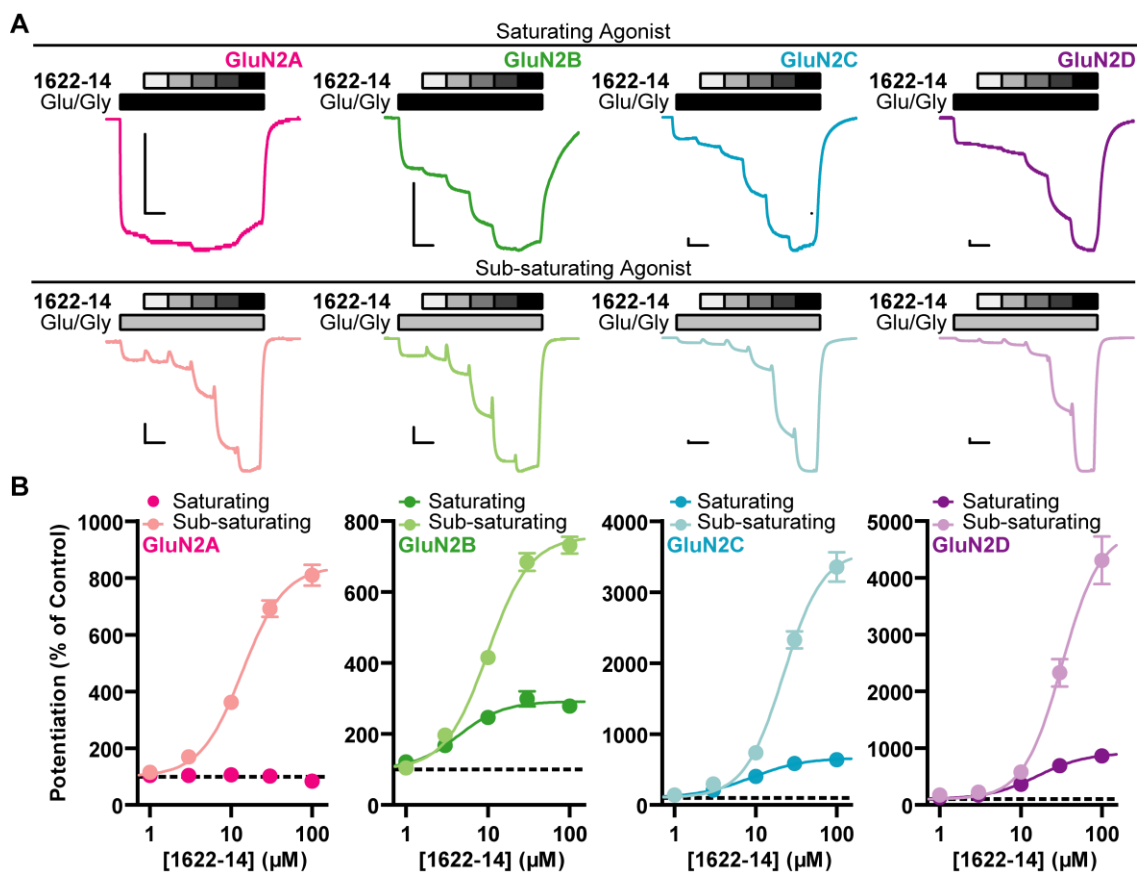
Figure 5.2. 1622-14 is a more potent and efficacious PAM, potentiation is enhanced at sub-saturating agonist responses.

A) Concentration-response curves of **1622-14** (1, 3, 10, 30, 100 μM) at saturating (*top*, 100 μM glutamate, 30 μM glycine) and sub-saturating (*bottom*, in μM for each receptor-glutamate/glycine concentration, GluN1/GluN2A-1.5/0.8 μM, GluN1/GluN2B-1.5/0.45 μM, GluN1/GluN2C-0.85/0.2 μM, GluN1/GluN2D-0.3/0.07 μM) agonist responses at all the diherteromeric NMDARs. Scale bars indicate 100 nA and 50 seconds. B) Average concentration-response data on saturating and sub-saturating agonist responses fit by the Hill equation. Data are from P. Le and R. Perszyk, and analyzed by R. Perszyk.

GluN1/GluN2D (Figure 5.2B,C, Table 5.1, data from P. Le and R. Perszyk). Greater potentiation of **1622-14** at sub-saturating agonist responses is likely a result of the ability of the modulator series to enhance agonist potency as shown by **1622**.

Next, I investigated the ability of **1622-14** to enhance NMDARs expressed in HEK293 cells when activated by brief applications (5 ms) of glutamate, similar to synaptic-like responses (Figure 5.3, data from J. Zhang and R. Perszyk). Comparable to **1622-14**'s actions on equilibrium effects on agonist-saturated responses, the peak responses of agonist application are potentiated by **1622-14** at GluN1/GluN2B, GluN1/GluN2C, and GluN1/GluN2D but not GluN1/GluN2A receptors (Figure 5.3A,C, Table 5.4). **1622-14** prolongs the deactivation time course (τ_w) of all NMDARs (Figure 5.3B,D, Table 5.4). The enhancement of the deactivation time course should be tightly correlated to the enhancement of agonist potency. Accordingly, the enhancement of GluN1/GluN2D deactivation is less than GluN1/GluN2B, reflecting a parallel activity pattern to **1622** enhancement of agonist potency (Table 5.4). In experiments with longer agonist applications times, similar trends are observed. The deactivation time-courses in these recordings are prolonged at all receptors in the presence of **1622-14** (Figure 5.4). The largest fold change in the weighted tau of deactivation occurs at GluN1/GluN2A, followed by similar fold changes in deactivation of GluN1/GluN2B and GluN1/GluN2C responses, and GluN1/GluN2D response deactivation increases the least (Table 5.5). Additionally, the rise time of the brief and 1.5 s glutamate responses are slowed in the presence of **1622-14** at all receptors except for GluN1/GluN2C for the 1.5 s glutamate application and GluN1/GluN2A for both glutamate application (Figure 5.4, Table 5.5).
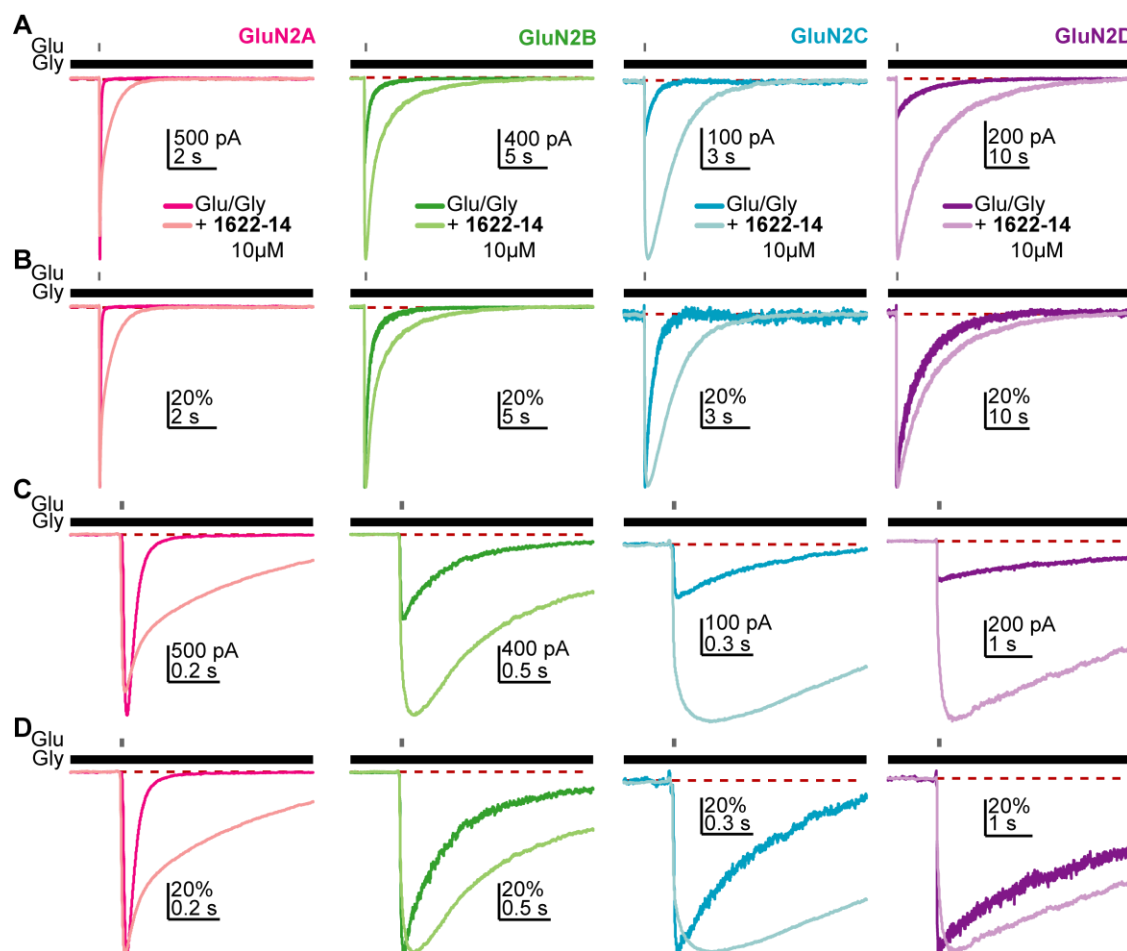
Figure 5.3. 1622-14 enhances NMDAR responses to brief glutamate exposures in HEK293 and prolongs deactivation.

A) Representative NMDAR responses to the 5 ms application of glutamate (100 μM, grey bar) in sustained exposure of glycine (30 μM, black bar) and with or without **1622-14** (10 μM, black bar, presence denoted by the legend). B) Same responses as in **A** but normalized to the peak response. C) Same traces as in **A** expanded to highlight the activation portion of the response. D) Same responses as in **B** expanded to highlight the deactivation of unmodulated and modulated response. Data are from J. Zhang and R. Perszyk, and analyzed by R. Perszyk.

Table 5.4. 1622-14, 10 µM, actions on 5 ms glutamate NMDAR responses.

	GluN2A		GluN2B		GluN2C		GluN2D	
	Control	**1622-14**	Control	**1622-14**	Control	**1622-14**	Control	**1622-14**
	($N = 8$)		($N = 6$)		($N = 6$)		($N = 7$)	
Peak$_{amp}$ (pA)	2281±689	1519±218	487±183	683±190	309±207	776±395	151±23.4	667±90.2
Fold	0.85±0.11		1.72±0.32*		3.33±0.31*		4.66±0.61*	
Rise Time (ms)	10.6±0.448	10.2±0.463	20.0±1.65	75.9±14.0	19.7±2.56	154±35.6	38.9±5.38	138±15.3
Fold	0.96±0.03		3.90±0.73*		9.24±3.12*		3.86±0.64*	
τ_{FAST} (ms)	37.9±5.72	54.0±7.63	304±38.7	1330±314	317±36.5	1250±196	1630±196	2850±454
Fold	1.56±0.21		4.45±0.97		3.54±0.94		1.93±0.46	
τ_{SLOW} (ms)	321±125	615±85.1	1180±190	4240±1300	1160±439	3790±2340	8390±738	13800±1970
Fold	4.96±1.59		3.74±1.01		3.53±1.62		1.63±0.14	
τ_w (ms)	48.1±7.49	302±26.7	592±46.4	1930±366	615±134	1570±168	6410±474	10700±1180
Fold	7.11±1.08*		3.33±0.57*		2.84±0.45*		1.66±0.07*	
% τ_{FAST}	83.7±10.3	52.9±4.96	61.4±9.74	69.6±9.11	49.9±12.3	58.1±13.3	28.9±1.96	26.3±5.48
Fold	-		-		-		-	

Fold values are **1622-14** divided by control. *indicates p<0.05 as determined by paired t-test using the Holm–Bonferroni method to correct for the family-wise error rate, comparing peak$_{amp}$, rise time, and τ_w. Data are from J. Zhang and R. Perszyk, and analyzed by R. Perszyk.
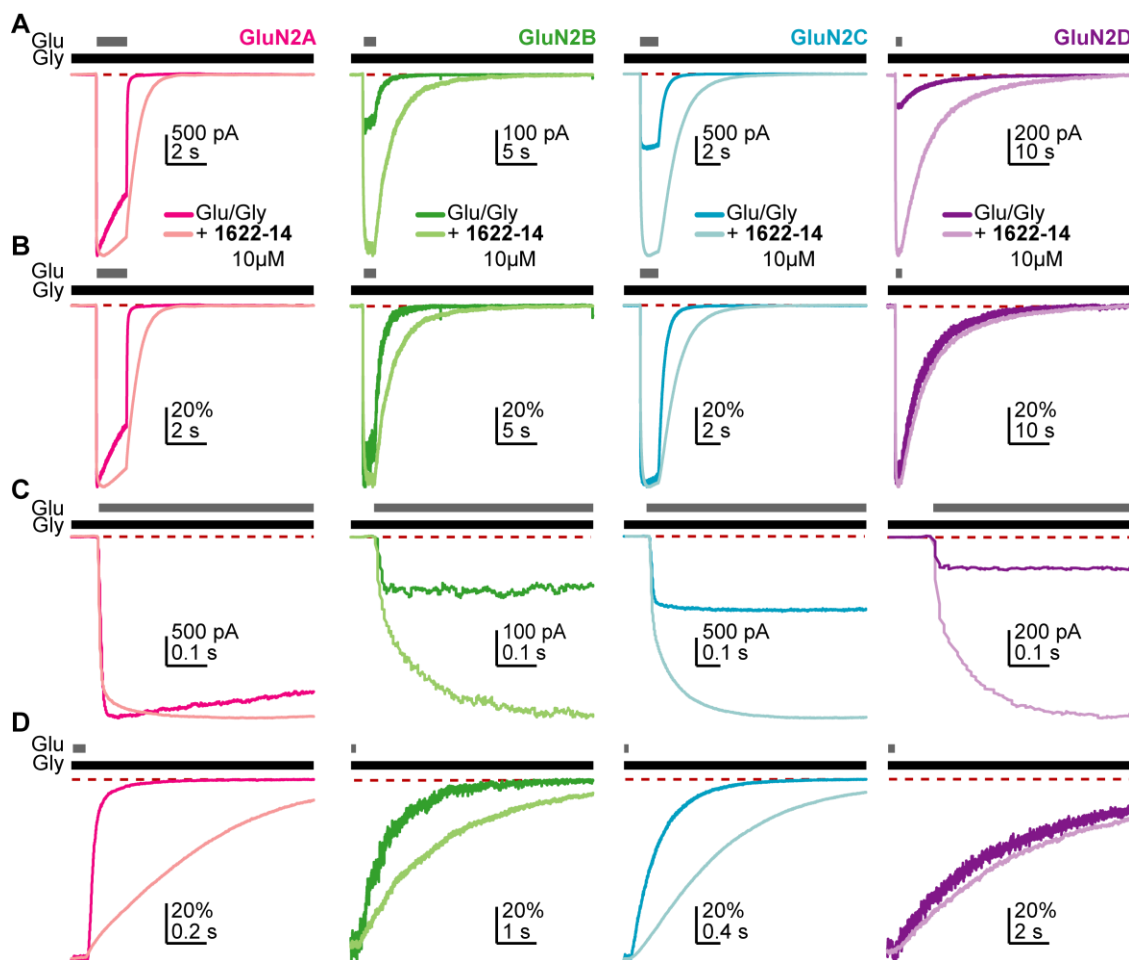
Figure 5.4. 1622-14 enhances NMDAR responses to 1.5 s glutamate exposures in HEK293 and prolongs deactivation.

A) Representative NMDAR responses to the 1.5 s application of glutamate (100 μM, grey bar) in sustained exposure of glycine (30 μM, black bar) and with or without **1622-14** (10 μM, black bar, presence denoted by the legend). B) Same responses as in **A** but normalized to the peak response. C) Same traces as in **A** expanded to highlight the activation portion of the response. D) Same responses as in **B** expanded to highlight the deactivation of unmodulated and modulated response. Data are from J. Zhang and R. Perszyk, and analyzed by R. Perszyk.

Table 5.5. 1622-14, 10 μM, actions on 1.5 s glutamate NMDAR responses.

	GluN2A		GluN2B		GluN2C		GluN2D	
	Control	**1622-14**	Control	**1622-14**	Control	**1622-14**	Control	**1622-14**
	($N = 8$)		($N = 6$)		($N = 5$)		($N = 7$)	
Peak_{amp} (pA)	2010±400	2100±350	536±186	849±193	176±55.2	603±133	198±24.8	846±103
Fold	1.08±0.05		1.91±0.33*		4.02±0.88*		4.37±0.44*	
Response_{ss} (pA)	1570±390	1780±300	400±156	730±200	176±50.0	598±128	200±24.9	837±103
Fold	1.28±0.13		2.29±0.51*		3.74±0.65*		4.27±0.42*	
Rise Time (ms)	14.8±1.23	53.1±17.3	82.2±32.1	187±41.2	160±62.4	291±48.1	131±21.6	199±18.5
Fold	3.53±1.04		4.31±2.02*		3.78±2.37		1.84±0.39*	
SS/Peak (%)	77.8 ±7.83	86.7±5.34	73.8±4.78	86.2±8.78	104±6.32	99.6±0.77	101±1.69	99.0±0.47
Fold	-		-		-		-	
τ_{FAST} (ms)	34.5±3.36	250±60.1	457±93.0	1470±247	284±75.2	1300±156	2460±326	4270±1030
Fold	5.97±2.17		3.83±0.77		5.48±1.22		1.81±0.41	
τ_{SLOW} (ms)	240±21.5	786±69.9	3700±2590	7770±1930	1110±296	4560±1230	9600±1230	21400±7410
Fold	3.37±0.30		6.30±2.35		3.73±1.31		2.48±0.94	
τ_w (ms)	74.6±9.49	666±52.3	788±80.6	2390±117	557±36.6	1970±395	6700±458	9770±802
Fold	9.40±0.85*		3.15±0.36*		3.62±0.77*		1.48±0.14*	
% τ_{FAST}	80.8±1.78	22.8±9.26	60.2±8.72	78.8±9.21	57.2±19.3	79.3±6.44	37.4±5.61	47.6±13.4
Fold	-		-		-		-	

Fold values are **1622-14** divided by control. *indicates p<0.05 as determined by paired t-test using the Holm–Bonferroni method to correct for the family-wise error rate, comparing peak$_{amp}$, response$_{ss}$, rise time, and τ_w. Data are from J. Zhang and R. Perszyk, and analyzed by R. Perszyk.

Although this experiment was not designed to directly address modulator action on the rise time of receptor responses, it seems likely that there is some effect of **1622-14** as the rise time, at most receptors, was slowed by at least 3-fold.

1622-14 potentiates the NMDAR-component of synaptic hippocampal excitatory transmission in both pyramidal cells and interneurons.

Before using this compound series in native tissue we wanted to assess the off-target profile of these compounds and how these molecules might interact with specific sub-types that exist. We used the National Institute of Mental Health Psychoactive Drug Screening Program to screened **1622** and **1622-14** in a binding assay against a panel of neuropsychiatric receptors (see *methods*) (Besnard 2012). Out of the panel of 45 receptors, **1622** causes a 50% reduction in binding of the ligand used in 2 receptors (peripheral benzodiazepine and sigma2) and **1622-14** reduced binding of antagonist probes for 5-TH$_{2C}$ and peripheral benzodiazepine receptors. Secondary testing was performed on these receptors to determine an affinity for these potential interactions. **1622** interacted with the peripheral benzodiazepine receptor with a K$_i$ of 1.7 µM and with sigma2 receptors with a K$_i$ of 6.1 µM. **1622-14** displaced the test ligand for 5-HT$_{2C}$ and peripheral benzodiazepine receptor with affinities of 0.42 and 0.98 µM, respectively. Additionally, **1622-14** was screened for interactions with several ionotropic receptors of various families (GABA$_A$ α1β2γ2s, GABA$_C$ ρ1, AMPAR GluA1, kainate GluK2, glycine α1, serotonin 5-HT$_{3A}$, nicotinic acetylcholine receptor α1β1γδ, α4β2, α7 and purinergic P2X2, data are from J. DiRaddo). Of this panel, **1622-14** only significantly modulates 5HT$_{3A}$ responses (71.4% of control, n=5, $p < 0.05$, data not shown).

NMDARs can form triheteromeric receptors that contain 2 different GluN2 subunits (Traynelis 2010). In the hippocampus there is evidence of the expression of GluN2A, GluN2B and GluN2D at synapses (von Engelhardt 2015, Perszyk 2016, Swanger 2017). To date there are only efficient means to robustly express GluN2 triheteromeric receptor containing GluN2A and GluN2B. **1622** (30 μM) potentiates GluN1/GluN2B/GluN2B receptors to 167 ± 5.5%, GluN1/GluN2A/GluN2A receptors to 106 ± 1.6%, and GluN1/GluN2A/GluN2B receptors to 125 ± 2.2% (one-way ANOVA, $F(2,15) = 61.79$, $p < 0.0001$, all groups are significantly different than each other via Tukey's multiple comparison test, $p < 0.05$). Additionally, **1622-14** (10 μM) potentiates GluN1/GluN2B/GluN2B receptors to 185 ± 5.5%, GluN1/GluN2A/GluN2A receptors to 101 ± 0.5%, and GluN1/GluN2A/GluN2B receptors to 116 ± 1.1% (one-way ANOVA, $F(2,14) = 266.7$, $p < 0.0001$, all groups are significantly different than each other via Tukey's multiple comparison test, $p < 0.05$). In a more comprehensive assessment of **1622-14** modulation of triheteromeric receptors, **1622-14** modulates GluN1/GluN2A/GluN2B receptors with low μM affinity to an extent of roughly 150% (Table 5.6).

I then sought to understand how 1622-14 modulates evoked synaptic NMDAR responses. I prepared ex vivo slices from young C57Bl/6 mice (P8-16). EPSCs were evoked by stimulating Schaffer collaterals and the NMDAR-component was isolated using pharmacology and recording at +40 mV (Figure 5.5, see methods). Ifenprodil (3 μM) is capable of inhibiting these responses by 50 ± 7 % (Table 5.7). 1622-14 (10 μM) did not enhance the peak response (79 ± 9%) but enhances the integrated charge transfer

Table 5.6. Actions of **1622-14** on specific triheteromeric NMDAR populations.

	EC$_{50}$ (µM) [conf. int.]^a		
	Maximal Degree of Modulation (% of control)^b		
Compound ID	**GluN2A/2A**	**GluN2A/2B**	**GluN2B/2B**
1622-14	-	2.6 [2.1, 3.2] 150 ± 4.6%	9.1 [7.7, 11] 360 ± 31%

^{a}EC$_{50}$ values were obtained by least-squares fitting of data from independent recordings by the Hill equation. Hill slope value was fixed to 1. EC$_{50}$ values are given as the mean with the 95% confidence interval determined from log(EC$_{50}$). Data are from 4-9 oocytes recordings from 1 experimental recording set. ^{b}Underlined values represent the extent of modulation as a percent of the control response in the absence of test compound. The maximal degree of modulation is given as mean ± SEM. Data were not fit (shown as -) if the response recorded at 30 µM of test compound did not differ by more than 20% from control.
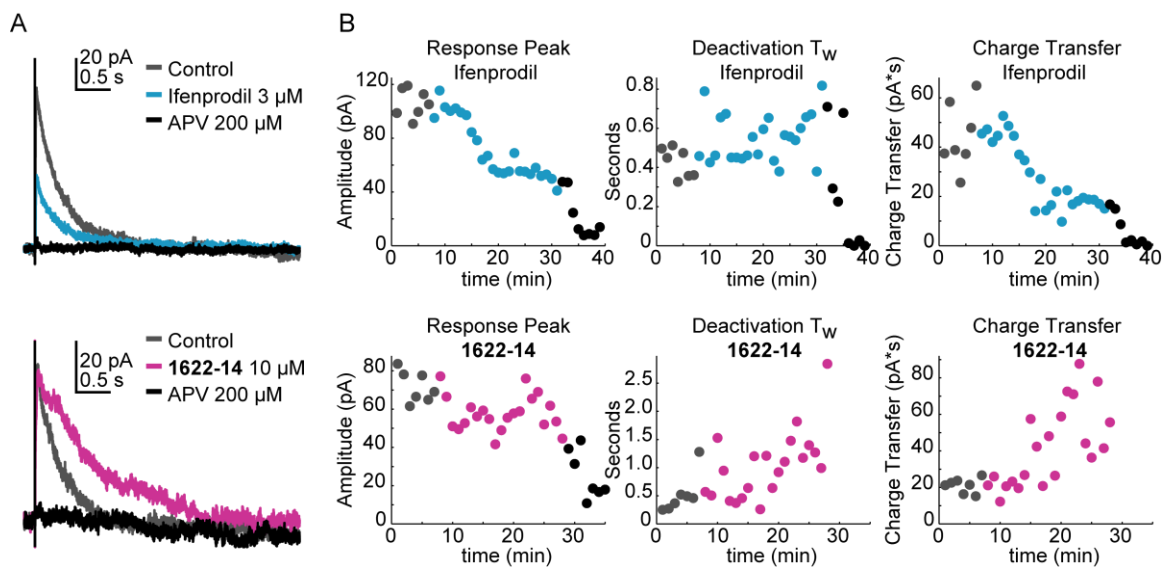
Figure 5.5. 1622-14 enhances net charge transfer of NMDAR responses of CA1 pyramidal cells.

A) Averaged evoked EPSCs with the NMDAR-component isolated highlighting the actions of ifenprodil (*top*) and **1622-14** (*bottom*); V_{HOLD} was +40 mV. B) Experimental time-course of the EPSC properties from **A**; the colors of data points correspond to experiment phases indicated by the legend in **A**. Solutions were changed at the beginning of each new phase of the experiment. The data from the APV-phase was not shown for τ_w and charge transfer due to variability of the diminished responses.

Table 5.7. 1622-14, 10 μM, effects on Shaffer collateral evoked EPSCs recorded from CA1 pyramidal cells.

	Control	Ifenprodil (3 μM)		APV (200 μM)
	($N = 6$)	Raw	Fold	Fold
Peak$_{amp}$ (pA)	105 ± 21	55.2 ± 16.4	0.50 ± 0.07*	0.11 ± 0.02
Rise Time (ms)	18.3 ± 3.3	15.2 ± 1.7	0.98 ± 0.18	
τ_{FAST} (ms)	67.1 ± 21.1	51.7 ± 13.9	1.23 ± 0.67	
τ_{SLOW} (ms)	543 ± 176	346 ± 79	0.98 ± 0.32	
τ_W (ms)	298 ± 39	243 ± 57	0.91 ± 0.26	
% τ_{FAST}	37.9 ± 11.1	45.8 ± 11.9	1.47 ± 0.24	
CT (ms*pA)	28.6 ± 5.59	13.7 ± 4.7	0.45 ± 0.09*	0.03 ± 0.01
	Control	**1622-14** (10 μM)		APV (200 μM)
	($N = 9$)	Raw	Fold	Fold
Peak$_{amp}$ (pA)	145 ± 23	108 ± 15	0.79 ± 0.09	0.16 ± 0.02
Rise Time (ms)	25.0 ± 3.8	51.3 ± 23.5	1.77 ± 0.49	
τ_{FAST} (ms)	79.8 ± 16.1	842 ± 241	16.0 ± 7.6	
τ_{SLOW} (ms)	440 ± 51	1980 ± 440	4.75 ± 1.3	
τ_W (ms)	363 ± 46	1280 ± 209	3.50 ± 0.41*	
% τ_{FAST}	21.0 ± 5.8	43.9 ± 13.8	3.06 ± 1.23	
CT (ms*pA)	55.0 ± 10.5	120 ± 27	2.24 ± 0.37*	0.15 ± 0.07

Fold values are **1622-14** or ifenprodil divided by control. CT stands for charge transfer. *indicates $p<0.05$ as determined by paired t-test using the Holm–Bonferroni method to correct for the family-wise error rate, comparing peak$_{amp}$, rise time, τ_w, and charge transfer.

(2.24 ± 0.37 fold), which is primarily due to a prolongation of the deactivation time-course of the $EPSC_{NMDAR}$ by 3.50 ± 0.41 fold (Table 5.7).

Next, I sought to determine if **1622-14** showed differential modulation of NMDARs on pyramidal cells and interneurons, given these cells express different NMDAR subunits (von Engelhardt 2015, Perszyk 2016, Swanger 2017). I recorded miniature EPSCs in both CA1 pyramidal cells and stratum radiatum interneurons in the presence of TTX (Figure 5.6A, B). Spontaneous events were detected and averaged (Figure 5.6C, see *methods*), and the mean composite mEPSC waveform was used for analysis (Figure 5.6D). In this dataset, interneuron mEPSCs, compared to pyramidal cells generally had larger AMPAR-components and smaller NMDAR-components (Figure 5.6, Table 5.8). Application of **1622-14** (10 μM) increases the NMDAR-component but not the AMPAR-component (Figure 5.6E-G, Table 5.8). Additionally, **1622-14** increases the net charge transfer of the NMDAR-component of the response in both cell types; a significant effect was determined between cell type, with drug application, and an interaction of factors was also detected (Figure 5.6G, Table 5.8). It appears that the increase in the charge transfer by **1622-14** is on average larger in interneurons than in pyramidal cells (Table 5.8).

1622-14 enhances theta-burst potentials but not low frequency EPSPs in the CA1.

Given NMDAR expression in multiple cell types in the hippocampus, I sought to assess how **1622-14** might alter network dynamics in the brain by performing field recording in the CA1. To focus on the excitatory connections, I performed experiments in the presence of picrotoxin to block fast inhibitory neurotransmission, with the Schaffer
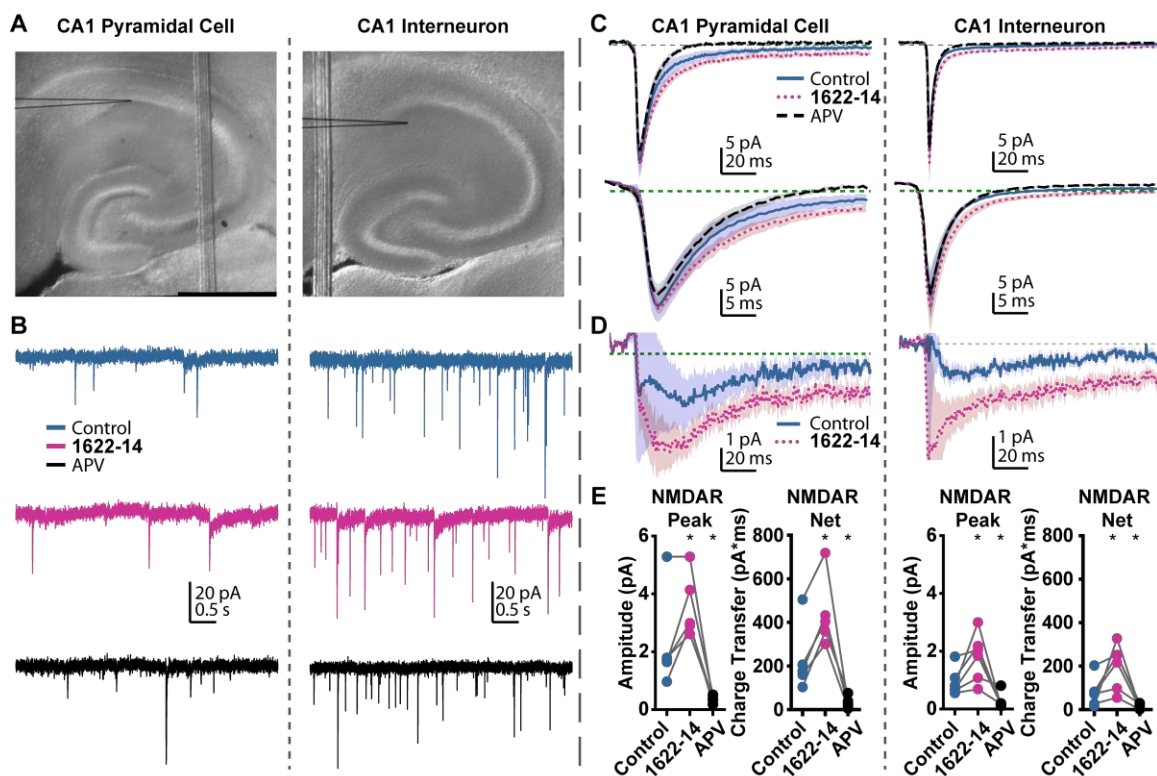
Figure 5.6. 1622-14 enhances the NMDAR-component of mEPSC from both CA1 pyramidal cells and stratum radiatum interneurons.

A) Images of mouse hippocampal brain slices during mEPSC recordings from a pyramidal cell (*left*) and an interneuron (*right*). The outline of the recording electrode is enhanced. B) Representative mEPSC recordings from a pyramidal cell (*left*) and an interneuron (*right*). C) Averaged composite mEPSCs (shaded area indicates the SEM of the averaged response) from each of the experimental phases indicated, lower panel shows an expanded view highlighting the AMPAR-component of the response. D) The averaged composite mEPSCs from **C** with the APV response subtracted from the other responses to highlight the NMDAR-component of the mEPSC. E) Experimental data of the NMDAR response amplitudes and net charge transfer from pyramidal cells (*left*) and interneurons (*right*). The concentration of **1622-14** used was 10 μM.

Table 5.8. 1622-14 effects on CA1 mEPSCs from pyramidal cells and interneurons.

	Control		**1622-14** (10 µM)		APV (200 µM)	
	Pyramidal N=5	Interneuron N=6	Pyramidal	Interneuron	Pyramidal	Interneuron
AMPA$_{peak}$ (pA)	21.7 ± 2.9	30.5 ± 6.7	22.3 ± 1.1	34.8 ± 8.2	24.3 ± 2.06	34.8 ± 8.3
Fold			1.08 ± 0.10	1.13 ± 0.03		
NMDA$_{peak}$ (pA)	2.28 ± 0.76	0.93 ± 0.19	3.59 ± 0.50*	1.81 ± 0.34*	0.36 ± 0.05*	0.26 ± 0.11*
Fold			1.94 ± 0.36	2.08 ± 0.40		
NMDA$_{CT}$ (pA*s)	230 ± 70	79.3 ± 27.2	314 ± 56*	200 ± 42*	32.7 ± 11.9*	16.8 ± 4.7*
Fold			2.23 ± 0.35	5.05 ± 2.95		
Frequency (s^{-1})	0.44 ± 0.04	0.62 ± 0.09	0.35 ± 0.05	0.52 ± 0.10	0.30 ± 0.10	0.49 ± 0.10
Fold			0.83 ± 0.18	1.04 ± 0.35		

Fold values are **1622-14** divided by control. *indicates $p < 0.05$ as determined by a Dunnett's multiple comparison test with control after a 2-way ANOVA. CT stands for charge transfer.

collaterals severed to control CA3 bursting (Figure 5.7A) (Le Duigou 2013). Low frequency EPSPs are not modulated by **1622-14** or D-APV, whereas potentials generated by theta-burst stimulation are enhanced by **1622-14** and reduced by D-APV (Figure 5.7B, C). The three theta-burst potentials recorded in picrotoxin appear to be limited by a form of desensitization or diminished NMDAR signaling, where the 2nd and 3rd bursts appear to be different than the first and not partially blocked by D-APV. However, this diminished theta-burst potential is augmented by **1622-14** (Figure 5.7B), suggesting that there is a substantial contribution to it by NMDA receptors that can be potentiated by **1622-14**.
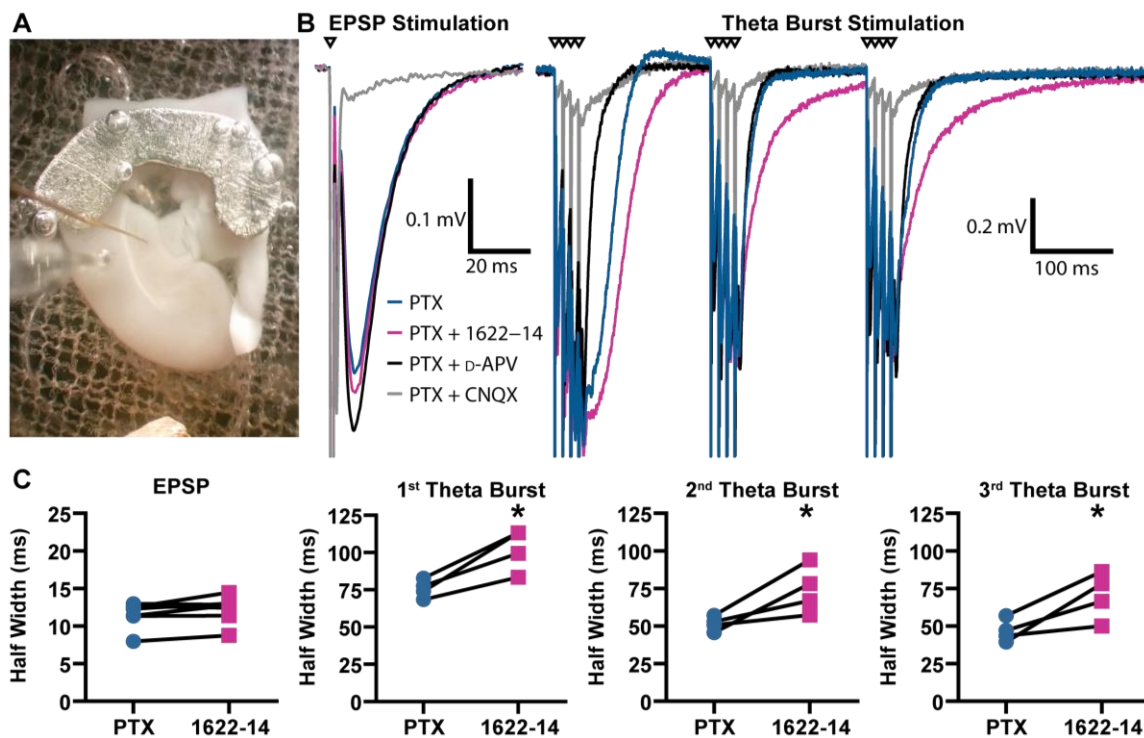
Figure 5.7. 1622-14 enhances theta-burst potentials but not low frequency EPSPs.

A) Image of a rat hippocampal brain slice in a field recording experiment, the CA3 was removed prior to experimentation to prevent recurrent CA3 bursting with the application of picrotoxin (10 μM). B) Representative CA1 stratum radiatum EPSPs (*left*) and theta-burst potentials (*right*) in different pharmacological agents (**1622-14** 10 μM, D-APV 50 μM, CNQX 10 μM) C) EPSP half-width and theta-burst half-width data from each recorded slice recorded.

Discussion

Here a novel compound series synthesized at Emory (Liebeskind, Liotta, Traynelis, unpublished) that are highly efficacious NMDAR potentiators has been described. This series also robustly enhances agonist potency, which can prolong receptor deactivation time-course following rapid removal of glutamate. The best-in-series (potency and efficacy) compound to date, **1622-14**, enhances saturated receptor responses from 300% (of control, GluN1/GluN2B) up to 930% (of control, GluN1/GluN2D). This compound also prolongs the deactivation of receptors from 1.6-fold (GluN1/GluN2D) to 7.1-fold (GluN1/GluN2A). **1622-14** is capable of augmenting NMDAR responses in neuronal tissue, where it appears to have heightened actions on synaptic currents in hippocampal interneurons as compared to hippocampal pyramidal cells. Additionally, this compound enhances NMDAR-dependent theta-burst potentials, a pattern of signaling that is associated with neuronal plasticity (Larson and Munkácsy 2015).

Mechanism and binding site

The **1622** compound series exhibits several common features to previously published NMDAR PAM series (Strong 2017, Wang 2017). The **1622** series acts on all diheteromeric NMDARs but at saturated responses only potentiates GluN1/GluN2B, GluN1/GluN2C, and GluN1/GluN2D, similar to IPQ-2 (Strong 2017). This series can potentate NMDARs robustly, to greater extents than the IPQ-2 series and potentially similar to GNE-9278 (Strong 2017, Wang 2017). The specific details of potentiation caused by GNE-9278 at different agonist concentrations are not reported and differences in receptor constructs make it difficult to fully reconcile potential differences with the

1622 series. **1622-14** does not appear have agonist-dependent actions, or agonist binding requirement for **1622-14** high affinity binding (see HEK cell experiments, Figure 5.3 and 5.4), making it distinct from GNE-9278 (Wang 2017). Given that **1622-14** enhances the agonist potency of NMDARs, in the apo state binding of **1622-14** must cause some conformation change of the agonist binding domain. This difference in agonist binding domain conformation may have a different response to the exposure to agonist, which may alter the time course of NMDA receptor activation. In our studies, **1622-14** prolonged the rise-time of some NMDAR subtypes in HEK293 cell recordings. A recent AMPAR study suggests that metastable glutamate binding sites, near the receptor-activating glutamate binding site, aid in glutamate association (Yu 2018). Thus in ionotropic glutamate receptors, the positioning of surface residues of the apo state agonist binding domain may be optimized for agonist binding. If **1622-14** alters the association of glutamate, it may impact neuronal actions of **1622-14** and necessitates further study. Mutagenesis studies suggest that the TMD of both GluN1 and GluN2 contribute to **1622** modulatory activity, which differentiates the **1622** series from GNE-9278, which has structural determinants primarily in the GluN1 M3. The **1622** series has structural determinants of action that are similar to IPQ-2 (unpublished data), although data suggests the enantiomers of IPQ-2 bind to either subunit, one having non-selective actions and the other having GluN1/GluN2C and GluN1/GluN2D selectivity (unpublished data). It is unclear precisely how **1622** interacts with NMDARs; it may interact with both the GluN1 and GluN2 TMD, which both may contribute to heightened levels of potentiation achieved by this series. Data suggests that **1622** and **1622-14** can alter the channel conductance levels at GluN1/GluN2A and GluN1/GluN2B (Khatri and

Traynelis, unpublished studies). It remains unknown whether this effect is restricted to GluN1/GluN2A and GluN1/GluN2B, if so it may lead to potentially greater action on GluN1/GluN2C and GluN1/GluN2D. Examining the structural consequences for the receptor of the binding of the **1622** series may lead to greater understanding of the conformational transitions that occur during gating.

Actions at neuronal receptors

1622-14 has robust actions on synaptic NMDAR responses (Figure 5.5, Table 5.7). **1622-14** application prolongs deactivation time course of EPSCs by 3.5-fold without increasing the peak amplitude. This is surprising given that **1622-14** should potentiate responses of GluN2B-containing receptors to saturating concentrations of agonist. The GluN2B-selective negative allosteric modulator ifenprodil reduced $EPSC_{NMDAR}$s amplitude by roughly half, suggesting that there is a considerable fraction of stimulated receptors that are diheteromeric GluN1/GluN2B receptors, taking into account ifenprodil's actions on triheteromeric GluN1/GluN2A/GluN2B receptors. Using the reported actions of ifenprodil on diheteromeric GluN1/GluN2B (12% of control) and triheteromeric GluN1/GluN2A/GluN2B (68% of control) receptors, the potential receptor pool compositions can be determined that produces the level of inhibition of observed (50% of control) (Hansen 2014). Based on this activity of ifenprodil, we can expect anywhere from, approximately, 33% to 55% to be diheteromeric GluN1/GluN2B and 0 to 66% triheteromeric GluN1/GluN2A/GluN2B receptors (see Figure 5.8). For any of these possibilities, the receptor pool would contain NMDARs that can be potentiated by **1622-14** (GluN1/GluN2B to 360% and GluN1/GluN2A/GluN2B to 150%), yet we do not

$$[2A/2A] + [2A/2B] + [2B/2B] = 1$$

$$aa_{inh}*[2A/2A] + ab_{inh}*[2A/2B] + bb_{inh}*[2B/2B] = EPSC_{inh}$$

$$aa_{inh}= 0\%, \ ab_{inh}= 32\%, \ bb_{inh}= 88\%, \ EPSC_{inh} = 50\%$$
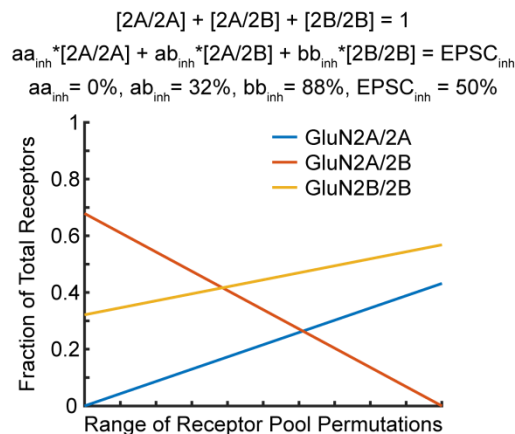
Figure 5.8. Range of potential composition of the NMDAR pool of CA1 pyramidal cells of this dataset.

A) The system of equations used to calculate the possible CA1 pyramidal cell NMDAR-pool composition of this dataset, which were inhibited by 50%. Ifenprodil inhibition is represented as percent of receptor response that is blocked (aa_{inh}, ab_{inh}, and bb_{inh}, values from Hansen 2014). B) Different fractions of receptor types permutations that results in the observed level of inhibition; for instance, a receptor pool of 66% GluN2A/GluN2B and 33% GluN2B/GluN2B or 45% GluN2A/GluN2A and 55% GluN2B/GluN2B would result in 50% inhibition by ifenprodil.

observe any potentiation (in fact slight inhibition) of the peak response of the NMDAR-component of stimulated EPSCs. Several possible explanations may account for this discrepancy, 1) the biophysical properties of the native NMDARs are sufficiently different to change the potency and efficacy of **1622-14** on these receptors, 2) modulation by **1622-14** slowed the rise time in activation, and the brief exposure of glutamate in the synaptic cleft prevents potentiation, 3) physiochemical properties restrict **1622-14** from fully achieving anticipated concentrations at synaptic spaces.

Robust prolongation of the deactivation time-course suggests that we are achieving penetration by **1622-14**. We cannot rule out at this point the idea that the biophysical properties are altered sufficiently to alter the modulators actions in native tissue. Other ionotropic glutamate receptors are known to have accessory subunits that alter receptor biophysical properties, and a recent study suggests that there is an auxiliary protein that impacts the function of NMDARs in *C. elegans* (Jackson and Nicoll 2011, Lei 2017). These factors may impact the ability of **1622-14** to modulate native NMDARs. **1622-14** slows the rise time at several NMDAR subtypes in HEK293 cells and it may slow the rise time of evoked EPSC, as it increased 1.77-fold but was not significant. This action on NMDARs may influence how **1622-14** alters synaptic responses but requires further study. Additionally, an unlikely scenario is that **1622-14** application might cause non-specific cellular actions or downregulation of NMDARs. Further study will be required for a full explanation of **1622**'s actions on native NMDARs.

Differences between pyramidal neurons and interneurons

Comparing the actions of **1622-14** on the NMDAR-component of mEPSCs from pyramidal and interneurons suggests that there is a difference in the capacity to potentiate. **1622-14** potentiates the NMDAR peak response equally in both types of neurons, roughly 2 fold. Identifying the NMDAR-component of mEPSCs is not as precise as measuring isolated NMDAR-component of evoked EPSCs, which may suggest why an increase in amplitude is observed. Alternatively, this different form of glutamate release might be a factor leading to this discrepancy. The integrated charge transfer of the NMDAR response is a more robust measure **1622-14** action. By this parameter, we see a heightened ability of **1622-14** to enhance the charge transfer in interneuron NMDAR responses. This is predicted from recent reports of the expression of the GluN2D subunits in hippocampal interneurons (Swanger 2015, von Engelhardt 2015, Perszyk 2016) and **1622-14**'s stronger actions on GluN1/GluN2D receptors. At the present time, we do not have any data describing the activity of **1622-14** on triheteromeric receptors containing GluN2D. However, extrapolating from the behavior of triheteromeric GluN1/GluN2A/GluN2B receptors we would expect greater potentiation capabilities of **1622-14** at any triheteromeric receptor containing one GluN2D subunit compared to a diheteromeric receptor of the other GluN2 subunit.

*Speculation about the in vivo actions of **1622-14***

The main question is how **1622-14** impacts neuronal networks. This is a complicated question given NMDAR expressed in multiple cell types. Preliminary attempts to address this question led to our final set of experiments. When blocking fast

synaptic inhibition using the GABAa receptor channel blocker picrotoxin, we observe no modulation by **1622-14** on low frequency EPSPs but robust enhancement of theta-burst potentials in the CA1 of the hippocampus. This experiment illustrates **1622-14** enhancement of burst firing via NMDAR signaling by isolating the direct excitatory input. Interestingly, the theta-burst potential waveform was not constant; the second and third bursts are smaller in width and not affected by NMDAR antagonism by APV. This may reflect desensitization of the NMDAR response or enhanced leak channels activity (Arai and Lynch 1992, Grover 2009). Interestingly, **1622-14** had effects on each of the three theta-bursts. **1622-14** may be capable of reducing NMDAR desensitization or augmenting the NMDAR to overcome factors contributing to this diminished response. Further investigation of this property is needed to interpret **1622-14** effects. Preliminary data (not shown), suggests that if inhibitory signaling is intact in the hippocampus, the actions of **1622-14** on theta-burst potentials drastically changes. **1622-14** has an opposite effect on burst width, causing a reduced burst potential. This would align with the observation that **1622-14** has enhanced capabilities at interneurons and can augments inhibitory signaling and results in pyramidal cell hyperpolarization that cannot be overcome by direct excitation. Persistent hyperpolarization would prevent Mg^{2+} dissociation and prevent NMDAR activity in the pyramidal cells, potentially leading to the reversed activity in the absence and presence of inhibitory signaling. This early result suggests the complexity of the role of NMDAR in the function of the hippocampus. This raises if four questions about the actions of this series of compounds: (1) are network effects of **1622-14** dominated by its actions at interneurons, (2) do biophysical or physiological factors give rise to this preferential activity, (3) is **1622-14's** impact on

network activity based on the types or patterns of signaling, and (4) do **1622** analogs with distinct pharmacological properties have different network activity? Data from another PAM, selective for GluN2A-containing receptors, suggests the activity dependency may be complex (Hackos 2016).

The **1622** series is highly interesting, with robust and reliable actions. Many questions remain about the properties, mechanisms, and potential of this series. We do know that **1622-14** crosses the blood-brain barrier (0.4 brain to plasma ratio, $t_{\frac{1}{2}brain} = 0.6$ hr, Janssen Pharmaceuticals, Inc., unpublished data), and so is a prototypical candidate for *in vivo* studies. Trial injections of **1622-14** up to 50 mg/kg were tolerated, a dosage that should result in active concentrations in the brain and did not produce any overt adverse effects. This suggests that the modulator is tolerated and that this class of compounds might be a tool for investigation of NMDAR-dependent physiological processes once its precise actions are delineated.

Chapter 6: Discussion

In the past decade, many new allosteric modulators of NMDAR function have been discovered (Bettini 2010, Costa 2010, Mosley 2010, Mullasseril 2010, Acker 2011, Costa 2012, Khatri 2014, Katzman 2015, Yuan 2015, Hackos 2016, Volkmann 2016, Strong 2017, Swanger 2017, Wang 2017). These new compounds will be useful in biological systems to gain a greater understanding of NMDAR involvement in the neuronal processing. In addition, NMDARs are implicated in many neurological diseases and have been identified as a potential drug target (Hallett and Standaert 2004, Kalia 2008, Coyle 2012, Collingridge 2013, Paoletti 2013). Previous clinical trial attempts using NMDAR targeting compounds have failed, in part, due to on-target side effects (Ikonomidou and Turski 2002, Chen and Lipton 2006). However, newer compounds with different modes of action may have greater chance for clinical success. The ability to discriminate between various populations of NMDAR by subunit-selectivity, activity-dependence, or other means may be fruitful, because neuronal systems are highly complex and NMDARs are found in many cell types, contributing to their propensity for on-target side effects. The more information we have concerning the mechanism of action of a novel pharmacological agent, the greater ability we will have in predicting how these agents will act on NMDARs in native tissues in response to physiological stimulation. Additionally, by studying mechanism of action of pharmacological agents, new mechanisms of action may suggest novel therapeutic strategies. By constructing models that accurately predict the activity of these novel pharmacological agents, predictions can be made about how they may respond in neuronal systems. Thus, modeling can drive new experimentation and refine working hypotheses.

In this dissertation three compound series have been presented. First, a series (1794) possessed a spectrum of activity, with analogs capable of negative to positive modulation along with several mechanistic properties that allow these compounds to have distinct activity based on agonist concentration. Second, a series (CIQ) that is selective for GluN1/GluN2C and GluN1/GluN2D and is capable of selectively acting at NMDAR in hippocampal interneurons. Third, a series (1622) is highly efficacious and may have selective actions on certain neurons based on subunit expression; this series has interesting action on native receptors in response to physiological stimulation. Here, I will discuss my current working hypothesis for how the function of these positive allosteric modulator series actions can best be modeled. I would propose that mechanistically relevant models are preferred, as they have greater predictive capabilities and may drive forward to developing new compounds with scientific utility and potential therapeutic utility.

Biophysical constraints on potentiation

The Traynelis lab has had access to a many distinct series of allosteric modulators as a result of previous screening efforts by the lab. Many series have been developed and expanded due to productive synthetic chemistry collaborators. Thanks to diligent work to characterize the basic properties of these compounds, modulator EC_{50} and maximal extent of modulation, there is now a large dataset of modulator actions, when complemented with other published series that can inform modeling of allosteric modulation of NMDARs.

Early work focused on positive and negative allosteric modulators (CIQ**,** QNZ**,** DQP) that possessed selectivity for GluN1/GluN2C and GluN1/GluN2D over GluN1/GluN2A and GluN1/GluN2B. Additionally, there were also several PAM series with diverse scaffolds that displayed a different selectivity profile (Figure 6.1, data procured by P. Le, J. Zhang, and past lab members). Initially, these modulators (IPQ, 1622, 1794) appeared to be GluN1/GluN2B-, GluN1/GluN2C-, and GluN1/GluN2D-selective when studied at saturating agonist concentration. A number of observations (both unpublished, and described in chapters 3, 5), suggest that these PAMs may enhance agonist potency. Interestingly, CIQ and similar compounds (R-enantiomers of IPQ analogs) enhanced agonist potency at GluN1/GluN2C, but GluN1/GluN2D the effect was less pronounced or absent (Table 6.1). As for the GluN1/GluN2B-, GluN1/GluN2C-, and GluN1/GluN2D-selective PAM (1622-14, IPQ-2, S-enantiomers of IPQ analogs, and the 1794 series), modulation resulted in enhanced agonist potency at all diheteromeric NMDARs, except for GluN1/GluN2D in several cases (Table 6.1). The 1794 series, as well as the GluN2C-/GluN2D-selective NAMs and GNE-9278, displayed various forms of agonist-dependency. The diverse array of modulator properties are perplexing and are difficult to explain, as some properties have different subunit selectivity.
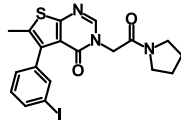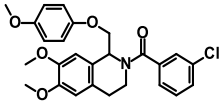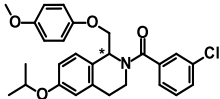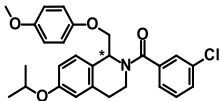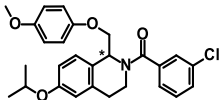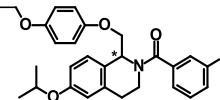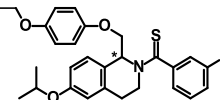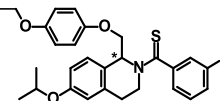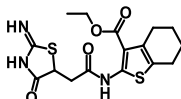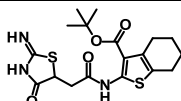
With these observations, I sought to identify models that could more actually represent the diverse modulator properties and that could accurately simulate NMDAR responses and modulator effects. Several points were crucial for potential models. First, the observation that there was a trend in maximal potentiation across multiple series (Figure 6.1, GluN1/GluN2D = GluN1/GluN2C > GluN1/GluN2B > GluN1/GluN2A ~ 100% or no potentiation). Second, the conversion of a non-selective NAM, in 1794-2**,** to
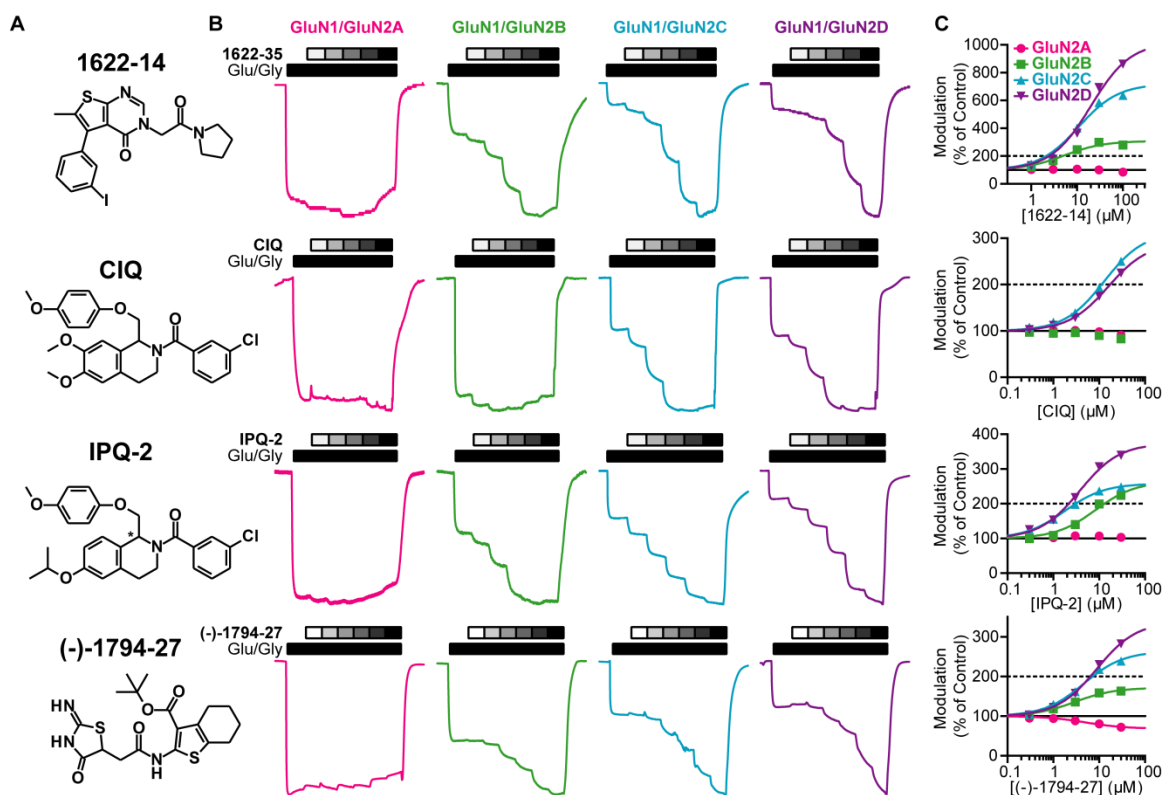
Figure 6.1. Several NMDAR modulator series display similar profiles of potentiation.

A) Chemical structures of exemplifying members of several PAM series; 1622 (1622-14), 1180 (CIQ, IPQ-2), and 1794 ((-)-1794-27). B) Representative two-electrode voltage-clamp oocyte recordings exemplifying the concentration-response of the compound shown in **A** (gray scale boxes – 0.3, 1, 3, 10, 30 μM for 1622-14, CIQ, and IPQ-2, 0.1. 0.3, 1, 3, 10, 30 μM for (-)-1794-27) on the diheteromeric NMDARs stimulated with saturating concentrations of agonist (black bar, 100 μM glutamate and 30 μM glycine). C) Concentration-response curves illustrating the modulatory actions of the compounds in **A** on the 4 diheteromeric NMDARs.

Table 6.1: The agonist potency shift several members of distinct modulator series.

Compound	ID	Conc (µM)	GluN2A	GluN2B	GluN2C	GluN2D
(structure)	**1622-14**[†]	10[*]	7.1	3.3	2.8	1.7
(structure)	**CIQ**	20	0.93	0.94	2.0	1.0
(structure)	**IPQ-2**[†]	30 30[*]	2.8 3.3	1.4 1.5	3.6 1.8	1.7 1.5
(structure)	**S-IPQ-2**[†]	20 10 15[*]	4.6 3.8 4.3	1.8 1.6 1.6	1.6 2.0 1.4	1.1 1.0 1.1
(structure)	**R-IPQ-2**[†]	10	0.9	1.1	2.6	1.4
(structure)	**S-IPQ-97**[†]	10	1.8	1.6	2.2	1.1
(structure)	**S-IPQ-142**[†]	10	2.3	1.4	1.4	0.92
(structure)	**R-IPQ-142**[†]	10	1.1	1.1	1.4	0.85
(structure)	**1794-4**	10	2.4	2.0	3.2	3.9
(structure)	**1794-27**	10	2.3	2.0	3.3	5.3

Represented values, unless stated otherwise, are direct measurements of agonist potency.

[*]Deactivation prolongation is correlated with glutamate potency enhancement. The data for these analogs were collected by P. Le, J. Zhang, and R. Perszyk. [†]unpublished data.

a highly similar analog that possessed this pattern of selectivity (GluN1/GluN2B-, GluN1/GluN2C-, and GluN1/GluN2D-selective), in the PAM 1794-27, was poignant. Given the similarity in chemical structure, we hypothesized that these molecules would share a binding site, so these analogs should share certain aspects of their mechanism of action but also have to potential for both positive and negative modulation and this pattern of selectivity. Third, there needs to be rationale for the ability of NAMs to enhance agonist potency, as the agonist-dependent GluN2C/GluN2D-selective molecule QNZ-46. Thus, I sought a model that could represent these diverse allosteric modulator activities.

The allosteric two-state receptor model

Various allosteric models have been proposed throughout the years to represent the activity of ligands, allosteric modulators, and receptors (Hall 2000, Christopoulos 2002). The allosteric two-state model is most appropriate as the desire is to represent the actions of an agonist and an allosteric modulator (Figure 6.2). These types of models are capable of accurately representing the actions of agonists and modulators of receptor system at equilibrium. To facilitate interpretation, focusing on the agonist actions is best to start. The two-state model of receptor activation illustrates the conformational changes of a receptor (R), which can either be inactive (R_i) or active (R_a) based on E, or intrinsic efficacy (Figure 6.2A). The binding of an agonist (A) to the inactive state, defined as affinity (K_A), induces an enhancement of the intrinsic efficacy by a factor, α. As a result of conservation of energy, α must also enhance the association of agonist in the between the active states, producing an apparent affinity of αK_A, relating the apo-receptor state
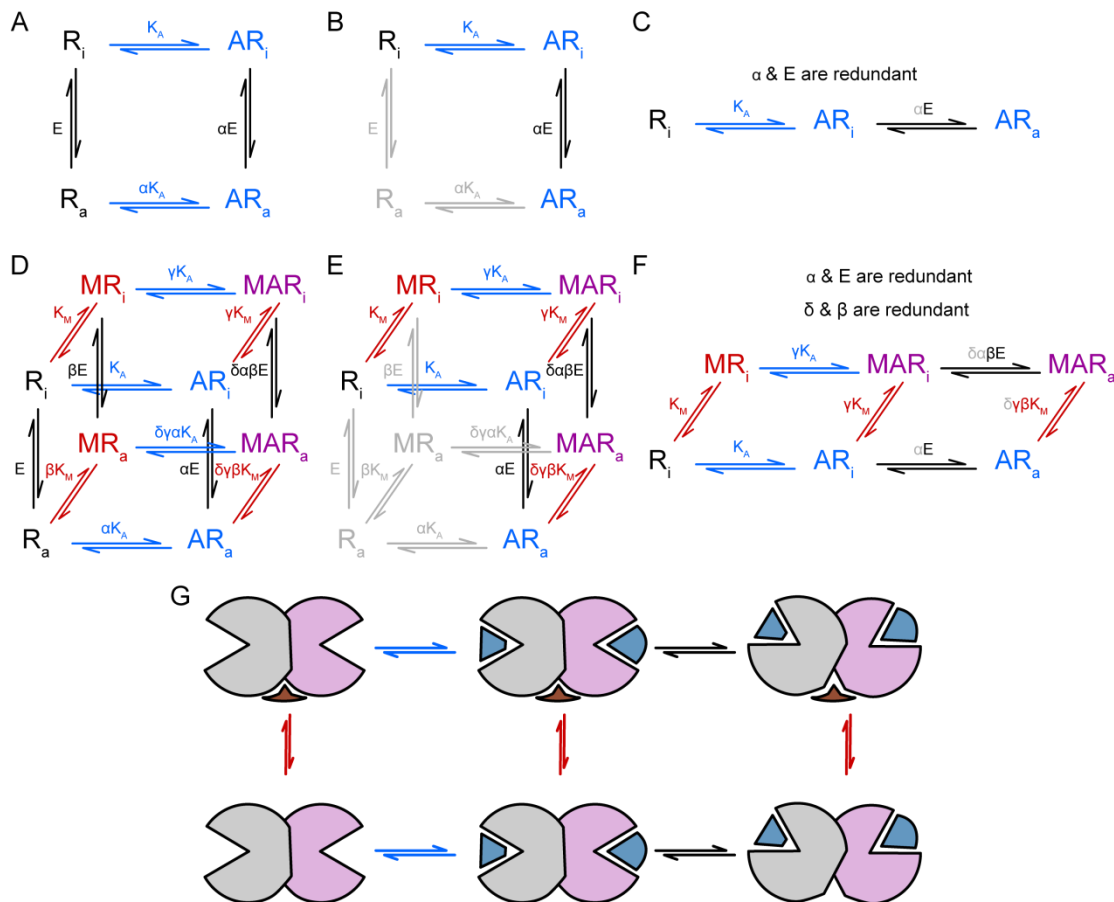
Figure 6.2. The allosteric two-state model describing the interaction of multiple ligands with a receptor.

A) The two-state model of receptor activation illustrates the conformational changes of a receptor being activated by an agonist. B) A simplification of the two-state model, given very low intrinsic receptor activation by eliminating the greyed state and transitions. C) A rearrangement of **B** illustrating its overlap with del Castillo and Katz model of receptor activation. D) The allosteric two-state model, where the dimension of an allosteric modulator is built on to the agonist activation of the two-state model. E') Assuming intrinsic receptor activity is very low and that the allosteric modulator is not an allosteric agonist, the allosteric two-state model can be simplified by eliminating the greyed states and transitions. F) A rearrangement of the simplified allosteric two-state model, shown in

E. G) A cartoon representation of hypothetical receptor conformations of the simplified allosteric two-state model, shown in **F**.

(R_a) and the active agonist bound state (AR_a). In NMDARs, spontaneous activation is very low additionally suggesting E is very low and the Ra is almost never exists (Figure 6.2B). Relatedly, agonist is not believed to dissociate while the ABD clamshell is closed, suggesting α is very large (Madden 2002). With these assumptions the model can be simplified, which results in a form that is identical to the del Castillo and Katz model of receptor activation (Figure 6.2C) (Del Castillo and Katz 1957). Next the actions of a modulator can be reintroduced (Figure 6.2D). K_M defines the affinity of the allosteric modulator (M). The enhancement of intrinsic activation of the modulator bound receptor is defined by the factor β. The enhancement of agonist binding by the modulator bound receptor (or vice-versa) is determined by the factor γ. Lastly, the enhancement of efficacy of the modulator/agonist-bound receptor over the agonist-bound receptor is determined by δ. Using the above assumption, that the receptor almost never activates in the absence of agonist and that the allosteric modulator tested do not result direct receptor activation, the model can be simplified (Figure 6.2E,F). This model can be conceptualized easily by considering the ABD, the introduction of agonists, the actions of an allosteric modulator and the conformations of the ABD is known to adopt during activation (Furukawa 2005, Karakas and Furukawa 2014, Twomey and Sobolevsky 2017). With this simplified allosteric two-state model, the various parameters that control receptor-agonist-modulator activity can be conceptually investigated. Examining the allosteric two-state model based on the factor γ, or allosteric cooperativity, helps elucidate the behaviors of various allosteric modulators (Figure 6.3).
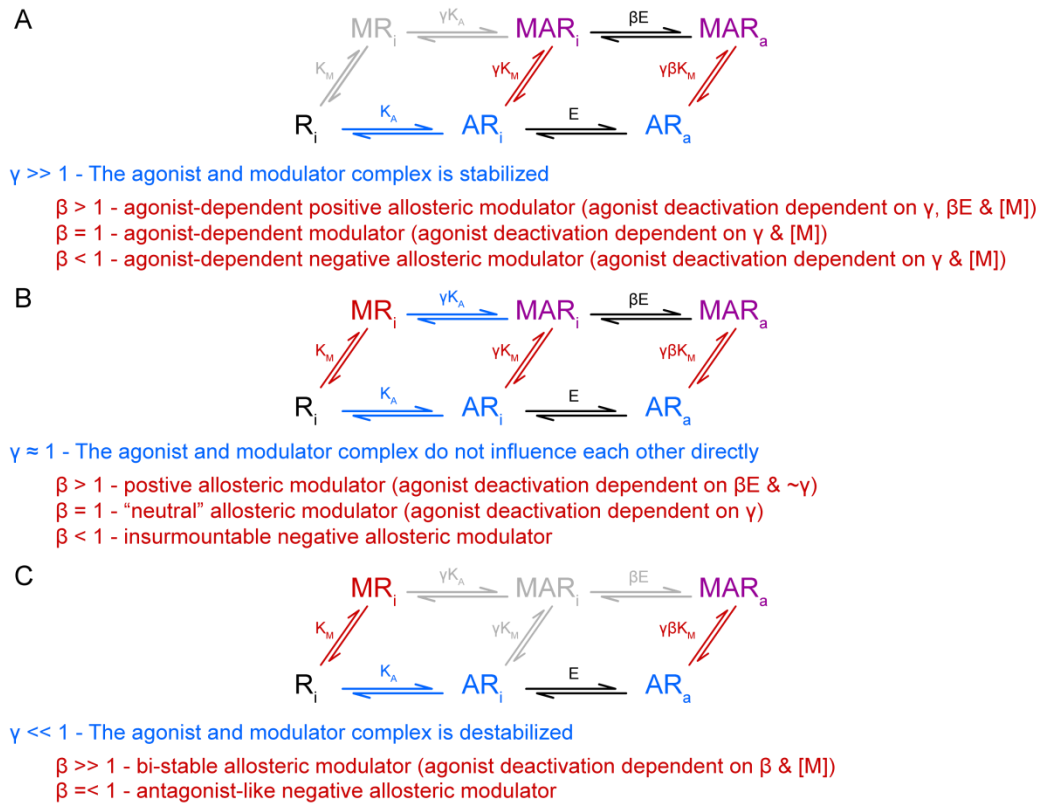
Figure 6.3. The actions of an allosteric modulator change based on its ability to couple with the agonist.

A) The simplified allosteric two-state model based on if the allosteric modulator and the agonist have strong positive cooperativity ($\gamma \gg 1$) and the effect of the possibilities of various values of β. Based on the magnitude of γ the model can be simplified further, states and transitions would tend to become insignificant are greyed (also changes based on β). B) The simplified allosteric two-state model based on if the allosteric modulator and the agonist do not influence each other ($\gamma \approx 1$) and the effect of the possibilities of various values of β. C) The simplified allosteric two-state model based on if the allosteric modulator and the agonist have negative cooperativity ($\gamma < 1$) and the effect of the possibilities of various values of β. If γ is sufficiently low, the greyed state and transitions would become insignificant (also based on β).

The allosteric two-state receptor model: high γ

The first case to be considered used the case of high ligand cooperativity ($\gamma \gg 1$) (Figure 6.3A). If γ is large enough, the only relevant binding of a modulator must occur if modulator affinity is very low for the apo-state receptor. This assumption is similar to how the general allosteric two-state model was simplified by suggesting the intrinsic efficacy of the apo-state receptor was very low, so that the only appreciable rate of modulator binding occurs when the receptor is already bound to agonist (Figure 6.2B). With this simplification, in this case the model represents modulators with the property of agonist-dependent binding (Figure 6.3A). Based on β, the modulator actions can change producing different actions on receptor function; if $\beta < 1$, a negative allosteric modulator results, if $\beta > 1$, a positive allosteric modulator results, and if β is approximately 1 then a "neutral" modulator results (Figure 6.3A). However, all of these modulator types results in altered pathways for receptor deactivation. If agonist is rapidly removed from a period of receptor activation the time it takes to return to an apo-state (non-agonist bound state) is determined by intrinsic properties of the receptor (Lester 1990). In the presence of a constant concentration of modulator, those state transitions are altered (Figure 6.3A). Instead of simply transition from AR_a to AR_i and then to R_i, the receptor, which may be in the MAR_i state or MAR_a state, must first unbind the modulator before the agonist can dissociate. This alters the determinants of deactivation based on β to be dependent on; if $\beta < 1$, γ and the concentration of the modulator, if $\beta > 1$, γ, $\beta*E$ and the concentration of the modulator, and if $\beta = 1$ γ and the concentration of the modulator (Figure 6.3A). The reason why the concentration of the modulator becomes dependent in the deactivation of the receptors is due to its mechanism, if the modulator dissociates from this modeled receptor

then there is a chance of it deactivating, however if a modulator rebinds before the receptor can deactivate it effectively prevents the agonist from dissociating.

Interestingly, this allosteric two-state model resembles that activity of the 1794 series. The 1794 series contains both positive and negative allosteric modulators. The modulation produced by both types of modulators was found to be agonist-dependent. The deactivation of all types of diheteromeric NMDARs were prolonged in the presence of the 1794 series modulators with differing activity (to be discussed further later). One would suppose then that the cooperativity of the 1794 series analogs and the agonist is very high. Hypothetically, the analogs confer differing β factors, as positive, weakly negative and strongly negative modulators were found. Additionally, the non-selective PAM, GNE-9278, would fit this case as it potentiates, prolongs deactivation, and has agonist-dependence (Wang 2017).

The GluN2C/GluN2D-selective NAMs (QNZ-46, DQP-1105, and NAB-14) appear to fit this type of negative allosteric modulator ($\beta<1$) given their agonist-dependence (Acker 2011, Hansen and Traynelis 2011, Swanger 2017). QNZ-46 was shown to have a prolonged deactivation time-course in the presence of sub-saturating concentrations of the modulator and had a large shift in modulator potency in different concentrations of glutamate but not glycine. Alternatively, NAB-14 was shown to be less dependent on glutamate potency, suggesting it may have a lower γ than QNZ-46 or DPQ-1105.

The allosteric two-state receptor model: neutral γ

Next, in the case where γ≈1, there is very little ligand cooperativity observed (neither positive nor negative) between modulator and agonist (Figure 6.3B). In these cases, similar types of modulators result based on β. There are positive (β>1), "neutral" (β=1), and negative (β<1) allosteric modulators. In these hypothetical modulators, the agonist deactivation scheme is less complicated since the modulator can be bound to an apo-state receptor. For the positive allosteric modulators, of this cooperativity, deactivation depends on βE and on γ. However, γ cannot be too large since if it was then agonist dependence would be detected, which could be determined using functional assays but more accurate determinations would potentially be achieved using direct binding measurements. Interestingly, a supposed "neutral" allosteric modulator may exist, where it may not alter the steady state activation of the receptor but deactivation kinetics would be impacted.

Based on this level of cooperativity, the behavior of several NMDAR modulators appear to be represented. The positive allosteric modulators in the 1622 and 1180 series have properties that are highlighted by these examples. These series display a capability to potentiate at saturating agonist levels and they also impede agonist deactivation. The prolongation of deactivation rates (or relatedly agonist potency) is apparently correlated with the efficacy (or E) of the receptor subtype (Table 6.1). Ifenprodil and other GluN2B-selective NAMs may fall into this category of moderate γ and low β, but caveats will be discussed below.

The allosteric two-state receptor model: Low γ

Last, in the case where γ<<1 there is strong negative ligand cooperativity observed between modulator and agonist (Figure 6.3C). In these cases, β values of one or less represent antagonist-like negative allosteric modulators. Hypothetically, there are modulators with very large β factors which would behave as bi-modal modulators. These would inhibit activity if bound to the receptor in an inactive state but if they bound while the receptor was activated then they would promote activity.

The antagonist-like NAMs described by this set of modulator types, is similar to the TCN and MPX analogs. These compound appear to be competitive in nature but at high concentrations exhibit clear allosteric coupling. A study showed that TCN-201 has allosteric coupling constants (here γ, but α in the publications) of 0.007 (Yi 2016).

Conclusions of the allosteric two-state receptor model

The derivation of the allosteric two-state receptor model used here has a remarkable ability to capture the steady state activity of several NMDAR small molecule modulators. It's able to capture modulators that increase efficacy (E), enhance apparent affinity of agonists, the property of agonist dependent and allosteric coupling of antagonist-like modulators. Multiple parameters of modulator action need to be characterized in order to accurately categorize allosteric modulators, for instance, given the available data of the Genentech GluN2A-selective PAMs they cannot be properly evaluated (Hackos 2016, Volgraf 2016, Villemure 2017). This lack of categorization is due to insufficient information, concerning agonist-dependency, clear characterization of deactivation time-course prolongation and potentiation of agonist saturated responses.

Several assumptions were made to adapt the allosteric two-state model for easy interpretation. Namely, the activated apo-state and the activated modulator-bound receptor state were removed. This is likely a safe assumption given that desensitization from a closed ABD is very unfavorable and apo-state activations are not observed (Furukawa 2005, Karakas and Furukawa 2014, Lee 2014). Additionally, the model that ultimately preceded the allosteric two-state model, the MWC model, made the assumption that symmetrical oligomers were the source of cooperativity of protomer conformation changes and determine the actions of ligand binding (Monod 1965). Although, most later models have not including this strict requirement, it is still something to consider (Changeux and Edelstein 1998).

Another consideration is that this model only contains one of NMDAR's co-agonists. NMDARs require the binding of co-agonists to both GluN1 and GluN2 subunits which results in all-or-nothing gating (Schorge 2005). It is also know that the binding of glutamate and glycine, alter the apparent affinity of each other (Mayer 1989, Benveniste 1990, Lester 1993). Presumably, a more realistic model would be constructed using the allosteric two-state model to accommodate the actions of the both co-agonist. Due to their mutual ability to decrease the opposing co-agonist potency (see glycine-dependent desensitization), their binding would result in a $\gamma < 1$ and, due to the requirement of both being bound for receptor activation, a β equaling or being greater than 1 is requires. Additionally, the only active state in this NMDAR allosteric two-state model would be the co-ligand bound activated state (in Figure 6.2F state MAR_a). From this model, a modulator-binding dimension could then be built in, doubling the number of states and adding to the complexity. Potentially this dual agonist model may help explain the action

of ifenprodil. Ifenprodil enhances glutamate potency; additionally its inhibitor effect is reduced in the presence of increasing concentrations of glycine (Williams 1993). Perhaps, ifenprodil's mechanism of action is to enhance glutamate binding and as a result increase glycine-dependent desensitization. This may be a farfetched possibility, but there must be a mechanistic basis for these interactions. An argument could be made for the inclusion of ATD actions and desensitization to such a model. Studies have shown that it can play a role in modal gating and has an allosteric interaction with the ABD (Zheng 2001, Popescu and Auerbach 2003, Gielen 2008, Vance 2012, Vance 2013). Generalized ligand-independent desensitization is also an important determinant of NMDAR function that is not encapsulated by this model (Sather 1990, Sather 1992). These features are known to influence baseline NMDAR function and likely impact NMDAR modulator action.

Between different classes of modulators we see varying abilities to enhance agonist potency (or prolong agonist-deactivation, Table 6.1, including Hansen 2011, Hackos 2016, and Wang 2017). This includes agonist-dependent modulators and non-agonist dependent modulators. The enhancement of agonist potency for non-agonist dependent modulators (shown in Table 6.1) displays a profile that roughly aligns roughly with the relative open probability (hence to βE). Alternatively, agonist-dependent modulators appear to display a profile with the largest enhancement of agonist potency results at the receptor with the lowest open probability (GluN1/GluN2D). There may be subtype specific differences in γ and β, but as some of these modulators are thought to bind to GluN1 (found in all NMDARs) it may be more parsimonious to conclude that these factors are the same across subtype but interact differently with E which is already

known to differ between subunits. These differences in the ability to enhance agonist potency may be important factors highlighting the differences they have in allosteric modulation of receptor activation.

One of the downfalls of this model is that is provides a description of equilibrium responses of agonist and modulator binding. As shown, it provides insight but cannot accurately represent single channel records, which are stochastic in nature and based on a number of structurally linked receptor conformations (see Chapter 1). When this model is reduced to the highlight agonist binding and activation, it reduces to the del Castillo and Katz model of end-plate receptor activation which is incapable of accurately representing single channel open and shut state sequences. Additionally as this model predicts, but also there is evidence for, the possibility that neutral allosteric ligands. These may be missed in equilibrium analyses, given the inability of these ligands to alter receptor equilibrium, however they may have the capacity to alter the activation or deactivation of receptors (Kostenis and Mohr 1996). These types of modulators could be missed by equilibrium based assays, but could be useful as they may alter activation and deactivation of receptors but might preserve the overall level of activity (may just change the time course of depolarization). Potentially this may be a useful tool in probing synaptic summation or integration of signals.

The ambiguity of this "activated" state in the allosteric two-state model is also less than ideal. In many cases, having a unmodulated and modulated activated state (AR_a and MAR_a) that are identical may be representative. For instance, attempting to apply the actions of CIQ to this model would suggest that since CIQ did not alter open time histograms of GluN1/GluN2D channels model may be sufficient. In other cases this may

be insufficient, for example 1622-14 actions on GluN1/GluN2A channels results in a dramatic shift in open probability but also a reduction of the conductance levels (unpublished data) and preliminary data suggests that 1794-27 reduces Ca^{2+} permeability of the GluN1/GluN2A channel. Therefore the activated receptor, denoted by AR_a and MAR_a, are not equivalent.

This allosteric equilibrium model has its benefits but it does not appear to be capable in fitting receptor channel records. Kinetically defined models that can represent microscopic and macroscopic NMDAR activity, including the actions of various modulators, would be a useful tool in probing NMDARs in native tissues. However, they would need to be capable of recapitulating the properties, illustrated here, that control allosteric modulator action.

Coupling of positive allosteric modulator enhancement and apparent agonist potency

Several PAMs above were proposed to fit into a modulator class defined as low agonist/modulator cooperativity ($\gamma \approx 1$) and a positive modulator factor (β). These modulators would produce a shift in in the apparent affinity of the agonist based on several factors. The normal deactivation time-course related to the EC_{50} of the agonist; the impact agonist and modulator parameters have on agonist EC_{50} is evaluated below.

Using the allosteric two-state model, that best fit this type of positive allosteric modulator above, and focusing on just the agonist binding steps allow for initial interpretation of the basic principles of this interaction. This model resembles the del Castillo and Katz model of receptor activation and has been thoroughly evaluated elsewhere (Colquhoun 1998, Kenakin 2016). Briefly, covering the impact of the agonist

properties on the agonist EC_{50} consideration should be given to the construction of the model. This model possesses two steps, an agonist binding and a gating step.

Scheme 6.1

$$A + R \underset{b_-}{\overset{b_+}{\rightleftharpoons}} RA \underset{k_-}{\overset{k_+}{\rightleftharpoons}} O$$
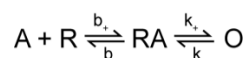
In scheme 6.1, the receptor is represented by (R) and an agonist (A) that associate based on the rate b_+ and dissociate based on b_-. The dissociation constant (K_A) is defined as the ratio b_- over b_+. The agonist bound receptor (RA) can then transition to the open state (O) base on the forward (k_+, also referred to as β) and reverse (k_-, also referred to as α) rates. The occupancy of this model based on agonist concentration can be calculated easily as described by Colquhoun in his 1998 published seminar. In Figure 6.4A, the effect of E on the open probability is shown by various concentration response curves. For very low E, the curve does not saturate at 1. With increasing E values, the concentration response curve reaches closer to a Po of 1 and, when approaching 1, the EC_{50} of the curve shifts to the left (even though binding affinity is constant), this divergent activity (based on E) can be more clearly seen in Figure 6.4B. This interaction between agonist efficacy and EC_{50} is a complicated concept and as a result in confusion when studying perturbations of receptor function (Colquhoun 1998). For example a mutation that greatly enhances or reduces efficacy can also enhance or reduce agonist EC_{50}, respectively. Equations can be derived mathematically that display the correlations between these parameters.

A few parameters of this model's behavior can be defined by a few subsequent equations. The gating equilibrium constant (E, which equals k_+/k_-) predicts the maximal open probability that can be achieved given saturating agonist.

$$\lim_{[A] \to \infty} Po = \frac{E}{1 + E} \tag{6.1}$$
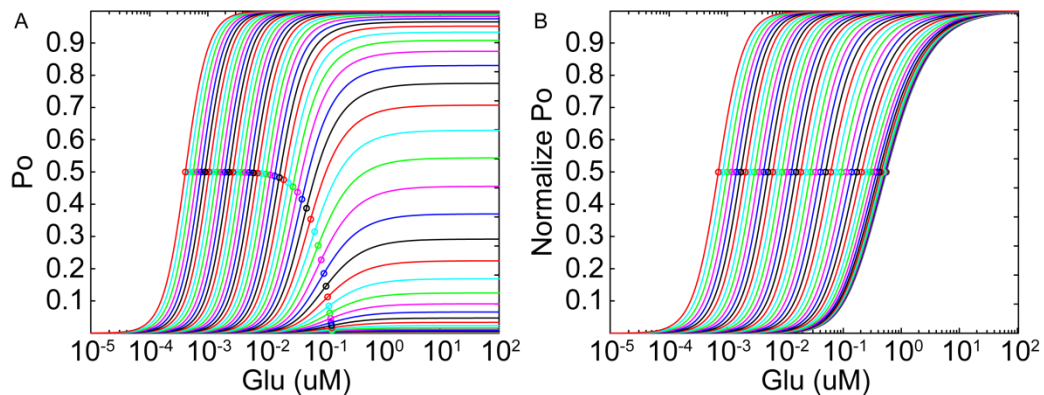
Figure 6.4. Calculated open probability of the del Castillo and Katz model highlights the impact of E' on maximal effect and agonist potency.

A) A range of open probability concentration responses curves, calculated with a wide range of values of E' (10^{-5} up to 10^{5}). B) The family of curves in **A** normalized to the maximal Po of each curve.

An explicit derivation of the EC_{50} of the agonist involves the binding affinity constant (K_A) as well as the efficacy term, as predicted by the curve in Figure 6.4.

$$EC_{50} = \frac{K_A}{1 + E} \qquad (6.2)$$

Essentially, since all states are dependent on each other there is a linkage between EC_{50} and E. If one equilibrium is perturbed it induces a change in the other equilibrium and the overall equilibrium of the receptor model. By this effect, a change in just the efficacy term can lead to an overall equilibrium shift in the receptor. This was used to show that mutation of residues that are involved receptor gating can impact the EC_{50} of an agonist (Colquhoun 1998). More specific experimentation is required to tease apart these two properties.

Using the allosteric two-state model ($\gamma \approx 1$, $\beta > 1$), assuming modulator is constantly bound we are left with a model that is identical to the modulator-lacking model except for the introduction of the two terms γ and β. Thus, by rough approximation, an allosteric modulator's interaction with a receptor and its actions on the agonist EC_{50} can be probed.
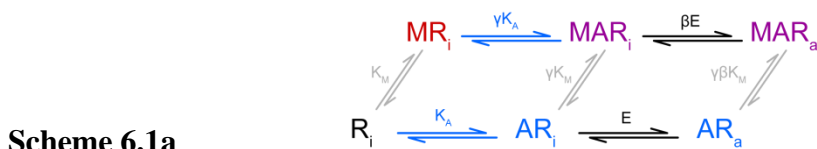
Scheme 6.1a

In terms of CIQ, modulation was found to prolong the deactivation of GluN1/GluN2C receptors but not GluN1/GluN2D (Mullasseril 2010). Using Scheme 6.1a different shifts in agonist EC_{50} can be calculated based on various perturbations by γ and β, a receptor with a maximal *Po* of 0.2 is potentiated by a modulator to have a maximal *Po* of 0.4 (β = 2.555), the model predicts an increase in agonist EC_{50} of 1.266 fold in the presence of the modulator. Potentiation of a lower *Po* receptor would result in less agonist potency shift and a higher *Po* receptor would have a larger shift, this effect can be seen in Figure 6.4,

as differences in E can approximate potentiation of a receptor. At GluN1/GluN2C we observe >200% potentiation and a 2.0-fold enhancement of agonist potency by CIQ modulation. Given the receptor's low *Po* (0.01), the shift cannot fully be accounted for by the increase in efficacy. However, the activity at GluN1/GluN2D is similar >200% potentiation, but lacks an effect on agonist potency (Mullasseril 2010 and unpublished data). Additionally, other PAMs have been found that do not potentiate saturated responses of GluN1/GluN2A receptors but do lead to increases in agonist potency (see IPQ, 1622).

Two possibilities could explain these observations. One, the ability to enhance agonist potency could be due to γ and steric differences between NMDAR subtypes (γ of GluN1/GluN2C is greater than GluN1/GluN2D). Two, the activation scheme of this model is too simplistic to recapitulate these modulator activities. 1622-14 has an ability to reduce channel shut times and prolong open times of GluN1/GluN2A channels, suggesting that it has an ability to enhance receptor efficacy, whereas this aspect of modulation is absent in other assays (unpublished data). 1622-14 has an ability to reduce channel conductance, which may impact the interpretation of these observations (unpublished data). Additionally, structural determinants of the IPQ series tracks to the GluN1 subunit, which is present in all NMDAR (unpublished observation). IPQ analogs alter agonist potency to different degrees based on NMDAR subtypes (Table 6.1). However, at GluN1/GluN2D, the level of agonist potency enhancement is close to 1, or is less than other NMDAR subtypes. This suggests that perhaps a fixed enhancement of agonist potency by these modulators does not accurately represent their biological effect.

One of the main goals in understanding the mechanistic action of NMDARs modulators was to produce models that can accurately represent microscopic and macroscopic receptor responses. These models would have useful predictive potential for simulating purposed. In addition to the points above, and as previously discussed in Chapter 1, NMDAR channel records cannot accurately be represented by simplistic models containing limited agonist bound shut states and open states. These points argue against the possibility that this model will be useful in these endeavors. Based on this I examined the behavior of other receptor models.

The actions of a positive allosteric modulator on a model with multiple gating steps

The del Castillo and Katz (and the extended Lester and Jahr model) reflects a reductionist approach that allows for interpretation of each step of receptor activation but it fails to capture accurate details of single channel properties (as previously discussed). On the other hand, the proposed models that more accurately reflect NMDAR channel properties (Scheme 1.2-1.6) are more complicated, more difficult to solve algebraically, and are not intuitive in terms of their prediction. I solved a receptor state equation that was more complicated, to begin to explore the effect of modulators of specific receptor transitions on agonist potency.

The model chosen, scheme 6.2, has one more state than the Lester and Jahr model.

Scheme 6.2
$$R \underset{b_-}{\overset{2b_+}{\rightleftharpoons}} RA \underset{2b_-}{\overset{b_+}{\rightleftharpoons}} RA_2 \underset{k_{1-}}{\overset{k_{1+}}{\rightleftharpoons}} R^*A_2 \underset{k_{2-}}{\overset{k_{2+}}{\rightleftharpoons}} O_1$$
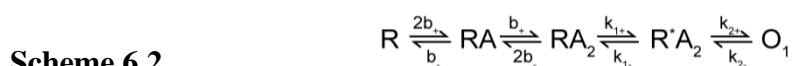
This model (two-step gating model) contains two binding steps to reflect the binding of two glutamate molecules, thus has two dissociation constants K_1 and K_2. It contains an

agonist bound states, that include an inactivated agonist bound state (RA_2) and an intermediate activation state (R^*A_2) that is non-conducting. Recent receptor structures of the iGluR family have been shown to adopt an intermediate activation states, in certain conditions (Tajima 2016, Twomey and Sobolevsky 2017). The equilibrium constant T (transactivation) defines this transition, from the inactivated agonist bound state to the intermediate activation state. This model's final transition equilibrium is defined by E', which is differs from the classical definition of efficacy. An equation relating the fraction of receptors in the open state and the agonist concentration, at steady state, can be determined for this model by solving a series of equations. First, the equations defining the equilibrium constants based on the transition rates, of each step, can be written.

$$K_1 = \frac{[A][R]}{[RA]} = \frac{b_-}{2b_+} \tag{6.3}$$

$$K_2 = \frac{[A][RA]}{[RA_2]} = \frac{2b_-}{b_+} \tag{6.4}$$

$$T = \frac{[R^*A_2]}{[RA_2]} = \frac{k_{1+}}{k_{1-}} \tag{6.5}$$

$$E' = \frac{[O]}{[R^*A_2]} = \frac{k_{2+}}{k_{2-}} \tag{6.6}$$

The proportions (of the total) of each possible receptor state must add up to one.

$$[R] + [RA] + [RA_2] + [R^*A_2] + [O] = 1 \tag{6.7}$$

Rearrangement of equations 6.3, 6.4, 6.5, and 6.6 then substituted into 6.7 can be formulated to solve for $[O]$.

$$\frac{K_1 K_2 [O]}{[A]^2 TE'} + \frac{K_2 [O]}{[A]^2 TE'} + \frac{[O]}{TE'} + \frac{[O]}{E'} + [O] = 1$$

$$[O] = \frac{[A]^2 TE'}{K_1 K_2 + [A]K_2 + [A]^2 + [A]^2 T + [A]^2 TE'} \tag{6.8}$$

Using equation 6.8, an expression for the maximal *Po* can be determined at saturating agonist concentration.

$$\lim_{[A]\to\infty}[O] = \frac{TE'}{1+T+TE'} = Po \tag{6.9}$$

Combining the two equations 6.8 and 6.9, by finding the concentration of *A* that corresponds to the half maximal *Po* response, the EC_{50} of the model can be derived from with some algebraic rearrangement.

$$\frac{1}{2}\lim_{[A]\to\infty}[O] = \frac{[A]^2 TE'}{K_1 K_2+[A]K_2+[A]^2+[A]^2 T+[A]^2 TE'}, \text{where } x = EC_{50}$$

$$\frac{1}{2}\frac{TE}{1+T+TE} = \frac{x^2 TE'}{K_1 K_2+xK_2+x^2+x^2 T+x^2 TE'}$$

$$0 = (1 + T + TE')x^2 - K_2 x - K_1 K_2 \tag{6.10}$$

The quadratic equation can be used on equation 6.10 to solve for the roots of *x*, and eliminating the potential irrational solutions of *x* results in the following equation for EC_{50} as a function of the model's equilibrium constants.

$$EC_{50} = \frac{K_2 + \sqrt{K_2^2 + 4K_1 K_2 (1+T+TE')}}{2*(1+T+TE')}$$

$$K_{2=}4K_1 \tag{6.11}$$

$$EC_{50} = \frac{2K_1 + \sqrt{(2+T+TE')}}{(1+T+TE')} \tag{6.12}$$

Equation 6.11 was used to simplify the EC_{50} equation to the form in 6.12. These equations can be used to evaluate equilibrium receptor responses to potentiation under various conditions and provide theoretical shifts in agonist potency.

Returning to the allosteric two-state model, we could suppose that instead of the single transition from agonist bound receptor to active (now MO and O are the active

states, MAR_a and AR_a are inactive, which was previously supposed to the open state) that there are two states that must be traversed.

$$MR_i \underset{}{\overset{\gamma K_A}{\rightleftharpoons}} MAR_i \underset{}{\overset{T}{\rightleftharpoons}} MAR_a \underset{}{\overset{E'}{\rightleftharpoons}} MO$$
$$K_M \updownarrow \quad \gamma K_M \updownarrow \quad \gamma K_M \updownarrow \quad \gamma K_M \updownarrow$$
$$R_i \underset{}{\overset{K_A}{\rightleftharpoons}} AR_i \underset{}{\overset{T}{\rightleftharpoons}} AR_a \underset{}{\overset{E'}{\rightleftharpoons}} O$$
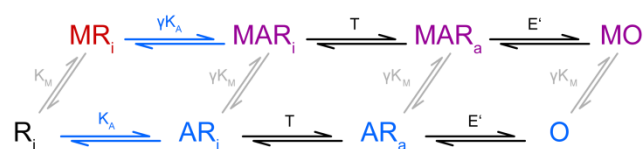
Taking some liberties, we could then suppose that the effect of modulator could occur at either gating states and introduce a modulation term to characterize the properties of the modulator. The behavior of the modulated arm can be compared to the unmodulated arm, using equations 6.8 and 6.12, by introducing the modulator factors next to the equilibrium constants from the model.

Using these equations, the response of the two-step gating model can be calculated easily over a wide range of conditions. A factor (ρ) can be introduced into the equations to represent the actions of a positive allosteric modulator. Supposing the PAM acts at the final gating state, the potentiation factor can be introduced into equation 6.8 with each instance of E' (Figure 6.5A, B). Three cases were determined to illustrate the response of the two-step gating model by potentiating the E' step (Figure 6.5C). A low *T/E'* case was calculated; this case has a very low maximal *Po* (0.0000897) at saturating agonist concentrations. Calculating the effect of potentiation factors, stretching two orders of magnitude (ρ = 3, 10, 30, 100), resulted in dramatic increase on *Po* (ρ =100, *Po* = 0.0089, 99.2 fold potentiation). The effect of modulation in this scenario was restricted solely to *Po,* with minimal effect on agonist potency enhancement (Figure 6.5D). The next scenario has *T* set relatively high (10) with *E'* still at a low value. To put this into context, an equilibrium constant of 1 for T means that RA_2 and R^*A_2 are equal in proportion, so a value of 10 means R^*A_2 is 10 times as abundance compared to the RA_2.
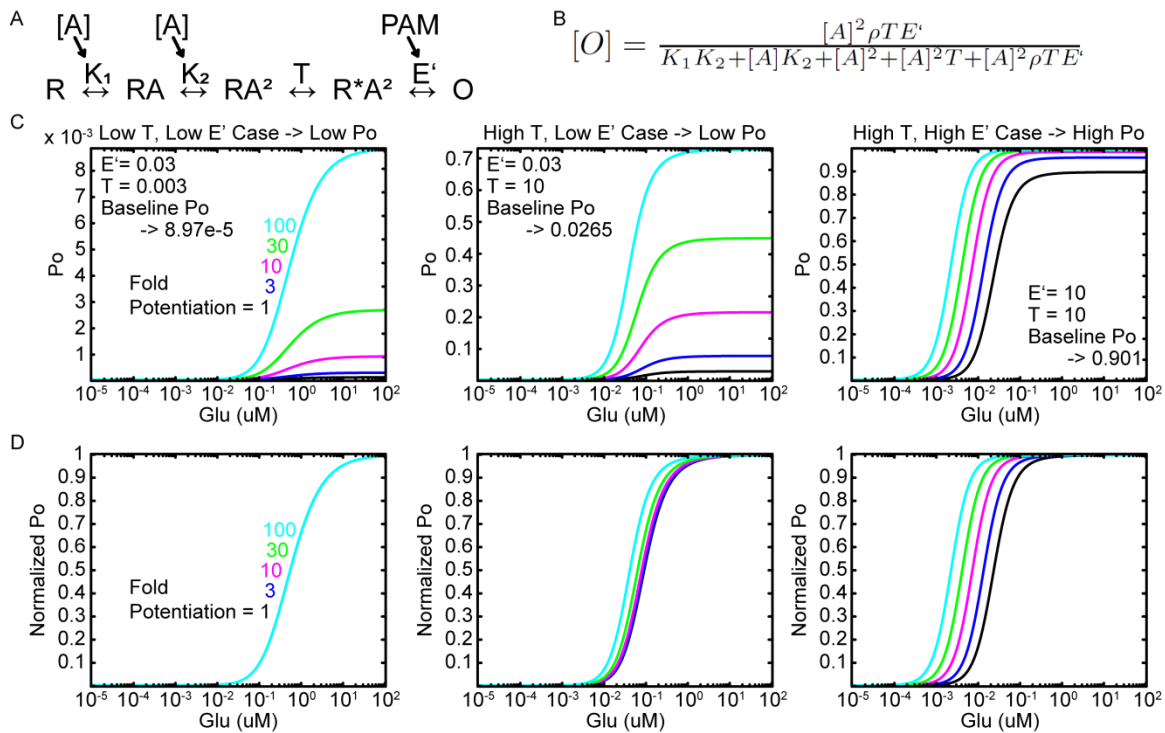
Figure 6.5. Agonist potency shifts in the two-step gating model, where a PAM acts on the gating step, are linked to Po.

A) The two-step gating model indicating the site of PAM action. B) Equations relating equilibrium response of the two-step gating model in **A** to agonist concentrations, ρ is introduced to modulate the constant E'. C) Calculated concentration-response curve given fixed E' and T constants (*left,* Low T/E'; middle, *High* T/Low E'; *right*, High T/E') and 5 different values for the degree of potentiation (1, 3, 10, 30, 100). D) The same concentration-response curves as in **C** here normalized to the maximal response.

This very much favors the right hand side of the transition, based on other equilibrium constants a change of a single equilibrium can have "small" scale (local) or "large" scale (global) effects on the state of the receptor, based on how much the change impacts the equilibrium of other states. With this high value for T, the receptor has a relatively low Po (0.0265). Potentiation of E' by a factor of 100 is capable of raising the maximal Po substantially (0.732, 27.6 fold potentiation, Figure 6.5C). The ability to shift agonist potency was observed in this scenario but only appreciably in the most extreme cases (ρ = 30, 100, Figure 6.5D). In the final case, both T and E' were set to 10 resulting in a receptor with a baseline maximal Po of 0.901. Potentiation in this case resulted in a limited capacity to increase Po due to a ceiling effect, rising to 0.999 with 100 fold potentiation (1.11 fold potentiation, Figure 6.5C). Potentiation did result in robust enhancement of agonist potency with 100 fold potentiation enhancing the EC_{50} by 10.3 fold (Figure 6.5D). This final transition illustrates the overall equilibrium shift in the receptor model by altering one equilibrium constant. If E' is large enough, it is able to dominate compared to the others, it drastically increase the number of receptors in the open state and in doing so deplete the fraction of receptors in the other states. Being that the receptor must be in the RA_2 state for agonist to dissociate the receptor spends more time as bound and results in an increase EC_{50}. Potentiating the E' step, in this two-step gating model, results in a coupling that requires Po to be high before appreciable shifts in agonist potency occur. This behavior is similar to the response of the del Castillo and Katz model as well as the Lester and Jahr model.

If instead supposing the PAM acts at the transactivation (T) step, of the two-step gating model, a different coupling between potentiation and agonist potency

enhancement occurs (Figure 6.6). Similar to the previous model, the potentiation factor (ρ) can be inserted into equation 6.8 at each instance of T, to produce the equation show in Figure 6.6. Likewise, three cases were calculated using the same values of E' and T, which results with the same baseline curves as the previous model (Low T/E' Po = 0.0000897, high T/low E' Po = 0.0265, high T/E' Po = 0.901). Similarly in the low T/E' case, potentiation resulted in a substantial increase in Po (ρ = 100. Po = 0.0069, 76.6 fold potentiation) and minimal enhancement of agonist potency. However, in the high T/low E' case, Po could only be marginally augmented (ρ = 100, Po = 0.0291, 1.10 fold potentiation). Whereas, in this case Po could not be augmented, there was a robust capability to enhance agonist potency (ρ =100, 12.4 fold enhancement, Figure 6.6D). Lastly, the high T/E' case could not be potentiated, due to its high baseline Po (ρ = 100, Po = 0.909, 1.01 fold potentiation), but the agonist potency could be enhanced (ρ = 100, 10.8 fold enhancement), similar to the previous model. This result suggest that by manipulating this middle transition in the receptor model (T) to a high enough equilibrium constant, that once agonist binding occurs the receptor accumulates in an agonist-bound pre-active state (R^*A_2) which can then gate based on E'. Given the magnitude of T, it limits the ability of the receptor to transition back to RA_2 and limits the dissociation of agonist, which leads to an enhanced EC_{50}. These cases illustrate key difference in the agonist potency coupling of the two-step gating model, based on which step a modulator interacts. This is a critical conclusion as different steps likely represent different conformational changes involving different parts of the receptor. When the PAM acts on the transactivation (T) step, the ability to enhance agonist potency was no longer directly coupled to the maximal Po of the model.
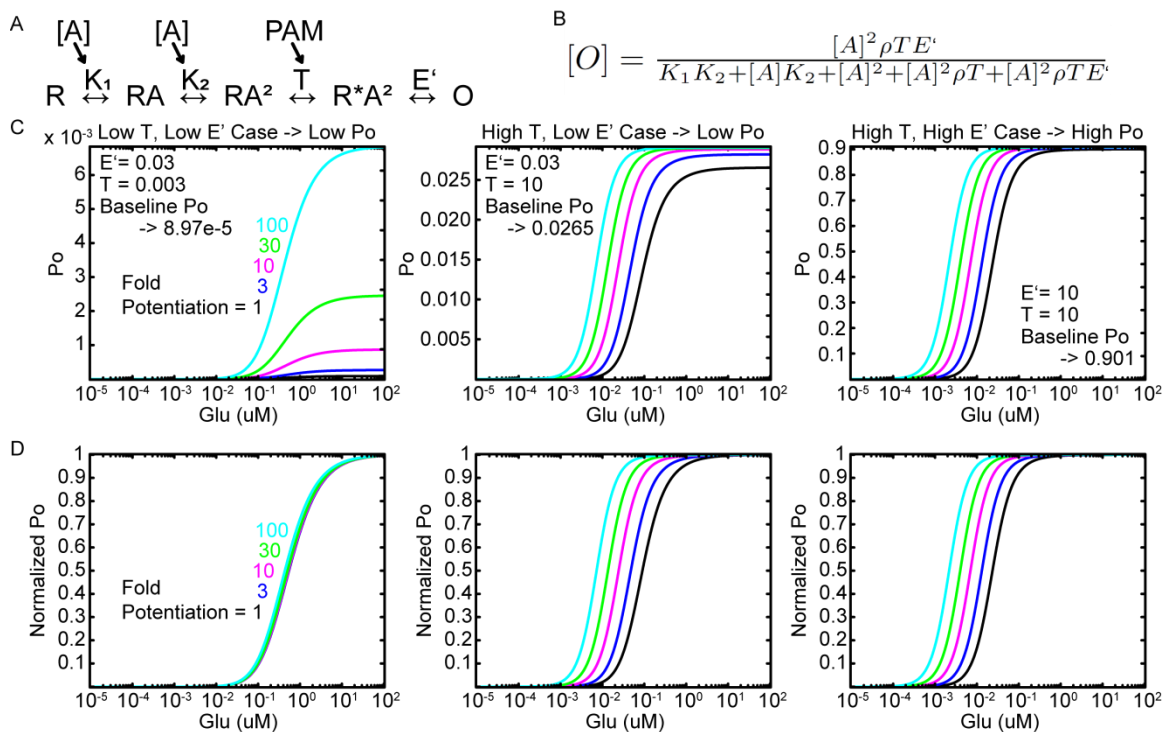
Figure 6.6. Agonist potency shifts in the two-step gating model, where a PAM acts on the transactivation (T) step, are not linked to Po.

A) The two-step gating model indicating the site of PAM action. B) Equations relating equilibrium response of the two-step gating model in **A** to agonist concentrations, ρ is introduced to modulate the constant T. C) Calculated concentration-response curve given fixed E' and T constants (*left,* Low T/E'; middle, *High* T/Low E'; *right*, High T/E') and 5 different values for the degree of potentiation (1, 3, 10, 30, 100). D) The same concentration-response curves as in **C** here normalized to the maximal response.

In this model, when a PAM acts at the transactivation (T) step, E' sets a theoretical ceiling on maximal Po that can be achieved by potentiation. It appears that if this ceiling is reached by potentiation, then the effect of a modulator shifts from potentiation to induce a greater enhancement of agonist potency. Using eq. 6.9 we can understand how T and E' influence baseline maximal Po and by inserting ρ we can observe the ceiling Po that is set by E'.

$$\lim_{[A]\to\infty}[O] = \frac{\rho TE'}{1+\rho T+\rho TE'} = Po$$

$$Po_{\rho=1} = \frac{\rho TE'}{1+\rho T+\rho TE'} = \frac{TE'}{1+T+TE'} = Po_{baseline} \tag{6.13}$$

$$\lim_{\rho\to\infty} Po = \frac{\rho TE'}{1+\rho T+\rho TE'} = \frac{\rho TE'}{\rho T+\rho TE'} = \frac{E'}{1+E'} = Po_{ceil} \tag{6.14}$$

Being that these models displays drastically different agonist potency coupling, the response of agonist EC_{50} to potentiation based on different gating equilibrium constants, T and E', was examined.

Using equation 6.12, the potentiation factor was inserted into the appropriate places for each model (Figure 6.7A, B). Given that this equation possessed multiple variables, ρ was fixed to 4, then T and E' were taken in turn to be fixed and the other varied over a range of values. By doing this, a family of curves was generated and allows for an evaluation of the behavior of agonist potency coupling (Figure 6.7C, D). In figure 6.7C, these curves were plotted as the fold enhancement of EC_{50} (EC_{50}/EC_{50PAM}) vs baseline Po, which was calculated using eq. 6.13. Examining the relationship of the first model, where the PAM acts at the E' step, potentiation only results in enhancement of EC_{50} when Po gets sufficiently high (Figure 6.7C). Alternatively, for the second model, where the PAM acts at the transactivation (T) step, we see parallel curves of the same magnitude based on each value of E' (Figure 6.7C). Each model with a different value of
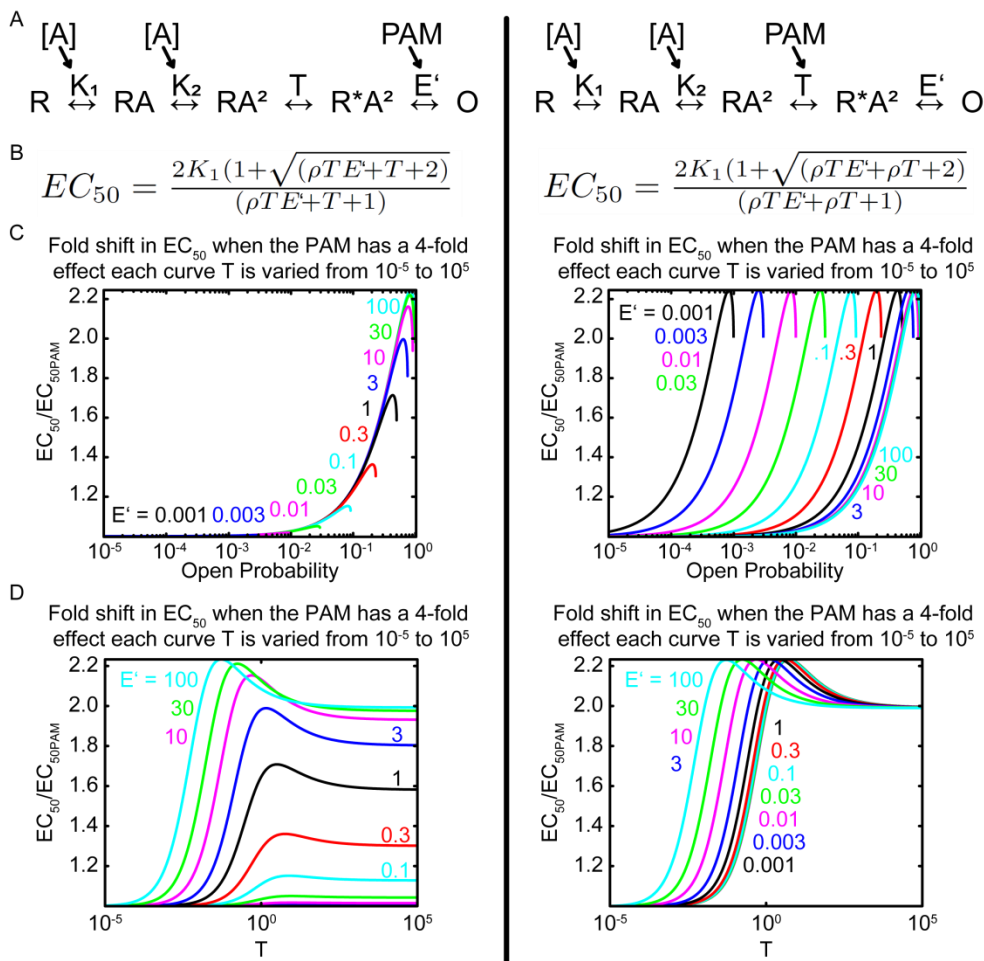
Figure 6.7. Theoretical PAMs have different agonist potency coupling based which step they act.

A) The two-step gating model schematic illustrating the transition state of PAM action, the E' step (*left*) or transactivation (T) step (*right*). B) Expression for EC_{50} from the two models in **A**, containing K_1, T, E' and ρ as variables. C) The agonist potency shift due to PAM action ($\rho = 4$) plotted as a function of Po. The family of curves was calculated using fixed values of E' and T was varied from 10^{-5} to 10^5. The Po range of each curve was calculated using the equation 6.9. D) The agonist potency shift due to PAM action ($\rho = 4$) plotted as a function of T. The family of curves was calculated using fixed values of E' and T was varied from 10^{-5} to 10^5.

E', possesses a different propensity for agonist potency enhancement. As *E'* is reduced, the break point where increases in Po stop occurring is reduced, as a consequence enhancement of agonist potency also occurs at lower Po.

Another consequence of this two-step gating model, that it creates, is a bottleneck effect or rate-limiting steps. Agonist potency coupling curves, plotted versus T, illustrates this feature (Figure 6.7D). When the final gating step (E') is potentiated, if T is low enough (producing lower Po receptors) it reduces the agonist potency coupling, even if E' is very high. If instead the transactivation step is potentiated, T still needs to be high enough to induce agonist potency coupling, but higher values of E' facilitate agonist potency enhancement.

This snapshot of the two-step gating model highlights specific factors of modulator behavior, but is still a reduced and simplified model so must be interpreted with caution. With that being said, there are some conclusions that can be drawn from this model. The phenomenon of agonist potency coupling is an inherent property of PAMs, but their activity is influenced the specific step of receptor activation they interact with. This property is not directly correlated with the baseline *Po*, if a PAM interacts at a step other than the step that sets the maximal *Po*. Potentiation can be restricted by a ceiling effect, if either Po is approaching 1 or a different theoretical ceiling. If approaching a theoretical Po limit, potentiation then leads to agonist potency enhancement. Additionally, rate-limiting steps can also restrict how potentiation of one step then influences the equilibrium of other distal states. This is a simplified, reductionist model that allows for theoretical interpretation and needs to be validated for

biological receptors. This conceptual modeling many assist in a conceptual representation of allosteric theory in single channel models of NMDAR.

The actions of a positive allosteric modulator on NMDA receptor hidden Markov gating models suggest activity is based at which step modulation occurs

Thus, we return to NMDAR models built from biological data with the concepts gained from the two-step gating model in hand. Initial observations of several NMDAR channel models show clear correlates to the two-step gating model (Banke and Traynelis 2003, Popescu 2004, Erreger 2005, Schorge 2005, Dravid 2008, Vance 2012). In both NMDAR models, there are multiple gating transition steps that separate the agonist binding and open states (Figure 6.8A) (Banke and Traynelis 2003, Popescu 2004, Erreger 2005, Dravid 2008). The Popescu model is highly similar possessing three agonist-bound unopen states in sequential linear order (Popescu 2004). Additionally, the Banke and later derivative models possess multiple shut states (3-4), 1-2 open states, and contain a split path to receptor activation. Most comparable to the Popescu model is scheme 3a from Dravid 2008, which both have two open states and three gating transitions. These models differ in that the Popescu model has a fixed transition order, whereas the Dravid model allows for an independent order to two pre-gating steps. Additionally in (Dravid 2008), the two models presented in Figure 6.8A were fit to the same data set resulting in nearly identical fitted parameters and producing only small differences simulating the activation of macroscopic responses.

With these NMDAR models possessing the features that influence the activity of a PAM identified in the study of the two-step gating model, we next considered what the
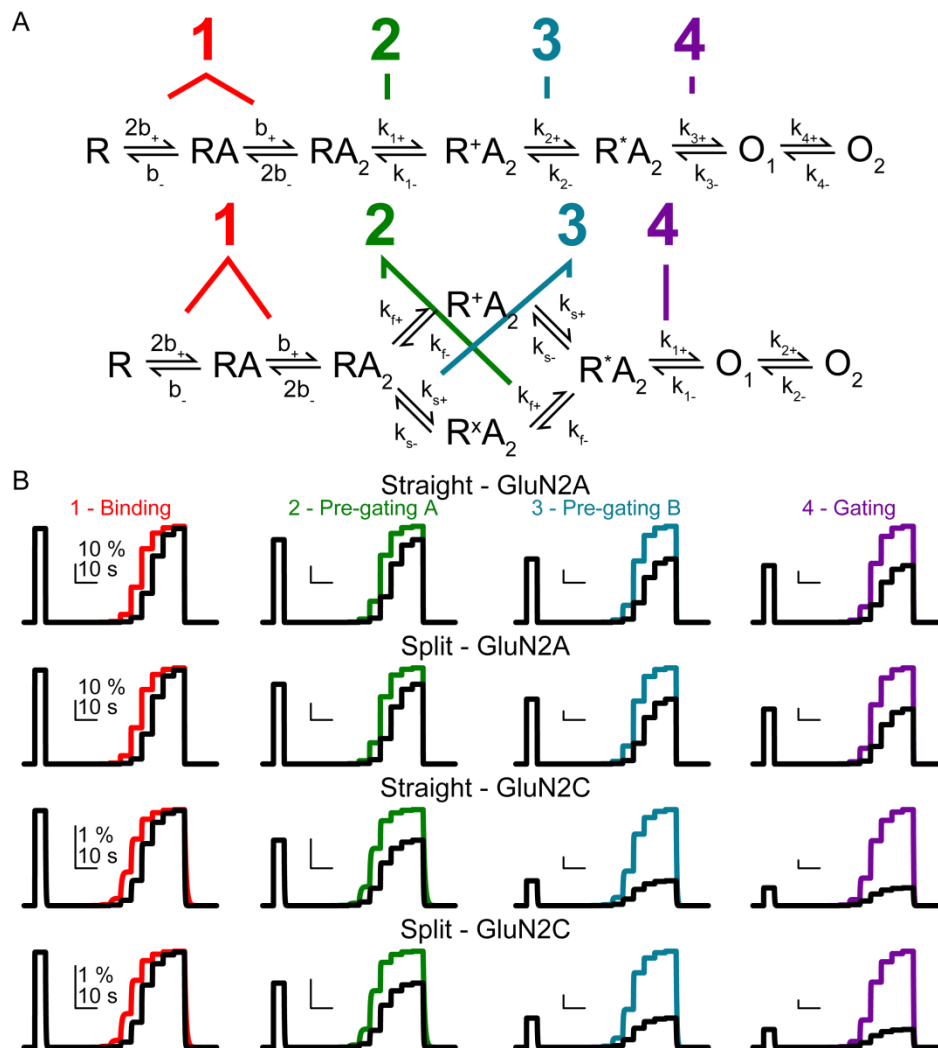
Figure 6.8. Modulation of NMDAR models varies based on the site of modulation.

A) Two NMDAR models generated previously (Erreger 2005, Dravid 2008). In the Dravid models, the straight and split models shown here were fit to the same data set and generated nearly identical transition rates. In order to produce a comparable set of models, the straight and split GluN1/GluN2A models were adapted from the three shut, two open state linear model from (Erreger 2005). Each step of the model was systematically potentiated (1-Binding, 2-Pre-gating A/Slow, 3-Pre-gating B/Fast, and 4-Gating). In each case, the forward rates were multiplied by a factor of 6 except for the 1-

Binding where the two unbinding rates were divided by a factor of 3. B) Simulated responses of the models described in **A**, with the systematic investigation of potentiation. Each model was initially simulated with a saturating concentration of agonist then by a range of agonist concentration (0.03, 0.1, 0.3, 1, 3, 10, 30, 100, 300) with (colored) and without (black) potentiation. See table 6.2 for transition rates of the models.

Table 6.2. Transition rates of NMDAR models used to simulate modulator action in Figure 6.8 and 6.6.

	GluN1/GluN2A[a] Straight & Split	GluN1/GluN2C[b] Straight	GluN1/GluN2C[b] Split
$b_+{}^{\dagger}$	31.6	1.3	1.4
b_-	1010	7.5	8.8
k_{1+}	356	66	65
k_{1-}	201	48	43
K_1	*1.77*	*1.37*	*1.51*
k_{2+}	944	560	590
k_{2-}	2758	3200	3300
K_2	*0.34*	*0.18*	*0.18*
k_{3+}	2849	580	590
k_{3-}	2835	3500	3400
K_3	*1.00*	*0.17*	*0.17*
k_{4+}	4979	1400	1300
k_{4-}	970	2600	2500
K_4	*5.13*	*0.54*	*0.52*

All units are in s^{-1}, except for binding rates ($\dagger$), which were in $\mu M^{-1}s^{-1}$. [a] (Erreger 2005), [b] (Dravid 2008). Equilibrium constants were calculated for each transition.

effect of modulating various transitions would have on the overall model function (Figure 6.8). The 2 GluN1/GluN2C schemes, from Dravid 2008, were constructed as well as 2 similar GluN1/GluN2A schemes, from Erreger 2005. In all models, desensitization was removed for simplicity. Then in a sequential manner, different transitions were modulated. In total, the agonist binding steps, the first or slow gating step, the second or fast step, and the final gating step were modulated. Two agonist concentration-response curves were simulated, with and without modulation, for each scenario to examine the steady-state effect of modulation (Figure 6.8B).

The GluN1/GluN2A simulation responses had higher saturating Po than the GluN1/GluN2C simulation responses. Distinct modulation profiles were observed due to the site of action. Agonist concentration-response curves for the control and modulated responses were measured and fit by the Hill equation (Figure 6.9). Whereas modulation of the agonist binding does not alter the response to saturating concentration of agonist, it did enhance agonist potency (Figure 6.9A,B). On the other end of the spectrum, modulation of the final gating step (4) resulted in large potentiation of responses to saturating agonist and enhanced agonist potency to lesser extents. The modulation of the two intermediate gating steps had combinations of these actions that varied based on subtype model. In all cases, modulation of site 2 (first step or slow split step) showed less potentiation of saturated responses as compared to either site 3 (second step or fast split step). Additionally, both site 2 and 3 showed less potentiation of saturated responses than 4. In terms of agonist potency enhancement, site 2 was more efficacious than site 3, which were both less efficacious than directly modulating binding (site 1). Similar to theoretical models, the ability to enhance saturated responses and to enhance agonist
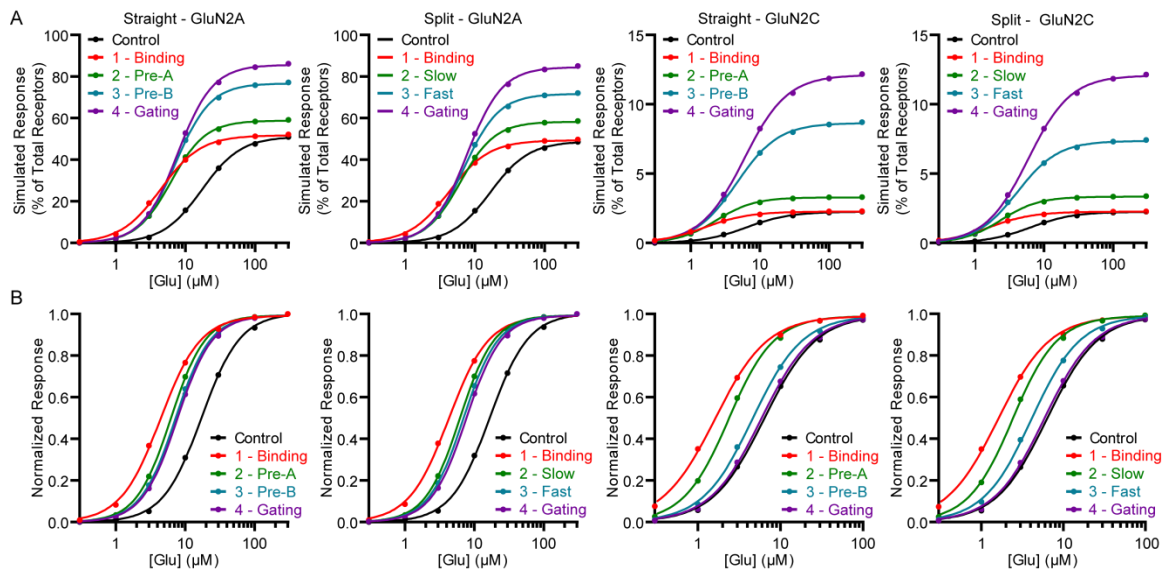
Figure 6.9. Modulator activity is dependent on the step in which it acts.

A) Concentration-response curves of the simulated NMDAR models from Figure 6.8, illustrating hypothetical modulators interacting with different transition steps. B) Normalized concentration-response curves highlighting the modulators actions on agonist potency.

potency (including cases for low *Po* receptors) were observed with these realistic NMDAR models. Additionally, the effect of modulating receptor activity had drastically different results based on where in the activation scheme modulation occurs.

Properties of several modulator series align with receptor modeling predictions

What evidence is there that the PAM series conform to the rules and limitations put forth by the simulated models? We lack high quality single channel recordings illustrating the effects of many of these series of PAMs, which would be able to directly address this question. Making due with currently published data, we can draw some conclusions with a set of multi-channel GluN1/GluN2D patches where CIQ was applied (Mullasseril 2010). In this data set, the open time histogram was unaffected CIQ by potentiation. Additionally, although rigorous analysis could not be performed on this dataset, CIQ altered several of the shut time histogram fitted exponentials but not the fastest two exponentials (the fastest two shut times would structurally represent the closest shut states, thermodynamically as compared to the open state). In the context of hidden Markov models of allosteric modulation, these two observations taken together suggest a site of action of this modulator is removed from the final gating transitions. If the final gating step was enhanced longer open times would be expected. Some unpublished data concerning the actions of 1622-14 suggest that this more efficacious PAM prolongs the open times of NMDARs (unpublished data). These observation may align with this two-step gating model if CIQ and 1622-14 act at different states, resulting in more potentiation by 1622-14 and less in CIQ.

Another property of the two-step gating model, which was important in the activity of allosteric modulators, was the tradeoff between potentiation and enhancement of agonist potency. The two-step model illustrated a ceiling effect of potentiation when approaching a *Po* of 1 or a theoretical *Po* ceiling (*E'* of the receptor is limiting). Most evident for GluN1/GluN2A, since it has the highest Po and potentiation would cause it to approach 1 more readily. Additionally, in most cases, no potentiation of saturated responses is observed when potentiating GluN1/GluN2A receptors, but robust agonist potency enhancement is observed in all of these cases. Also to this point, the agonist potency of GluN1/GluN2C can be enhanced by several PAMs, with diverse scaffolds, even though it is a low Po receptor. Potentially, GluN2C may have divergent polypeptide segments that contribute to a shared binding site for these modulators that induces greater cooperativity between modulator and agonist. Alternatively, the properties of GluN1/GluN2C channels are sufficiently different, than GluN1/GluN2D, such that potentiation by these modulations is approaching a proposed theoretical ceiling Po and resulting in greater enhancement of agonist potency as a consequence.

Several NMDAR PAM series have been studied by the lab containing in some cases, hundreds of analogs, which may help suggest this theoretically restricted Po exists for GluN1/GluN2C preventing it from reaching high levels based by potentiation by mechanistically similar modulators. The maximal potentiation of 1180 series of PAMs at different diheteromeric receptors were cross plotted (Figure 6.10). If the concentration-response data could not be fit, the potentiation at the highest concentration tested was used to complete the dataset. In general, GluN1/GluN2C and GluN1/GluN2D are the most a like in terms of receptor properties and modulator capabilities (Monyer 1994,
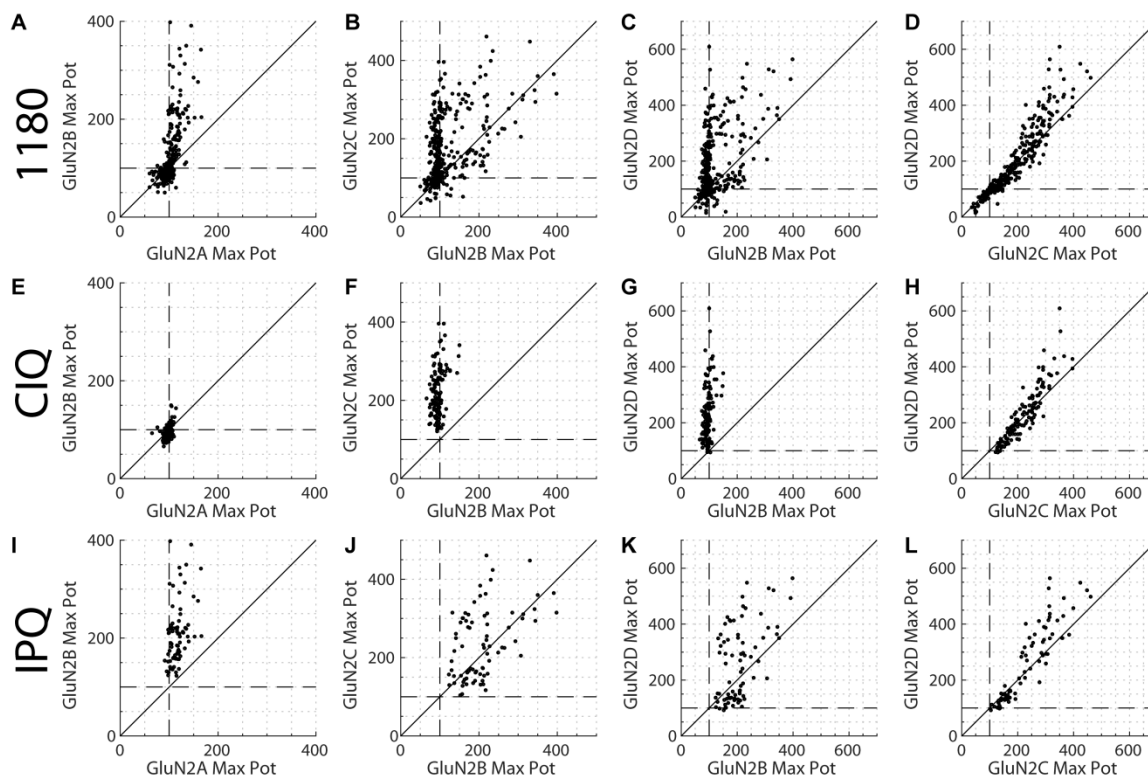
Figure 6.10. The subsets of the 1180 series have distinct modulatory activity.

Maximal potentiation scatter plots of the 1180 series analogs cross plot at different diheteromeric NMDAR. All 1180 analogs (A-D) were separated based on the ability to potentiate GluN2B diheteromeric receptors; CIQ-like (E-H, lacking GluN2B potentiation), and IPQ-like (I-L, possessing GluN2B potentiation) are plotted separately to identify differences in activity. If the fit of the Hill equation failed to converge, the average potentiation of the highest modulator concentration tested was used. The solid line illustrates unity in the two plotted modulator attributes, the dashed lines 100% modulation or no activity. The inactive (lacking either GluN1/GluN2C and GluN1/GluN2D activity) CIQ and IPQ analogs of the 1180 series were removed (372 total analogs, 171 inactive analogs). A,E,I) Cross-plot of analog activity at GluN1/GluN2B versus GluN1/GluN2D. B,F,J) Cross-plot of analog activity at GluN1/GluN2B versus GluN1/GluN2C. C,G,K) Cross-plot of analog activity at

GluN1/GluN2A versus GluN1/GluN2B. D,H,L) Cross-plot of analog activity at GluN1/GluN2C versus GluN1/GluN2D. The data for these analogs were collected by P. Le, P. Lyuboslavsky, K. Vellano, J. Zhang, and likely other lab members.

Vicini 1998, Mullasseril 2010, Acker 2011, Hansen and Traynelis 2011, Siegler Retchless 2012, Swanger 2017). Unsurprisingly, the highest correlation in maximal potentiation occurs in the comparison of GluN1/GluN2C and GluN1/GluN2D (Figure 6.10D,H,L). The 1180 series (both CIQ- and IPQ-like) closely follow the 1 to 1 correlation (Figure 6.10D,H). However, the slope of a fitted line through the 1180, CIQ- and IPQ-like data significantly diverges from 1 (fitted line runs through $x = 100$ $y = 100$, *slope* [*CI*], 1180 - 1.19 [1.16 1.23] $p < 0.0001$, CIQ - 1.15 [1.09 1.21] $p < 0.0001$, IPQ - 1.25 [1.17 1.33] $p < 0.0001$). This suggests that potentiation extent of GluN1/GluN2D is generally greater than at GluN1/GluN2C in all series.

Intriguingly, the cross-plot of the maximal potentiation of PAMs at GluN1/GluN2C versus GluN1/GluN2D displays a curious pattern. Focusing on the 1180 series, compounds with modest levels of potentiation (100-300%) perform equally well at GluN1/GluN2C and GluN1/GluN2D (Figure 6.10D). However, at higher levels of potentiation (>300%) most compound are capable of potentiating GluN1/GluN2D preferentially over GluN1/GluN2C (Figure 6.10D). This capability occurs regardless of subclass, CIQ or IPQ (Figure 6.10H,L). This may suggest that modulation, by these mechanistically similar compounds, is resulting in potentiated of GluN1/GluN2C receptors that have begun to approach a theoretical limit in *Po*. The two-step gating model, suggests that if a theoretical limit (being set by E') is approached modulation will tend to lead to reduced increases in Po but should result in a greater shift in agonist potency for GluN1/GluN2C compared to GluN1/GluN2D. In fact this trend is observed, the enhancement of agonist potency has been measured using several 1180 analogs (CIQ

and IPQ analogs) and in every case the shift is larger for GluN1/GluN2C than for GluN1/GluN2D (Table 6.1). In order for this aspect be a result of a structural subtype specific component of the 1180 series it would have to interact with all compound analogs, as many aspects of the modulator chemical structure have been changed, this seems less likely to be the case.

Another peculiar observation from this cross plots, is that there appears to be a clustering of analogs in the 1180 series analogs at very low levels of potentiation (<150%) of GluN1/GluN2D and slightly more modest levels of potentiation of GluN1/GluN2C (~200%, Figure 6.10D). This may reflect a slight preference for GluN1/GluN2C or perhaps, as these represent low potency analogs; the 1180 series generally has limited solubility and slight differences in potency may be significant (unpublished data). Perhaps as outline by the allosteric two-state theory, the actions of an allosteric modulator on an agonist are reciprocal (Christopoulos 2002). With GluN1/GluN2C receptors have preferentially agonist potency coupling, then potentially the modulator potency is also enhanced preferentially at GluN1/GluN2C receptors. In fact, the 1180 series shows higher potency at GluN1/GluN2C versus GluN1/GluN2D (Figure 6.11). In 101 cases of 173 total the EC_{50} at GluN1/GluN2C was less (more potent) than GluN1/GluN2D (permutation test, 10^6 permutations, p = 0.041) (Camargo 2008).

As various lines of evidence suggest, modulation by various NMDAR PAMs require more mechanistically informed models of allosteric modulation. Greater validity of this mechanistic concept would be strengthened by a detailed single channel modeling of potentiated GluN1/GluN2C and GluN1/GluN2D. Additionally, these models could be
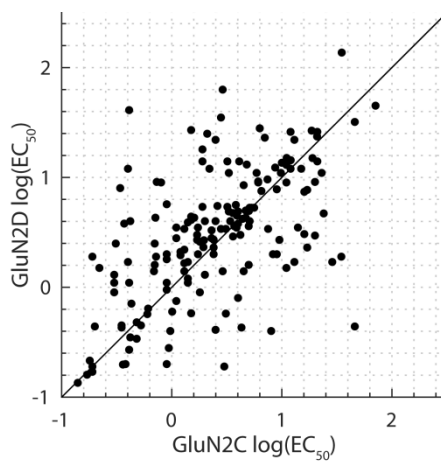
Figure 6.11. The 1180 series is more potent at GluN1/GluN2C than GluN1/GluN2D. GluN1/GluN2C and GluN1/GluN2D $\log(EC_{50})$ scatter plot of 1180 series analogs. EC_{50} were in μM before transformation. The solid line illustrates unity in the two plotted modulator attributes. The data for these analogs were collected by P. Le, P. Lyuboslavsky, K. Vellano, J. Zhang, and likely other lab members.

validated using partial agonists in tandem with allosteric modulators. The canonical effect that partial agonists have on receptor gating kinetics is that they cause reduced receptor efficacy and shown for various NMDAR partial agonists (Erreger 2005, Kussius and Popescu 2009). Presumably, PAMs would have a heightened ability to potentiate saturated responses of receptors activated by partial agonist than by full agonists. Additionally, given the proposed trade off of potentiation and enhancement of agonist potency, likely PAMs would result in less enhancement of partial agonist potency compared to full agonists. These mechanistic allosteric receptor models would be very useful in predicting allosteric modulator action in native tissue to physiological receptor stimulation patterns.

Which model is best?

The pharmacology of the NMDAR presents a complex picture of a myriad of ligands with diverse actions. Most of these features can be represented by perturbations of the allosteric two-state model adapted for NMDARs. Allosteric theory is built from a reductionist model and quantifies the steady state responses due to the interactions of ligands and receptors (Colquhoun 1998, Hall 2000). The original allosteric theory is based on cooperative symmetrical conformational changes in protein oligomers (Monod 1965), although now this theory is more widely applied to receptors and proteins without the need of symmetry (Hall 2000, Christopoulos 2002). On the other hand, NMDAR are large and built from an assembly of subunits, each comprised of a number of semi-autonomous domains with homologous independent analog gene origins (O'Hara 1993, Armstrong 1998, Panchenko 2001). Each domain has an independent homolog, which

had its own function and conformational motions. Are these semiautonomous domains now adapted to act as one functioning machine or are their interactions more complex and not perfectly concerted? Other smaller receptors have much more straightforward allosteric interactions including GPCRs and pentameric ligand gated ion channels (Christopoulos 2002, Pin and Prézeau 2007, Calimet 2013, Lindsley 2016). Perhaps these models of allostery are too simplified for accurate description of NMDAR interactions although the major principle still applies.

The hidden Markov models of NMDAR channel activity are more realistic representations of the underlying biological phenomena. However, the impact of modulators on specific states is not intuitive and thus explicit models must be designed explicitly for each receptor subtype and analog. These types of models, possessing realistic channel transition and modulator actions, would allow for a greater ability to assess potential candidate drug in various physiological setting. These models may also help in identifying new mechanistic details that could have utility or provide a way to quantify the desired properties of modulators to aid development of newer better analogs.

The theoretical two-step gating model suggests that the principles of the allosteric two-state model may be adaptable to models with increasing number of connected states. This is required since the allosteric two-state model does not contain the complexity to represent NMDAR channel records, since it lacks a sufficient number of open and shut states. Perhaps since the ABD is the major dominating factor in determining receptor activation and dominates the steady state response of the allosteric two-state model, where as other factors impact the sub-millisecond time scale of receptor channel activity. For instance, the ABD, of iGluRs, is known to adopted different conformation states in

the absence of agonist, and stabilized distinct states based on agonist or partial agonist binding (Madden 2002, Jin 2003, Cooper 2015, Dolino 2017). The interactions between glutamate and glycine are well defined and may be an appropriate starting point for developing a more kinetically accurate allosteric model. Other domains and key gating elements of the receptor are known to dramatically impact receptor function; including the ATD, the Pre-M1, and the M3 (Schorge 2005, Yuan 2009, Vance 2012, Vance 2013, Ogden 2017, Wang 2017, Yelshanskaya 2017). The ATD is known to influence modal gating of certain NMDAR subtypes (Popescu and Auerbach 2003, Vance 2013), which indicates an allosteric action. Mutations and modulators that interact with the TMD have very strong abilities to alter receptor activation suggesting the natural role is critical (Ogden 2017, Wang 2017, Yelshanskaya 2017). The selectivity filter has been suggested to play a part in ion flow and contributes to channel activity in K^+ channels (Chakrapani 2011). In NMDARs, a single GluN2 residue of the M3 that is closer to the intracellular side of the TMD controls Ca^{2+} permeability and channel conductance (Siegler Retchless 2012). All of these must influence each other allosterically and could be modeled. Potentially when taking into account these various factors an allosteric model may begin to approximate the properties of single channel recordings. However, generating a model that taking into account all these factors may contain too many degrees of freedom and may not be feasible to constrain. More efficient ways to collect channel recordings to fit hidden Markov models may the more useful way forward in modeling NMDARs.

Moving forward in pursuit of novel NMDAR modulators with utility

The aim of developing of novel pharmacological agents is to produce tools that will allow for greater understanding of NMDARs role in biological systems, how specific physiological processes can be targeted and how disease pathologies be rectified using therapeutic agents. NMDARs in the brain are comprised by distinct gene with specific expression patterns, subpopulations that are expressed in various cell surface areas of neurons and there are different signaling profiles that signal to NMDARs (Monyer 1994, Groc 2006, Papouin and Oliet 2014). The compound series covered in this document have potential properties that may lend themselves to achieving some of these goals. Those properties and potential improvements will be discussed here.

The 1180 series

This series has several interesting features, the capability to selectively modulate GluN2C- and GluN2D-containing receptors in the CIQ-like modulator subset. The data that (+)-CIQ has the capability to enhance the inhibitory tone in the hippocampus illustrates one important utility. Interneurons are thought to enhance signal processing via various forms of feedforward and feedback control (Freund and Buzsaki 1996). The actions of these modulators could enhance this control and alter information processing by these brain regions (Kullmann and Lamsa 2007). Alternatively, the increase inhibitory control may be suppressed excessive or even normal signaling. The other subclass, IPQ, having non-selective actions should have drastically different behavior. This type of molecule should impact NMDAR in inhibitory interneurons as well as excitatory pyramidal cells, thus alter neuronal systems in a very different way. This may lead to

enhanced connectivity and promote rhythmic signaling (Klausberger and Somogyi 2008, Somogyi 2014). Other selectivity profiles are desired (GluN2B selective PAM, GluN2D selective PAM) but no compounds, to date, are highly efficacious and possess sufficient selectivity (50-fold or greater). Hopefully with advances in structural determinations of the receptor (crystallization or cyro-EM) binding poses of modulators will lead to structurally guided pursuits of different subunit selectivity.

The 1622 series

The 1622 series may act similarly to the IPQ series given the similar selectivity profile but the much greater potentiation capabilities may cause different physiological activity. Additionally, the dramatic ability to prolong deactivation may have a profound impact on the integration and summation of afferent signaling. This may change the rules of neuronal plasticity and could robustly impact a wide array of behaviors (Tang 1999, Hackos 2016). Recent unpublished work, suggests that this series has the capability to alter the prevalence of channel sub-conductance levels. In GluN1/GluN2A, 1622-14 shifts the channel conductance levels to be primarily subconductance levels (unpublished data). This suggests that other channel properties may also be altered by these modulators. There may be different rules to how these channel properties are impacted by modulators in the series which could be exploited. Lower channel conductance may also be associated with altered ion permeability which could impact the physiological impact of NMDARs. Indeed, Shaker potassium channels have been shown to possess different ion permeability based on conductance level (Zheng and Sigworth 1997, Zheng and Sigworth 1998). The micro-domains of calcium ions surrounding channels are tightly

controlled and are tuned for high fidelity of consequential signaling cascades that may be disrupted or altered with modulation (Karakas and Furukawa 2014). This series is highly interesting given the mechanistic properties to possess as well as highly efficacious modulator capabilities. However, given NMDAR's role in excitotoxicity, these series analogs may have potential liabilities, even in pre-clinical studies (in basic science exploratory research). The activity of 1622 analogs may be honed through careful delineation of the structure activity relationship of the series to produce desired modulatory effects and preventing toxicity.

The 1794 series

There is a lot of potential and possibilities in the 1794 series. The series has the property of agonist-dependence, requiring both agonists. Additionally, it appears that the series has a full range of modulation possibilities, from full inhibition, to partial inhibition, and to potentiation. Lastly, these modulators are capable of enhancing agonist potency. The combination of agonist potency enhancement with partial inhibition creates a compound with the potential to selectively act at NMDAR that experience low levels of agonist exposure (Figure 6.12). Alternatively, compound with agonist-dependency coupled with full inhibition, partial inhibition or potentiation could serve as molecular agents that selectively act during high frequency stimulation events each with different actions (Figure 6.13). Theoretical modulators with different association rate, dissociation rate, degree of agonist-dependence, and effect on channel gating all have different implications for how they may respond in native tissue. Predictions from the allosteric two-state model suggest that these parameters are tractable quantities and may vary
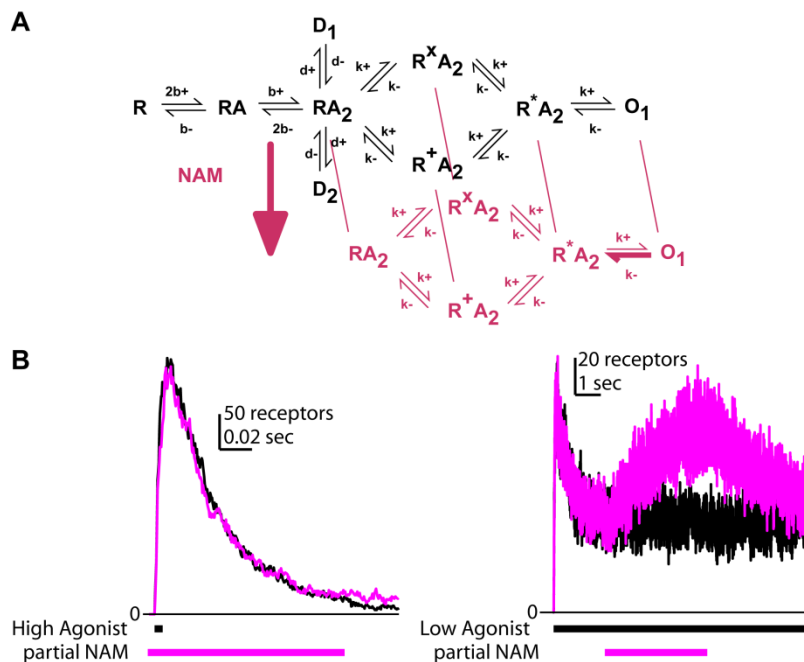
Figure 6.12. Simulations of a hypothetical partial-NAM with agonist-dependence illustrates potential selectivity for low agonist concentration-responses.

A) Model used to simulate synaptic- and extrasynaptic-like NMDAR responses. The model used is similar to the glutamate model from (Erreger 2005). The total association rate of the NAM was 1.572 $\mu M^{-1}s^{-1}$ and the dissociation rate was 1.572 s^{-1} (which was split over each state where NAM binding could occur). The only difference in the two arms of the model is the final gating equilibrium was divided by a factor of 4. B) *Left*, Simulation of a synaptic-like NMDAR response (glutamate concentration was 1000 μM, 5ms) in the presence and absence of a partial NAM, similar to 1794-4. *Right*, Simulation of an extrasynaptic-like NMDAR response (glutamate concentration was 3 μM) with the application of a partial NAM, similar to 1794-4.
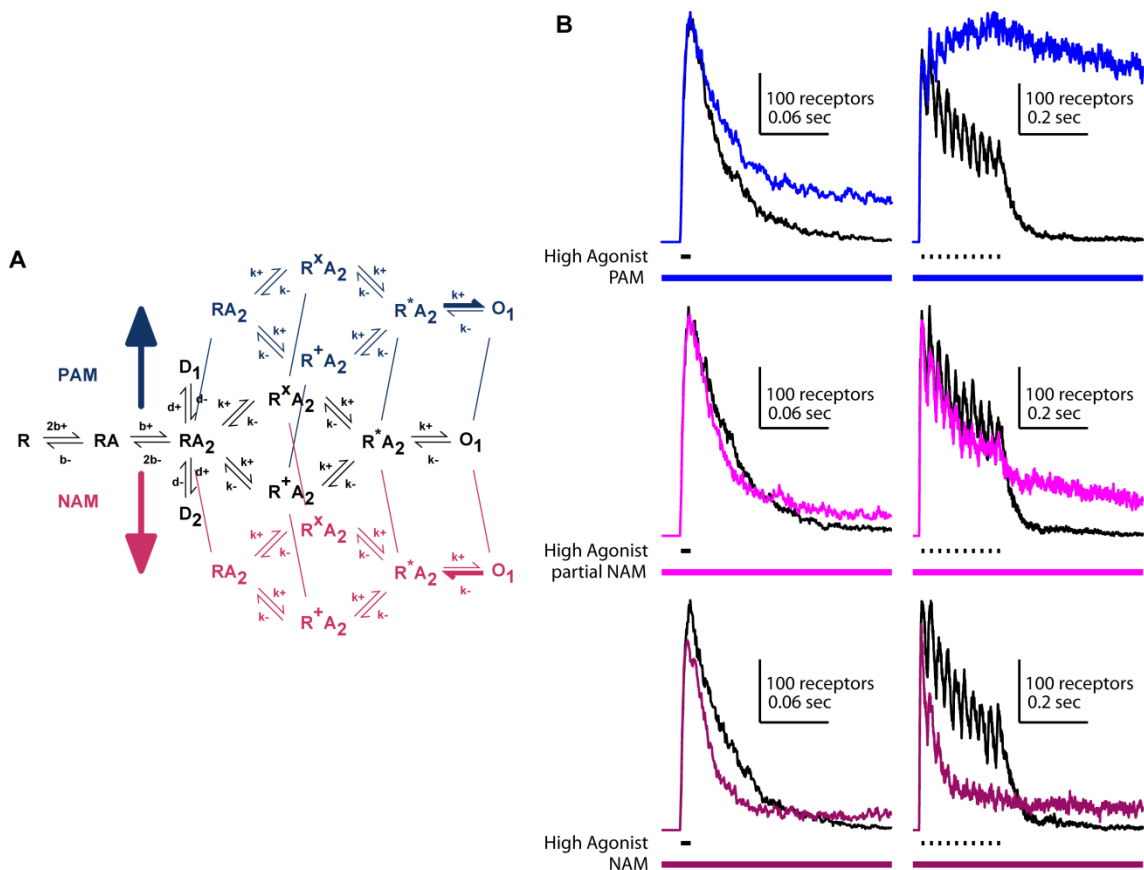
Figure 6.13. Hypothetical modulators with agonist-dependence and a spectrum of activity have diverse actions on burst stimulation of modeled NMDARs.

A) Model used (same as 6.12) to simulate low and high frequency stimulated NMDAR model responses. B) *Left*, low frequency NMDAR model responses (glutamate concentration was 1000 µM, 5 ms) in the presence and absence of diverse allosteric modulators (*top* PAM, *middle* partial NAM, *bottom* full NAM). *Right*, high frequency NMDAR model responses (1000 µM, 5 ms, 20 ms interval between stimulations, 10 stimulations) in the presence and absence of diverse allosteric modulators. The association rate of the PAM was 0.786 µM^{-1}s^{-1}, partial NAM was 1.572 µM^{-1}s^{-1}, and full NAM was 1.572 µM^{-1}s^{-1}. The disassociation rate of the PAM was 0. 786 s^{-1}, partial NAM

was 1.572 s^{-1}, and full NAM was 1.572 s^{-1}. The gating equilibrium constant modulation factor for the PAM arm was 2, partial NAM arm was 1/4, and full NAM arm was 1/16.

between analogs. Thus quantification of these mechanistic properties is crucial for accurate interpretation of the actions of each analog. In addition to the complexity, there are neutral allosteric ligands of GPCRs that do not alter the steady state activity of a receptor but alters the kinetics of activation and deactivation (Kostenis and Mohr 1996). The 1794 series displays a capacity for a range of activity and related analogs may be neutral ligands. However, with our current means of assaying NMDAR ligands, we have no efficient means to quantify these differences in activation and deactivation rate to identify these hypothetical ligands.

The future of pharmacological agent development

In order to advance our pursuit of novel pharmacological agents, we need more efficient tools that are capable of collecting detailed information about the mechanistic parameters of modulator series. If our knowledge about modulators series parameters is restricted to efficacy and potency, we are limited in our ability to reliably predict how a compound will work once you introduce it to neuronal tissue. This then requires deliberate characterization of a number of different parameters (use-dependence, association rate, etc) to have a reasonable idea of how a compound will respond in a neuronal system. Detailed information concerning the mechanistic properties, discussed in this dissertation, could be added to the structure activity relationship the compound series being studied, great benefits would be reaped. With the growing prospect of personalized medicine, more detailed libraries of potential therapeutic agents may allow for greater potential targeting and specificity of treatments. The ability to identify the optimal modulator for a specific disease treatment may be a possibility.

There is a great need for more efficient ways to test novel compounds in neuronal tissue. Many examples show that a compound with ideal pre-clinical testing can result in clinical trial failure (Ikonomidou and Turski 2002). The complexities of the brain, especially in targeting NMDARs that are in many places in the brain, will create unpredictable differences in drug action. This may be alleviated if we could more readily screen libraries of compound on biological tissue and on biological relevant endpoints. This would provide a much greater confidence in a compound ability to produce a desired therapeutic effect. For example, if testing could be done on the 1622 series, a correlation may be derived to explain the different factors contribute to 1622-14's robust effects the NMDAR-component of the EPSC but a lack of amplitude potentiation. Additionally due to the complex nature of neuronal networks, similar compounds (memantine versus PCP) or even different doses of the same compound (ketamine) can produce drastically different physiological effects (Krystal 1994, Johnson and Kotermanski 2006, Iacobucci 2017). A rapid ability to collect concentration-response information in biological systems with physiological end-points would greatly enhance our ability to drive forward drug discovery in the field of neuroscience.

Conclusions

Unlocking the complexities of the brain remains one of the greatest scholarly pursuits of our time. Since the earliest depictions of the neurons and glia of the brain, scientists have sought to understand how all these components work together to produce behavior, social interactions, consciousness. There are many ways to approach this question. One powerful way that advances our capability to comprehend diverse

functions of the brain and to treat disease, is through development of pharmacological agents of cell surface receptors. We are learning more about the range of possibilities of how different molecules interact with cell surface receptors and this dissertation discussed several new modulator series that alter the function of NMDARs. Constructing models of these modulatory actions aids in the understanding patterns of activity of analogs. These models also illustrate the potential limitations and the fundamental mechanistic properties leading to their activity. Speculations about how the attributes of these compound series may allow for new ways of altering neuronal processes have been discussed. The tools and ideas within this work progresses us closer to the goal of making sense of the processes, responses, outputs of the brain.

Chapter 7: References

Acker, T. M., A. Khatri, K. M. Vance, C. Slabber, J. Bacsa, J. P. Snyder, S. F. Traynelis and D. C. Liotta (2013). Structure-activity relationships and pharmacophore model of a noncompetitive pyrazoline containing class of GluN2C/GluN2D selective antagonists. *J Med Chem* **56**(16): 6434-6456.

Acker, T. M., H. Yuan, K. B. Hansen, K. M. Vance, K. K. Ogden, H. S. Jensen, P. B. Burger, P. Mullasseril, J. P. Snyder, D. C. Liotta and S. F. Traynelis (2011). Mechanism for noncompetitive inhibition by novel GluN2C/D N-methyl-D-aspartate receptor subunit-selective modulators. *Mol Pharmacol* **80**(5): 782-795.

Akazawa, C., R. Shigemoto, Y. Bessho, S. Nakanishi and N. Mizuno (1994). Differential expression of five N-methyl-D-aspartate receptor subunit mRNAs in the cerebellum of developing and adult rats. *The Journal of Comparative Neurology* **347**(1): 150-160.

Alsaloum, M., R. Kazi, Q. Gan, J. Amin and L. P. Wollmuth (2016). A Molecular Determinant of Subtype-Specific Desensitization in Ionotropic Glutamate Receptors. *J Neurosci* **36**(9): 2617-2622.

Amin, J. B., C. L. Salussolia, K. Chan, M. C. Regan, J. Dai, H.-X. Zhou, H. Furukawa, M. E. Bowen and L. P. Wollmuth (2017). Divergent roles of a peripheral transmembrane segment in AMPA and NMDA receptors. *The Journal of General Physiology* **149**(6): 661-680.

Anis, N. A., S. C. Berry, N. R. Burton and D. Lodge (1983). The dissociative anaesthetics, ketamine and phencyclidine, selectively reduce excitation of central mammalian neurones by N-methyl-aspartate. *Br J Pharmacol* **79**(2): 565-575.

Arai, A. and G. Lynch (1992). Factors regulating the magnitude of long-term potentiation induced by theta pattern stimulation. *Brain Research* **598**(1): 173-184.

Armstrong, N., Y. Sun, G.-Q. Chen and E. Gouaux (1998). Structure of a glutamate-receptor ligand-binding core in complex with kainate. *Nature* **395**: 913.

Aroniadou-Anderjaska, V., V. I. Pidoplichko, T. H. Figueiredo and M. F. M. Braga (2018). Oscillatory Synchronous Inhibition in the Basolateral Amygdala and its Primary Dependence on NR2A-containing NMDA Receptors. *Neuroscience*.

Arunlakshana, O. and H. O. Schild (1959). Some quantitative uses of drug antagonists. *Br J Pharmacol Chemother* **14**(1): 48-58.

Ascher, P. and L. Nowak (1988). The role of divalent cations in the N-methyl-D-aspartate responses of mouse central neurones in culture. *J Physiol* **399**: 247-266.

Ataman, Z. A., L. Gakhar, B. R. Sorensen, J. W. Hell and M. A. Shea (2007). The NMDA Receptor NR1 C1 Region Bound to Calmodulin: Structural Insights into Functional Differences between Homologous Domains. *Structure* **15**(12): 1603-1617.

Auberson, Y. P., H. Allgeier, S. Bischoff, K. Lingenhoehl, R. Moretti and M. Schmutz (2002). 5-Phosphonomethylquinoxalinediones as competitive NMDA receptor antagonists with a

preference for the human 1A/2A, rather than 1A/2B receptor composition. *Bioorganic & Medicinal Chemistry Letters* **12**(7): 1099-1102.

Auerbach, A. and Y. Zhou (2005). Gating reaction mechanisms for NMDA receptor channels. *J Neurosci* **25**(35): 7914-7923.

Ault, B., R. H. Evans, A. A. Francis, D. J. Oakes and J. C. Watkins (1980). Selective depression of excitatory amino acid induced depolarizations by magnesium ions in isolated spinal cord preparations. *The Journal of Physiology* **307**(1): 413-428.

Awadalla, P., J. Gauthier, R. A. Myers, F. Casals, F. F. Hamdan, A. R. Griffing, M. Côté, E. Henrion, D. Spiegelman and J. Tarabeux (2010). Direct measure of the de novo mutation rate in autism and schizophrenia cohorts. *The American Journal of Human Genetics* **87**(3): 316-324.

Bachtiar, V. and C. J. Stagg (2014). The role of inhibition in human motor cortical plasticity. *Neuroscience* **278**: 93-104.

Banke, T. G. and S. F. Traynelis (2003). Activation of NR1/NR2B NMDA receptors. *Nat Neurosci* **6**(2): 144-152.

Barnard, E. A., P. Skolnick, R. W. Olsen, H. Mohler, W. Sieghart, G. Biggio, C. Braestrup, A. N. Bateson and S. Z. Langer (1998). International Union of Pharmacology. XV. Subtypes of γ-Aminobutyric Acid A Receptors: Classification on the Basis of Subunit Structure and Receptor Function. *Pharmacological Reviews* **50**(2): 291-314.

Benveniste, M., J. Clements, L. Vyklicky, Jr. and M. L. Mayer (1990). A kinetic analysis of the modulation of N-methyl-D-aspartic acid receptors by glycine in mouse cultured hippocampal neurones. *J Physiol* **428**: 333-357.

Bergeron, R., T. M. Meyer, J. T. Coyle and R. W. Greene (1998). Modulation of N-methyl-d-aspartate receptor function by glycine transport. *Proceedings of the National Academy of Sciences* **95**(26): 15730-15734.

Besnard, J., G. F. Ruda, V. Setola, K. Abecassis, R. M. Rodriguiz, X. P. Huang, S. Norval, M. F. Sassano, A. I. Shin, L. A. Webster, F. R. Simeons, L. Stojanovski, A. Prat, N. G. Seidah, D. B. Constam, G. R. Bickerton, K. D. Read, W. C. Wetsel, I. H. Gilbert, B. L. Roth and A. L. Hopkins (2012). Automated design of ligands to polypharmacological profiles. *Nature* **492**(7428): 215-220.

Bettini, E., A. Sava, C. Griffante, C. Carignani, A. Buson, A. M. Capelli, M. Negri, F. Andreetta, S. A. Senar-Sancho, L. Guiral and F. Cardullo (2010). Identification and characterization of novel NMDA receptor antagonists selective for NR2A- over NR2B-containing receptors. *J Pharmacol Exp Ther* **335**(3): 636-644.

Bhatt, J. M., A. Prakash, P. S. Suryavanshi and S. M. Dravid (2013). Effect of ifenprodil on GluN1/GluN2B N-methyl-D-aspartate receptor gating. *Mol Pharmacol* **83**(1): 9-21.

Biscoe, T. J., R. H. Evans, A. A. Francis, M. R. Martin, J. C. Watkins, J. Davies and A. Dray (1977). D-alpha-Aminoadipate as a selective antagonist of amino acid-induced and synaptic excitation of mammalian spinal neurones. *Nature* **270**(5639): 743-745.

Bliss, T. V. and G. L. Collingridge (1993). A synaptic model of memory: long-term potentiation in the hippocampus. *Nature* **361**(6407): 31-39.

Bliss, T. V. P. and T. Lømo (1973). Long-lasting potentiation of synaptic transmission in the dentate area of the anaesthetized rabbit following stimulation of the perforant path. *The Journal of Physiology* **232**(2): 331-356.

Bolhuis, J. J. and I. C. Reid (1992). EFFECTS OF INTRAVENTRICULAR INFUSION OF THE N-METHYL-D-ASPARTATE (NMDA) RECEPTOR ANTAGONIST AP5 ON SPATIAL MEMORY OF RATS IN A RADIAL ARM MAZE. *Behavioural Brain Research* **47**(2): 151-157.

Bolshakov, K. V., V. E. Gmiro, D. B. Tikhonov and L. G. Magazanik (2003). Determinants of trapping block of N-methyl-d-aspartate receptor channels. *Journal of Neurochemistry* **87**(1): 56-65.

Bordji, K., J. Becerril-Ortega, O. Nicole and A. Buisson (2010). Activation of Extrasynaptic, But Not Synaptic, NMDA Receptors Modifies Amyloid Precursor Protein Expression Pattern and Increases Amyloid-β Production. *The Journal of Neuroscience* **30**(47): 15927-15942.

Borlongan, C. V., J. Burns, N. Tajiri, C. E. Stahl, N. L. Weinbren, H. Shojo, P. R. Sanberg, D. F. Emerich, Y. Kaneko and H. R. van Loveren (2013). Epidemiological Survey-Based Formulae to Approximate Incidence and Prevalence of Neurological Disorders in the United States: a Meta-Analysis. *PLOS ONE* **8**(10): e78490.

Borovska, J., V. Vyklicky, E. Stastna, V. Kapras, B. Slavikova, M. Horak, H. Chodounska and L. Vyklicky, Jr. (2012). Access of inhibitory neurosteroids to the NMDA receptor. *Br J Pharmacol* **166**(3): 1069-1083.

Brickley, S. G., C. Misra, M. H. Mok, M. Mishina and S. G. Cull-Candy (2003). NR2B and NR2D subunits coassemble in cerebellar Golgi cells to form a distinct NMDA receptor subtype restricted to extrasynaptic sites. *J Neurosci* **23**(12): 4958-4966.

Brothwell, S. L., J. L. Barber, D. T. Monaghan, D. E. Jane, A. J. Gibb and S. Jones (2008). NR2B- and NR2D-containing synaptic NMDA receptors in developing rat substantia nigra pars compacta dopaminergic neurones. *J Physiol* **586**(3): 739-750.

Buard, I., S. J. Coultrap, R. K. Freund, Y.-S. Lee, M. L. Dell'Acqua, A. J. Silva and K. U. Bayer (2010). CaMKII "autonomy" is required for initiating but not for maintaining neuronal long-term information storage. *Journal of Neuroscience* **30**(24): 8214-8220.

Buchanan, K. L., J. L. Grindstaff and V. V. Pravosudov (2013). Condition dependence, developmental plasticity, and cognition: implications for ecology and evolution. *Trends in Ecology & Evolution* **28**(5): 290-296.

Buller, A. L. and D. T. Monaghan (1997). Pharmacological heterogeneity of NMDA receptors: characterization of NR1a/NR2D heteromers expressed in Xenopus oocytes. *Eur J Pharmacol* **320**(1): 87-94.

Burnashev, N., Z. Zhou, E. Neher and B. Sakmann (1995). Fractional calcium currents through recombinant GluR channels of the NMDA, AMPA and kainate receptor subtypes. *The Journal of Physiology* **485**(2): 403-418.

Cais, O., M. Sedlacek, M. Horak, I. Dittert and L. Vyklicky, Jr. (2008). Temperature dependence of NR1/NR2B NMDA receptor channels. *Neuroscience* **151**(2): 428-438.

Calimet, N., M. Simoes, J.-P. Changeux, M. Karplus, A. Taly and M. Cecchini (2013). A gating mechanism of pentameric ligand-gated ion channels. *Proceedings of the National Academy of Sciences of the United States of America* **110**(42): E3987-E3996.

Camargo, A., F. Azuaje, H. Wang and H. Zheng (2008). Permutation – based statistical tests for multiple hypotheses. *Source Code for Biology and Medicine* **3**: 15-15.

Carroll, R. C. and R. S. Zukin (2002). NMDA-receptor trafficking and targeting: implications for synaptic transmission and plasticity. *Trends in Neurosciences* **25**(11): 571-577.

Cauli, B., J. T. Porter, K. Tsuzuki, B. Lambolez, J. Rossier, B. Quenet and E. Audinat (2000). Classification of fusiform neocortical interneurons based on unsupervised clustering. *Proc Natl Acad Sci U S A* **97**(11): 6144-6149.

Chakrapani, S., J. F. Cordero-Morales, V. Jogini, A. C. Pan, D. M. Cortes, B. Roux and E. Perozo (2011). On The Structural Basis of Modal Gating Behavior in K(+) Channels. *Nature structural & molecular biology* **18**(1): 67-74.

Chamorro, Á., U. Dirnagl, X. Urra and A. M. Planas (2016). Neuroprotection in acute stroke: targeting excitotoxicity, oxidative and nitrosative stress, and inflammation. *The Lancet Neurology* **15**(8): 869-881.

Changeux, J.-P. and S. J. Edelstein (1998). Allosteric Receptors after 30 Years. *Neuron* **21**(5): 959-980.

Chazot, P. L. and F. A. Stephenson (1997). Molecular dissection of native mammalian forebrain NMDA receptors containing the NR1 C2 exon: direct demonstration of NMDA receptors comprising NR1, NR2A, and NR2B subunits within the same complex. *J Neurochem* **69**(5): 2138-2144.

Chen, B. S. and K. W. Roche (2007). Regulation of NMDA receptors by phosphorylation. *Neuropharmacology* **53**(3): 362-368.

Chen, H. S. and S. A. Lipton (2006). The chemical biology of clinically tolerated NMDA receptor antagonists. *J Neurochem* **97**(6): 1611-1626.

Chen, N., A. Moshaver and L. A. Raymond (1997). Differential sensitivity of recombinant N-methyl-D-aspartate receptor subtypes to zinc inhibition. *Mol Pharmacol* **51**(6): 1015-1023.

Chen, N. S., B. Li, T. H. Murphy and L. A. Raymond (2004). Site within N-methyl-D-aspartate receptor pore modulates channel Gating. *Molecular Pharmacology* **65**(1): 157-164.

Chen, P. E., M. T. Geballe, E. Katz, K. Erreger, M. R. Livesey, K. K. O'Toole, P. Le, C. J. Lee, J. P. Snyder, S. F. Traynelis and D. J. A. Wyllie (2008). Modulation of glycine potency in rat recombinant NMDA receptors containing chimeric NR2A/2D subunits expressed in Xenopus laevis oocytes. *The Journal of Physiology* **586**(1): 227-245.

Chen, W., C. Shieh, S. A. Swanger, A. Tankovic, M. Au, M. McGuire, M. Tagliati, J. M. Graham, S. Madan-Khetarpal, S. F. Traynelis, H. Yuan and T. M. Pierson (2017). GRIN1 mutation associated with intellectual disability alters NMDA receptor trafficking and function. *J Hum Genet* **62**(6): 589-597.

Chenard, B. L., J. Bordner, T. W. Butler, L. K. Chambers, M. A. Collins, D. L. De Costa, M. F. Ducat, M. L. Dumont, C. B. Fox, E. E. Mena and et al. (1995). (1S,2S)-1-(4-hydroxyphenyl)-2-(4-hydroxy-4-phenylpiperidino)-1-propanol: a potent new neuroprotectant which blocks N-methyl-D-aspartate responses. *J Med Chem* **38**(16): 3138-3145.

Chesler, M. (2003). Regulation and modulation of pH in the brain. *Physiol Rev* **83**(4): 1183-1221.

Choi, D. W. (1992). Excitotoxic cell death. *Journal of Neurobiology* **23**(9): 1261-1276.

Choi, D. W. and S. M. Rothman (1990). The Role of Glutamate Neurotoxicity in Hypoxic-Ischemic Neuronal Death. *Annual Review of Neuroscience* **13**(1): 171-182.

Choi, U. B., R. Kazi, N. Stenzoski, L. P. Wollmuth, V. N. Uversky and M. E. Bowen (2013). Modulating the intrinsic disorder in the cytoplasmic domain alters the biological activity of the N-methyl-D-aspartate-sensitive glutamate receptor. *J Biol Chem* **288**(31): 22506-22515.

Choi, Y. B. and S. A. Lipton (1999). Identification and mechanism of action of two histidine residues underlying high-affinity Zn2+ inhibition of the NMDA receptor. *Neuron* **23**(1): 171-180.

Christie, B. R., K. M. Franks, J. K. Seamans, K. Saga and T. J. Sejnowski (2000). Synaptic plasticity in morphologically identified CA1 stratum radiatum interneurons and giant projection cells. *Hippocampus* **10**(6): 673-683.

Christopoulos, A. (2002). Allosteric binding sites on cell-surface receptors: novel targets for drug discovery. *Nat Rev Drug Discov* **1**(3): 198-210.

Christopoulos, A. and T. Kenakin (2002). G Protein-Coupled Receptor Allosterism and Complexing. *Pharmacological Reviews* **54**(2): 323-374.

Ciabarra, A. M., J. M. Sullivan, L. G. Gahn, G. Pecht, S. Heinemann and K. A. Sevarino (1995). Cloning and characterization of chi-1: a developmentally regulated member of a novel class of the ionotropic glutamate receptor family. *J Neurosci* **15**(10): 6498-6508.

Clark, A. L. and F. Mitchelson (1976). THE INHIBITORY EFFECT OF GALLAMINE ON MUSCARINIC RECEPTORS. *British Journal of Pharmacology* **58**(3): 323-331.

Clark, G. D., D. B. Clifford and C. F. Zorumski (1990). The effect of agonist concentration, membrane voltage and calcium on N-methyl-D-aspartate receptor desensitization. *Neuroscience* **39**(3): 787-797.

Clarke, R. J. and J. W. Johnson (2006). NMDA Receptor NR2 Subunit Dependence of the Slow Component of Magnesium Unblock. *The Journal of Neuroscience* **26**(21): 5825-5834.

Cohen, S. M., R. W. Tsien, D. C. Goff and M. M. Halassa (2015). The impact of NMDA receptor hypofunction on GABAergic neurons in the pathophysiology of schizophrenia. *Schizophrenia research* **167**(1): 98-107.

Collingridge, G. L., J. T. Isaac and Y. T. Wang (2004). Receptor trafficking and synaptic plasticity. *Nat Rev Neurosci* **5**(12): 952-962.

Collingridge, G. L., S. J. Kehl and H. McLennan (1983). Excitatory amino acids in synaptic transmission in the Schaffer collateral-commissural pathway of the rat hippocampus. *The Journal of Physiology* **334**(1): 33-46.

Collingridge, G. L., A. Volianskis, N. Bannister, G. France, L. Hanna, M. Mercier, P. Tidball, G. Fang, M. W. Irvine, B. M. Costa, D. T. Monaghan, Z. A. Bortolotto, E. Molnar, D. Lodge and D. E. Jane (2013). The NMDA receptor as a target for cognitive enhancement. *Neuropharmacology* **64**: 13-26.

Colquhoun, D. (1998). Binding, gating, affinity and efficacy: the interpretation of structure-activity relationships for agonists and of the effects of mutating receptors. *Br J Pharmacol* **125**(5): 924-947.

Colquhoun, D. and A. G. Hawkes (1977). Relaxation and fluctuations of membrane currents that flow through drug-operated channels. *Proc R Soc Lond B Biol Sci* **199**(1135): 231-262.

Colquhoun, D. and A. G. Hawkes (1995). A Q-matrix cookbook: How to write only one program to calculate the single-channel and macroscopic predictions for any kinetic mechanism.

Colquhoun, D. and F. J. Sigworth (1995). Fitting and Statistical Analysis of Single-Channel Records. Single-Channel Recording. B. Sakmann and E. Neher. Boston, MA, Springer US**:** 483-587.

Cooper, D. R., D. M. Dolino, H. Jaurich, B. Shuang, S. Ramaswamy, C. E. Nurik, J. Chen, V. Jayaraman and C. F. Landes (2015). Conformational transitions in the glycine-bound GluN1 NMDA receptor LBD via single-molecule FRET. *Biophys J* **109**(1): 66-75.

Costa, B. M., M. W. Irvine, G. Fang, R. J. Eaves, M. B. Mayo-Martin, B. Laube, D. E. Jane and D. T. Monaghan (2012). Structure-activity relationships for allosteric NMDA receptor inhibitors based on 2-naphthoic acid. *Neuropharmacology* **62**(4): 1730-1736.

Costa, B. M., M. W. Irvine, G. Fang, R. J. Eaves, M. B. Mayo-Martin, D. A. Skifter, D. E. Jane and D. T. Monaghan (2010). A novel family of negative and positive allosteric modulators of NMDA receptors. *J Pharmacol Exp Ther* **335**(3): 614-621.

Cotman, C. W. and D. T. Monaghan (1988). Excitatory Amino Acid Neurotransmission: NMDA Receptors and Hebb-Type Synaptic Plasticity. *Annual Review of Neuroscience* **11**(1): 61-80.

Coyle, J. T. (2012). NMDA Receptor and Schizophrenia: A Brief History. *Schizophrenia Bulletin* **38**(5): 920-926.

Coyle, J. T., G. Tsai and D. Goff (2003). Converging evidence of NMDA receptor hypofunction in the pathophysiology of schizophrenia. *Ann N Y Acad Sci* **1003**: 318-327.

Cull-Candy, S. G. and M. M. Usowicz (1987). Multiple-conductance channels activated by excitatory amino acids in cerebellar neurons. *Nature* **325**: 525.

Curtis, D. R. and J. C. Watkins (1963). Acidic amino acids with strong excitatory actions on mammalian neurones. *J Physiol* **166**: 1-14.

Danysz, W., J. T. Wroblewski and E. Costa (1988). LEARNING IMPAIRMENT IN RATS BY N-METHYL-D-ASPARTATE RECEPTOR ANTAGONISTS. *Neuropharmacology* **27**(6): 653-656.

Davies, J. and J. C. Watkins (1979). Selective antagonism of amino acid-induced and synaptic excitation in the cat spinal cord. *J Physiol* **297**(0): 621-635.

De Lean, A., J. M. Stadel and R. J. Lefkowitz (1980). A ternary complex model explains the agonist-specific binding properties of the adenylate cyclase-coupled beta-adrenergic receptor. *Journal of Biological Chemistry* **255**(15): 7108-7117.

del Castillo, J. and B. Katz (1954). Quantal components of the end-plate potential. *The Journal of Physiology* **124**(3): 560-573.

del Castillo, J. and B. Katz (1957). Interaction at end-plate receptors between different choline derivatives. *Proc R Soc Lond B Biol Sci* **146**(924): 369-381.

Diamond, J. S. (2001). Neuronal Glutamate Transporters Limit Activation of NMDA Receptors by Neurotransmitter Spillover on CA1 Pyramidal Cells. *The Journal of Neuroscience* **21**(21): 8328-8338.

Dityatev, A., M. Schachner and P. Sonderegger (2010). The dual role of the extracellular matrix in synaptic plasticity and homeostasis. *Nature Reviews Neuroscience* **11**: 735.

Dolino, D. M., S. Chatterjee, D. M. MacLean, C. Flatebo, L. D. C. Bishop, S. A. Shaikh, C. F. Landes and V. Jayaraman (2017). The structure-energy landscape of NMDA receptor gating. *Nat Chem Biol* **13**(12): 1232-1238.

Dravid, S. M., K. Erreger, H. Yuan, K. Nicholson, P. Le, P. Lyuboslavsky, A. Almonte, E. Murray, C. Mosely, J. Barber, A. French, R. Balster, T. F. Murray and S. F. Traynelis (2007). Subunit-specific mechanisms and proton sensitivity of NMDA receptor channel block. *J Physiol* **581**(Pt 1): 107-128.

Dravid, S. M., A. Prakash and S. F. Traynelis (2008). Activation of recombinant NR1/NR2C NMDA receptors. *J Physiol* **586**(18): 4425-4439.

Dulla, C. G., D. A. Coulter and J. Ziburkus (2016). From Molecular Circuit Dysfunction to Disease:Case Studies in Epilepsy, Traumatic Brain Injury, and Alzheimer's Disease. *The Neuroscientist* **22**(3): 295-312.

Edman, S., S. McKay, L. J. MacDonald, M. Samadi, M. R. Livesey, G. E. Hardingham and D. J. A. Wyllie (2012). TCN 201 selectively blocks GluN2A-containing NMDARs in a GluN1 co-agonist dependent but non-competitive manner. *Neuropharmacology* **63**(3): 441-449.

Ehlers, M. D., E. T. Fung, R. J. O'Brien and R. L. Huganir (1998). Splice variant-specific interaction of the NMDA receptor subunit NR1 with neuronal intermediate filaments. *J Neurosci* **18**(2): 720-730.

Ehlers, M. D., S. Zhang, J. P. Bernhadt and R. L. Huganir (1996). Inactivation of NMDA receptors by direct interaction of calmodulin with the NR1 subunit. *Cell* **84**(5): 745-755.

Ehlert, F. J. (1988). Estimation of the affinities of allosteric ligands using radioligand binding and pharmacological null methods. *Molecular Pharmacology* **33**(2): 187-194.

Endele, S., G. Rosenberger, K. Geider, B. Popp, C. Tamer, I. Stefanova, M. Milh, F. Kortüm, A. Fritsch and F. K. Pientka (2010). Mutations in GRIN2A and GRIN2B encoding regulatory subunits of NMDA receptors cause variable neurodevelopmental phenotypes. *Nature genetics* **42**(11): 1021.

Erreger, K., S. M. Dravid, T. G. Banke, D. J. Wyllie and S. F. Traynelis (2005). Subunit-specific gating controls rat NR1/NR2A and NR1/NR2B NMDA channel kinetics and synaptic signalling profiles. *J Physiol* **563**(Pt 2): 345-358.

Erreger, K., M. T. Geballe, S. M. Dravid, J. P. Snyder, D. J. Wyllie and S. F. Traynelis (2005). Mechanism of partial agonism at NMDA receptors for a conformationally restricted glutamate analog. *Journal of Neuroscience* **25**(34): 7858-7866.

Erreger, K., M. T. Geballe, A. Kristensen, P. E. Chen, K. B. Hansen, C. J. Lee, H. Yuan, P. Le, P. N. Lyuboslavsky, N. Micale, L. Jørgensen, R. P. Clausen, D. J. A. Wyllie, J. P. Snyder and S. F. Traynelis (2007). Subunit-Specific Agonist Activity at NR2A-, NR2B-, NR2C-, and NR2D-Containing N-Methyl-d-aspartate Glutamate Receptors. *Molecular Pharmacology* **72**(4): 907-920.

Erreger, K. and S. F. Traynelis (2005). Allosteric interaction between zinc and glutamate binding domains on NR2A causes desensitization of NMDA receptors. *Journal of Physiology-London* **569**(2): 381-393.

Erreger, K. and S. F. Traynelis (2008). Zinc inhibition of rat NR1/NR2A N-methyl-D-aspartate receptors. *J Physiol* **586**(3): 763-778.

Evans, R. H., A. A. Francis, K. Hunt, D. J. Oakes and J. C. Watkins (1979). Antagonism of excitatory amino acid-induced responses and of synaptic excitation in the isolated spinal cord of the frog. *Br J Pharmacol* **67**(4): 591-603.

Evans, R. H., A. A. Francis, A. W. Jones, D. A. Smith and J. C. Watkins (1982). The effects of a series of omega-phosphonic alpha-carboxylic amino acids on electrically evoked and excitant amino acid-induced responses in isolated spinal cord preparations. *Br J Pharmacol* **75**(1): 65-75.

Evans, R. H., A. A. Francis and J. C. Watkins (1977). Selective antagonism by Mg2+ of amino acid-induced depolarization of spinal neurones. *Experientia* **33**(4): 489-491.

Evans, R. H., A. A. Francis and J. C. Watkins (1978). Mg2+-like selective antagonism of excitatory amino acid-induced responses by alpha, epsilon-diaminopimelic acid, D-alpha-aminoadipate and HA-966 in isolated spinal cord of frog and immature rat. *Brain Res* **148**(2): 536-542.

Eyo, U. B., A. Bispo, J. Liu, S. Sabu, R. Wu, V. L. DiBona, J. Zheng, M. Murugan, H. Zhang, Y. Tang and L.-J. Wu (2018). The GluN2A Subunit Regulates Neuronal NMDA receptor-Induced Microglia-Neuron Physical Interactions. *Scientific Reports* **8**(1): 828.

Feng, B., R. M. Morley, D. E. Jane and D. T. Monaghan (2005). The effect of competitive antagonist chain length on NMDA receptor subunit selectivity. *Neuropharmacology* **48**(3): 354-359.

Feng, B., H. W. Tse, D. A. Skifter, R. Morley, D. E. Jane and D. T. Monaghan (2004). Structure-activity analysis of a novel NR2C/NR2D-preferring NMDA receptor antagonist: 1-(phenanthrene-2-carbonyl) piperazine-2,3-dicarboxylic acid. *Br J Pharmacol* **141**(3): 508-516.

Fischer, G., V. Mutel, G. Trube, P. Malherbe, J. N. Kew, E. Mohacsi, M. P. Heitz and J. A. Kemp (1997). Ro 25-6981, a highly potent and selective blocker of N-methyl-D-aspartate receptors containing the NR2B subunit. Characterization in vitro. *J Pharmacol Exp Ther* **283**(3): 1285-1292.

Foster, A. C., J. Farnsworth, G. E. Lind, Y.-X. Li, J.-Y. Yang, V. Dang, M. Penjwini, V. Viswanath, U. Staubli and M. P. Kavanaugh (2016). D-Serine Is a Substrate for Neutral Amino Acid Transporters ASCT1/SLC1A4 and ASCT2/SLC1A5, and Is Transported by Both Subtypes in Rat Hippocampal Astrocyte Cultures. *PLoS ONE* **11**(6): e0156551.

Freund, T. F. and G. Buzsaki (1996). Interneurons of the hippocampus. *Hippocampus* **6**(4): 347-470.

Frizelle, P. A., P. E. Chen and D. J. Wyllie (2006). Equilibrium constants for (R)-[(S)-1-(4-bromo-phenyl)-ethylamino]-(2,3-dioxo-1,2,3,4-tetrahydroquino xalin-5-yl)-methyl]-phosphonic acid (NVP-AAM077) acting at recombinant NR1/NR2A and NR1/NR2B N-methyl-D-aspartate receptors: Implications for studies of synaptic transmission. *Molecular Pharmacology* **70**(3): 1022-1032.

Fromer, M., A. J. Pocklington, D. H. Kavanagh, H. J. Williams, S. Dwyer, P. Gormley, L. Georgieva, E. Rees, P. Palta and D. M. Ruderfer (2014). De novo mutations in schizophrenia implicate synaptic networks. *Nature* **506**(7487): 179.

Furukawa, H., S. K. Singh, R. Mancusso and E. Gouaux (2005). Subunit arrangement and function in NMDA receptors. *Nature* **438**(7065): 185-192.

Gaddum, J. H. (1937). The quantitative effects of antagonistic drugs. *J Physiol* **89**: 7-9.

Gardoni, F., A. Caputi, M. Cimino, L. Pastorino, F. Cattabeni and M. Di Luca (1998). Calcium/calmodulin-dependent protein kinase II is associated with NR2A/B subunits of NMDA receptor in postsynaptic densities. *J Neurochem* **71**(4): 1733-1741.

Ghosh, A. and M. Greenberg (1995). Calcium signaling in neurons: molecular mechanisms and cellular consequences. *Science* **268**(5208): 239-247.

Gibb, A. J. and D. Colquhoun (1992). Activation of N-methyl-D-aspartate receptors by L-glutamate in cells dissociated from adult rat hippocampus. *The Journal of Physiology* **456**: 143-179.

Gielen, M., A. Le Goff, D. Stroebel, J. W. Johnson, J. Neyton and P. Paoletti (2008). Structural rearrangements of NR1/NR2A NMDA receptors during allosteric inhibition. *Neuron* **57**(1): 80-93.

Gielen, M., B. Siegler Retchless, L. Mony, J. W. Johnson and P. Paoletti (2009). Mechanism of differential control of NMDA receptor activity by NR2 subunits. *Nature* **459**(7247): 703-707.

Giffard, R. G., H. Monyer, C. W. Christine and D. W. Choi (1990). Acidosis reduces NMDA receptor activation, glutamate neurotoxicity, and oxygen-glucose deprivation neuronal injury in cortical cultures. *Brain Res* **506**(2): 339-342.

Gilmour, G., S. Dix, L. Fellini, F. Gastambide, N. Plath, T. Steckler, J. Talpos and M. Tricklebank (2012). NMDA receptors, cognition and schizophrenia – Testing the validity of the NMDA receptor hypofunction hypothesis. *Neuropharmacology* **62**(3): 1401-1412.

Gladding, C. M. and L. A. Raymond (2011). Mechanisms underlying NMDA receptor synaptic/extrasynaptic distribution and function. *Molecular and Cellular Neuroscience* **48**(4): 308-320.

Glasgow, N. G. (2016). Mechanisms of NMDA receptor inhibition by memantine and ketamine. Doctoral Dissertation.

Goldman, D. E. (1943). POTENTIAL, IMPEDANCE, AND RECTIFICATION IN MEMBRANES. *The Journal of General Physiology* **27**(1): 37-60.

Golgi, C. (1873). Sulla struttura della sostanza grigia della cervello. *Gazz. Med. Ital. Lombardia.* **6**: 244–246.

Gonzalez, J., J. C. Jurado-Coronel, M. F. Ávila, A. Sabogal, F. Capani and G. E. Barreto (2015). NMDARs in neurological diseases: a potential therapeutic target. *International Journal of Neuroscience* **125**(5): 315-327.

Gooch, C. L., E. Pracht and A. R. Borenstein (2017). The burden of neurological disease in the United States: A summary report and call to action. *Annals of Neurology* **81**(4): 479-484.

Groc, L., M. Heine, S. L. Cousins, F. A. Stephenson, B. Lounis, L. Cognet and D. Choquet (2006). NMDA receptor surface mobility depends on NR2A-2B subunits. *Proc Natl Acad Sci U S A* **103**(49): 18769-18774.

Grover, L. M., E. Kim, J. D. Cooke and W. R. Holmes (2009). LTP in hippocampal area CA1 is induced by burst stimulation over a broad frequency range centered around delta. *Learning & Memory* **16**(1): 69-81.

Hackos, D. H. and J. E. Hanson (2017). Diverse modes of NMDA receptor positive allosteric modulation: Mechanisms and consequences. *Neuropharmacology* **112**(Pt A): 34-45.

Hackos, D. H., P. J. Lupardus, T. Grand, Y. Chen, T. M. Wang, P. Reynen, A. Gustafson, H. J. Wallweber, M. Volgraf, B. D. Sellers, J. B. Schwarz, P. Paoletti, M. Sheng, Q. Zhou and J. E. Hanson (2016). Positive Allosteric Modulators of GluN2A-Containing NMDARs with Distinct Modes of Action and Impacts on Circuit Function. *Neuron* **89**(5): 983-999.

Hage, T. A. and Z. M. Khaliq (2015). Tonic Firing Rate Controls Dendritic Ca(2+) Signaling and Synaptic Gain in Substantia Nigra Dopamine Neurons. *The Journal of Neuroscience* **35**(14): 5823-5836.

Hájos, N., T. F. Freund and I. Mody (2002). Comparison of single NMDA receptor channels recorded on hippocampal principal cells and oriens/alveus interneurons projecting to stratum lacunosum-moleculare (O-LM cells). *Acta Biologica Hungarica* **53**(4): 465-472.

Hall, D. A. (2000). Modeling the Functional Effects of Allosteric Modulators at Pharmacological Receptors: An Extension of the Two-State Model of Receptor Activation. *Molecular Pharmacology* **58**(6): 1412-1423.

Hallett, P. J. and D. G. Standaert (2004). Rationale for and use of NMDA receptor antagonists in Parkinson's disease. *Pharmacol Ther* **102**(2): 155-174.

Hamdan, F. F., J. Gauthier, Y. Araki, D.-T. Lin, Y. Yoshizawa, K. Higashi, A.-R. Park, D. Spiegelman, S. Dobrzeniecka and A. Piton (2011). Excess of de novo deleterious mutations in genes associated with glutamatergic systems in nonsyndromic intellectual disability. *The American Journal of Human Genetics* **88**(3): 306-316.

Hansen, K. B., K. K. Ogden and S. F. Traynelis (2012). Subunit-selective allosteric inhibition of glycine binding to NMDA receptors. *J Neurosci* **32**(18): 6197-6208.

Hansen, Kasper B., Kevin K. Ogden, H. Yuan and Stephen F. Traynelis (2014). Distinct Functional and Pharmacological Properties of Triheteromeric GluN1/GluN2A/GluN2B NMDA Receptors. *Neuron* **81**(5): 1084-1096.

Hansen, K. B., N. Tajima, R. Risgaard, R. E. Perszyk, L. Jorgensen, K. M. Vance, K. K. Ogden, R. P. Clausen, H. Furukawa and S. F. Traynelis (2013). Structural Determinants of Agonist Efficacy at the Glutamate Binding Site of NMDA Receptors. *Molecular Pharmacology*.

Hansen, K. B. and S. F. Traynelis (2011). Structural and Mechanistic Determinants of a Novel Site for Noncompetitive Inhibition of GluN2D-Containing NMDA Receptors. *The Journal of Neuroscience* **31**(10): 3650-3661.

Hao, J. and T. G. Oertner (2012). Depolarization gates spine calcium transients and spike-timing-dependent potentiation. *Current Opinion in Neurobiology* **22**(3): 509-515.

Hardingham, G. E. and H. Bading (2010). Synaptic versus extrasynaptic NMDA receptor signalling: implications for neurodegenerative disorders. *Nat Rev Neurosci* **11**(10): 682-696.

Hardingham, G. E., Y. Fukunaga and H. Bading (2002). Extrasynaptic NMDARs oppose synaptic NMDARs by triggering CREB shut-off and cell death pathways. *Nature Neuroscience* **5**: 405.

Harris, A. Z. and D. L. Pettit (2007). Extrasynaptic and synaptic NMDA receptors form stable and uniform pools in rat hippocampal slices. *The Journal of Physiology* **584**(2): 509-519.

Harris, A. Z. and D. L. Pettit (2008). Recruiting Extrasynaptic NMDA Receptors Augments Synaptic Signaling. *Journal of Neurophysiology* **99**(2): 524-533.

Hashimoto, K., B. Malchow, P. Falkai and A. Schmitt (2013). Glutamate modulators as potential therapeutic drugs in schizophrenia and affective disorders. *Eur Arch Psychiatry Clin Neurosci* **263**(5): 367-377.

Hatton, C. J. and P. Paoletti (2005). Modulation of triheteromeric NMDA receptors by N-terminal domain ligands. *Neuron* **46**(2): 261-274.

Haydon, P. G. and G. Carmignoto (2006). Astrocyte control of synaptic transmission and neurovascular coupling. *Physiol Rev* **86**(3): 1009-1031.

Hebb, D. O. (1949). The organization of behavior; a neuropsychological theory. New York,, Wiley.

Hess, S. D., L. P. Daggett, J. Crona, C. Deal, C. C. Lu, A. Urrutia, L. Chavez-Noriega, S. B. Ellis, E. C. Johnson and G. Velicelebi (1996). Cloning and functional characterization of human heteromeric N-methyl-D-aspartate receptors. *J Pharmacol Exp Ther* **278**(2): 808-816.

Hess, S. D., L. P. Daggett, C. Deal, C. C. Lu, E. C. Johnson and G. Velicelebi (1998). Functional characterization of human N-methyl-D-aspartate subtype 1A/2D receptors. *J Neurochem* **70**(3): 1269-1279.

Hildebrand, M. E., G. M. Pitcher, E. K. Harding, H. Li, S. Beggs and M. W. Salter (2014). GluN2B and GluN2D NMDARs dominate synaptic responses in the adult spinal cord. *Scientific Reports* **4**: 4094.

Hodgkin, A. L. and A. F. Huxley (1952). A quantitative description of membrane current and its application to conduction and excitation in nerve. *The Journal of Physiology* **117**(4): 500-544.

Hollmann, M., J. Boulter, C. Maron, L. Beasley, J. Sullivan, G. Pecht and S. Heinemann (1993). Zinc potentiates agonist-induced currents at certain splice variants of the NMDA receptor. *Neuron* **10**(5): 943-954.

Horak, M., K. Vlcek, H. Chodounska and L. Vyklicky, Jr. (2006). Subtype-dependence of N-methyl-D-aspartate receptor modulation by pregnenolone sulfate. *Neuroscience* **137**(1): 93-102.

Horak, M., K. Vlcek, M. Petrovic, H. Chodounska and L. Vyklicky, Jr. (2004). Molecular mechanism of pregnenolone sulfate action at NR1/NR2B receptors. *J Neurosci* **24**(46): 10318-10325.

Hu, B. and F. Zheng (2005). Molecular determinants of glycine-independent desensitization of NR1/NR2A receptors. *J Pharmacol Exp Ther* **313**(2): 563-569.

Huettner, J. E. and B. P. Bean (1988). Block of N-methyl-D-aspartate-activated current by the anticonvulsant MK-801: selective binding to open channels. *Proceedings of the National Academy of Sciences of the United States of America* **85**(4): 1307-1311.

Iacobucci, G. J., O. Visnjevac, L. Pourafkari and N. D. Nader (2017). Ketamine: An Update on Cellular and Subcellular Mechanisms with Implications for Clinical Practice. *Pain Physician* **20**(2): E285-e301.

Ikeda, K., M. Nagasawa, H. Mori, K. Araki, K. Sakimura, M. Watanabe, Y. Inoue and M. Mishina (1992). Cloning and expression of the epsilon 4 subunit of the NMDA receptor channel. *FEBS Lett* **313**(1): 34-38.

Ikonomidou, C. and L. Turski (2002). Why did NMDA receptor antagonists fail clinical trials for stroke and traumatic brain injury? *Lancet Neurol* **1**(6): 383-386.

Ishii, T., K. Moriyoshi, H. Sugihara, K. Sakurada, H. Kadotani, M. Yokoi, C. Akazawa, R. Shigemoto, N. Mizuno, M. Masu and et al. (1993). Molecular characterization of the family of the N-methyl-D-aspartate receptor subunits. *J Biol Chem* **268**(4): 2836-2843.

Jackson, Alexander C. and Roger A. Nicoll (2011). The Expanding Social Network of Ionotropic Glutamate Receptors: TARPs and Other Transmembrane Auxiliary Subunits. *Neuron* **70**(2): 178-199.

Jahr, C. E. and C. F. Stevens (1987). Glutamate activates multiple single channel conductances in hippocampal neurons. *Nature* **325**: 522.

Javitt, D. C. and S. R. Zukin (1991). Recent advances in the phencyclidine model of schizophrenia. *Am J Psychiatry* **148**(10): 1301-1308.

Jin, R., T. G. Banke, M. L. Mayer, S. F. Traynelis and E. Gouaux (2003). Structural basis for partial agonist action at ionotropic glutamate receptors. *Nat Neurosci* **6**(8): 803-810.

Johnson, J. W. and P. Ascher (1987). Glycine potentiates the NMDA response in cultured mouse brain neurons. *Nature* **325**(6104): 529-531.

Johnson, J. W. and S. E. Kotermanski (2006). Mechanism of action of memantine. *Current Opinion in Pharmacology* **6**(1): 61-67.

Jones, S. and A. J. Gibb (2005). Functional NR2B- and NR2D-containing NMDA receptor channels in rat substantia nigra dopaminergic neurones. *J Physiol* **569**(Pt 1): 209-221.

Kaiser, T. M., S. A. Kell, H. Kusumoto, G. Shaulsky, S. Bhattacharya, M. P. Epplin, K. L. Strong, E. J. Miller, B. D. Cox, D. S. Menaldino, D. C. Liotta, S. F. Traynelis and P. B. Burger (2017). The bioactive protein-ligand conformation of GluN2C-selective positive allosteric modulators bound to the NMDA receptor. *Mol Pharmacol*.

Kalia, L. V., S. K. Kalia and A. E. Lang (2015). Disease-modifying strategies for Parkinson's disease. *Movement Disorders* **30**(11): 1442-1450.

Kalia, L. V., S. K. Kalia and M. W. Salter (2008). NMDA receptors in clinical neurology: excitatory times ahead. *The Lancet Neurology* **7**(8): 742-755.

Karakas, E. and H. Furukawa (2014). Crystal structure of a heterotetrameric NMDA receptor ion channel. *Science* **344**(6187): 992-997.

Karakas, E., N. Simorowski and H. Furukawa (2009). Structure of the zinc-bound amino-terminal domain of the NMDA receptor NR2B subunit. *EMBO J* **28**(24): 3910-3920.

Karakas, E., N. Simorowski and H. Furukawa (2011). Subunit arrangement and phenylethanolamine binding in GluN1/GluN2B NMDA receptors. *Nature* **475**(7355): 249-U170.

Kari, A. J., P. J. Conn and M. N. Colleen (2009). Glutamate Receptors as Therapeutic Targets for Parkinsons Disease. *CNS & Neurological Disorders - Drug Targets* **8**(6): 475-491.

Karlin, A. (1967). On the application of "a plausible model" of allosteric proteins to the receptor for acetylcholine. *Journal of Theoretical Biology* **16**(2): 306-320.

Kashiwagi, K., J. Fukuchi, J. Chao, K. Igarashi and K. Williams (1996). An aspartate residue in the extracellular loop of the N-methyl-D-aspartate receptor controls sensitivity to spermine and protons. *Mol Pharmacol* **49**(6): 1131-1141.

Kashiwagi, K., A. J. Pahk, T. Masuko, K. Igarashi and K. Williams (1997). Block and modulation of N-methyl-D-aspartate receptors by polyamines and protons: role of amino acid residues in the transmembrane and pore-forming regions of NR1 and NR2 subunits. *Mol Pharmacol* **52**(4): 701-713.

Katz, B. and R. Miledi (1972). The statistical nature of the acetylcholine potential and its molecular components. *The Journal of Physiology* **224**(3): 665-699.

Katzman, B. M., R. E. Perszyk, H. Yuan, Y. A. Tahirovic, A. E. Sotimehin, S. F. Traynelis and D. C. Liotta (2015). A novel class of negative allosteric modulators of NMDA receptor function. *Bioorganic & Medicinal Chemistry Letters* **25**(23): 5583-5588.

Kenakin, T. (2016). The mass action equation in pharmacology. *British Journal of Clinical Pharmacology* **81**(1): 41-51.

Kew, J. N., G. Trube and J. A. Kemp (1996). A novel mechanism of activity-dependent NMDA receptor antagonism describes the effect of ifenprodil in rat cultured cortical neurones. *J Physiol* **497 (Pt 3)**: 761-772.

Kew, J. N. C. and J. A. Kemp (1998). An allosteric interaction between the NMDA receptor polyamine and ifenprodil sites in rat cultured cortical neurones. *The Journal of Physiology* **512**(1): 17-28.

Khatri, A., P. B. Burger, S. A. Swanger, K. B. Hansen, S. Zimmerman, E. Karakas, D. C. Liotta, H. Furukawa, J. P. Snyder and S. F. Traynelis (2014). Structural Determinants and Mechanism of Action of a GluN2C-selective NMDA Receptor Positive Allosteric Modulator. *Molecular Pharmacology* **86**(5): 548-560.

Klausberger, T. and P. Somogyi (2008). Neuronal Diversity and Temporal Dynamics: The Unity of Hippocampal Circuit Operations. *Science* **321**(5885): 53-57.

Kleckner, N. W. and R. Dingledine (1988). Requirement for glycine in activation of NMDA-receptors expressed in Xenopus oocytes. *Science* **241**(4867): 835-837.

Kohr, G. and P. H. Seeburg (1996). Subtype-specific regulation of recombinant NMDA receptor-channels by protein tyrosine kinases of the src family. *J Physiol* **492 (Pt 2)**: 445-452.

Koleske, A. J. (2013). Molecular mechanisms of dendrite stability. *Nature Reviews Neuroscience* **14**: 536.

Korinek, M., V. Vyklicky, J. Borovska, K. Lichnerova, M. Kaniakova, B. Krausova, J. Krusek, A. Balik, T. Smejkalova, M. Horak and L. Vyklicky (2015). Cholesterol modulates open probability and desensitization of NMDA receptors. *J Physiol* **593**(10): 2279-2293.

Kornau, H., L. Schenker, M. Kennedy and P. Seeburg (1995). Domain interaction between NMDA receptor subunits and the postsynaptic density protein PSD-95. *Science* **269**(5231): 1737-1740.

Kostandy, B. B. (2012). The role of glutamate in neuronal ischemic injury: the role of spark in fire. *Neurol Sci* **33**(2): 223-237.

Kostenis, E. and K. Mohr (1996). Kostenis and Mohr reply. *Trends in Pharmacological Sciences* **17**(12): 443-444.

Kotaleski, J. H. and K. T. Blackwell (2010). Modelling the molecular mechanisms of synaptic plasticity using systems biology approaches. *Nature Reviews Neuroscience* **11**: 239.

Kotermanski, S. E. and J. W. Johnson (2009). Mg2+ imparts NMDA receptor subtype selectivity to the Alzheimer's drug memantine. *J Neurosci* **29**(9): 2774-2779.

Krupp, J. J., B. Vissel, S. F. Heinemann and G. L. Westbrook (1996). Calcium-dependent inactivation of recombinant N-methyl-D-aspartate receptors is NR2 subunit specific. *Molecular Pharmacology* **50**(6): 1680-1688.

Krupp, J. J., B. Vissel, C. G. Thomas, S. F. Heinemann and G. L. Westbrook (1999). Interactions of calmodulin and alpha-actinin with the NR1 subunit modulate Ca2+-dependent inactivation of NMDA receptors. *J Neurosci* **19**(4): 1165-1178.

Krystal, J. H., L. P. Karper, J. P. Seibyl and et al. (1994). Subanesthetic effects of the noncompetitive nmda antagonist, ketamine, in humans: Psychotomimetic, perceptual, cognitive, and neuroendocrine responses. *Archives of General Psychiatry* **51**(3): 199-214.

Kullmann, D. M. and K. P. Lamsa (2007). Long-term synaptic plasticity in hippocampal interneurons. *Nat Rev Neurosci* **8**(9): 687-699.

Kuner, T. and R. Schoepfer (1996). Multiple Structural Elements Determine Subunit Specificity of Mg^{2+} Block in NMDA Receptor Channels. *The Journal of Neuroscience* **16**(11): 3549-3558.

Kussius, C. L. and G. K. Popescu (2009). Kinetic basis of partial agonism at NMDA receptors. *Nat Neurosci* **12**(9): 1114-1120.

Kutsuwada, T., N. Kashiwabuchi, H. Mori, K. Sakimura, E. Kushiya, K. Araki, H. Meguro, H. Masaki, T. Kumanishi, M. Arakawa and et al. (1992). Molecular diversity of the NMDA receptor channel. *Nature* **358**(6381): 36-41.

Lacaille, J. C., A. L. Mueller, D. D. Kunkel and P. A. Schwartzkroin (1987). Local circuit interactions between oriens/alveus interneurons and CA1 pyramidal cells in hippocampal slices: electrophysiology and morphology. *J Neurosci* **7**(7): 1979-1993.

Lai, T. W., S. Zhang and Y. T. Wang (2014). Excitotoxicity and stroke: identifying novel targets for neuroprotection. *Prog Neurobiol* **115**: 157-188.

Landwehrmeyer, G., D. Standaert, C. Testa, J. Penney and A. Young (1995). NMDA receptor subunit mRNA expression by projection neurons and interneurons in rat striatum. *The Journal of Neuroscience* **15**(7): 5297-5307.

Larson, J. and E. Munkácsy (2015). Theta-burst LTP. *Brain Research* **1621**: 38-50.

Lau, C. G. and R. S. Zukin (2007). NMDA receptor trafficking in synaptic plasticity and neuropsychiatric disorders. *Nature Reviews Neuroscience* **8**: 413.

Laube, B., H. Hirai, M. Sturgess, H. Betz and J. Kuhse (1997). Molecular determinants of agonist discrimination by NMDA receptor subunits: analysis of the glutamate binding site on the NR2B subunit. *Neuron* **18**(3): 493-503.

Laube, B., J. Kuhse and H. Betz (1998). Evidence for a tetrameric structure of recombinant NMDA receptors. *J Neurosci* **18**(8): 2954-2961.

Laurie, D. and P. Seeburg (1994). Regional and developmental heterogeneity in splicing of the rat brain NMDAR1 mRNA. *The Journal of Neuroscience* **14**(5): 3180-3194.

Le Duigou, C., J. Simonnet, M. T. Teleñczuk, D. Fricker and R. Miles (2013). Recurrent synapses and circuits in the CA3 region of the hippocampus: an associative network. *Frontiers in Cellular Neuroscience* **7**: 262.

Lee, C. H., W. Lu, J. C. Michel, A. Goehring, J. Du, X. Song and E. Gouaux (2014). NMDA receptor structures reveal subunit arrangement and pore architecture. *Nature* **511**(7508): 191-197.

Leff, P. (1995). The two-state model of receptor activation. *Trends in Pharmacological Sciences* **16**(3): 89-97.

Legendre, P., C. Rosenmund and G. L. Westbrook (1993). Inactivation of NMDA channels in cultured hippocampal neurons by intracellular calcium. *J Neurosci* **13**(2): 674-684.

Lei, N., J. E. Mellem, P. J. Brockie, D. M. Madsen and A. V. Maricq (2017). NRAP-1 Is a Presynaptically Released NMDA Receptor Auxiliary Protein that Modifies Synaptic Strength. *Neuron* **96**(6): 1303-1316.e1306.

Leonard, A. S., K.-U. Bayer, M. A. Merrill, I. A. Lim, M. A. Shea, H. Schulman and J. W. Hell (2002). Regulation of Calcium/Calmodulin-dependent Protein Kinase II Docking toN-Methyl-d-aspartate Receptors by Calcium/Calmodulin and α-Actinin. *Journal of Biological Chemistry* **277**(50): 48441-48448.

Leonard, A. S., I. A. Lim, D. E. Hemsworth, M. C. Horne and J. W. Hell (1999). Calcium/calmodulin-dependent protein kinase II is associated with the N-methyl-d-aspartate receptor. *Proceedings of the National Academy of Sciences* **96**(6): 3239-3244.

Lester, R. and C. Jahr (1992). NMDA channel behavior depends on agonist affinity. *The Journal of Neuroscience* **12**(2): 635-643.

Lester, R. A. J., J. D. Clements, G. L. Westbrook and C. E. Jahr (1990). Channel kinetics determine the time course of NMDA receptor-mediated synaptic currents. *Nature* **346**(6284): 565-567.

Lester, R. A. J., G. Tong and C. E. Jahr (1993). Interactions between the Glycine and Glutamate Binding-Sites of the NMDA Receptor. *Journal of Neuroscience* **13**(3): 1088-1096.

Lind, G. E., T. C. Mou, L. Tamborini, M. G. Pomper, C. De Micheli, P. Conti, A. Pinto and K. B. Hansen (2017). Structural basis of subunit selectivity for competitive NMDA receptor antagonists with preference for GluN2A over GluN2B subunits. *Proc Natl Acad Sci U S A* **114**(33): E6942-E6951.

Lindsley, C. W., K. A. Emmitte, C. R. Hopkins, T. M. Bridges, K. J. Gregory, C. M. Niswender and P. J. Conn (2016). Practical Strategies and Concepts in GPCR Allosteric Modulator Discovery: Recent Advances with Metabotropic Glutamate Receptors. *Chemical Reviews* **116**(11): 6707-6741.

Lipton, S. A. (2006). Paradigm shift in neuroprotection by NMDA receptor blockade: Memantine and beyond. *Nature Reviews Drug Discovery* **5**: 160.

Lipton, S. A. (2007). Pathologically-activated therapeutics for neuroprotection: mechanism of NMDA receptor block by memantine and S-nitrosylation. *Curr Drug Targets* **8**(5): 621-632.

Lipton, S. A. and P. A. Rosenberg (1994). Excitatory Amino Acids as a Final Common Pathway for Neurologic Disorders. *New England Journal of Medicine* **330**(9): 613-622.

Lisman, J., R. Yasuda and S. Raghavachari (2012). Mechanisms of CaMKII action in long-term potentiation. *Nat Rev Neurosci* **13**(3): 169-182.

Lisman, J. E., J. T. Coyle, R. W. Green, D. C. Javitt, F. M. Benes, S. Heckers and A. A. Grace (2008). Circuit-based framework for understanding neurotransmitter and risk gene interactions in schizophrenia. *Trends in Neurosciences* **31**(5): 234-242.

Liu, D.-d., Q. Yang and S.-t. Li (2013). Activation of extrasynaptic NMDA receptors induces LTD in rat hippocampal CA1 neurons. *Brain Research Bulletin* **93**: 10-16.

Liu, X.-B., K. D. Murray and E. G. Jones (2004). Switching of NMDA Receptor 2A and 2B Subunits at Thalamic and Cortical Synapses during Early Postnatal Development. *The Journal of Neuroscience* **24**(40): 8885-8895.

Low, C.-M. and K. S.-L. Wee (2010). New Insights into the Not-So-New NR3 Subunits of N-methyl-d-aspartate Receptor: Localization, Structure, and Function. *Molecular Pharmacology* **78**(1): 1-11.

Low, C. M., P. Lyuboslavsky, A. French, P. Le, K. Wyatte, W. H. Thiel, E. M. Marchan, K. Igarashi, K. Kashiwagi, K. Gernert, K. Williams, S. F. Traynelis and F. Zheng (2003). Molecular determinants of proton-sensitive N-methyl-D-aspartate receptor gating. *Mol Pharmacol* **63**(6): 1212-1222.

Low, C. M., F. Zheng, P. Lyuboslavsky and S. F. Traynelis (2000). Molecular determinants of coordinated proton and zinc inhibition of N-methyl-D-aspartate NR1/NR2A receptors. *Proc Natl Acad Sci U S A* **97**(20): 11062-11067.

Lu, W. and M. Constantine-Paton (2004). Eye Opening Rapidly Induces Synaptic Potentiation and Refinement. *Neuron* **43**(2): 237-249.

Lüllmann, H., F. K. Ohnesorge, G. C. Schauwecker and O. Wassermann (1969). Inhibition of the actions of carbachol and DFP on guinea pig isolated atria by alkane-bis-ammonium compounds. *European Journal of Pharmacology* **6**(3): 241-247.

Luo, J., Y. Wang, R. P. Yasuda, A. W. Dunah and B. B. Wolfe (1997). The majority of N-methyl-D-aspartate receptor complexes in adult rat cerebral cortex contain at least three different subunits (NR1/NR2A/NR2B). *Mol Pharmacol* **51**(1): 79-86.

Lussier, M. P., A. Sanz-Clemente and K. W. Roche (2015). Dynamic Regulation of NMDA and AMPA Receptors by Posttranslational Modifications. *Journal of Biological Chemistry*.

MacDermott, A. B., M. L. Mayer, G. L. Westbrook, S. J. Smith and J. L. Barker (1986). NMDA-receptor activation increases cytoplasmic calcium concentration in cultured spinal cord neurones. *Nature* **321**(6069): 519-522.

Mackie, G. O. (1990). The Elementary Nervous System Revisited1. *American Zoologist* **30**(4): 907-920.

Macrez, R., P. K. Stys, D. Vivien, S. A. Lipton and F. Docagne (2016). Mechanisms of glutamate toxicity in multiple sclerosis: biomarker and therapeutic opportunities. *The Lancet Neurology* **15**(10): 1089-1102.

Madden, D. R. (2002). The structure and function of glutamate receptor ion channels. *Nature Reviews Neuroscience* **3**: 91.

Magee, J. C. (2000). Dendritic integration of excitatory synaptic input. *Nature Reviews Neuroscience* **1**: 181.

Maki, B. A., T. K. Aman, S. A. Amico-Ruvio, C. L. Kussius and G. K. Popescu (2012). C-terminal domains of N-methyl-D-aspartic acid receptor modulate unitary channel conductance and gating. *J Biol Chem* **287**(43): 36071-36080.

Malayev, A., T. T. Gibbs and D. H. Farb (2002). Inhibition of the NMDA response by pregnenolone sulphate reveals subtype selective modulation of NMDA receptors by sulphated steroids. *Br J Pharmacol* **135**(4): 901-909.

Malenka, R. C. and R. A. Nicoll (1999). Long-term potentiation--a decade of progress? *Science* **285**(5435): 1870-1874.

Mangialasche, F., A. Solomon, B. Winblad, P. Mecocci and M. Kivipelto (2010). Alzheimer's disease: clinical trials and drug development. *The Lancet Neurology* **9**(7): 702-716.

Marambaud, P., U. Dreses-Werringloer and V. Vingtdeux (2009). Calcium signaling in neurodegeneration. *Molecular Neurodegeneration* **4**(1): 20.

Martin, S. J., P. D. Grimwood and R. G. M. Morris (2000). Synaptic Plasticity and Memory: An Evaluation of the Hypothesis. *Annual Review of Neuroscience* **23**(1): 649-711.

Masuko, T., K. Kashiwagi, T. Kuno, N. D. Nguyen, A. J. Pahk, J. Fukuchi, K. Igarashi and K. Williams (1999). A regulatory domain (R1-R2) in the amino terminus of the N-methyl-D-aspartate receptor: effects of spermine, protons, and ifenprodil, and structural similarity to bacterial leucine/isoleucine/valine binding protein. *Mol Pharmacol* **55**(6): 957-969.

Masuko, T., T. Kuno, K. Kashiwagi, T. Kusama, K. Williams and K. Igarashi (1999). Stimulatory and Inhibitory Properties of Aminoglycoside Antibiotics at N-Methyl-d-Aspartate Receptor. *Journal of Pharmacology and Experimental Therapeutics* **290**(3): 1026-1033.

Matta, J. A., K. A. Pelkey, M. T. Craig, R. Chittajallu, B. W. Jeffries and C. J. McBain (2013). Developmental origin dictates interneuron AMPA and NMDA receptor subunit composition and plasticity. *Nat Neurosci* **16**(8): 1032-1041.

Mayer, M. L., L. Vyklicky, Jr. and J. Clements (1989). Regulation of NMDA receptor desensitization in mouse hippocampal neurons by glycine. *Nature* **338**(6214): 425-427.

Mayer, M. L. and G. L. Westbrook (1987). Permeation and block of N-methyl-D-aspartic acid receptor channels by divalent cations in mouse cultured central neurones. *J Physiol* **394**: 501-527.

Mayer, M. L., G. L. Westbrook and P. B. Guthrie (1984). Voltage-dependent block by Mg2+ of NMDA responses in spinal cord neurones. *Nature* **309**: 261.

McBain, C. J. and R. Dingledine (1993). Heterogeneity of synaptic glutamate receptors on CA3 stratum radiatum interneurones of rat hippocampus. *The Journal of Physiology* **462**(1): 373-392.

McKay, S., N. H. Griffiths, P. A. Butters, E. B. Thubron, G. E. Hardingham and D. J. A. Wyllie (2012). Direct pharmacological monitoring of the developmental switch in NMDA receptor subunit composition using TCN 213, a GluN2A-selective, glycine-dependent antagonist. *British Journal of Pharmacology* **166**(3): 924-937.

McLennan, H. and D. Lodge (1979). The antagonism of amino acid-induced excitation of spinal neurones in the cat. *Brain Res* **169**(1): 83-90.

Medina, I., N. Filippova, G. Charton, S. Rougeole, Y. Ben-Ari, M. Khrestchatisky and P. Bregestovski (1995). Calcium-dependent inactivation of heteromeric NMDA receptor-channels expressed in human embryonic kidney cells. *J Physiol* **482 (Pt 3)**: 567-573.

Meguro, H., H. Mori, K. Araki, E. Kushiya, T. Kutsuwada, M. Yamazaki, T. Kumanishi, M. Arakawa, K. Sakimura and M. Mishina (1992). Functional characterization of a heteromeric NMDA receptor channel expressed from cloned cDNAs. *Nature* **357**(6373): 70-74.

Monaghan, D. T., M. W. Irvine, B. M. Costa, G. Fang and D. E. Jane (2012). Pharmacological modulation of NMDA receptor activity and the advent of negative and positive allosteric modulators. *Neurochemistry International* **61**(4): 581-592.

Monod, J., J. P. Changeux and F. Jacob (1963). Allosteric proteins and cellular control systems. *J Mol Biol* **6**: 306-329.

Monod, J. and F. Jacob (1961). General conclusions: teleonomic mechanisms in cellular metabolism, growth, and differentiation. Cold Spring Harbor symposia on quantitative biology, Cold Spring Harbor Laboratory Press.

Monod, J., J. Wyman and J.-P. Changeux (1965). On the nature of allosteric transitions: a plausible model. *Journal of Molecular Biology* **12**: 88-118.

Mony, L., S. Zhu, S. Carvalho and P. Paoletti (2011). Molecular basis of positive allosteric modulation of GluN2B NMDA receptors by polyamines. *EMBO J* **30**(15): 3134-3146.

Monyer, H., N. Burnashev, D. J. Laurie, B. Sakmann and P. H. Seeburg (1994). Developmental and regional expression in the rat brain and functional properties of four NMDA receptors. *Neuron* **12**(3): 529-540.

Monyer, H., R. Sprengel, R. Schoepfer, A. Herb, M. Higuchi, H. Lomeli, N. Burnashev, B. Sakmann and P. H. Seeburg (1992). Heteromeric NMDA receptors: molecular and functional distinction of subtypes. *Science* **256**(5060): 1217-1221.

Moriyoshi, K., M. Masu, T. Ishii, R. Shigemoto, N. Mizuno and S. Nakanishi (1991). Molecular cloning and characterization of the rat NMDA receptor. *Nature* **354**(6348): 31-37.

Morley, R. M., H. W. Tse, B. Feng, J. C. Miller, D. T. Monaghan and D. E. Jane (2005). Synthesis and pharmacology of N1-substituted piperazine-2,3-dicarboxylic acid derivatives acting as NMDA receptor antagonists. *Journal of Medicinal Chemistry* **48**(7): 2627-2637.

Morris, R. G. M. (1989). SYNAPTIC PLASTICITY AND LEARNING - SELECTIVE IMPAIRMENT OF LEARNING IN RATS AND BLOCKADE OF LONG-TERM POTENTIATION INVIVO BY THE N-METHYL-D-ASPARTATE RECEPTOR ANTAGONIST AP5. *Journal of Neuroscience* **9**(9): 3040-3057.

Morris, R. G. M. (2013). NMDA receptors and memory encoding. *Neuropharmacology* **74**: 32-40.

Morris, R. G. M., E. Anderson, G. S. Lynch and M. Baudry (1986). SELECTIVE IMPAIRMENT OF LEARNING AND BLOCKADE OF LONG-TERM POTENTIATION BY AN N-METHYL-D-ASPARTATE RECEPTOR ANTAGONIST, AP5. *Nature* **319**(6056): 774-776.

Mosley, C. A., T. M. Acker, K. B. Hansen, P. Mullasseril, K. T. Andersen, P. Le, K. M. Vellano, H. Brauner-Osborne, D. C. Liotta and S. F. Traynelis (2010). Quinazolin-4-one derivatives: A novel class of noncompetitive NR2C/D subunit-selective N-methyl-D-aspartate receptor antagonists. *J Med Chem* **53**(15): 5476-5490.

Mothet, J.-P., A. T. Parent, H. Wolosker, R. O. Brady, D. J. Linden, C. D. Ferris, M. A. Rogawski and S. H. Snyder (2000). d-Serine is an endogenous ligand for the glycine site of the N-methyl-d-aspartate receptor. *Proceedings of the National Academy of Sciences* **97**(9): 4926-4931.

Mott, D. D., J. J. Doherty, S. Zhang, M. S. Washburn, M. J. Fendley, P. Lyuboslavsky, S. F. Traynelis and R. Dingledine (1998). Phenylethanolamines inhibit NMDA receptors by enhancing proton inhibition. *Nat Neurosci* **1**(8): 659-667.

Muir, K. W. (2006). Glutamate-based therapeutic approaches: clinical trials with NMDA antagonists. *Current Opinion in Pharmacology* **6**(1): 53-60.

Mullasseril, P., K. B. Hansen, K. M. Vance, K. K. Ogden, H. Yuan, N. L. Kurtkaya, R. Santangelo, A. G. Orr, P. Le, K. M. Vellano, D. C. Liotta and S. F. Traynelis (2010). A subunit-selective potentiator of NR2C- and NR2D-containing NMDA receptors. *Nat Commun* **1**: 90.

Murakoshi, H., H. Wang and R. Yasuda (2011). Local, persistent activation of Rho GTPases during plasticity of single dendritic spines. *Nature* **472**(7341): 100-104.

Neher, E. and B. Sakmann (1976). Single-channel currents recorded from membrane of denervated frog muscle fibres. *Nature* **260**: 799.

Nicholson, E. and D. M. Kullmann (2014). Long-term potentiation in hippocampal oriens interneurons: postsynaptic induction, presynaptic expression and evaluation of candidate retrograde factors. *Philosophical Transactions of the Royal Society B: Biological Sciences* **369**(1633).

Niethammer, M., E. Kim and M. Sheng (1996). Interaction between the C terminus of NMDA receptor subunits and multiple members of the PSD-95 family of membrane-associated guanylate kinases. *The Journal of Neuroscience* **16**(7): 2157-2163.

Nowak, L., P. Bregestovski, P. Ascher, A. Herbet and A. Prochiantz (1984). Magnesium gates glutamate-activated channels in mouse central neurones. *Nature* **307**: 462.

O'Hara, P. J., P. O. Sheppard, H. Thógersen, D. Venezia, B. A. Haldeman, V. McGrane, K. M. Houamed, C. Thomsen, T. L. Gilbert and E. R. Mulvihill (1993). The ligand-binding domain in metabotropic glutamate receptors is related to bacterial periplasmic binding proteins. *Neuron* **11**(1): 41-52.

Ogden, K. K., W. Chen, S. A. Swanger, M. J. McDaniel, L. Z. Fan, C. Hu, A. Tankovic, H. Kusumoto, G. J. Kosobucki, A. J. Schulien, Z. Su, J. Pecha, S. Bhattacharya, S. Petrovski, A. E. Cohen, E. Aizenman, S. F. Traynelis and H. Yuan (2017). Molecular Mechanism of Disease-Associated Mutations in the Pre-M1 Helix of NMDA Receptors and Potential Rescue Pharmacology. *PLOS Genetics* **13**(1): e1006536.

Ogden, K. K., A. Khatri, S. F. Traynelis and S. A. Heldt (2014). Potentiation of GluN2C/D NMDA receptor subtypes in the amygdala facilitates the retention of fear and extinction learning in mice. *Neuropsychopharmacology* **39**(3): 625-637.

Ogden, K. K. and S. F. Traynelis (2011). New advances in NMDA receptor pharmacology. *Trends Pharmacol Sci* **32**(12): 726-733.

Ogden, K. K. and S. F. Traynelis (2013). Contribution of the M1 Transmembrane Helix and Pre-M1 Region to Positive Allosteric Modulation and Gating of N-Methyl-d-Aspartate Receptors. *Molecular Pharmacology* **83**(5): 1045-1056.

Oren, I., W. Nissen, D. M. Kullmann, P. Somogyi and K. P. Lamsa (2009). Role of Ionotropic Glutamate Receptors in Long-Term Potentiation in Rat Hippocampal CA1 Oriens-Lacunosum Moleculare Interneurons. *The Journal of Neuroscience* **29**(4): 939-950.

Pahk, A. J. and K. Williams (1997). Influence of extracellular pH on inhibition by ifenprodil at N-methyl-D-aspartate receptors in Xenopus oocytes. *Neuroscience Letters* **225**(1): 29-32.

Palmer, G. C. (2001). Neuroprotection by NMDA Receptor Antagonists in a Variety of Neuropathologies. *Current Drug Targets* **2**(3): 241-271.

Panchenko, V. A., C. R. Glasser and M. L. Mayer (2001). Structural Similarities between Glutamate Receptor Channels and K$^+$ Channels Examined by Scanning Mutagenesis. *The Journal of General Physiology* **117**(4): 345-360.

Paoletti, P., P. Ascher and J. Neyton (1997). High-affinity zinc inhibition of NMDA NR1-NR2A receptors. *J Neurosci* **17**(15): 5711-5725.

Paoletti, P., C. Bellone and Q. Zhou (2013). NMDA receptor subunit diversity: impact on receptor properties, synaptic plasticity and disease. *Nat Rev Neurosci* **14**(6): 383-400.

Paoletti, P. and J. Neyton (2007). NMDA receptor subunits: function and pharmacology. *Current Opinion in Pharmacology* **7**(1): 39-47.

Paoletti, P., J. Neyton and P. Ascher (1995). Glycine-independent and subunit-specific potentiation of NMDA responses by extracellular Mg2+. *Neuron* **15**(5): 1109-1120.

Papouin, T. and S. H. R. Oliet (2014). Organization, control and function of extrasynaptic NMDA receptors. *Philosophical Transactions of the Royal Society B: Biological Sciences* **369**(1654).

Paul, S. M., J. J. Doherty, A. J. Robichaud, G. M. Belfort, B. Y. Chow, R. S. Hammond, D. C. Crawford, A. J. Linsenbardt, H.-J. Shu, Y. Izumi, S. J. Mennerick and C. F. Zorumski (2013). The Major Brain Cholesterol Metabolite 24(S)-Hydroxycholesterol Is a Potent Allosteric Modulator of N-Methyl-d-Aspartate Receptors. *The Journal of Neuroscience* **33**(44): 17290-17300.

Pelkey, K. A., R. Chittajallu, M. T. Craig, L. Tricoire, J. C. Wester and C. J. McBain (2017). Hippocampal GABAergic Inhibitory Interneurons. *Physiological Reviews* **97**(4): 1619-1747.

Perin-Dureau, F., J. Rachline, J. Neyton and P. Paoletti (2002). Mapping the binding site of the neuroprotectant ifenprodil on NMDA receptors. *J Neurosci* **22**(14): 5955-5965.

Perszyk, R. E., J. O. DiRaddo, K. L. Strong, C. M. Low, K. K. Ogden, A. Khatri, G. A. Vargish, K. A. Pelkey, L. Tricoire, D. C. Liotta, Y. Smith, C. J. McBain and S. F. Traynelis (2016). GluN2D-containing NMDA receptors mediate synaptic transmission in hippocampal interneurons and regulate interneuron activity. *Mol Pharmacol*.

Petrovic, M., M. Sedlacek, M. Horak, H. Chodounska and L. Vyklický (2005). 20-Oxo-5β-Pregnan-3α-yl Sulfate Is a Use-Dependent NMDA Receptor Inhibitor. *The Journal of Neuroscience* **25**(37): 8439-8450.

Pin, J.-P. and L. Prézeau (2007). Allosteric Modulators of GABA(B) Receptors: Mechanism of Action and Therapeutic Perspective. *Current Neuropharmacology* **5**(3): 195-201.

Popescu, G. and A. Auerbach (2003). Modal gating of NMDA receptors and the shape of their synaptic response. *Nat Neurosci* **6**(5): 476-483.

Popescu, G., A. Robert, J. R. Howe and A. Auerbach (2004). Reaction mechanism determines NMDA receptor response to repetitive stimulation. *Nature* **430**(7001): 790-793.

Porter, J. T., B. Cauli, J. F. Staiger, B. Lambolez, J. Rossier and E. Audinat (1998). Properties of bipolar VIPergic interneurons and their excitation by pyramidal neurons in the rat neocortex. *Eur J Neurosci* **10**(12): 3617-3628.

Preskorn, S., M. Macaluso, D. V. Mehra, G. Zammit, J. R. Moskal, R. M. Burch and t. G.-C. S. Group (2015). Randomized Proof of Concept Trial of GLYX-13, an N-Methyl-D-Aspartate Receptor Glycine Site Partial Agonist, in Major Depressive Disorder Nonresponsive to a Previous Antidepressant Agent. *Journal of Psychiatric Practice®* **21**(2): 140-149.

Preskorn, S. H., B. Baker, S. Kolluri, F. S. Menniti, M. Krams and J. W. Landen (2008). An Innovative Design to Establish Proof of Concept of the Antidepressant Effects of the NR2B Subunit Selective N-Methyl-D-Aspartate Antagonist, CP-101,606, in Patients With Treatment-Refractory Major Depressive Disorder. *Journal of Clinical Psychopharmacology* **28**(6): 631-637.

Priestley, T., P. Laughton, J. Myers, B. Le Bourdelles, J. Kerby and P. J. Whiting (1995). Pharmacological properties of recombinant human N-methyl-D-aspartate receptors comprising NR1a/NR2A and NR1a/NR2B subunit assemblies expressed in permanently transfected mouse fibroblast cells. *Mol Pharmacol* **48**(5): 841-848.

Punnakkal, P., P. Jendritza and G. Kohr (2012). Influence of the intracellular GluN2 C-terminal domain on NMDA receptor function. *Neuropharmacology* **62**(5-6): 1985-1992.

Ramon y Cajal, S. (1894). The Croonian lecture.—La fine structure des centres nerveux. *Proceedings of the Royal Society of London* **55**(331-335): 444-468.

Retchless, B. S., W. Gao and J. W. Johnson (2012). A single GluN2 subunit residue controls NMDA receptor channel properties via intersubunit interaction. *Nat Neurosci* **15**(3): 406-413.

Romero-Hernandez, A., N. Simorowski, E. Karakas and H. Furukawa (2016). Molecular Basis for Subtype Specificity and High-Affinity Zinc Inhibition in the GluN1-GluN2A NMDA Receptor Amino-Terminal Domain. *Neuron* **92**(6): 1324-1336.

Rosenmund, C., A. Feltz and G. L. Westbrook (1995). Calcium-dependent inactivation of synaptic NMDA receptors in hippocampal neurons. *Journal of Neurophysiology* **73**(1): 427-430.

Rosenmund, C., Y. Stern-Bach and C. F. Stevens (1998). The tetrameric structure of a glutamate receptor channel. *Science* **280**(5369): 1596-1599.

Rosenmund, C. and G. L. Westbrook (1993). Calcium-induced actin depolymerization reduces NMDA channel activity. *Neuron* **10**(5): 805-814.

Rossi, P., E. Sola, V. Taglietti, T. Borchardt, F. Steigerwald, J. K. Utvik, O. P. Ottersen, G. Kohr and E. D'Angelo (2002). NMDA receptor 2 (NR2) C-terminal control of NR open probability regulates synaptic transmission and plasticity at a cerebellar synapse. *J Neurosci* **22**(22): 9687-9697.

Rudolf, G. D., C. A. Cronin, G. B. Landwehrmeyer, D. G. Standaert, J. B. Penney, Jr. and A. B. Young (1996). Expression of N-methyl-D-aspartate glutamate receptor subunits in the prefrontal cortex of the rat. *Neuroscience* **73**(2): 417-427.

Rudolph, U. and F. Knoflach (2011). Beyond classical benzodiazepines: novel therapeutic potential of GABAA receptor subtypes. *Nature Reviews Drug Discovery* **10**: 685.

Rusakov, D. A. and D. M. Kullmann (1998). Extrasynaptic glutamate diffusion in the hippocampus: ultrastructural constraints, uptake, and receptor activation. *J Neurosci* **18**(9): 3158-3170.

Ryan, T. J. and S. G. N. Grant (2009). The origin and evolution of synapses. *Nature Reviews Neuroscience* **10**: 701.

Rycroft, B. K. and A. J. Gibb (2004). Regulation of single NMDA receptor channel activity by alpha-actinin and calmodulin in rat hippocampal granule cells. *The Journal of Physiology* **557**(Pt 3): 795-808.

Sahlender, D. A., I. Savtchouk and A. Volterra (2014). What do we know about gliotransmitter release from astrocytes? *Philosophical Transactions of the Royal Society B: Biological Sciences* **369**(1654).

Saneyoshi, T. and Y. Hayashi (2012). The Ca2+ and Rho GTPase signaling pathways underlying activity-dependent actin remodeling at dendritic spines. *Cytoskeleton (Hoboken)* **69**(8): 545-554.

Sans, N., R. S. Petralia, Y.-X. Wang, J. Blahos, J. W. Hell and R. J. Wenthold (2000). A Developmental Change in NMDA Receptor-Associated Proteins at Hippocampal Synapses. *The Journal of Neuroscience* **20**(3): 1260-1271.

Santangelo Freel, R., K. Ogden, K. Strong, A. Khatri, K. Chepiga, H. Jensen, S. Traynelis and D. Liotta (2013). Synthesis and structure activity relationship of tetrahydroisoquinoline-based potentiators of GluN2C and GluN2D containing N-methyl-D-aspartate receptors. *Journal of medicinal chemistry* **56**(13): 5351-5381.

Santangelo Freel, R. M., K. K. Ogden, K. L. Strong, A. Khatri, K. M. Chepiga, H. S. Jensen, S. F. Traynelis and D. C. Liotta (2014). Correction to Synthesis and Structure Activity Relationship of Tetrahydroisoquinoline-Based Potentiators of GluN2C and GluN2D Containing N-Methyl-d-aspartate Receptors. *Journal of Medicinal Chemistry* **57**(11): 4975-4975.

Santangelo, R. M., T. M. Acker, S. S. Zimmerman, B. M. Katzman, K. L. Strong, S. F. Traynelis and D. C. Liotta (2012). Novel NMDA Receptor Modulators: An Update. *Expert opinion on therapeutic patents* **22**(11): 1337-1352.

Sather, W., S. Dieudonne, J. F. MacDonald and P. Ascher (1992). Activation and desensitization of N-methyl-D-aspartate receptors in nucleated outside-out patches from mouse neurones. *Journal of Physiology* **450**: 643-672.

Sather, W., J. W. Johnson, G. Henderson and P. Ascher (1990). Glycine-insensitive desensitization of NMDA responses in cultured mouse embryonic neurons. *Neuron* **4**(5): 725-731.

Schneggenburger, R. (1996). Simultaneous measurement of Ca2+ influx and reversal potentials in recombinant N-methyl-D-aspartate receptor channels. *Biophys J* **70**(5): 2165-2174.

Schorge, S. and D. Colquhoun (2003). Studies of NMDA receptor function and stoichiometry with truncated and tandem subunits. *J Neurosci* **23**(4): 1151-1158.

Schorge, S., S. Elenes and D. Colquhoun (2005). Maximum likelihood fitting of single channel NMDA activity with a mechanism composed of independent dimers of subunits. *J Physiol* **569**(Pt 2): 395-418.

Shapiro, M. L. and Z. Caramanos (1990). NMDA ANTAGONIST MK-801 IMPAIRS ACQUISITION BUT NOT PERFORMANCE OF SPATIAL WORKING AND REFERENCE MEMORY. *Psychobiology* **18**(2): 231-243.

Sheng, M., J. Cummings, L. A. Roldan, Y. N. Jan and L. Y. Jan (1994). Changing subunit composition of heteromeric NMDA receptors during development of rat cortex. *Nature* **368**(6467): 144-147.

Sherrington, C. (1910). The integrative action of the nervous system, CUP Archive.

Shipton, O. A. and O. Paulsen (2014). GluN2A and GluN2B subunit-containing NMDA receptors in hippocampal plasticity. *Philos Trans R Soc Lond B Biol Sci* **369**(1633): 20130163.

Siegler Retchless, B., W. Gao and J. W. Johnson (2012). A single GluN2 subunit residue controls NMDA receptor channel properties via intersubunit interaction. *Nat Neurosci* **15**(3): 406-413, S401-402.

Sirrieh, R. E., D. M. MacLean and V. Jayaraman (2015). Subtype-dependent N-methyl-D-aspartate receptor amino-terminal domain conformations and modulation by spermine. *J Biol Chem* **290**(20): 12812-12820.

Smith, G. G., K. M. Williams and D. M. Wonnacott (1978). Factors affecting the rate of racemization of amino acids and their significance to geochronology. *The Journal of Organic Chemistry* **43**(1): 1-5.

Sobolevsky, A. I., S. G. Koshelev and B. I. Khodorov (1999). Probing of NMDA Channels with Fast Blockers. *The Journal of Neuroscience* **19**(24): 10611-10626.

Sobolevsky, A. I. and M. V. Yelshansky (2000). The trapping block of NMDA receptor channels in acutely isolated rat hippocampal neurones. *The Journal of Physiology* **526**(3): 493-506.

Somogyi, P., L. Katona, T. Klausberger, B. Lasztóczi and T. J. Viney (2014). Temporal redistribution of inhibition over neuronal subcellular domains underlies state-dependent rhythmic change of excitability in the hippocampus. *Philosophical Transactions of the Royal Society B: Biological Sciences* **369**(1635).

Standaert, D. G., C. M. Testa, A. B. Young and J. B. Penney (1994). Organization of N-methyl-D-aspartate glutamate receptor gene expression in the basal ganglia of the rat. *The Journal of Comparative Neurology* **343**(1): 1-16.

Staubli, U., O. Thibault, M. Dilorenzo and G. Lynch (1989). ANTAGONISM OF NMDA RECEPTORS IMPAIRS ACQUISITION BUT NOT RETENTION OF OLFACTORY MEMORY. *Behavioral Neuroscience* **103**(1): 54-60.

Stefanescu, R. A. and S. Shore (2015). NMDA receptors mediate stimulus-timing-dependent plasticity and neural synchrony in the dorsal cochlear nucleus. *Frontiers in Neural Circuits* **9**.

Steigerwald, F., T. W. Schulz, L. T. Schenker, M. B. Kennedy, P. H. Seeburg and G. Köhr (2000). C-Terminal Truncation of NR2A Subunits Impairs Synaptic But Not Extrasynaptic Localization of NMDA Receptors. *The Journal of Neuroscience* **20**(12): 4573-4581.

Stern, P., P. Behe, R. Schoepfer and D. Colquhoun (1992). Single-channel conductances of NMDA receptors expressed from cloned cDNAs: comparison with native receptors. *Proc Biol Sci* **250**(1329): 271-277.

Stern, P., M. Cik, D. Colquhoun and F. A. Stephenson (1994). Single channel properties of cloned NMDA receptors in a human cell line: comparison with results from Xenopus oocytes. *J Physiol* **476**(3): 391-397.

Stockton, J. M., N. J. Birdsall, A. S. Burgen and E. C. Hulme (1983). Modification of the binding properties of muscarinic receptors by gallamine. *Molecular Pharmacology* **23**(3): 551-557.

Strack, S. and R. J. Colbran (1998). Autophosphorylation-dependent Targeting of Calcium/ Calmodulin-dependent Protein Kinase II by the NR2B Subunit of theN-Methyl- d-aspartate Receptor. *Journal of Biological Chemistry* **273**(33): 20689-20692.

Stroebel, D., D. L. Buhl, J. D. Knafels, P. K. Chanda, M. Green, S. Sciabola, L. Mony, P. Paoletti and J. Pandit (2016). A novel binding mode reveals two distinct classes of NMDA receptor GluN2B-selective antagonists. *Mol Pharmacol*.

Stroebel, D., S. Carvalho, T. Grand, S. Zhu and P. Paoletti (2014). Controlling NMDA receptor subunit composition using ectopic retention signals. *J Neurosci* **34**(50): 16630-16636.

Strong, K. L., M. P. Epplin, J. Bacsa, C. J. Butch, P. B. Burger, D. S. Menaldino, S. F. Traynelis and D. C. Liotta (2017). The Structure–Activity Relationship of a Tetrahydroisoquinoline Class of N-Methyl-d-Aspartate Receptor Modulators that Potentiates GluN2B-Containing N-Methyl-d-Aspartate Receptors. *Journal of Medicinal Chemistry* **60**(13): 5556-5585.

Strong, K. L., Y. Jing, A. R. Prosser, S. F. Traynelis and D. C. Liotta (2014). NMDA receptor modulators: an updated patent review (2013-2014). *Expert Opin Ther Pat* **24**(12): 1349-1366.

Sucher, N. J., S. Akbarian, C. L. Chi, C. L. Leclerc, M. Awobuluyi, D. L. Deitcher, M. K. Wu, J. P. Yuan, E. G. Jones and S. A. Lipton (1995). Developmental and regional expression pattern of a novel NMDA receptor-like subunit (NMDAR-L) in the rodent brain. *J Neurosci* **15**(10): 6509-6520.

Sugihara, H., K. Moriyoshi, T. Ishii, M. Masu and S. Nakanishi (1992). Structures and properties of seven isoforms of the NMDA receptor generated by alternative splicing. *Biochem Biophys Res Commun* **185**(3): 826-832.

Surmeier, D. J., J. N. Guzman, J. Sanchez-Padilla and J. A. Goldberg (2010). Chapter 4 - What causes the death of dopaminergic neurons in Parkinson's disease? <u>Progress in Brain Research</u>. A. Björklund and M. A. Cenci, Elsevier. **183:** 59-77.

Surmeier, D. J. and P. T. Schumacker (2013). Calcium, Bioenergetics, and Neuronal Vulnerability in Parkinson's Disease. *Journal of Biological Chemistry* **288**(15): 10736-10741.

Suryavanshi, P. S., R. R. Ugale, D. Yilmazer-Hanke, D. J. Stairs and S. M. Dravid (2014). GluN2C/GluN2D subunit-selective NMDA receptor potentiator CIQ reverses MK-801-induced impairment in prepulse inhibition and working memory in Y-maze test in mice. *Br J Pharmacol* **171**(3): 799-809.

Swanger, S. A., W. Chen, G. Wells, P. B. Burger, A. Tankovic, S. Bhattacharya, K. L. Strong, C. Hu, H. Kusumoto, J. Zhang, D. R. Adams, J. J. Millichap, S. Petrovski, S. F. Traynelis and H. Yuan (2016). Mechanistic Insight into NMDA Receptor Dysregulation by Rare Variants in the GluN2A and GluN2B Agonist Binding Domains. *Am J Hum Genet* **99**(6): 1261-1280.

Swanger, S. A., K. M. Vance, T. M. Acker, S. S. Zimmerman, J. O. DiRaddo, S. J. Myers, C. Bundgaard, C. A. Mosley, S. L. Summer, D. S. Menaldino, H. S. Jensen, D. C. Liotta and S. F. Traynelis (2017). A Novel Negative Allosteric Modulator Selective for GluN2C/2D-Containing NMDA Receptors Inhibits Synaptic Transmission in Hippocampal Interneurons. *ACS Chemical Neuroscience*.

Swanger, S. A., K. M. Vance, J.-F. Pare, F. Sotty, K. Fog, Y. Smith and S. F. Traynelis (2015). NMDA Receptors Containing the GluN2D Subunit Control Neuronal Function in the Subthalamic Nucleus. *The Journal of Neuroscience* **35**(48): 15971-15983.

Sweatt, J. D. (2016). Neural plasticity and behavior – sixty years of conceptual advances. *Journal of Neurochemistry*.

Tajima, N., E. Karakas, T. Grant, N. Simorowski, R. Diaz-Avalos, N. Grigorieff and H. Furukawa (2016). Activation of NMDA receptors and the mechanism of inhibition by ifenprodil. *Nature* **534**(7605): 63-68.

Talaei, S. A., A. Azami and M. Salami (2016). Postnatal development and sensory experience synergistically underlie the excitatory/inhibitory features of hippocampal neural circuits: Glutamatergic and GABAergic neurotransmission. *Neuroscience* **318**: 230-243.

Tang, Y.-P., E. Shimizu, G. R. Dube, C. Rampon, G. A. Kerchner, M. Zhuo, G. Liu and J. Z. Tsien (1999). Genetic enhancement of learning and memory in mice. *Nature* **401**: 63.

Tanzi, E. (1893). I fatti e le induzioni dell'odierna istologia del sistema nervoso. . *Riv. Sper. Fren. Med. Leg.* **19**: 419–472.

Thomas, G. M. and R. L. Huganir (2004). MAPK cascade signalling and synaptic plasticity. *Nature Reviews Neuroscience* **5**: 173.

Thompson, C. L., D. L. Drewery, H. D. Atkins, F. A. Stephenson and P. L. Chazot (2002). Immunohistochemical localization of N-methyl-d-aspartate receptor subunits in the adult murine hippocampal formation: evidence for a unique role of the NR2D subunit. *Molecular Brain Research* **102**(1-2): 55-61.

Thron, C. D. (1973). On the Analysis of Pharmacological Experiments in Terms of an Allosteric Receptor Model. *Molecular Pharmacology* **9**(1): 1-9.

Tovar, K. R., M. J. McGinley and G. L. Westbrook (2013). Triheteromeric NMDA receptors at hippocampal synapses. *J Neurosci* **33**(21): 9150-9160.

Tovar, K. R. and G. L. Westbrook (2002). Mobile NMDA Receptors at Hippocampal Synapses. *Neuron* **34**(2): 255-264.

Traynelis, S. F., M. F. Burgess, F. Zheng, P. Lyuboslavsky and J. L. Powers (1998). Control of voltage-independent zinc inhibition of NMDA receptors by the NR1 subunit. *J Neurosci* **18**(16): 6163-6175.

Traynelis, S. F. and S. G. Cull-Candy (1990). Proton inhibition of N-methyl-D-aspartate receptors in cerebellar neurons. *Nature* **345**(6273): 347-350.

Traynelis, S. F. and S. G. Cull-Candy (1991). Pharmacological properties and H+ sensitivity of excitatory amino acid receptor channels in rat cerebellar granule neurones. *Journal of Physiology* **433**: 727-763.

Traynelis, S. F., M. Hartley and S. F. Heinemann (1995). Control of proton sensitivity of the NMDA receptor by RNA splicing and polyamines. *Science* **268**(5212): 873-876.

Traynelis, S. F., L. P. Wollmuth, C. J. McBain, F. S. Menniti, K. M. Vance, K. K. Ogden, K. B. Hansen, H. Yuan, S. J. Myers and R. Dingledine (2010). Glutamate Receptor Ion Channels: Structure, Regulation, and Function. *Pharmacological Reviews* **62**(3): 405-496.

Twomey, E. C. and A. I. Sobolevsky (2017). Structural Mechanisms of Gating in Ionotropic Glutamate Receptors. *Biochemistry*.

Twomey, E. C., M. V. Yelshanskaya, R. A. Grassucci, J. Frank and A. I. Sobolevsky (2017). Channel opening and gating mechanism in AMPA-subtype glutamate receptors. *Nature* **549**(7670): 60-65.

Twomey, E. C., M. V. Yelshanskaya, R. A. Grassucci, J. Frank and A. I. Sobolevsky (2017). Structural Bases of Desensitization in AMPA Receptor-Auxiliary Subunit Complexes. *Neuron* **94**(3): 569-580 e565.

Ulbrich, M. H. and E. Y. Isacoff (2008). Rules of engagement for NMDA receptor subunits. *Proc Natl Acad Sci U S A* **105**(37): 14163-14168.

Vance, K. M., K. B. Hansen and S. F. Traynelis (2012). GluN1 splice variant control of GluN1/GluN2D NMDA receptors. *The Journal of Physiology* **590**(16): 3857-3875.

Vance, K. M., K. B. Hansen and S. F. Traynelis (2013). Modal gating of GluN1/GluN2D NMDA receptors. *Neuropharmacology* **71**: 184-190.

Verhoog, M. B., N. A. Goriounova, J. Obermayer, J. Stroeder, J. J. J. Hjorth, G. Testa-Silva, J. C. Baayen, C. P. J. de Kock, R. M. Meredith and H. D. Mansvelder (2013). Mechanisms Underlying the Rules for Associative Plasticity at Adult Human Neocortical Synapses. *The Journal of Neuroscience* **33**(43): 17197-17208.

Vicini, S., J. F. Wang, J. H. Li, W. J. Zhu, Y. H. Wang, J. H. Luo, B. B. Wolfe and D. R. Grayson (1998). Functional and Pharmacological Differences Between RecombinantN-Methyl-d-Aspartate Receptors. *Journal of Neurophysiology* **79**(2): 555-566.

Villarroel, A., N. Burnashev and B. Sakmann (1995). Dimensions of the narrow portion of a recombinant NMDA receptor channel. *Biophys J* **68**(3): 866-875.

Villemure, E., M. Volgraf, Y. Jiang, G. Wu, C. Q. Ly, P.-w. Yuen, A. Lu, X. Luo, M. Liu, S. Zhang, P. J. Lupardus, H. J. A. Wallweber, B. M. Liederer, G. Deshmukh, E. Plise, S. Tay, T.-M. Wang, J. E. Hanson, D. H. Hackos, K. Scearce-Levie, J. B. Schwarz and B. D. Sellers (2017). GluN2A-Selective Pyridopyrimidinone Series of NMDAR Positive Allosteric Modulators with an Improved in Vivo Profile. *ACS Medicinal Chemistry Letters* **8**(1): 84-89.

Volgraf, M., B. D. Sellers, Y. Jiang, G. Wu, C. Q. Ly, E. Villemure, R. M. Pastor, P. W. Yuen, A. Lu, X. Luo, M. Liu, S. Zhang, L. Sun, Y. Fu, P. J. Lupardus, H. J. Wallweber, B. M. Liederer, G. Deshmukh, E. Plise, S. Tay, P. Reynen, J. Herrington, A. Gustafson, Y. Liu, A. Dirksen, M. G. Dietz, Y. Liu, T. M. Wang, J. E. Hanson, D. Hackos, K. Scearce-Levie and J. B. Schwarz (2016). Discovery of GluN2A-Selective NMDA Receptor Positive Allosteric Modulators (PAMs): Tuning Deactivation Kinetics via Structure-Based Design. *J Med Chem* **59**(6): 2760-2779.

Volkmann, R. A., C. M. Fanger, D. R. Anderson, V. R. Sirivolu, K. Paschetto, E. Gordon, C. Virginio, M. Gleyzes, B. Buisson, E. Steidl, S. B. Mierau, M. Fagiolini and F. S. Menniti (2016). MPX-004 and MPX-007: New Pharmacological Tools to Study the Physiology of NMDA Receptors Containing the GluN2A Subunit. *PLoS One* **11**(2): e0148129.

von Engelhardt, J., C. Bocklisch, L. Tönges, A. Herb, M. Mishina and H. Monyer (2015). GluN2D-containing NMDA receptors-mediate synaptic currents in hippocampal interneurons and pyramidal cells in juvenile mice. *Frontiers in Cellular Neuroscience* **9**.

Vyklicky, L., Jr. (1993). Calcium-mediated modulation of N-methyl-D-aspartate (NMDA) responses in cultured rat hippocampal neurones. *J Physiol* **470**: 575-600.

Vyklicky, L., Jr., V. Vlachova and J. Krusek (1990). The effect of external pH changes on responses to excitatory amino acids in mouse hippocampal neurones. *J Physiol* **430**: 497-517.

Vyklicky, V., B. Krausova, J. Cerny, A. Balik, M. Zapotocky, M. Novotny, K. Lichnerova, T. Smejkalova, M. Kaniakova, M. Korinek, M. Petrovic, P. Kacer, M. Horak, H. Chodounska and L. Vyklicky (2015). Block of NMDA receptor channels by endogenous neurosteroids: implications for the agonist induced conformational states of the channel vestibule. *Sci Rep* **5**: 10935.

Wang, C. X. and A. Shuaib (2005). NMDA/NR2B selective antagonists in the treatment of ischemic brain injury. *Curr Drug Targets CNS Neurol Disord* **4**(2): 143-151.

Wang, T. M., B. M. Brown, L. Deng, B. D. Sellers, P. J. Lupardus, H. J. A. Wallweber, A. Gustafson, E. Wong, M. Volgraf, J. B. Schwarz, D. H. Hackos and J. E. Hanson (2017). A novel NMDA receptor positive allosteric modulator that acts via the transmembrane domain. *Neuropharmacology* **121**: 204-218.

Watkins, J. C. (1962). The Synthesis of Some Acidic Amino Acids Possessing Neuropharmacological Activity. *J Med Pharm Chem* **91**: 1187-1199.

Wilcox, M., N. G. Glasgow, A. L. Turcu, S. Vazquez and J. W. Johnson (2017). The uncharged form of memantine can access the NMDAR channel through a hydrophobic route. Program No. 558.07/C24. 2017 Neuroscience Meeting Planner. Washington, DC: Society for Neuroscience, 2017. Online.

Williams, K. (1993). Ifenprodil Discriminates Subtypes of the N-Methyl-D-Aspartate Receptor - Selectivity and Mechanisms at Recombinant Heteromeric Receptors. *Molecular Pharmacology* **44**(4): 851-859.

Williams, K. (1996). Separating dual effects of zinc at recombinant N-methyl-D-aspartate receptors. *Neuroscience Letters* **215**(1): 9-12.

Wo, Z. G. and R. E. Oswald (1995). A topological analysis of goldfish kainate receptors predicts three transmembrane segments. *J Biol Chem* **270**(5): 2000-2009.

Wollmuth, L. P., T. Kuner and B. Sakmann (1998). Adjacent asparagines in the NR2-subunit of the NMDA receptor channel control the voltage-dependent block by extracellular Mg2+. *J Physiol* **506 (Pt 1)**: 13-32.

Wollmuth, L. P., T. Kuner, P. H. Seeburg and B. Sakmann (1996). Differential contribution of the NR1- and NR2A-subunits to the selectivity filter of recombinant NMDA receptor channels. *J Physiol* **491 (Pt 3)**: 779-797.

Wollmuth, L. P. and A. I. Sobolevsky (2004). Structure and gating of the glutamate receptor ion channel. *Trends in Neurosciences* **27**(6): 321-328.

Wong, E. H., J. A. Kemp, T. Priestley, A. R. Knight, G. N. Woodruff and L. L. Iversen (1986). The anticonvulsant MK-801 is a potent N-methyl-D-aspartate antagonist. *Proc Natl Acad Sci U S A* **83**(18): 7104-7108.

Wood, M. W., H. M. VanDongen and A. M. VanDongen (1995). Structural conservation of ion conduction pathways in K channels and glutamate receptors. *Proc Natl Acad Sci U S A* **92**(11): 4882-4886.

Wootten, D., A. Christopoulos and P. M. Sexton (2013). Emerging paradigms in GPCR allostery: implications for drug discovery. *Nature Reviews Drug Discovery* **12**: 630.

Wyllie, D. J., P. Behe and D. Colquhoun (1998). Single-channel activations and concentration jumps: comparison of recombinant NR1a/NR2A and NR1a/NR2D NMDA receptors. *J Physiol* **510 (Pt 1)**: 1-18.

Wyllie, D. J., P. Behe, M. Nassar, R. Schoepfer and D. Colquhoun (1996). Single-channel currents from recombinant NMDA NR1a/NR2D receptors expressed in Xenopus oocytes. *Proc Biol Sci* **263**(1373): 1079-1086.

Wyllie, D. J. A., M. R. Livesey and G. E. Hardingham (2013). Influence of GluN2 subunit identity on NMDA receptor function. *Neuropharmacology* **74**: 4-17.

Xue, J.-G., T. Masuoka, X.-D. Gong, K.-S. Chen, Y. Yanagawa, S. K. A. Law and S. Konishi (2011). NMDA receptor activation enhances inhibitory GABAergic transmission onto

hippocampal pyramidal neurons via presynaptic and postsynaptic mechanisms. *Journal of Neurophysiology* **105**(6): 2897-2906.

Yamamoto, H., E. Kamegaya, W. Sawada, R. Hasegawa, T. Yamamoto, Y. Hagino, Y. Takamatsu, K. Imai, H. Koga, M. Mishina and K. Ikeda (2013). Involvement of the N-methyl-D-aspartate receptor GluN2D subunit in phencyclidine-induced motor impairment, gene expression, and increased Fos immunoreactivity. *Mol Brain* **6**: 56.

Yang, J., G. L. Woodhall and R. S. G. Jones (2006). Tonic Facilitation of Glutamate Release by Presynaptic NR2B-Containing NMDA Receptors Is Increased in the Entorhinal Cortex of Chronically Epileptic Rats. *The Journal of Neuroscience* **26**(2): 406-410.

Yelshanskaya, M. V., M. Li and A. I. Sobolevsky (2014). Structure of an agonist-bound ionotropic glutamate receptor. *Science* **345**(6200): 1070-1074.

Yelshanskaya, M. V., S. Mesbahi-Vasey, M. G. Kurnikova and A. I. Sobolevsky (2017). Role of the Ion Channel Extracellular Collar in AMPA Receptor Gating. *Sci Rep* **7**(1): 1050.

Yelshanskaya, M. V., A. K. Singh, J. M. Sampson, C. Narangoda, M. Kurnikova and A. I. Sobolevsky (2016). Structural Bases of Noncompetitive Inhibition of AMPA-Subtype Ionotropic Glutamate Receptors by Antiepileptic Drugs. *Neuron* **91**(6): 1305-1315.

Yenari, M. A., T. E. Bell, A. N. Kotake, M. Powell and G. K. Steinberg (1998). Dose Escalation Safety and Tolerance Study of the Competitive NMDA Antagonist Selfotel (CGS 19755) in Neurosurgery Patients. *Clinical Neuropharmacology* **21**(1): 28-34.

Yi, F., T. C. Mou, K. N. Dorsett, R. A. Volkmann, F. S. Menniti, S. R. Sprang and K. B. Hansen (2016). Structural Basis for Negative Allosteric Modulation of GluN2A-Containing NMDA Receptors. *Neuron* **91**(6): 1316-1329.

Yu, A., H. Salazar, A. J. R. Plested and A. Y. Lau (2018). Neurotransmitter Funneling Optimizes Glutamate Receptor Kinetics. *Neuron* **97**(1): 139-149.e134.

Yuan, H., K. B. Hansen, K. M. Vance, K. K. Ogden and S. F. Traynelis (2009). Control of NMDA Receptor Function by the NR2 Subunit Amino-Terminal Domain. *The Journal of Neuroscience* **29**(39): 12045-12058.

Yuan, H., K. B. Hansen, J. Zhang, T. M. Pierson, T. C. Markello, K. V. Fajardo, C. M. Holloman, G. Golas, D. R. Adams, C. F. Boerkoel, W. A. Gahl and S. F. Traynelis (2014). Functional analysis of a de novo GRIN2A missense mutation associated with early-onset epileptic encephalopathy. *Nat Commun* **5**: 3251.

Yuan, H., C.-M. Low, O. A. Moody, A. Jenkins and S. F. Traynelis (2015). Ionotropic GABA and Glutamate Receptor Mutations and Human Neurologic Diseases. *Molecular Pharmacology* **88**(1): 203-217.

Yuan, H., S. J. Myers, G. Wells, K. L. Nicholson, S. A. Swanger, P. Lyuboslavsky, Y. A. Tahirovic, D. S. Menaldino, T. Ganesh, L. J. Wilson, D. C. Liotta, J. P. Snyder and S. F. Traynelis (2015). Context-Dependent GluN2B-Selective Inhibitors of NMDA Receptor Function Are Neuroprotective with Minimal Side Effects. *Neuron* **85**(6): 1305-1318.

Zarei, M. M. and J. A. Dani (1995). Structural basis for explaining open-channel blockade of the NMDA receptor. *J Neurosci* **15**(2): 1446-1454.

Zhang, S., M. D. Ehlers, J. P. Bernhardt, C. T. Su and R. L. Huganir (1998). Calmodulin mediates calcium-dependent inactivation of N-methyl-D-aspartate receptors. *Neuron* **21**(2): 443-453.

Zhang, X., Z. J. Feng and K. Chergui (2014). Allosteric modulation of GluN2C/GluN2D-containing NMDA receptors bidirectionally modulates dopamine release: implication for Parkinson's disease. *British Journal of Pharmacology* **171**(16): 3938-3945.

Zhang, Y., P. Li, J. Feng and M. Wu (2016). Dysfunction of NMDA receptors in Alzheimer's disease. *Neurol Sci* **37**(7): 1039-1047.

Zheng, F., K. Erreger, C. M. Low, T. Banke, C. J. Lee, P. J. Conn and S. F. Traynelis (2001). Allosteric interaction between the amino terminal domain and the ligand binding domain of NR2A. *Nature Neuroscience* **4**(9): 894-901.

Zheng, J. and F. J. Sigworth (1997). Selectivity Changes during Activation of Mutant *Shaker* Potassium Channels. *The Journal of General Physiology* **110**(2): 101-117.

Zheng, J. and F. J. Sigworth (1998). Intermediate conductances during deactivation of heteromultimeric Shaker potassium channels. *J Gen Physiol* **112**(4): 457-474.

Zhu, S. and P. Paoletti (2015). Allosteric modulators of NMDA receptors: multiple sites and mechanisms. *Current Opinion in Pharmacology* **20**: 14-23.

Zhu, S., Richard A. Stein, C. Yoshioka, C.-H. Lee, A. Goehring, Hassane S. McHaourab and E. Gouaux (2016). Mechanism of NMDA Receptor Inhibition and Activation. *Cell* **165**(3): 704-714.

Zimmerman, S. S., A. Khatri, E. C. Garnier-Amblard, P. Mullasseril, N. L. Kurtkaya, S. Gyoneva, K. B. Hansen, S. F. Traynelis and D. C. Liotta (2014). Design, synthesis, and structure-activity relationship of a novel series of GluN2C-selective potentiators. *J Med Chem* **57**(6): 2334-2356.